INVESTIGATION OF INDOOR PROPAGATION ALGORITHMS FOR LOCALIZATION PURPOSES

Simulation and Measurements of Indoor Propagation Algorithms for Localization Applications using Wall Correction Factors, Local Mean Power Estimation and Ray Tracing Validations.

Huthaifa Ahmad Naji OBEIDAT

Submitted for the Degree of
Doctor of Philosophy

Faculty of Engineering and Informatics

University of Bradford

2018

Abstract

Huthaifa Ahmad Naji Obeidat

Investigation of Indoor Propagation Algorithms for Localization Purposes

Simulation and Measurements of Indoor Propagation Algorithms for Localization Applications using Wall Correction Factors, Local Mean Power Estimation and Ray Tracing Validations.

Keywords

Indoor Path Loss Model, Indoor Propagation, Received Signal Strength (RSS), Ray Tracing, Local Mean Power, Millimetre wave, Wireless Local Area Network (WLAN), Line of Sight (LoS), Time of Arrival (TOA), Angle of Arrival (AoA).

The objective of this work is to enhance the awareness of the indoor propagation behaviour, by a set of investigations including simulations and measurements. These investigations include indoor propagation behaviour, local mean power estimation, proposing new indoor path loss model and introducing a case study on 60 GHz propagation in indoor environments using ray tracing and measurements.

A summary of propagation mechanisms and manifestations in the indoor environment is presented. This comprises the indoor localization techniques using channel parameters in terms of angle of arrival (AOA), time of arrival (TOA) and received signal strength (RSS). Different models of path loss, shadowing and fast fading mechanisms are explored. The concept of MIMO channels is studied using many types of deterministic channel modelling such as Finite Difference Time Domain, Ray tracing and Dominant path model.

A comprehensive study on estimating local average of the received signal strength (RSS) for indoor multipath propagation is conducted. The effect of the required number of the RSS data and their Euclidian distances between the neighbours samples are investigated over 1D, 2D and 3D configurations. It was found that the effect of fast fading was reduced sufficiently using 2D horizontal's arrangement with larger spacing configuration.

A modified indoor path loss prediction model is presented namely effective wall loss model (EWLM). The modified model with wall correction factors is compared to other indoor path loss prediction models using simulation data (for 2.4, 5, 28, 60 and 73.5 GHz) and real-time measurements (for 2.4 and 5 GHz). Different operating frequencies and antenna polarizations are considered to verify the observations. In the simulation part, EWLM shows the best performance among other models. Similar observations were recorded from the experimental results.

Finally, a detailed study on indoor propagation environment at 60 GHz is conducted. The study is supported by Line of Sight (LoS) and Non-LoS measurements data. The results were compared to the simulated ones using Wireless-InSite ray tracing software. Several experiments have confirmed the reliability of the modelling process based on adjusted material properties values from measurements.

Dedication

To Mom, Dad and all beloved ones.

Acknowledgement

First and foremost, I would like to thank Allah (God) for giving me the Opportunity to expand my knowledge and horizons. I am also grateful to Allah (God) for the successful completion of my transfer report. I would also like to thank my parents, my family and friends, without them, none of these would even have been possible. They have always been my biggest fans and I appreciate that.

Special thanks and gratitude to my academic advisers my supervisor Prof Raed A Abd-Alhameed, Dr James M Noras and Dr Steve Jones for giving me the opportunity to conduct the research work under their supervision. Their scientific wisdom and experience have helped me in achieving my research objectives. I will never forget the many opportunities that they gave me in facilities, publications and support teaching experience.

I would like to thank my fellow graduate students in B3.26 and B3.19: Hanady, Wafa, Fathi, Khalid, Ali, Buhari, Mohammed, Ammar, Waqas and Issa who support me through this journey, and made my stay in Bradford pleasurable.

Table of Contents

List of Abbreviations

Acronym	Stands for
AOA	Angle of arrival
AP	Access point
AWGN	Additive white Gaussian noise
AWM	Averaged Wall Loss Model
BER	Bet error rate
BPL	Building penetration loss
BW	Bandwidth
COST	European Cooperative for Scientific and Technical Research
CP	Circular polarized
CRSS	Comparative received signal strength
DOA	Direction of arrival
DRSS	Differential received signal strength
DSM	Dual Slope Model
DSO	Digital Storage Oscilloscope
ERP	Effective radiated power
EWLM	Effective Wall Loss Model
FDTD	Finite difference time domain
GO	Geometric optics
GPS	Global position system
GRT	Generic Ray Tracing
GTD	General theory of diffraction
IEEE	Institute of Electrical and Electronics Engineers
IF	Intermediate frequency /inverse Fourier
IRT	Intelligent Ray Tracing
ITU	International Telecommunication Union
LAM	Linear Attenuation Model
LBS	Location Based Services
LLS	Linear least square
LOS	Line of sight
MAE	Mean average error
MF	Matched filter
MIMO	Multiple input multiple output
MKM	Motley Keenan Model
MLE	Maximum likelihood
MM-wave	Millimetre-wave
MUSIC	Multiple Signal Classification
NLOS	Non-line of sight
NLS	Non-linear least square
OSM	One Slope Model
PBX	Private branch exchange
PDF	Probability distribution functions
PDP	Power delay profile
PEL	Plane Earth loss
PM	Partitioned Model

PML	Perfectly Matched Layer
PS	Power Sum
RF	Radio-frequency
RMS	Root mean square
RMSE	Root mean square error
RP	Reference point
RSS	Received signal strength
Rx	Receiver
SNR	Signal to noise ratio
SS	Signal strength
STD	Standard deviation
TDOA	Time difference of arrival
TOA	Time of arrival
TP	Test point
Tx	Transmitter
VHF	Very high frequency
VP	Vertical polarized
VS	Vector Sum
UHF	Ultra-high frequency
ULA	Uniform linear array
UTD	Uniform theory of diffraction
UWB	Ultra-wideband
Wi-Fi	wireless fidelity
WINNER	Wireless World Initiative New Radio
WLAN	Wireless local area network
WSN	Wireless sensor network

List of Figures

List of Tables

Chapter 1

Introduction

1.1 Background

With the rapid evolution of wireless communication systems and the wide spread of Wi-Fi technology within indoor environments, indoor object localization emerges as a critical feature to many applications including supporting firefighters rescue process and assisting patients in hospitals and nurse homes. Detailed simultaneous localization methods have been addressed in terms of mapping of objects locations [1], and thus a brief review of the previous and recent developments could enhance the importance of such subject.

In the 1960s the US army developed satellite-based localization which was promoted later to the global positioning system (GPS) [2]. In 1983 GPS was utilized for public usage, with the improvements achieved in the research field, the accuracy enhanced from 100 m as achieved in 1990 to 3.5 m as achieved in 2014 [3]. While GPS is dependent on the availability of LOS propagation, which makes it widely used in the outdoor localization; however it's not recommended to use for indoor environments as the LOS path is weakened or even vanished due to high building penetration losses [4].

Outdoor localization is performed by GPS and mobile cellular networks whereas indoor localization is performed using personal area networks, wireless local area networks WLAN and wireless ad-hoc networks [5]. Due to different building materials, different building sizes, dimensions, furniture and people movements it becomes difficult to generalize a localization model for the indoor environment.

The ability to locate a target object in an indoor environment has many potential applications: e.g. in security, emergency services, healthcare and commercial fields [6-8]. However, it is difficult to provide accurate location by radio means because of the complex multipath propagation associated with buildings [9].

Multipath propagation of wireless signals within buildings has been extensively studied in the context of the deployment of cordless phones [10] and WLAN [11-13]. Propagation from outdoors to indoors has been studied in the context of cellular networks [14]. More recently, there has been significant interest in developing indoor location technologies, in many cases relying on the opportunistic exploitation of available WLAN signals [15] and deploying WLAN in the mm-Wave band [16].

Propagation models have been developed and broadly can be categorised as either predicting median signal strength (path loss and shadowing) like the Motley Keenan model [10] or channel behaviour (fading across time or frequency) like the Saleh Valenzuela model [17]. Path loss models predict the signal level (averaged over several wavelengths or a wide bandwidth) at a given distance from the transmitter [10], whilst channel models describe the stochastic or non-deterministic variation of the signal level (narrowband) and the time-dispersion (wideband) at that location [17]. The advent of multiple input, multiple output (MIMO) systems, and spatial channel models have been introduced to improve accuracy, based on the 3D indoor environment that comprises walls, floors, windows, doors, corridors, stairwells and lift-shafts, including fixtures and furniture which can be considered as clutter [18].

Multipath effects can be observed when the mobile terminal moves distances shorter compared to the correlation shadowing distance; due to these effects, signal strength recorded at the receiver becomes very sensitive to any small movement. In fact, even if the receiver is stationary, the recorded SS still varies noticeably; this makes the use of signal strength in localization impractical and inaccurate.

Researchers have developed techniques to remove the effect of multipath [19] so that the received signal strength (RSS) could be linked to path loss and shadowing only; such integrated representations makes the RSS-distance relationship more tractable. One of the main problems in localization using RSS is the non-monotonic fading of RSS level with distance; such a problem will lead to ambiguity of location estimation. The main objective is to make this relationship unambiguous (i.e. monotonically decreasing). A possible way to achieve this is by averaging over local areas to remove the effects of fast fading [19].

This highly complex channel behaviour is captured by ray-tracing software. However, there are practical limits on the accuracy with which the detail of building structures or clutter can be characterised or the extent to which the material electrical properties can be accurately known [9]. There are also compromises made in the number of ray paths that can be found by the software within the constraints of a reasonable run-time and memory requirement [20].

The ray-optical view of the propagation mechanisms leads naturally to a description of the channel in terms of its impulse response as given by [21]. In the indoor channel, rays have been observed to arrive in clusters, as modelled

by [17]. The clusters can be associated with angles of arrival and departure in developing spatial channel models [22]. The impulse response will vary with the position and if the terminal (or clutter) is moving, this translates into time variation.

1.2 Aims and Objectives

The aim of this research is to investigate and contribute to indoor propagation algorithms for better understanding and to enhance various indoor applications including location-based services. The aspects investigated in this research include local mean signal estimation, indoor path loss algorithm and ray tracing validation at millimetre-wave frequencies.

Objectives identified to achieve this aim to:

1. Conduct a comprehensive study of major propagation mechanism and manifestations for indoor and outdoor environments.
2. Present a broad study of indoor localization techniques using channel inferred parameters.
3. Full modelling process using Wireless InSite software and detailed Matlab programmes to be implemented for various indoor applications.
4. Perform an analytical study on local mean signal strength estimation to enhance localization performance.
5. Conduct experimental measurements and validate results with ray tracing software at mm-wave frequencies.

The major contributions of this work are:

1. A modified indoor path loss prediction model is presented in Chapter 4, namely, the effective wall loss model. The modified model is compared to other indoor path loss prediction models using simulation data and real-time measurements. Different operating frequencies and antenna polarizations are considered to verify the observations. In the simulation part, the effective wall loss model shows the best performance among other models as it outperforms by a factor of two the dual-slope model, which is the second-best performancer. Similar observations were recorded from the experimental results.

2. A comprehensive study on estimating local average signal strength for indoor multipath propagation is conducted in Chapter 5. The study covers the effect of the required number of collected point samples of signal strength, the distance between these sample points and the distribution of them. It was found that the effect of fast fading was reduced sufficiently using two-dimensional horizontal configuration samples; further, using the same number of samples with larger spacing enhanced averaging compared with small spacing. It was also noticed that for some arrangement types averaging improved for a smaller size as spacing increases.

3. Ray-tracing validation using real-time measurements are presented in Chapter 6, the comparison investigates effects of material electrical parameters on received signal strength. It was found that the ray tracing software results were varying depending on the input of the material electrical parameters; however, some results are comparable to measurements which imply that material electrical parameters values used are the most accurate.

4. A review on indoor propagation manifestations is conducted in Chapter 2, the study includes different models on path loss, shadowing and fast fading mechanisms. Different channel parameters including signal strength, power delay, coherence bandwidth, Doppler spread and the angle of arrival are explored. The study also explores many types of deterministic channel modelling such as Finite Difference Time Domain, ray tracing and dominant path model. Building material properties with frequency are also investigated, many models for the propagation through buildings are introduced.

1.3 Organization of the Thesis

Chapter 2: This chapter provides a comprehensive review on propagation in indoor environments, the study enlightens propagation differences between indoor and outdoor environments. Different indoor path loss models are presented, the study also explores many types of deterministic channel modelling including Finite Difference Time Domain, ray tracing and dominant path model. Building material properties with frequency are also investigated, the chapter also investigates building penetration losses models published in the literature.

Chapter 3: This chapter opens with an introduction to the term localization techniques including RSS, TOA and AOA. The study contains concepts, requirements and specifications for each category of techniques. The chapter also presents pros and cons for investigated localization techniques and conducts comparisons between them.

Chapter 4: This chapter presents a modified indoor path loss prediction model, the proposed model was compared to other models at different frequencies and antenna polarizations, simulation results were compared to collected measurements where good agreement was observed.

Chapter 5: A comprehensive study on estimating local average signal strength for indoor multipath propagation is conducted in Chapter 5. The study covers the effect of the required number of collected point samples of signal strength, the distance between these samples points and the distribution of them.

Chapter 6: Validation of Wireless InSite Ray-tracing software with measurements at 60 GHz is conducted in Chapter 6. The study includes LOS and NLOS propagation, the effect of using different electrical parameters values recorded in literature are investigated for different materials.

Chapter 7: This chapter summarizes the whole thesis and provides the outcomes of this research. Conclusions drawn from each chapter and how this work can be further extended are discussed in this chapter.

Chapter 2

Indoor Propagation Environment

2.1 Introduction

Wireless communication engineers struggle with the dynamic behaviour of wireless radio channels. Wireless channels are more susceptible than cabled channels to noise, interference and similar hindrances [23]. Therefore, they try to establish values of the received signal strength (RSS) at any location. The aim of this study is to introduce a survey on indoor radio propagation: understanding this is important for many applications, including location-based services (LBS) [9, 24].

With the vast expansion of mobile technologies, many indoor applications have become supported by 4G services [25, 26] and 5G services [27]. In 5G systems, indoor cells are linked to outdoor base stations through indoor base stations working at millimetre waves [28]. The usage of high data rate Multiple Input Multiple Output (MIMO) systems makes the prediction and planning for indoor systems extremely difficult [26]. Figure 2.1 highlights the general topics covered in this chapter.

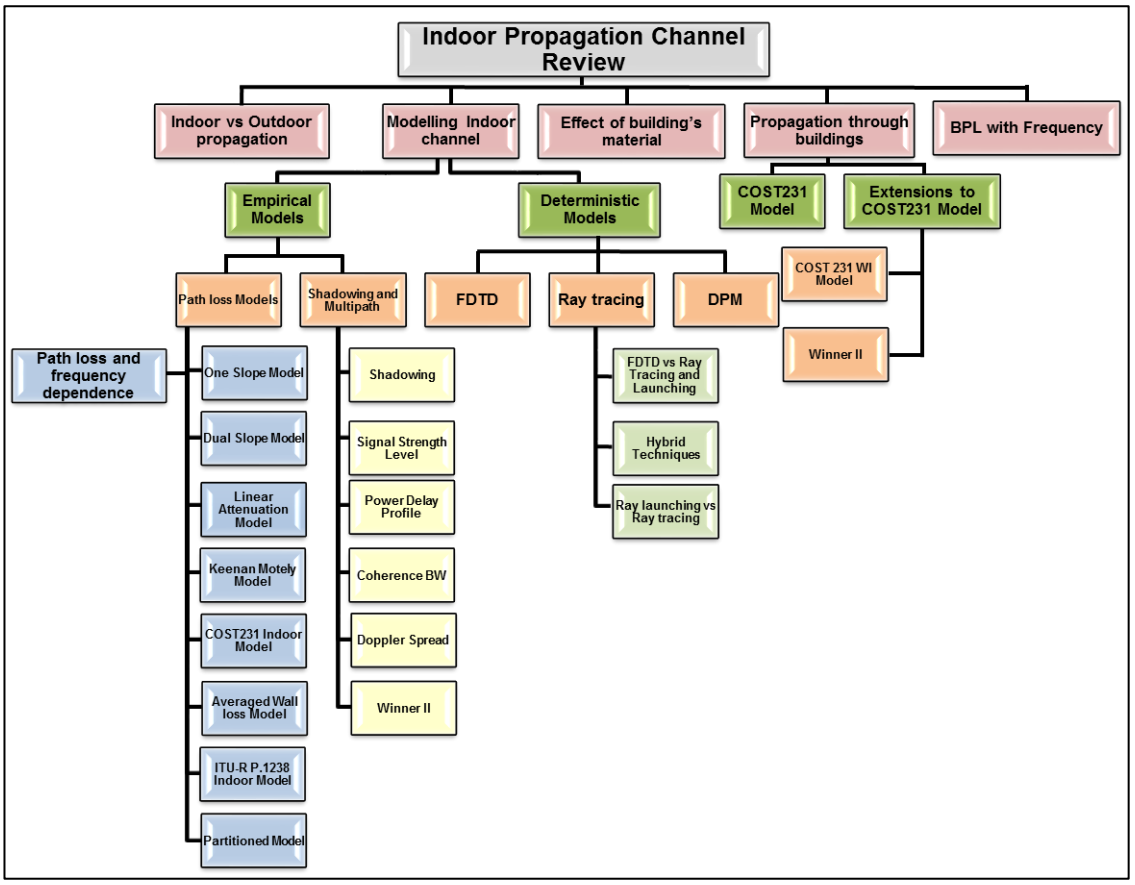

Figure 2.1: Indoor Propagation Channel Review Outlines.

2.2 Indoor and Outdoor Comparison

The indoor environment is more dynamic compared to the outdoor environment [29]: diffraction becomes an important phenomenon especially in the absence of LOS paths, and scattering from objects of size comparable to the wavelength also has major effects on signal level [21]. The indoor coverage is further constrained by high wall/floor attenuation and low transmitted power, which result in lower delay spread: typical delay spreads for indoor environments are in the range of tens of nanoseconds, while being in the range of tens of microseconds for outdoor environments [21]. While the only causes of a time-variant channel outdoors are the movements of the transmitter and/or the receiver, movement of people causes the indoor channel to be time-variant even if both transmitter and

receiver are stationary [26]. Note however that Doppler effects are neglected since the velocity within buildings is limited [21]. In the indoor case, a simple path loss exponent (n) model is less likely to be applied for path loss prediction due to its complexity [30].

Indoor propagation analysis depends on a building's geometry where frequency reuse in the building is widely used; however, the interference between the floors makes propagation analysis more challenging. Ray tracing techniques are widely used to model the channel in indoor and outdoor environments; however, once the size of any obstacles are comparable to the wavelength, ray tracing becomes invalid: this is the case in many indoor scenarios and as a result this will place restrictions on frequency bands predicted via ray tracing for indoor environments [31]. Path loss attenuation at the specific frequency allocated for a service can be different in indoor and outdoor environments: for example, frequency-dependent attenuation due to oxygen and water vapour particles will restrict the use of 60 GHz in outdoor environments [32] while it is attractive for indoor applications [33]. Indoor propagation is not affected by winds, storms and rainfall which can affect outdoor RSS [34], also path loss dependency on operating frequency tends to be more in the case of the indoor environment [35].

2.3 Frequency Allocation

Many organisations run their own local private wireless telephone network called private branch exchange (PBX), these networks use the 800-2000 MHz range [36]. Other frequency ranges include Bluetooth at 2400 MHz, WiMAX at 3500 MHz, IEEE 802.11 [a, b, n, g, ac, ad] in the frequency range 2400-5800 MHz and

free licences 433.05-434.79 MHz, 900-928 MHz, 2400-2483 MHz and 5700-5900 MHz [36] 60 GHz [37]. The availability for bandwidth is limited as many applications utilize these bands (e.g. at 2.4-2.5 GHz wireless devices are affected by the radiation from other microwave emissions like Bluetooth); hence proper coverage and interference reduction are indispensable [38]. Higher data rate achieved at 17-18 GHz [39], 6.8-8.5 GHz, 24 GHz bands [40] and millimetre wave system in the 38 GHz [41], 32.5 GHz, 60 GHz, 65 GHz and 73 GHz regions [42] [43] 42 GHz and 58 GHz [39].

2.4 Modelling Indoor Channel

Generally, there are two main approaches for indoor channel propagation modelling: empirical and deterministic [44]. In empirical modelling data are collected from measurements, then by using statistical analysis, channel coefficients are characterised to convert the data into parametric equations [45]. The signal level, phases, time of arrival, angle of arrival and many signal parameters are characterised by probability distributions to describe their behaviour [45].

Deterministic modelling depends on laws of physics whereby the electromagnetic wave distributions are solved to estimate the channel parameters at any location in the environment [45]. Environmental details like floor height, the location of doors and windows and their material types and furniture in the environment are carefully considered to predict signal parameters like the signal strength, angle of arrival and time of arrival [20]. The accuracy of the models depends strongly on the detail in which the environmental features are considered [44]. Generally, empirical models are applied to environments that have similar characteristics to

the environment used to construct the model, while deterministic models are created for a specific environment [44].

2.5 Empirical Models (Site General Models)

Before proceeding with the discussion of this section, it is appropriate to note that, although many models are based on measurements in typical indoor environments like houses and offices, the structure and ingredients are quite different from one culture to another; for instance houses may be made of brick, concrete, reinforced concrete, mud, wood and steel-framed which is used widely in industrial buildings. They may also be made of wood and plaster for interior partitions and concrete and brick for exterior partitions, etc. The same applies to “office environment”, where some offices are large and others are small. Some offices have hard partitions which are constructed with the building itself, others have soft partitions made from plaster or wood which are not extended to the ceiling and may be movable. These generalizations may lead to contradictions with observations in the literature unless the material and details of the environment are specified in detail [46-48].

2.5.1 Path loss

In this section different path loss models are presented; these models include the effects of walls, floors and the complexity of the environment. Many models have been proposed in literature including one slope model [49], dual slope model [50], linear attenuation model [51], partitioned model [52], Motley Keenan model [10], averaged wall loss model [53], ITU-R P.1238 model [54] COST 231 indoor model [55] and dominant path model [56].

One Slope Model (OSM)

This is a fast and simple model, also termed as the simplified path loss model where the received power at a point is given by [49]:

$$P_r(dB) = P_0(dB) - 10n\log_{10}(d) \quad (2.1)$$

Where P_0 is the received power at one metre from the transmitter which can be estimated using free space formula or experimentally [23], n is the path loss exponent which is calculated using interpolation [57] and d is the distance from the transmitter. Path loss is dependent on the range (distance) and path loss exponent [23]. In [58] various values of decay index n are presented, the values ranging from 1.2 due to waveguiding effects in corridors to 6.1 for a dense office environment [59]. In outdoor to indoor propagation at 1.7 GHz [51], decay index n found to be 1.495 for corridor on a single floor; 1.524 through separated corridors in that building and 3.25 for separate rooms on a single floor and 3.31 in rooms dispersed through a building. Typical path loss exponent for the indoor environment are given in Table 2-1, where OLOS stands for obstructed LOS.

Table 2-1: Typical path loss exponent for indoor environment [59].

Building	Frequency (MHz)	n
Store	914	1.8-2.2
Office	900	2.4
	1900	2.6
Factory LOS	1300	1.6-2.1
OLOS		3.3
House	900	3.0

Authors in [47] formulated the path loss exponent in mathematical equations as a function of the corresponding excess delay τ_{ex} and whether the propagation is LOS or Non-LOS (NLOS):

$$n_{LOS} = \begin{cases} 2.5 + \dfrac{\tau_{ex}}{39} & \tau_{ex} < 15\ ns \\ 3 + \dfrac{\tau_{ex} - 15.6}{380} & 15\ ns\ < \tau_{ex} < 250\ ns \\ 3.6 & 250\ ns\ < \tau_{ex} < 500\ ns \end{cases} \quad (2.2)$$

$$n_{NLOS} = \begin{cases} 3.65 + \dfrac{\tau_{ex}}{536} & \tau_{ex} < 310\ ns \\ 4.23 & 310\ ns\ < \tau_{ex} < 500\ ns \end{cases} \quad (2.3)$$

Linear Attenuation Model (LAM)

Authors in [60] proposed another approach: experiments were carried out over a range of frequencies (0.85, 1.9, 4.0 and 5.8 GHz) and it was concluded that total loss is the sum of free space loss L_{FS} and loss factor in the range of ($\alpha = 0.3 - 0.6\ dB/m$) depending on frequency and building [60].

$$P_r(dB) = P_0(dB) - 20\log_{10}(d) - a \cdot d \quad (2.4)$$

where d represents distance in metre. Equation 2.4 can be modified by adding wall losses to overall losses [61].

Dual Slope Model (DSM)

Propagation within indoor environment was categorized depending on first Fresnel zone clearance: firstly the “near transmitter propagation” where there is no obstruction in the first Fresnel zone and the path loss exponent is less than 2 due to waveguiding, and secondly “breakpoint propagation” when furniture falls

in the first Fresnel zone and path loss exponent becomes larger than 2, as shown in Equation 2.5 [50].

$$P_r = P_0 - 10\begin{cases} n_1 \log_{10}(d) & d < d_{bp} \\ n_1 \log_{10}(d_{bp}) + n_2 \log_{10}\left(\frac{d}{d_{bp}}\right) & d > d_{bp} \end{cases} \quad (2.5)$$

where n_1, n_2 are the path loss exponents and d_{bp} is the breakpoint distance. Calculation of the breakpoint distance is done either theoretically as in [50] or experimentally as in [62]. The authors in [63] claimed better performance for the DSM compared to the OSM, since their corresponding overall standard deviation are 4.9 dB and 17.2 dB respectively.

In indoor environments the direct path may not be the dominant path as other rays which are not direct may have a stronger signal, in [64] OSM and DSM were enhanced by infusing the concept of dominant direct path in the model instead of using the direct path, authors claimed better performance than the original models.

Partitioned Model (PM)

In this model, the path loss is estimated based on predetermined values of n and distance between transmitter and receiver [65]:

$$L = L(d_0) + k_d \quad (2.6)$$

Where $$k_d = \begin{cases} 20\log_{10} d, & 1m < d \le 10m \\ 20 + 30\log_{10}\frac{d}{10}, & 10m < d \le 20m \\ 29 + 60\log_{10}\frac{d}{20}, & 20m < d \le 40m \\ 47 + 120\log_{10}\frac{d}{40}, & d > 40m \end{cases}$$

Measurements show that OSM and DSM outperform the partitioned model [50], Ericsson Radio Systems have taken a similar approach while the path loss has upper and lower limits depending on the fading severity: the path loss exponent was found to be in the range from 2 to 12 as distance increased [30].

ITU-R P.1238 Indoor Model

This is an empirical model that accounts for the losses due to penetration through floors within the same building [54]:

$$L = 20\log_{10} f_{MHz} + 10n\log_{10}\frac{d}{d_0} + L_f\big(N(F)\big) - 28 \qquad (2.7)$$

Where $L_f\big(N(F)\big)$ is the floor penetration loss which varies with frequency, type of floor and number of floors. Based on a large number of measurements, the model gives typical values for n and $L_f\big(N(F)\big)$ for different indoor environments in Table 2-2 and Table 2-3 respectively [54]. Some guidelines should be considered when using these tables are given in the source literature [54], in the case where both transmitter and receiver are in the same floor then $L_f = 0$.

Table 2-2: Indoor power loss exponent [54].

Frequency	Residential	Office	Commercial	Factory	Corridor
900 MHz	-	3.3	2	-	-
1.25 GHz	-	3.2	2.2	-	-
1.9 GHz	2.8	3	2.2	-	-
2.1 GHz	-	2.55	2	2.1	1.7
2.4 GHz	2.8	3	-	-	-
3.2 GHz	-	2.7	-	-	-

2.625 GHz	-	4.4	-	3.3	-
4 GHz	-	2.8	2.2	-	-
5.2 GHz	3, 2.8	3.1	-	-	-
5.8 GHz	-	2.4	-	-	-
28 GHz	-	-	2.76	-	-
60 GHz(1)	-	2.2	1.7	-	1.6
70 GHz(1)	-	2.2	-	-	-

Table 2-3: Floor loss factor for m floors (dB) [54].

Frequency (GHz)	Residential	Office	Commercial
0.900	-	9 (1 floor) 19 (2 floors) 24 (3 floors)	-
1.8-2	4m	15+4(m-1)	6+3(m-1)
2.4	10, 5	14	-
3.5	-	18 (1 floor) 26 (2 floors)	-
5.2	13(1) (Apartment) 7(2) (house)	16 (1 floor)	-
5.8	-	22 (1 floor) 28 (2 floors)	-

(1) Per concrete wall (2) Wooden house

Motley-Keenan Model (MKM)

The wide range of n makes the use of one slope model inadequate [10], MKM considers the effect of walls and floors, including their types and numbers [10] [66].

$$L = L_{FS} + L_C + \sum_{i=1}^{I} N_{wi} L_{wi} + \sum_{j=1}^{J} N_{fj} L_{fj} \quad (2.8)$$

Where $L_{FS}, L_C, N_w, N_f, L_w, L_f, i$ and j are the free space loss, constant term (loss at $d_0 = 1\ m$), number of walls, number of floors, wall loss factor, floor loss factor,

type of wall and type of floor respectively. It's noteworthy that L_w and L_f were found to be lower as the number of interleaving wall/floor increased [67] [68]. This may be related to the fact that the signal will find other paths to propagate, such as corridors and doors in the same floor or via stairs for multi-floor buildings [69] as shown in Figure 2.2. Table 2-4 illustrates values for floor attenuation factor for different buildings: wall and floor losses tend to depend on thickness, types of materials, angle of incidence and frequency [70], floor loss factor was observed to increase as the frequency increases [71] and losses at oblique incidence tend to be larger compared to normal incidence [55].

Table 2-4: Floor attenuation factor (dB) for different buildings [59].

Building		Floor Attenuation factor
Building 1	Floor 1	12.9
	Floor 2	5.8
	Floor 3	5.7
	Floor 4	2.6
Building 2	Floor 1	16.2
	Floor 2	11.3
	Floor 3	4.1
Building 3	Floor 1	13.2
	Floor 2	4.9
	Floor 3	5.9
	Floor 4	3.0
	Floor 5	0.1

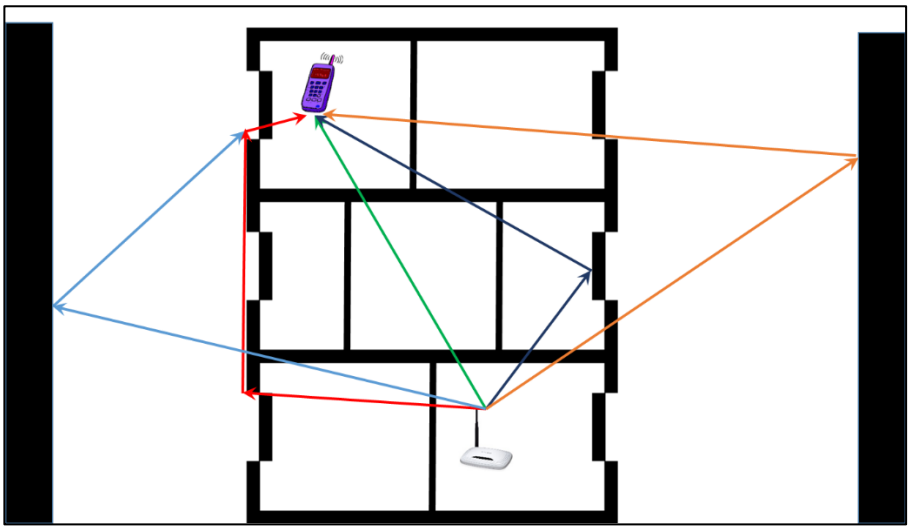

Figure 2.2: Propagation through floors.

COST231 Indoor Model

A more sophisticated model was given by COST231, which adopts the concept of MKM [55]. The model assumes a linear increase of loss as the number of walls increases, and a non-linear increase of loss as the number of floors increases, due to the decrease in floor losses; the model is given in Equation 2.9 [55] [72]:

$$L = L_{FS} + L_C + \sum_{i=1}^{I} N_{wi} L_{wi} + L_f n_f^{\left(\frac{(n_f+2)}{(n_f+1)} - b\right)} \quad (2.9)$$

where L_C is the resultant wall loss obtained by applying multiple linear regression to the measurements, n_f is the number of encountered floors and b is an empirical constant, L_{wi} is wall loss of type i and L_f is the floor loss. Two types of wall are defined: a light wall which has thickness <10 cm such as plasterboard, and a heavy wall with thickness >10 cm, such as brick or concrete [55]. Typical values for light wall loss are 1.9 dB at 900 MHz and 3.4 dB at 1800 MHz. For heavy walls, the average loss at 1800 MHz is around 6.9 dB [55]. Typical values for floor losses are 14.8 and 18.3 dB for 900 and 1800 MHz respectively. For different types of environments, the empirical constant b found to be 0.46 at 1800

MHz [55]. Figure 2.3 shows how floor individual losses decrease as the number of floors increases, and also how floor losses increase as frequency increases.

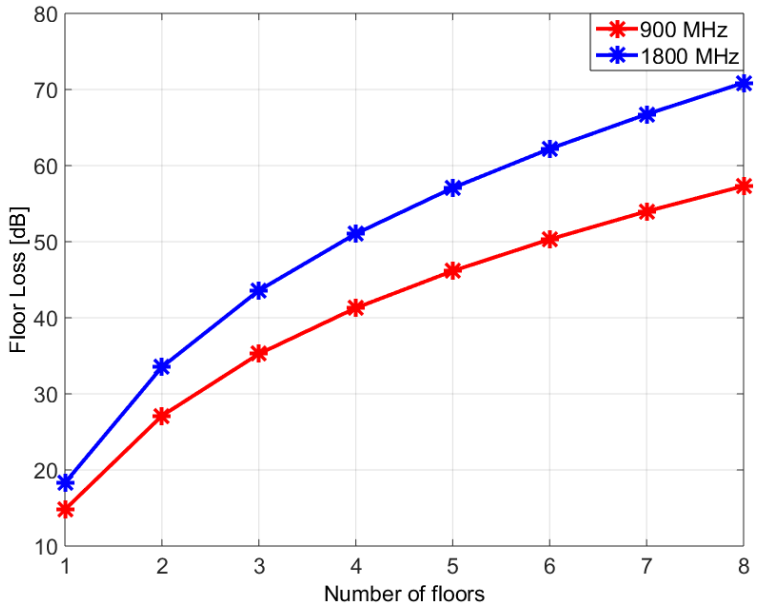

Figure 2.3: Floor losses for COST231 Indoor model.

As mentioned above, the model assumes that wall losses are linear as the number of walls increases, this makes the results to be pessimistic. An extension has been made so that individual wall losses decrease as the number of walls increases which claimed to give better performance [72].

Averaged Wall Loss Model (AWM)

AWM was proposed by [53]. This model is similar to the MKM, however, the way losses are calculated is different. The first wall loss is estimated by finding the difference between the path loss estimated from measurements and the losses due to free space propagation as shown in Equation 2.10 [53]:

$$W_1 = P_{r1} - P_0 + 20\log_{10}(d_1) \tag{2.10}$$

where P_{r1} is the RSS one meter from the first wall, and d_1 is the distance between the transmitter and the point where the P_{r1} measurement was taken. Losses of following walls are estimated similarly after excluding previous wall losses [53]. Averaged wall loss of the same type is given by:

$$W_{avg} = \frac{\sum_{i=1}^{v} W_i}{v} \tag{2.11}$$

where v is the total number of walls. The path loss at distance d can be expressed as shown in Equation 2.12, where L is the number of walls.

$$P_r(d) = P_0 - 20\log_{10}(d) - W_{avg} \cdot L \tag{2.12}$$

Path loss and frequency dependence

As the frequency increases, the ability of the wave to bind around corners decreases, causing diffraction to contribute less to overall signal strength and hence path loss tends to be larger at higher frequencies [67], [73]. According to [74] it was observed that the path loss exponent doesn't change with frequency, it was also observed that both path loss and path loss exponent do not change with bandwidth, modulation and polarization of the wave.

In [75] a set of experiments was carried out over the frequency range 3-11 GHz. It was observed that as frequency increases, the attenuations in NLOS scenarios are more severe compared with LOS cases. Another study on the same

frequency range found that path loss exponent, delay spread and power delay profile (PDP) have similar behaviour over this range of frequencies [76].

The frequency dependence of path loss exponent found to be related to LOS existence, as n was recorded to have a slightly different frequency dependence in LOS cases: it was observed to have more dependence on frequency in the NLOS cases [77].

2.5.2 Shadowing and Multipath

Similarly to outdoor propagation, indoor fading occurred on the large scale (path attenuation and shadowing) and on the small scale (multipath and Doppler spread), the channel could also be narrowband or wideband.

Shadowing

Fading due to shadowing in an indoor environment tends to follow a Log-Normal distribution. Typical values for location variability σ_L for an office are given in Table 2-5 [54]:

Table 2-5 Location variability for indoor office.

Frequency (GHz)	σ_L(dB)
1.8-2	10
3.5	8
5.2	12
5.8	17

Signal Strength Level

Signal strength levels can be described by many distributions, depending on the circumstances of the experiments. In the case where NLOS is dominant it was found that signal level follows a Rayleigh distribution [17] [78], but in the presence

of the LOS component, the signal envelope follows a Rician distribution [79], [80]. Experiments in other circumstances show a Log-Normal distribution [52, 81], Suzuki distribution [82], Nakagami distribution [83, 84], exponential distribution [85] and Weibull distribution [73, 84, 86].

The Suzuki distribution [87] applies in many locations as it combines the Log-Normal with Rayleigh distributions, so it gives the signal fading due to shadowing superimposed with the Rayleigh fading due to multipath propagation [82].

The Weibull distribution has the flexibility to cover a range of circumstances, as presented in [86]. Here different transmitter-receiver separation distances were applied, LOS and NLOS cases and the effect of Doppler spread were considered. Several different probability distribution functions (PDFs) were tested to fit the measurements: the percentage was as follow: Rayleigh 1%, Lognormal 7.8% Rician 22.3%, Nakagami 31.8% and Weibull 37%. The indoor environment is very complicated, therefore signal parameters will not follow the same behaviour in all environments. Since it has three parameters, the Weibull distribution offers flexibility so that even the environment changes Weibull still represents the signal level fading [73].

$$p(x, m, \epsilon, \rho) = \frac{m}{\epsilon}\left(\frac{x-\rho}{\epsilon}\right)^{m-1} e^{-\left(\frac{x-\rho}{\epsilon}\right)m} \tag{2.13}$$

where m, ϵ and ρ are the shape parameter, scale parameter and location parameter respectively. The Weibull distribution becomes a Rayleigh distribution when *m=2* [88].

Impulse Response

The Saleh-Valenzuela (SV) model is popular and widely used for describing arrival time sequence and amplitude in the case of resolvable multipath. The model describes the behaviour of multipath in indoor environments suggesting that rays come in clusters as shown in Figure 2.4. The number of clusters tends to decrease with increasing frequency [89] and as the separation between transmitter and receiver is increased [90].

The number of clusters tends to follow a modified Poisson distribution [91]. Considering the first ray of each cluster and aggregate them together, it was found that the best fit for the amplitude of these rays follows a negative exponential distribution while their inter-arrival times of each cluster follow a modified Poisson distribution and their corresponding amplitudes follow a negative exponential distribution [17].

The amplitude of each individual ray follows a Rayleigh distribution or Normal distribution in the Ultra-Wide Band (UWB) propagation case, while its phase follows a Normal distribution [36]. The indoor channel based on SV-model is described by:

$$h(t) = \sum_{l=0}^{\infty} \sum_{k=0}^{\infty} \beta_{kl} e^{j\varphi_{kl}} \delta(t - T_l - \tau_{kl}) \qquad (2.14)$$

where β_{kl} is the multipath gain, φ is the phase associated with the l^{th} cluster and k^{th} ray, l is the number of clusters, k the number of arrival rays within the l^{th} cluster, T_l is the arrival time of the l^{th} cluster and τ_{kl} is the arrival time of k^{th} ray within the l^{th} cluster. Note that the SV model was developed for wideband systems, it was also found to be valid for UWB systems [92].

The work done in [17] was updated by [22] to include the behaviour of the angle of arrival in the indoor environment, they found that the arrival waves tend to be clustered in time and angle as shown in Equation 2.15 [22]. For all rays within a cluster, the mean of their angles of arrival is known as the *cluster arrival angle* Θ_l.

$$h(t,\theta) = \sum_{l=0}^{\infty}\sum_{k=0}^{\infty} \beta_{kl} e^{j\varphi_{kl}} \delta(t - T_l - \tau_{kl}) \delta(\theta - \Theta_l - \omega_{kl}) \qquad (2.15)$$

where ω_{kl} is the arrival angle of the k^{th} ray of the l^{th} cluster. The distribution for Θ_l is uniform, while the k^{th} ray's arrival angle ω_{kl} follows a Laplacian distribution [22].

$$p(\omega_{kl}) = \frac{1}{\sqrt{2}\sigma} e^{-|\sqrt{2}\omega_{kl}/\sigma|} \qquad (2.16)$$

where σ is the standard deviation. Table 2-6 gives the mean value for angular spread in an indoor environment.

Table 2-6: Typical mean value for angular spread in the indoor environment [54].

Indoor Scenario	LOS	NLOS
Hall	23.7°	-
Office	14.8°	54°
Home	21.4°	25.5°
Corridor	5°	14.76°

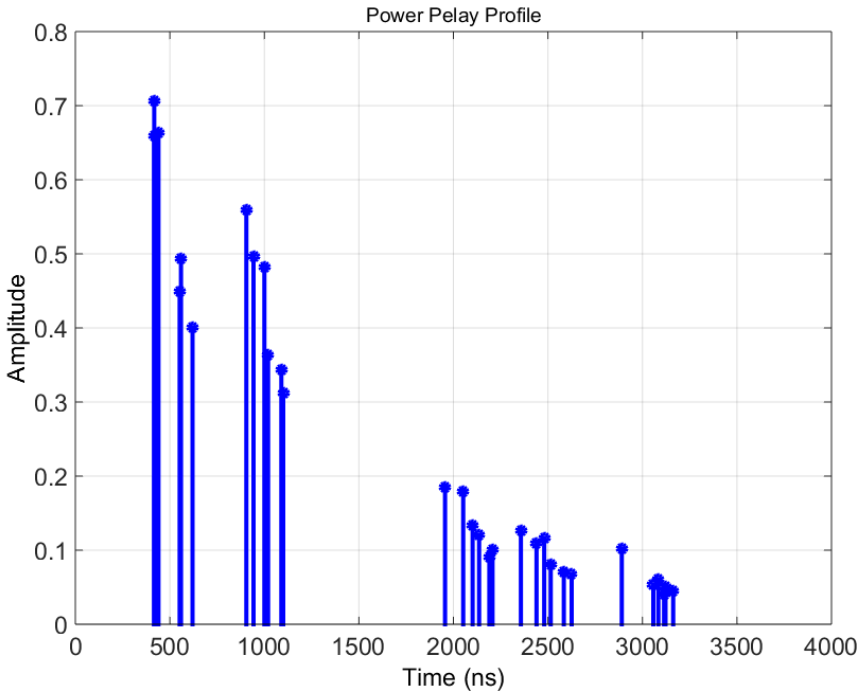

Figure 2.4: Saleh Valenzuela Model.

Delay Spread

RMS Delay spread σ_{rms} tends to follow a normal distribution and has a clear dependence on the distance between the transmitter and receiver [86]. Typical values for average indoor mean delay spread are in the range of 20-30 ns over the frequency range of 0.9-1.3 GHz [86] [93].

In [36], statistics of RMS delay spread were measured by their mean, median and standard deviation, it was found that LOS propagation has lower metrics values compared to NLOS propagation, a similar observation was recorded by [94]. σ_{rms} was found to be larger as the transmitter-receiver (Tx-Rx) separation increases [93] [95] and as the area of floor becomes larger [54]. Equation 2.17 shows a proportional relationship between delay spread and floor's area F_a up to 1000 m^2 at 2 GHz [54]:

$$\log \sigma_{rms} = 0.23 \log(F_a) + 1.1 \quad (2.17)$$

In propagation between floors, σ_{rms} tends to be larger due to more reflection, diffraction and transmission occurring [96]. It was found that increasing the operating frequency caused the mean of σ_{rms} to fall [97] [89]. Table 2-7 summarizes the median RMS delay spread in different indoor environments at different frequencies.

Table 2-7: Median RMS delay spread in different environments [54].

Frequency (GHz)	Environment	Median RMS delay spread (ns)
1.9	House	70
	Office	100
	Commercial	150
2.625	Office	11
	Corridor	18.53
	Air cabin	11.89
	Factory	69.2
3.7	House	22
	Office	38
	Commercial	145
5.2	House	23
	Office	60
	Commercial	190
60	Office	1.77

Number of Paths

The number of detected paths depends on receiver sensitivity and transmitter-receiver separation. Higher sensitivity means that more paths are expected to be detected, as distance gets longer the probability to receive a multipath component

reduced [98], this probability is further reduced in open spaces compared to a dense built environment since more reflection and scattering are likely to occur in dense environments: measurements show that the number of detected paths follows a modified Beta distribution [98-100], a Gaussian distribution [81], or a Poisson distribution. In the case where the threshold is lower, the distribution tends to be Normal [101].

Coherence Bandwidth (B_C)

Since the relationship between B_C and σ_{rms} is inversely proportional, it is expected for B_C to have opposite characteristics [36]. B_C was found to be larger for LOS cases compared to NLOS, also as the transmitter-receiver separation increases B_C tends to be smaller [36].

Doppler Spread

In indoor environments the movement of people could affect the channel response and cause Doppler spread; however due to the limited mobile velocity in indoor environment, Doppler spreads are negligible as shown in [102] where Doppler spread was found to be in the range of 0.3-6.1 Hz, also in [86] the observed range was (0.35-4.54 Hz). In [103] a set of measurements were conducted on the range of frequencies (3.1-10.6 GHz), it was observed that Doppler spread shows a frequency dependent behaviour. In the case of outdoor-indoor propagation (e.g. satellite to indoor), Doppler effects can no longer be ignored [104]. Doppler spread tends to increase as frequency increases; in [105] a relationship between coherence time and antenna beamwidth was observed, it was concluded that coherence time is inversely proportional to antenna beamwidth for millimetre wave.

WINNER II

In the WINNER II project [106] a set of measurements were conducted on different propagation scenarios in the range of frequencies from 2 to 6 GHz. Two general indoor cases were considered, the first being an indoor floor that could be an office or residential, and the second case is a very large hall, such as a conference hall or railway stations. The path loss is given by Equation 2.18 [106].

$$PL = A \cdot \log_{10}(d) + B + C \cdot \log_{10}\left(\frac{f_c}{5}\right) + X \qquad (2.18)$$

where *X* represents additional losses and C= 20 dB for all cases except for large indoor hall in NLOS propagation as it equals 23 dB, other parameters are given in Table 2-8.

Table 2-8: Typical values for WINNER II Indoor Models [106].

		A	*B*	*X*	*σ*
Indoor Office/ residential	LOS	18.7	46.8	-	3
	NLOS†	36.8	43.8	$5(n_w - 1)$	4
	NLOS††	36.8	43.8	$12(n_w - 1)$	
	NLOS†††	20	46.4	$5n_w$	6
	NLOS††††	20	46.4	$12n_w$	8
Large Indoor hall	LOS	13.9	64.4	-	3
	NLOS	37.8	36.5	-	4

†: Corridor-room propagation and light walls.
††: Corridor-room propagation and heavy walls.
†††: Room-room propagation and light walls.
††††: Room-room propagation and heavy walls.

n_w is the number of walls and *σ* is the shadowing fading standard deviation. In the case where transmitter and receiver are on different floors an additional loss is added as in Equation 2.19 [106]:

$$L_{floor} = 17 + 4(n_f - 1) \quad (2.19)$$

where n_f is the number of floors. For both cases the delay spread was found to follow an exponential distribution, the number of clusters in both cases was larger in the NLOS compared to LOS, while the correlation distance are larger in LOS compared to NLOS. Other propagation parameters are discussed in [106].

2.6 Deterministic Models (Site Specific Models)

In a deterministic model, the channel and signal parameters are determined for every location in the environment. The most accurate results would be obtained by solving Maxwell's equations; however, such a task is effectively impossible even with high-speed computers due to the complexity of specifying boundary conditions [107]. Deterministic techniques for indoor propagation includes the Finite Difference Time Domain (FDTD), ray tracing [107] and dominant Path model (DPM) [108].

2.6.1 Finite Difference Time Domain (FDTD)

Maxwell's equations provide the solution to estimate the signal parameters everywhere, however finding analytical solutions is not always possible, and hence approximations and assumptions have been adopted as an alternative way to solve Maxwell's equations. One of the well-known methods is by using the FDTD method to build a deterministic model for the indoor environment [109, 110]:

The FDTD is a time domain solution that can cover a wide range of frequencies [111]. The main idea is to replace the Maxwellian derivatives with finite difference approximations which can be evaluated at each point in space and time [112-114].

The method had been applied in an indoor scenario in an area of 990 m^2 at 433 MHz [115], the results showed a standard deviation of about 15.5 dB but it was observed that the resource requirements tend to increase exponentially with frequency as the dimension of the simulated environment increases.

In [116] a full wave description for indoor office at WLAN and WiMAX frequencies were estimated using FDTD. The authors found that the path loss exponent was estimated accurately, while the standard deviation for the estimated path loss level was around 5.5 dB.

2.6.2 Ray Tracing

Most deterministic models nowadays adopt the ray tracing technique for indoor propagation prediction since it requires less computational time compared to FDTD [117]. As long as the wavelength is smaller than the sizes of the obstacles the waves can be considered as rays and ray theory can be applied [118]. Both transmitter and receiver are considered as source points where wave propagation between them is described as rays. Early ray tracing models adopt geometric optics and considered only reflection and refraction [119], but later the effect of diffraction was included enhancing propagation parameter prediction

[120]. Rays can be generated by two methods; the first method is performed by launching many rays through many angles where only those which have power above a certain threshold are considered, this method is known as "*Ray launching*" Figure 2.5-b.

The ith ray received electric field using ray launching technique is calculated as [120]:

$$E_i = E_0 U_{ti} U_{ri} L_{FSL}(r) \left[\prod_j R_j \prod_p T_p \prod_l D_l A_l(S_l, S_l') \right] e^{-jkr} \qquad (2.20)$$

where $L_{FSL}(r)$, $U_{(t/r)i}$, R_j, T_p, D_l, S_l, S_l', k: are Free space loss, transmitter/receiver radiation pattern, reflection coefficient of the (j) reflection, transmission coefficient of the (p) transmission, Diffraction coefficient of the (l) diffraction, path length from the transmitter to diffraction edge, path length from diffraction edge to the receiver and wave number respectively.

The second method considers only the paths between the transmitter and the receiver, where the ray paths are established by considering multiple images of the transmitter which occur as a result of reflection of walls. The path is found by drawing straight lines between the multiple images to the receiver: this method is known as "*Multiple images or Ray Tracing*" Figure 2.5-a [121].

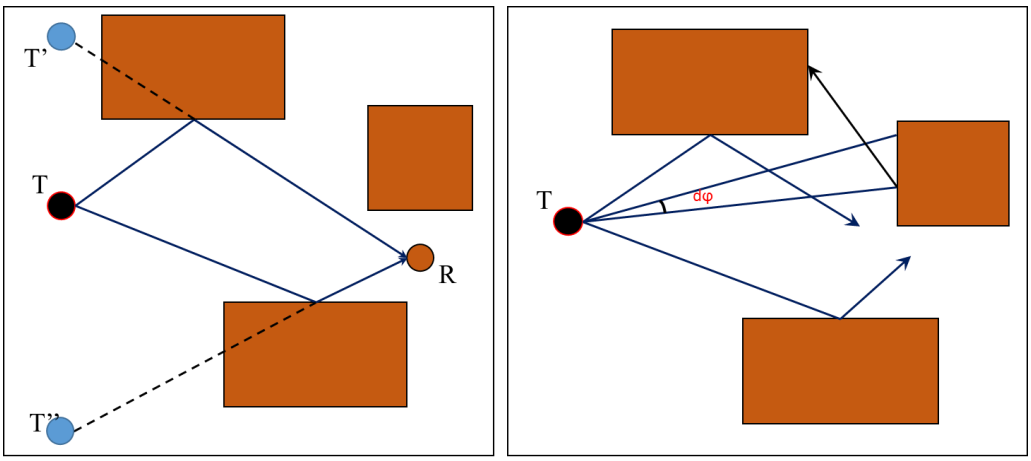

Figure 2.5: (a) Ray Tracing, (b) Ray Launching.

Signal prediction in NLOS scenarios is more sensitive to modelling errors [122], it was also found that changing the values of material electrical properties, walls will have more impact on signal predictions compared to floors and ceilings [122]. Ray tracing techniques can be fastened by using space divisions and simplifications into 2D and 2.5D maps techniques [123].

Several commercial software tools are available to simulate the environment in 3D structure and to emulate the wave propagation to predict channel parameters. The accuracy of these predictions depends on how accurately the environment is constructed. Popular software packages include Wireless InSite® [18], WinProp® [124], EDX SignalPro® [125] and iBWAVE Wi-Fi® [126].

Ray launching vs Ray tracing

Ray tracing guarantees tracing all rays between transmitter and receiver, however, it suffers from exponential increments of computational time as the number of interactions increases while ray launching shows linear dependency. On the other hand, ray launching suffers from the disadvantage of constant angle

increment, which means that some of the surfaces such as corners may not be hit [118]. Also even if the incremental angle were small, as the receiver is moved further away from the transmitter rays may not pass through field point; however by using a reception sphere around the field point, vicinity adequately rays are used to predict signal.

Ray tracing is suitable for point to point prediction while ray launching is suitable for area prediction [118]. One possible way to reduce the computational time is by using *Intelligent Ray Tracing* (IRT) [127]. Using the basic generic ray tracing (GRT) it was observed that while receiving a large number of rays, most of the energy is delivered by a small number of rays, those rays are almost the same for slightly closed receivers. It was also observed that the visibility between walls and edges is independent of transmitter location, thus by doing pre-processing for the environment; the visibility relationships are stored and used for signal prediction, this method removes the redundancy in pathfinding [127]. On the other hand by using (IRT) the prediction time is much less than the GRT, although less accurate results are obtained due to pre-processing [128].

Hybrid Techniques and FDTD vs Ray Tracing and Launching:

The FDTD is a time domain technique which has the advantage of program simplicity; however, it suffers from very large computation time requirement [111]. The ray tracing and launching are frequency-domain techniques and hence narrowband, although they have smaller computation times compared with FDTD [111]; however, the programming is more complicated and also in complex geometries many rays cannot be traced. Using low frequencies in indoor environments, many objects may be smaller than the wavelength and in these

circumstances, the UTD will no longer be applicable [129]. For 2D FDTD simulation, the total number of numerical operations is [130]:

$$F_{FDTD} = \sqrt{\varepsilon_r} \cdot N_{FDTD} \cdot (N_{FDTD} + 2N_{PML})^2 \quad (2.21)$$

where N_{FDTD}: is the number of FDTD grids and N_{PML} is the thickness grid element of the absorbing boundary of the perfectly matched layer (PML). The total number of numerical operations for the Ray Launching technique is [130]:

$$F_{RL} = N_{RL}^2 \cdot i(i+1) \quad (2.22)$$

where $N_{RL}$is the number of discretization steps, and i is the number of interactions. As seen, the complexity orders for the 2D FDTD and Ray launching methods around $\sim N_{FDTD}^3$ and $\sim N_{RL}^2$ respectively [111].

A hybrid technique combining the FDTD and ray launching has been proposed to reduce the computational time and to increase prediction accuracy [131]. The environment is divided into two main categories: the places which have irregularity are studied by the FDTD method which has better performance in these kinds of regions [129]. Other regions will be studied by ray launching which has the same performance compared to FDTD but with less computational time. The total number of numerical operations for the proposed hybrid technique T is [131]:

$$T = k_{RL}(N_{FDTD}^2 - N_{RL}^2) + k_{FDTD}N_{FDTD}^3 \quad (2.23)$$

where $k_{RL}$and k_{FDTD} are the complexity factors for ray launching and FDTD respectively. The hybrid technique has been claimed to be useful especially for inhomogeneous walls [132].

A similar hybrid technique is proposed in [133] where LOS and NLOS scenarios had been examined, better results are observed by using the hybrid technique. Averaged standard deviation error of the hybrid results were 1.85 for LOS propagation and 3.62 dB for the NLOS propagation. For ray tracing only averaged standard deviations were 3.42 dB and 7.18 dB for the LOS and NLOS propagation respectively. FDTD may replace ray tracing in future as the computer capabilities are promising to increase as suggested by [134].

2.6.3 Dominant Path Model

Empirical models (like Motley-Keenan) assume the direct ray between the transmitter and the receiver to be the strongest path [135], which is not the case in most NLOS scenarios, as it contributes less to the total received power [108]. Ray tracing, on the other hand, considers a large number of rays travelling between the transmitter and receiver which will take a long computational time, while only a few rays contribute 95% of the total received power [136]. Even using pre-processing the computation time is relatively high [5] [137].

Dominant path models (DPM), is similar to the MKM; however, instead of considering the direct ray, dominant rays are considered [138]. It considers the main rays which contribute most of the energy, hence using this model will reduce the requirement of having a fine detailed simulated environment and it also reduces the computational time as it considers fewer rays. As this model considers specific information about the environment it shows a time-invariant

behaviour which makes it attractive as claimed by [138]. Figure 2.6 illustrates the main ideas for the Motley-Keenan model, ray tracing model and DPM.

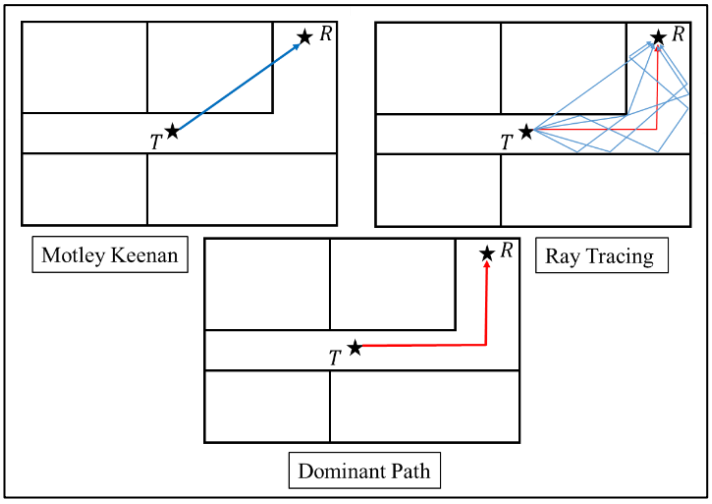

Figure 2.6: Empirical model, Ray tracing and DPM.

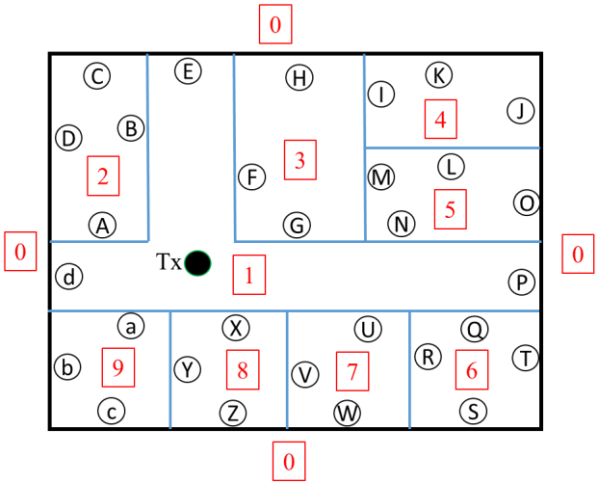

Figure 2.7: DPM determination of paths.

Signal prediction in DPM includes two main procedures: determination of propagation paths and calculation of signal strength [138, 139]. In the first stage rooms and walls in an indoor floorplan are termed as seen in Figure 2.7. Reflections and diffractions are not taken into consideration, rays passing the same room and transmitting same walls are represented by one dominant path.

For example for a transmitter (Tx) located in room 1, a signal can reach 2 (through A and B), 3 (through F and G), 5 (through N), 6 (through Q), 7 (through U), 8 (through X) and 9 (through a). This is represented in Figure 2.8 as seen in Tx-Layer 1. If we consider rays penetrating room 2, the only neighbour room is 1, then the path will be through B (walls are not allowed to be repeated in each root), and so on [140]. Finally, the dominant paths are chosen, depending on how many paths required the computation time will vary [108]. In DPM most selected paths are those with shortest distances, or have fewer interactions, or have fewer transmissions [108].

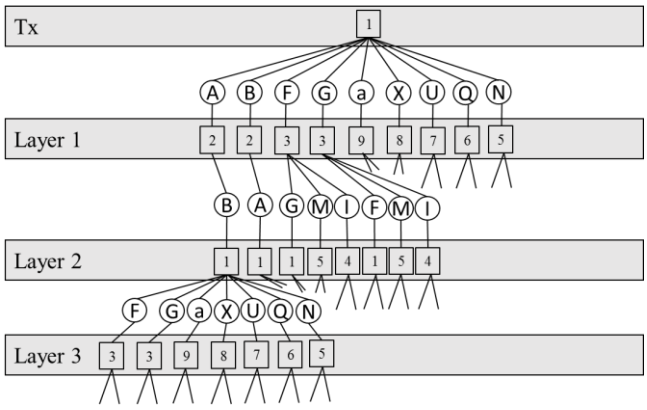

Figure 2.8: DPM path determination tree

The prediction of signal strength is accomplished either using empirical regression measurements [140] or neural network [139]. The input parameters for the neural network includes transmission loss, waveguiding effect, free space loss at distance l, and total bent angle [139]. Minimum losses for DPM are computed as in Equation 2.24 [139]:

$$L = L_{FS} + \sum_{i=1}^{k} WL_j + \sum_{j=1}^{p} w_I \tag{2.24}$$

where L_{FS} is the free space loss, *WL* is cumulated wall losses, and w_I is interaction loss which depends on the type of wall, operating frequency, and the angle of bend made by the propagation.

Table 2-9 shows a performance comparison between different models. The table shows the standard deviation for the prediction models compared to measurements [108]. As shown, the DPM shows better performance compared to other prediction models. In [128], IRT was compared to DPM; although both methods share the property of fast processing, in terms of prediction accuracy the former shows less accurate results in the case where the receiver is far away from the transmitter.

Table 2-9: Performance comparison between signal strength prediction models [108].

	Ray tracing	DPM	Motley-Keenan
Transmitter 1	12.11 dB	5.85 dB	11.39 dB
Transmitter 2	7.23 dB	6.36 dB	9.83 dB
Transmitter 3	9.76 dB	5.64 dB	6.04 dB
Transmitter 4	6.04 dB	5.12 dB	5.82 dB

2.7 Effects of building's materials

Reflected and transmitted rays are estimated through solving Fresnel coefficients; however, those coefficients are functions of many parameters including complex permittivity; therefore the type of material used in constructing the building has a significant impact on wireless channel in the indoor environment. Material dependency on operating frequency plays a major role in determining radio coverage, as shown in Equation 2.25 the attenuation rate A

(dB/m) is a function of conductivity σ, relative permittivity ε_r and operating frequency f [141].

$$A = \begin{cases} 1636\dfrac{\sigma}{\sqrt{\varepsilon_r}} & Dielectric \\ 545.8\sqrt{\sigma f_{GHz}} & Conductor \end{cases} \quad (2.25)$$

Complex permittivity is a function of ϵ_r, σ and frequency [142]:

$$\epsilon_c = \epsilon_0\epsilon_r - j\frac{\sigma}{\omega} \quad (2.26)$$

In [141] a relationship between complex permittivity parameters and operating frequency was formulated as shown in Equation 2.27 and 2.28.

$$\sigma = \alpha f_{GHz}^{\beta}\ S/m \quad (2.27)$$

$$\epsilon_r = \rho f_{GHz}^{\gamma} \quad (2.28)$$

Typical values of α, β and ρ for different types of materials are given in Table 2-10, while γ =-0.1, -0.4 for medium dry and wet grounds respectively but zero elsewhere [141].

Table 2-10: Material frequency dependent parameters [141].

Material	(ρ)	(α)	(β)	Frequency (GHz)
Vacuum	1	0	0	0.001-100
Concrete	5.31	0.03265	0.809	1-100
Brick	3.75	0.038	0	1-10
Plasterboard	2.94	0.0116	0.7076	1-100
Wood	1.99	0.0047	1.0718	0.001-100
Glass	6.27	0.0043	1.1925	0.1-100
Ceiling board	1.5	0.0005	1.1634	1-100

Chipboard	2.58	0.0217	0.78	1-100
Floorboard	3.66	0.0044	1.3515	50-100
Metal	1	10^7	0	1-100
Very dry ground	3	0.0015	2.52	1-10
Medium dry ground	15	0.035	1.63	1-10

A comprehensive review on material properties and their relationship with frequency was presented in [143], the values presented in Table 2-11 are for specific frequencies and measurements conditions, comments on these values are illustrated in the table [143]:

Table 2-11: A summary of material properties presented in [143].

Material	ε_r	σ	Freq. (GHz)	Thickness (m)	Notes
Brick	4.62	0.0174	1.7	-	-
	3.7-4	0.0200	3	0.015-0.0215	0% water volume
	3.7-4	0.0600	9	0.015-0.0215	0% water volume
	3.7-4	0.8	24	0.015-0.0215	0% water volume
	19	0.2917	3	0.015-0.0215	30% water volume
	14	1.1875	9	0.015-0.0215	30% water volume
	4.11	0.0364	18	-	-
Concrete	7	0.0150	0.9	-	Reinforced Concrete
	7	0.0300	1.8	-	Reinforced Concrete
	2	0.0278	1	-	Aerated
	8	0.0833	3	0.02	Water/cement ratio (w/c) 22%

	10	0.0833	3	0.0195	w/c 28%
	7	0.1250	3	0.021	w/c 32.5%
	6	0.1667	3	0.2	w/c 40%
	7	0.2453	9	0.0195	w/c 28%
	6.5	0.2830	9	0.021	w/c 32.5%
	6.5	0.1887	9	0.189	w/c 34%
	6	1.3333	24	0.0195	w/c 28%
	5.5	2.3693	24	0.021	w/c 32.5%
	6.5	1.3333	24	0.189	w/c 34%
	6.2	1.8114	95.9	-	Hardened concrete
Wood	2.15	0.0038	1	0.005-0.03	Oven Dry wood p_0=0.7 g/cm^3
	1.95	0.0479	10	0.005-0.03	Oven Dry wood p_0=0.7 g/cm^3
	2.5	0.2867	60	0.005-0.03	Oven Dry wood p_0=0.7 g/cm^3
	1.9	0.2639	100	0.005-0.03	Oven Dry wood p_0=0.7 g/cm^3

A set of measurements was conducted to explore the relationship between the dielectric constant of building materials and frequency [144]. The investigated materials included wallboard, cloth office partition, structural wood, wooden door, plywood, glass, Styrofoam, bricks and concrete blocks. Detailed dimensions and specifications for the materials are given in [144].

Wallboard was tested over the range 0.62-13.92 GHz, its ε_r has almost no dependence on frequency, this was also observed for structural wood which was tested over the range 0.81-14.11 GHz, Styrofoam over the range 0.52-0.13.82 GHz and concrete blocks over the range of 2.02-6.82 GHz. Cloth partition walls were examined over the range 0.52-13.82 GHz and it was found that ε_r tended to decrease slightly with frequency within the range 1.36-1.07. Similar behaviour

was recorded for a wooden door which was examined over the range 1.01-14.31 GHz and plywood over the range 2-14.6 GHz where their corresponding ε_r were in the ranges 2.08-1.98 and 2.55-2.35 respectively.

On the other hand, some material tend to have larger ε_r as frequency increases, as in the case of glass and bricks. Glass was tested over 1.01-14.31 GHz and bricks over the range 1.01-7.01 GHz their corresponding ε_r are 6.35-6.71 and 3.73-4.48 respectively. Figure 2.9 summarises the dielectric relationship with frequency for measurements recorded in [144].

In [145], the authors aimed to measure the reflection coefficient for different material types over the X band (8-12.5 GHz), the investigated materials include Polyvinyl chloride (PVC), Beechwood, Sipo, plaster, plaster with silica, mortar and concrete with different water to cement ratios. The materials were assumed to be homogenous, dry and at room temperature. Mortar is different from concrete as it is made from small grains of sand where the maximum diameter for the grain is 4 mm, while the maximum diameter for concrete is 16 mm. Table 2-12 gives the mean values for complex permittivity.

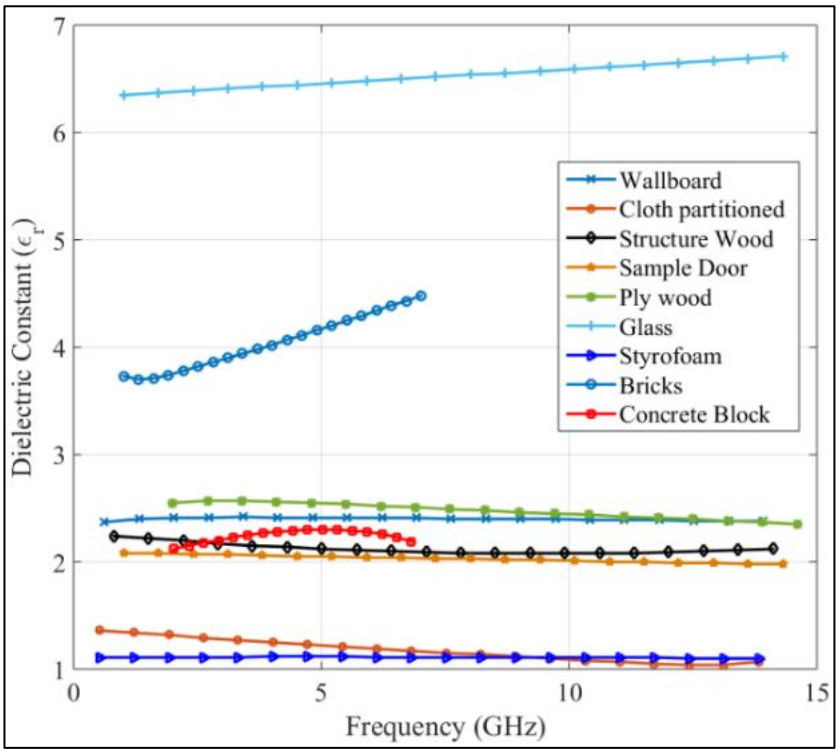

Figure 2.9: Dielectric constant with frequency for measurements collected in [144].

Table 2-12: Mean complex permittivity for investigated materials [145].

Material	Complex Permittivity
PVC	4.34-j0.028
Beechwood (*S*)	3.81-j0.2
Beechwood (*P*)	4.54-j0.23
Sipo	3.7-j0.17
Plaster	5.74-j0.06
Plaster (80%) and Silica (20%)	4.33-j0.095
Mortar	7.1-j0.27
Concrete (water/cement=0.5)	7.7-j0.33
Concrete (water/cement=0.7)	6.9-j0.4

Where *S* and *P* respectively refer to parallel and perpendicular polarization of the electric field to the wood fibre. Figure 2.10 shows the real part of the complex permittivity with frequency for the tested materials [145]. As seen in the figure,

material permittivity behaviour with respect to frequency is not straightforward; however the general behaviour can be observed, regarding plaster with silica and Beechwood showed a slight trend for ε_r to increase with frequency, while the average value for other material remains the same especially in the 9-12.5 GHz band. Due to greater porosity for concrete 0.7 the real part of its permittivity is less than that for concrete 0.5.

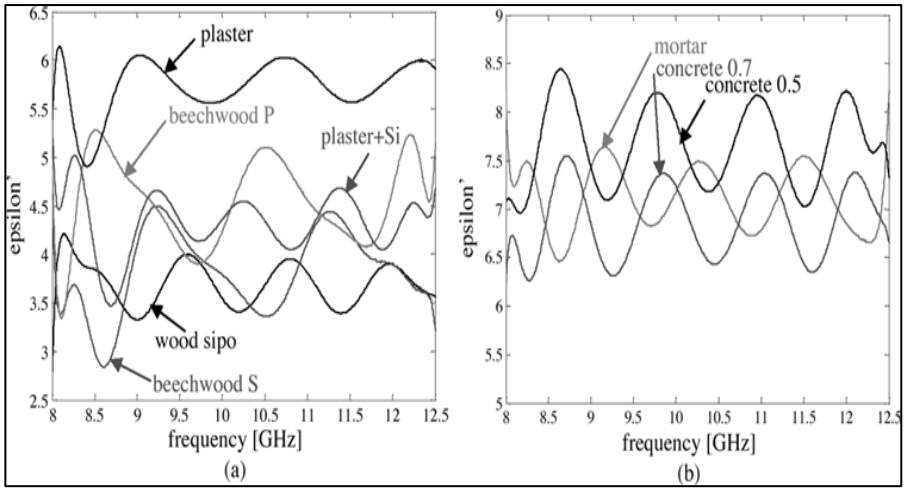

Figure 2.10: Real part of permittivity relationship with frequency [145].

In [146] measurements were conducted at 2.4 GHz to study the permittivity for stone, concrete and glass walls. The average results were 5.4 for the concrete, 2.3 for the glass while for indoor and outdoor stone walls the permittivity recorded were 4.5 and 7.9 respectively. The difference between the permittivities of indoor and outdoor stone walls is due to differences in the percentage of wall moisture [146]. Values of glass permittivity given by [146, 147] differ significantly, depending on the types of glass used in the experiments.

2.8 Propagation through buildings

Since most cell phones spend most of the time inside buildings, the received service level inside should be above the receiver threshold level. Therefore, building penetration loss should be taken into account [55]. Building penetration loss (BPL) depends on the environment, antenna heights, LOS/NLOS propagation, operating frequency, angle of incidence and on material type [148].

2.8.1 COST231 Building Penetration Studies

Extensive sets of measurements were developed by the European COST "**Co**-operation in the field of **S**cientific and **T**echnical research" program 231 to study outdoor to indoor propagation models. The measurements being conducted in the range of 900-1800 MHz, valid for 500 m distance between the base station and the building of interest where the base station height is less than 30 meters [55, 96].

In the case of LOS propagation, the total path loss L_T between two isotropic antennas is given by Equation 2.29 where one is located outside the building and the other is located inside as shown in Figure 2.11 [55]. The total loss can be considered in three categories: outdoor loss L_{out}, penetration loss L_{pen} and indoor loss L_{in}.

$$L_T = L_{out} + L_{pen} + L_{in} \tag{2.29}$$

Where:

$$L_{out} = L_{FS} \tag{2.30}$$

$$L_{pen} = L_e + L_g(1 - \cos\theta)^2 \tag{2.31}$$

$$L_{in} = \max(n_w L_i\,, \alpha(d_i - 2)(1 - \cos\theta)) \tag{2.32}$$

where θ is the angle of incidence which is given by $\cos^{-1}(D/d)$, L_{FS} is free space path loss for path $(d_i + d)$, L_e is the external wall loss at $\theta = 0^0$, L_g is the additional external loss at $\theta = 90^0$, n_w is the number of walls, L_i is the internal wall loss, d_i' is the unobstructed path and α is the d_i' specific attenuation (dB/m). Typical values for parameters in Equations 2.29-2.32 are given in Table 2-13.

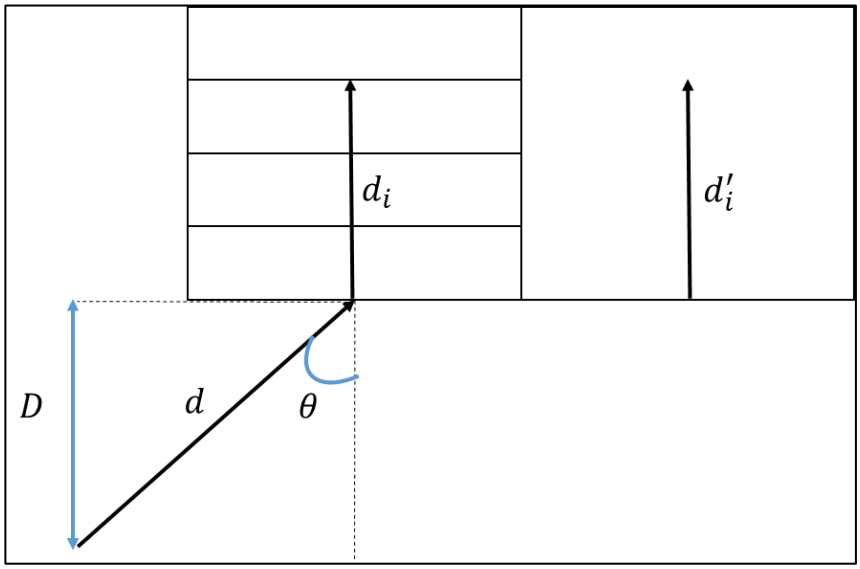

Figure 2.11: COST 231 LOS BPL model.

Table 2-13: Typical values for $(L_e, L_g, L_{in} \& \alpha)$ [55]:

Parameter	Material	Loss value
L_e/L_{in}	Concrete Wall	7 dB
	Wood/Plaster Wall	4 dB
L_g	Concrete Wall	20 dB
α	-	0.6 dB/m

Concrete walls can increase the losses to the range of 10-20 dB in the case where walls are without windows. Walls with larger window sizes tend to have less loss, while metalized windows tend to have larger loss [55].

In the case of NLOS propagation, the COST 231 model relates the penetration loss to an outer reference on the side of the nearest wall of interest at a height of 2 m [55].

$$L_{out} = L_{FS} \tag{2.33}$$

$$L_{pen} = L_e + L_{ge} - G_{FH} \tag{2.34}$$

$$L_{in} = \max(n_w L_i\,, \alpha d_i) \tag{2.35}$$

Given that:

$$G_{FH} = n \cdot G_n \text{ or } h \cdot G_h \tag{2.36}$$

where L_{ge}, n, G_n, h and G_h are tuning correction factor for L_e [96], floor number, floor height gain (dB/floor), height above the outdoor reference and height gain (dB/m). Typical values for parameters in Equations 2.34 and 2.36 are given in Table 2-14.

Table 2-14: Typical values for COST231 model parameters [55].

Parameter	Loss	Comments
L_{ge}	3-5	900 MHz
	5-7	1800 MHz
	7-8	2100 MHz [149]
G_n	1.5-2	900/1800 MHz, building height below 4-5 m
	4-7	900/1800 MHz, building height above 4-5 m
G_h	1.1-1.6	1800 MHz, building height above 4-5 m

2.8.2 Extensions to COST231 Model

In [150] experiments were performed in 71 floors within 17 buildings of two types (office buildings and multi-storey car park). A wide range of frequencies was

investigated (0.8, 2.2, 4.7 and 8.45 GHz). L_{pen} is defined as the difference between the indoor losses and outdoor losses as given by Equation 2.37 [150]:

$$L_{pen} = L_{in} - L_{out} = \alpha d - G_h h + \alpha_{LOS} k + \alpha_f \log f + W \quad (2.37)$$

where $\alpha, d, h, k, \alpha_{LOS}, \alpha_f$ and W are penetration distance coefficient, building penetration distance, floor height, LOS constant, LOS coefficient, frequency coefficient and constant loss respectively. Typical values for Equation 2.37 parameters are given in Table 2-15 [150].

Table 2-15: Typical values for the proposed BPL parameters.

Parameter	Value
d	0-20 m
α	0.6 dB/m
G_h	0.6 dB/m
h	1.5-30 m
α_{LOS}	-0.8 and -3.9
α_f	-1.1
k	1: LOS 0: NLOS
W	10 dB

It was also observed that α increases slightly as frequency increases; while no dependence on distance between the base station and the building.

In [151], authors proposed a modification to COST 231 LOS model as the latter assumes the penetration through walls without considering the effect of windows and doors existence, the proposed model assumes the dominant rays are those

propagate through wall openings, doors and windows. The model also includes the effect of angle's dependency on penetration losses, L_{in} and L_{pen} are updated to [151]:

$$L_{in} = \alpha d_1 \tag{2.38}$$

$$L_{pen} = L_e + L_g(1 - \cos\theta')^2 + f(\varphi) \tag{2.39}$$

where d_1 is the distance between the door and the receiver, θ' is the angle of incidence at the door and $f(\varphi)$ is the angular dependency factor (φ is the angle between the refracted ray and the receiver). $f(\varphi)$ is found to be close to $(L_g \cdot \sin\varphi)$.

COST 231 Walfisch-Ikegami Model:

In [152] a modification of the COST 231 was proposed for LOS conditions, the free space loss factor in Equation 2.30 was replaced by a LOS COST 231 Walfisch-Ikegami mode:

$$L_{out} = 42.6 + 26\log(D) + 20\log(f) \tag{2.40}$$

where D is in km and f in MHz. The Walfisch-Ikegami model is valid over the frequency range of 0.8-2 GHz, and over distances from 0.02 to 5 km and for base station heights 4-50 m [55]. The other modification is a simplification for the indoor loss term which is replaced by Equation 2.41 [153] provided that there is one internal wall per ten meters. This modification reduces the requirement for detailed knowledge of the position of the mobile station [154]. The model is

claimed to have better performance compared to the original COST 231 model [154].

$$L_{in} = \alpha \cdot d_i \tag{2.41}$$

WINNER II Model:

Another modification to the COST 231 on the NLOS propagation is the WINNER II (Wireless World Initiative New Radio) [106]. In this, the receiver antenna heights are around 1-2 metre in addition to the floor height. The receiver building is up to 3 floors, the model is valid over the range of frequencies 2-6 GHz.

The first model termed as "*WINNER II B4 model*" considers propagation through an urban microcell environment. The base station is 10 m on top of surrounding buildings, and distance range 3-1000 m between the transmitter and receiver.

$$L_{out} = \max\left(41 + 22.7\log_{10}(D + d_i) + 20\log_{10}\frac{f}{5}, L_{FS}\right) \tag{2.42}$$

$$L_{pen} = 14 + 15(1 - \cos\theta)^2 \tag{2.43}$$

$$L_{in} = 0.5d_i \tag{2.44}$$

where f is the operating frequency in GHz [155].

The other model is for the urban macro propagation case: this model is termed the "*WINNER II C4 model*". The base station is 25 m on top of surrounding buildings, and distance range 50-5000 m between the transmitter and receiver were considered.

$$L_{out} = (44.9 - 6.55\log_{10} h_b)\log_{10}(D + d_i) + 20\log_{10}\frac{f}{5} + 5.83\log_{10} h_b + 26.46 \quad (2.45)$$

$$L_{tw} = 17.4 + 0.8h \quad (2.46)$$

$$L_{in} = 0.5d_i \quad (2.47)$$

where f is in GHz, h_b is the base station height. It should be noted that the WINNER II models are applicable only when the mobile station is above ground level, (i.e. they do not apply for negative mobile heights) [155].

2.8.3 Building Penetration Loss (BPL)

In the literature, information about the relationship between BPL and frequency are rather conflicting, while some researchers stated that BPL increases as frequency increases [156] [157] [158] [159] [160] [161] [162] [163] [164] [165], another group claimed the opposite [166] [167] [168] [78] [149] [169]. A third group claimed that either no frequency dependency exists or there is an irregular frequency dependency [170] [150]. Figure 2.12 and Figure 2.13 show a literature summary on BPL dependence on frequency.

Measurements in [150] show interesting observations, using the same set of frequencies and equipment, losses for some material are increasing with frequency, while for other materials don't as shown in Figure 2.14, this may give an explanation for the conflicting results in the literature.

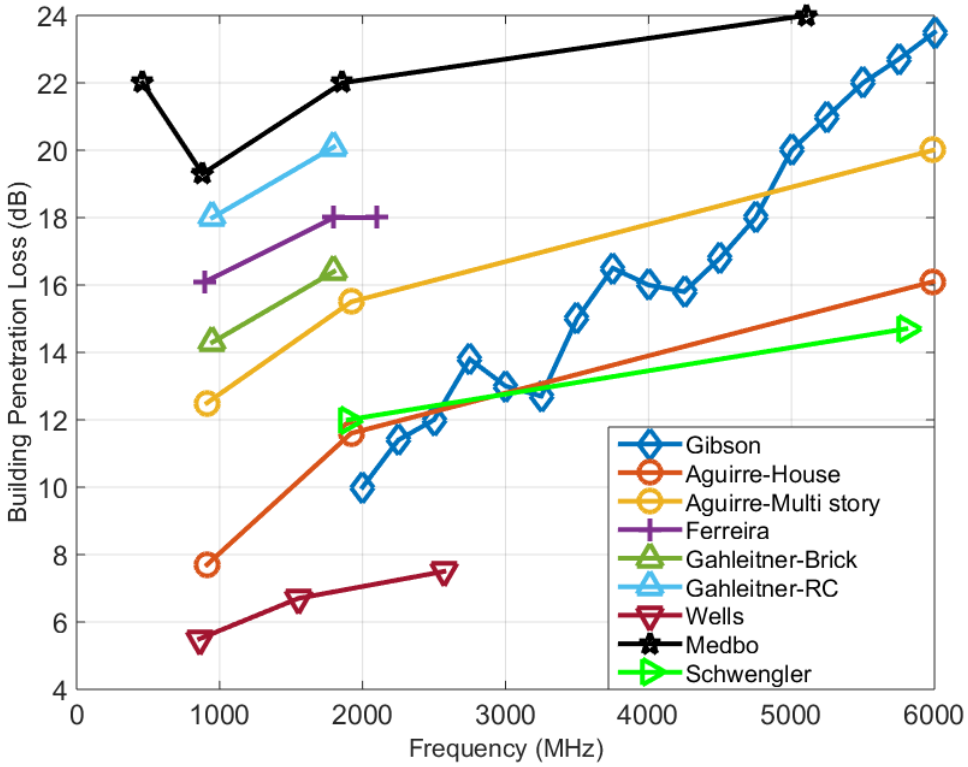

Figure 2.12: BPL increase with increasing frequency.

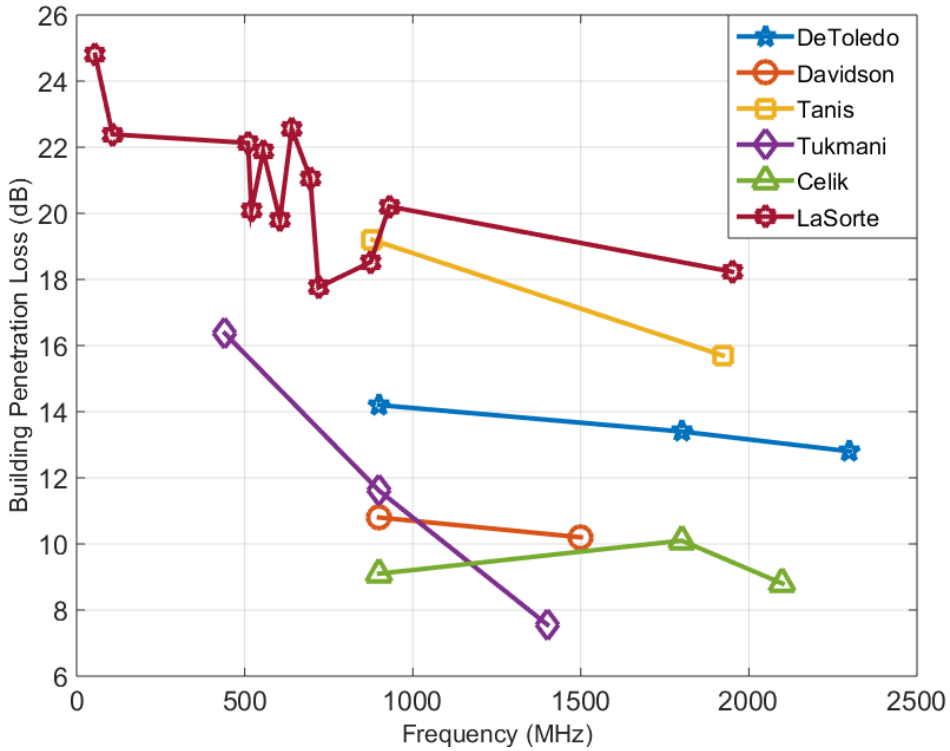

Figure 2.13: BPL decrease with increasing frequency.

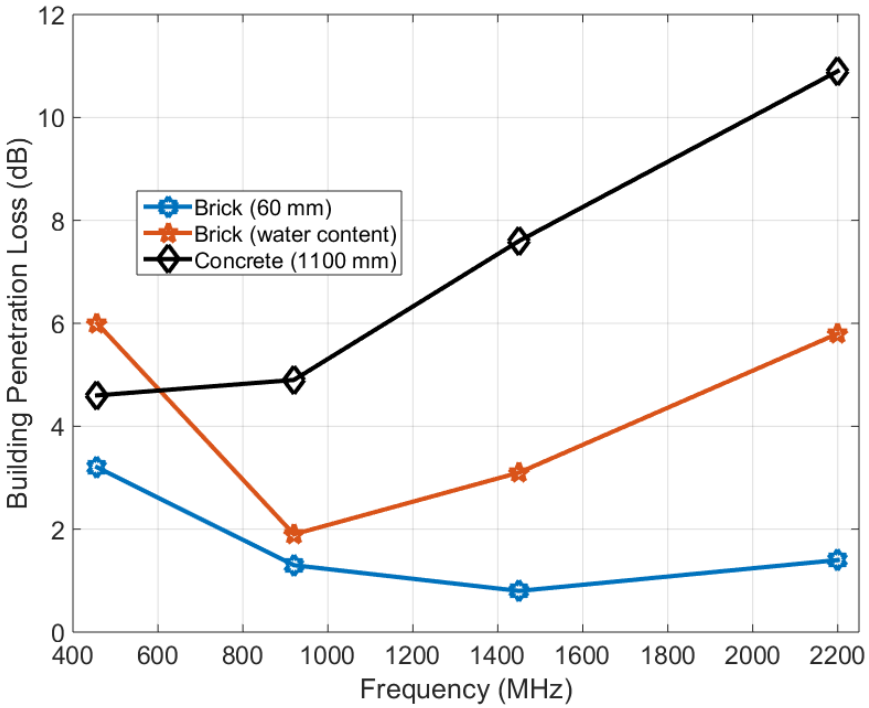

Figure 2.14: BPL behaviour with frequency for different types of buildings.

It was observed in [150] that BPL has no clear dependence on frequency, among the applied frequencies, BPL was around (10 dB and 3 dB) for office buildings and multi-storey car park respectively. It was also observed that BPL increases proportionally as the distance between the mobile station and as the window of the outer wall increases.

In [171], the authors explored the effect of opening and closing the windows on BPL. Data were collected at distances from 0.2 to 5 m away from the wall at 1800 MHz, over this range, BPL difference between opened and closed window cases were almost the same at around 11 dB. BPL tended to increase as signals travelled deeper into the building, and decreases when observed on higher floors in the building [158]. A study on satellite-indoor services over the band from 2 to 6.5 GHz concluded that BPL increases monotonically as the elevation angle

increases in both LOS and NLOS cases [172], similar results were also obtained by [173, 174]. BPL was found to be larger as the incidence angle increased towards grazing incidence [148].

Chee et al [175] conducted measurements at 800 and 3500 MHz for seven residential buildings. The BPL observed showed no frequency dependence, in the case of walls with windows measurements, showed that a 5-6 dB reduction in the BPL value was observed compared to the case of walls without windows.

In summary, for most studies BPL tend to increase as frequency increases and as the angle of incidence increased and tend to decrease as moving up in the floors and if walls have more windows.

Chapter 3

Indoor Localization Techniques

3.1 Introduction

Indoor localization is applied widely in many environments including hospitals, airports, train stations and even households [176]. Patient's movements in hospitals could be tracked to provide quick assist when needed. In cases of evacuations firefighters locations could be identified, such that if anyone suffered suffocation and fell down or was trapped, he could be located and rescued [177]. In households kids' location inside the house can be inferred, elders who are taking healthcare services at homes can be tracked and monitored to give quick assessment once needed.

WLAN and Radio-Frequency Identification RFID systems can be utilized for localization purposes by using the inferred channel parameters, these parameters include power level of arrival paths, paths' arrival time, angle of arrivals and departures [178].

Localization technique procedure includes having geographic information of the tested area and computation targets' location according to collected data. The choice and design of the localization algorithm is made depending on availability of resources and the required level of accuracy [179], in this chapter indoor localization using Received Signal Strength (RSS), Time of Arrival (TOA) and Angle of Arrival (AOA) are introduced as shown in Figure 3.1.

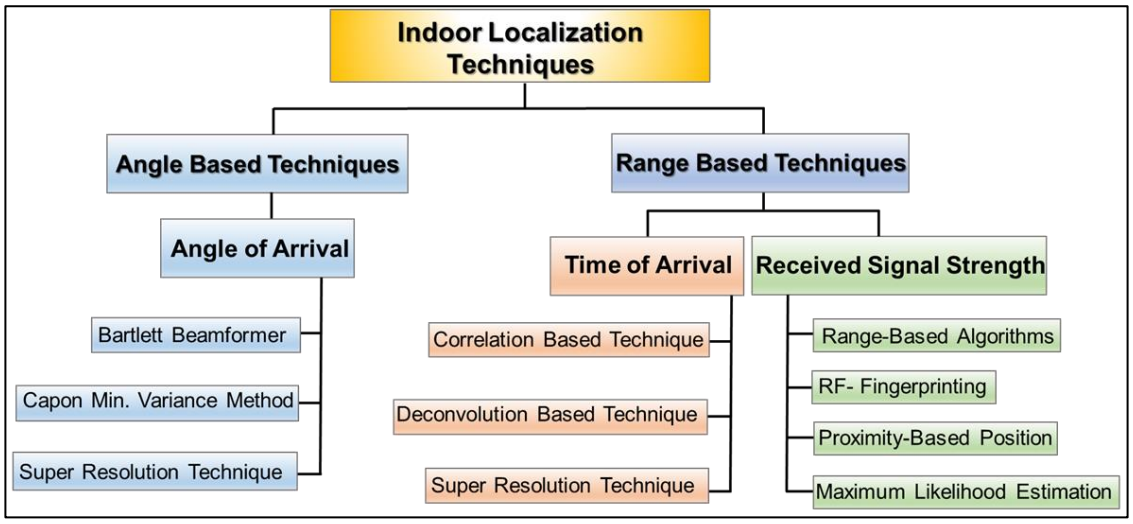

Figure 3.1: Indoor Positioning Techniques.

3.2 Received Signal Strength

3.2.1 Introduction

The idea behind localization using RSS is to establish a one to one relationship between the target location and its RSS [180]. RSS level decreases with the distance between transmitter and receiver (known as the decay law of RSS with distance). However, RSS-distance relationship is not necessarily to be linear especially in indoor environments due to the effect of multipath [4]. Moreover, since 50% of the human body is water, people movement cause fluctuations of RSS with time which reduce localization accuracy [181-183].

RSS measuring requires only power detectors which are available in WLAN, UWB, Zigbee, Bluetooth and infrared devices. Utilizing WLAN for localization purposes is advantageous due to its continuous monitoring, low cost and its capability of working unattended for years [184, 185]; however this may introduce interference problems with other devices works on the same frequency bands such as microwave ovens and Bluetooth devices, thus, the probability of error

may increase although by using different channels the correlation becomes trivial. [4]

RSS systems do not rely on timing information, this makes them more robust to multipath. Moreover, synchronization between devices is not required [186]. RSS localization systems excel in short range distances, however, it provides lower accuracy in long-range distances comparing to TOA systems which are favourable for outdoor applications [187].

On the other hand, training and complex matching algorithms are needed to perform localization [188]. Moreover, RSS is sensitive to shadowing, low signal to noise ratio (SNR), and NLOS propagation.

3.2.2 RSS-Based Localization Algorithms

Many RSS-based localization algorithms are presented in literature including range based position, radio frequency fingerprinting technique, proximity-based position and probabilistic estimation [15], a brief discussion on these algorithms are introduced in the following subsections.

3.2.2.1 Range based position

Localization using range-based technique includes two steps: *ranging* and *lateration* [189], in the first step a distance-power relationship is formulated depending on the observed RSS values, in the latter step mobile's location is inferred based on the distances obtained using *least square techniques.* Using this type of localization is preferred due to its ease; however, it suffers from varying RSS measurements [190].

RSS values vary in a random manner within indoor environments. As the Tx-Rx distance increases, the SS level does not follow a monotonic decrease. Figure 3.2 shows the relationship between RSS and Tx-Rx distance along a building hallway.

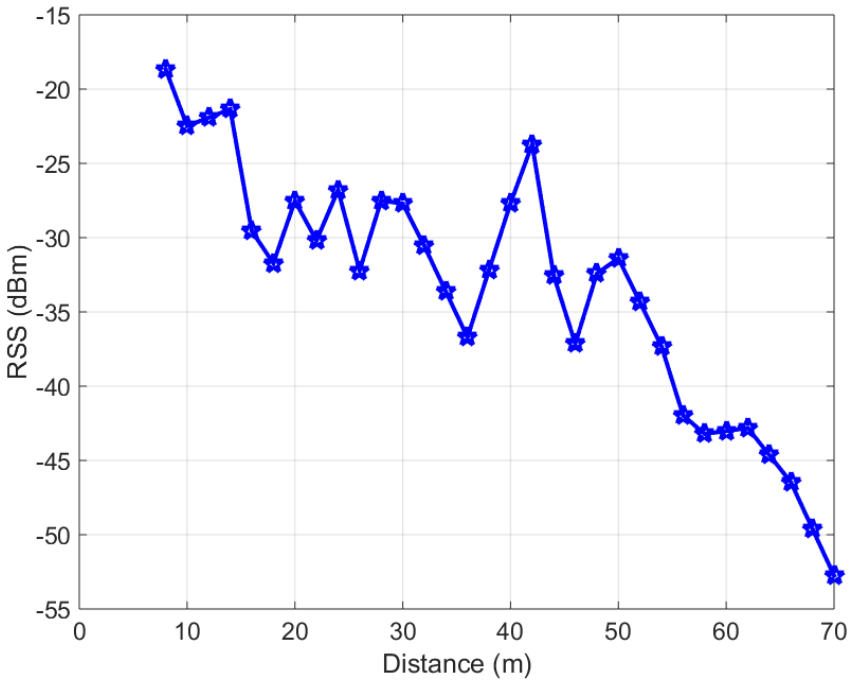

Figure 3.2 Attenuation of RSS within a hallway

The figure shows a nonlinear relationship between RSS and Tx-Rx distance, this nonlinearity arises due to fading effect. At any receiver point, the received power is the transmitted power from transmitter minus losses; those losses are due to distance (the area mean propagation loss), shadowing (local mean propagation loss) and multipath (fast fading). In indoor environments access points (AP) locations tend to be known while mobile's location is unknown. For AP located at known location (x_i, y_i) and a mobile located at unknown location (x, y), the received power at the mobile is given by Equation 3.1 [15, 191]:

$$P(d_i) = P_t - \overline{PL}(d_0) - 10n \log_{10}\left(\frac{d_i}{d_0}\right) + \chi_\sigma \quad (3.1)$$

where d_i is the distance between i^{th} AP and the mobile, P_t is the transmitted power, $\overline{PL}(d_0)$ is the average path loss at reference distance (usually 1 m) and χ_σ is a Gaussian random variable with zero mean represents shadow fading. Equation 3.1 can be rewritten as:

$$P(d_i) = P_0 - 10n \log_{10}\left(\frac{d_i}{d_0}\right) + \chi_\sigma \quad (3.2)$$

where $(P_0 = P_t + \overline{PL}(d_0))$ is the received power at the reference distance calculated experimentally or by applying Equation 3.3:

$$P_0 = P_t \left(\frac{\lambda}{4\pi d_0}\right)^2 \quad (3.3)$$

Solving Equation 3.2 for d_i gives the distance between AP and the mobile:

$$d_i = d_0 \left[10^{\frac{P(d_i) - P_0 + \chi_\sigma}{10}}\right]^{\frac{-1}{n}} \quad (3.4)$$

For an omnidirectional antenna, mobile possible locations may lie on a circle, mobile coordinates are the solution of the circle equation shown below:

$$d_i{}^2 = (x - x_i)^2 + (y - y_i)^2 \quad (3.5)$$

Provided that d_i value is given by applying Equation 3.4.

Since d_i and (x_i, y_i) are known, the remaining unknowns are (x, y), which needs at least another equation to be solved; however with two equations there will be two possible solutions, in order to have a unique solution three equations are required, the intersection of these equations will determine the location of the

mobile as shown in Figure 3.3, if the problem is in 3D (x, y, z) then four APs are used at least to have unique solution [192].

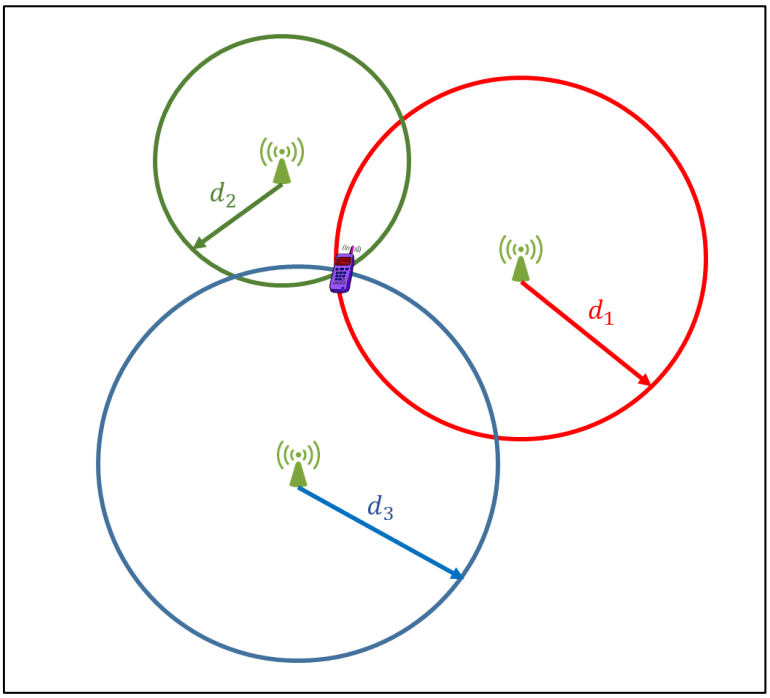

Figure 3.3 Trilateration localization using RSS

Estimation of environmental parameters χ_σ and n is accomplished by taking a training data (SS collected from known locations), by fitting these data into a model using *linear regression* the unknown parameters are estimated [193].

Least Square Technique

Due to the effect of noise and NLOS the exact solution for a mobile's location may not exist. In this case, least square methods are applied. These methods are categorized into *Non-linear least square* (NLS) and *linear least square* (LLS)[15]. The principle is as follows: the available information includes *known* parameters (x_i, y_i) and the *measured* parameter d_i. The target is to estimate the *unknown* location of the mobile (x, y). This is accomplished by searching for all possible

locations $(\hat{x}, \hat{y})$ such that the distance between this point and (x_i, y_i) is approaching d_i as much possible for all N APs, as shown in Equation 3.6 [15]:

$$(\hat{x}, \hat{y}) = \arg\min_{x,y} \sum_{i=1}^{N} \left[(x - x_i)^2 + (y - y_i)^2 - {d_i}^2 \right] \tag{3.6}$$

The above approach is the NLS method, which depends on its initial guess, therefore its required to perform several iterations in order to get better results; however, this requires huge computations. For a less computational cost LLS approach is performed; nevertheless less accurate results are obtained [15].

A possible way to perform linearization is by taking the mean of all APs measurements then perform a subtraction from each observation [15].

$$\frac{1}{N} \sum_{i=1}^{N} [(x - x_i)^2 + (y - y_i)^2] = \frac{1}{N} \sum_{i=1}^{N} {d_i}^2 \tag{3.7}$$

The K[th] AP measurement becomes:

$$\left[y_k - \frac{1}{N} \sum_{i=1}^{N} y_i \right] y + \left[x_k - \frac{1}{N} \sum_{i=1}^{N} x_i \right] x$$

$$= 0.5 \left(\left[{y_k}^2 - \frac{1}{N} \sum_{i=1}^{N} {y_i}^2 \right] + \left[{x_k}^2 - \frac{1}{N} \sum_{i=1}^{N} {x_i}^2 \right] - \left[{d_k}^2 - \frac{1}{N} \sum_{i=1}^{N} {d_i}^2 \right] \right) \tag{3.8}$$

For all N-APs, a matrix can be represented as ($\boldsymbol{Az} = \boldsymbol{b}$) where ($\boldsymbol{z} = \begin{bmatrix} y \\ x \end{bmatrix}$)

$$\boldsymbol{A} = \begin{pmatrix} y_1 - \frac{1}{N} \sum_{i=1}^{N} y_i & x_1 - \frac{1}{N} \sum_{i=1}^{N} x_i \\ \vdots & \\ y_N - \frac{1}{N} \sum_{i=1}^{N} y_i & x_N - \frac{1}{N} \sum_{i=1}^{N} x_i \end{pmatrix} \tag{3.9}$$

$$\boldsymbol{b} = \begin{pmatrix} 0.5\left(\left[{y_1}^2 - \frac{1}{N}\sum_{i=1}^{N}{y_i}^2\right] + \left[{x_1}^2 - \frac{1}{N}\sum_{i=1}^{N}{x_i}^2\right] - \left[{d_1}^2 - \frac{1}{N}\sum_{i=1}^{N}{d_i}^2\right]\right) \\ \vdots \\ 0.5\left(\left[{y_N}^2 - \frac{1}{N}\sum_{i=1}^{N}{y_i}^2\right] + \left[{x_N}^2 - \frac{1}{N}\sum_{i=1}^{N}{x_i}^2\right] - \left[{d_N}^2 - \frac{1}{N}\sum_{i=1}^{N}{d_i}^2\right]\right) \end{pmatrix} \quad (3.10)$$

The mobile location can be estimated as:

$$\boldsymbol{z} = (\boldsymbol{A}^T\boldsymbol{A})^{-1}\boldsymbol{A}^T\boldsymbol{b} \quad (3.11)$$

Lateration is prone to outliers (when the estimated location is extremely far away from the actual one), in order to give robustness to the system, outliers measurements are excluded by taking the median value of the sum [194]:

$$(\hat{x}, \hat{y}) = \arg\min_{x,y} median_i \sum_{i=1}^{N} \left[(x - x_i)^2 + (y - y_i)^2 - {d_i}^2\right] \quad (3.12)$$

Differential RSS (DRSS)

Equation 3.2 can be expressed in normalized form as:

$$P_i = P(d_i) - P_0 = -10n\log_{10}\left(\frac{d_i}{d_0}\right) + \chi_\sigma \quad (3.13)$$

As can be seen from Equation 3.2 or 3.13 measurements accuracy depend on many parameters including the unknown transmitted power P_t, another problem is the fluctuation of RSS values with time. In order to remove the need for having a priori knowledge of P_t and to reduce effects of environmental changes, Differential RSS (DRSS) is adopted [195, 196].

$$P_{ij} = P_i - P_j = 10n\log_{10}\left(\frac{d_j}{d_i}\right) + \chi_{\sigma_{ij}} \quad (3.14)$$

where ($\chi_{\sigma_{ij}} = \chi_{\sigma_i} - \chi_{\sigma_j}$). P_i and P_j have a variance of σ^2, P_{ij} have a variance of $2\sigma^2$ [193].

Generally, if m APs are collaborating in localization there will be ($\frac{m(m-1)}{2}$) formulated DRSS equations, among these equations $(m-1)$ are basic equations, while the rest are redundant, the solution of each basic equation will lie on a hyperbola, the intersection of these hyperbolas gives the mobile's coordinates [197].

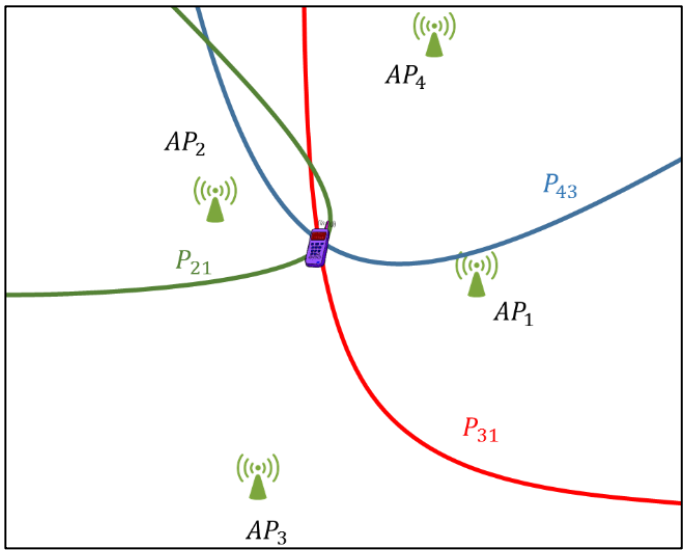

Figure 3.4 Hyperbolic localization using DRSS.

For example, using 3 APs system, there will be 2 basic equations (P_{21} and P_{31}) while (P_{32}) is a linear combination of (P_{21} and P_{31}), in order to have a unique solution three basic equations are required which is achieved by adding another AP in Figure 3.4. The generated basic equations are (P_{21}, P_{31} and P_{43}), while (P_{41} and P_{42}) are a linear combination of the basic function ($P_{43} - P_{31}, P_{43} - P_{32}$) respectively.

Although this method reduces dependence on knowing the value of P_t, it has poor performance in indoor environments compared to RSS [196].

3.2.2.2 Radio-Frequency Fingerprinting

Constructing a signal propagation model can be a very challenging task due to complexities of indoor environments, rather than modelling RSS behaviour another approach can be used known as Radio Frequency-fingerprinting technique [185, 198, 199].

RF–fingerprinting consists of two phases; the offline phase and the online phase. In the offline phase (Training phase) the area of interest is divided into grids, in each grid, many RSS are collected from surrounding APs and averaged to remove the fast fading effect, averaged RSS with corresponding location (also called *reference points* RP) are stored in a database known as *Radio map* [200].

In Online phase (Real-time phase) RSS measurements are collected from unknown locations called *test point*s (TP), these measurements are then compared with the database built in the offline phase. One possible method is to estimate the smallest Euclidean distance between the test point measurements and the radio map subspace [201]. The RP with corresponding smallest Euclidean distance represents the closest location to TP [200] as shown in Equation 3.15.

$$\arg\min_{RP(k)} \sqrt{\sum_{l=1}^{L}(TP_l - RP(k)_l)^2} \;\; \forall \, \mathrm{k} = 1{:}\,\mathrm{K} \tag{3.15}$$

where k is the k^{th} RP. Other methods return the k-nearest locations which has the lowest values of Equation 3.15 [202].

The level of achieved accuracy depends heavily on how many APs and RPs used. Adding more APs will reduce the possibility of having ambiguous results and tend to enhance the localization process. Adding more RPs will enhance resolution; however, this will cost more labour work. Another disadvantage of this approach is the need for regular updates for the radio map as the building layout or the number of operating APs may be changed [15, 203]. Figure 3.5 shows the distribution of APs, RPs and TPs.

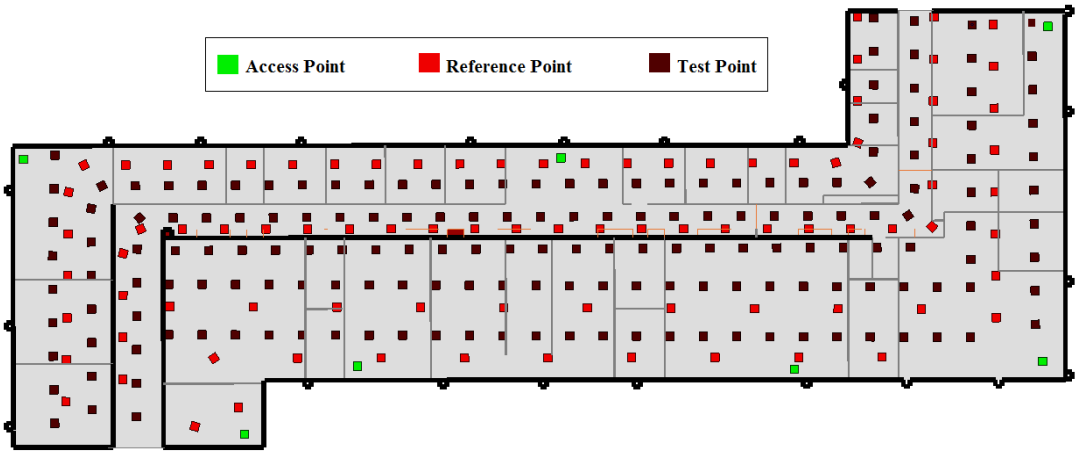

Figure 3.5: RF-fingerprinting approach

3.2.2.3 ***Proximity-based position (Free Range Localization)***

Proximity measurements (relative positioning) have been suggested as a cheap and simple mean to estimate the range between mobile and AP location.

In contrast to range-based localization which suffers from the fading differences in the propagation channel, proximity approach does not matter if the mobile and the AP are exposed to same fading channel or not, as long as they are within communication range [204].

The location for the mobile is estimated using the coordinates of the AP. Proximity approach is simple and widely used, however, accuracy is limited to AP radio coverage [205].

3.2.2.4 Maximum Likelihood Estimation

In this method RSS behaviour is modelled as a random variable, two stages are performed similar to RF-Fingerprinting approach. In the first stage SS measurements are collected from the area of interest, these data are processed to give a probabilistic distribution for the SS behaviour in each location, in the second stage mobile's RSS from surrounding APs are collected from unknown location and stored in vector and then mobile's location is inferred based on Maximum Likelihood Estimation (MLE) as shown in Equation 3.16 [206]:

$$(\hat{x}, \hat{y}) = \arg\max_{L_j} \left(P\left(L_j | \boldsymbol{ss}\right) \right) \tag{3.16}$$

where $P\left(L_j | \boldsymbol{ss}\right)$ is the probability that the mobile is located at location L_j given that the RSS vector is ($\boldsymbol{ss}$).

In the first stage, the study area is divided into grids, in each grid, the signal strength is measured from each AP extensively. If we assume a 4-grids environment with one AP, where many measurements were taken in each. At each grid the probability distribution of RSS from AP-1 $P\left(ss^j\right)$ will follow certain behaviour as seen in Figure 3.6. This distribution also can be considered as the probability of having ss at grid j ($P\left(ss | L_j\right)$).

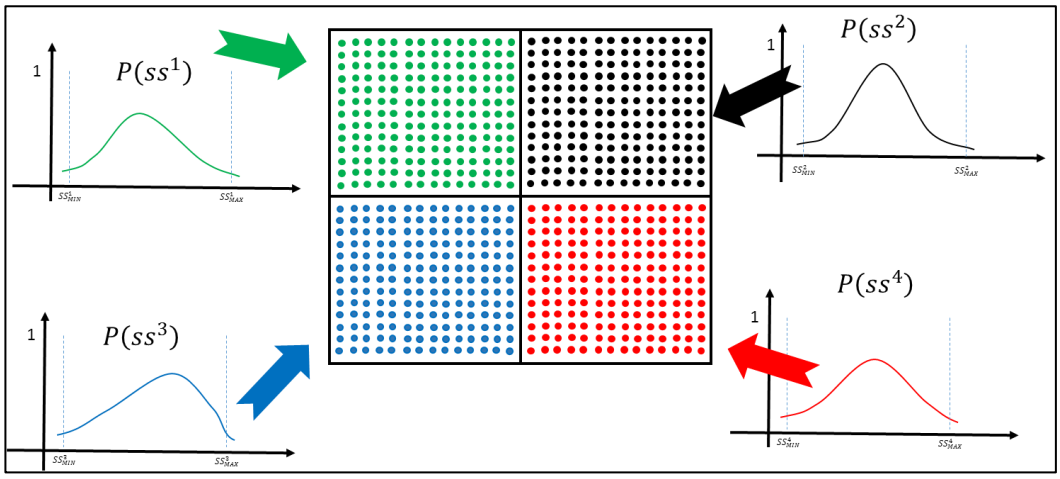

Figure 3.6: Example of MLE RSS positioning methodology.

$$P(ss^j) = P(ss|L_j) \tag{3.17}$$

where j=1:4.

The probability for RSS from AP-1 in all grids will be:

$$P(ss) = \frac{1}{4}\sum_{j=1}^{4} P(ss^j) \tag{3.18}$$

If we have M-APs then Equations 3.17 and 3.18 will be respectively:

$$P(\boldsymbol{ss}|L_j) = \prod_{i=1}^{M} P(ss_i|L_j) \tag{3.19}$$

$$P(\boldsymbol{ss}) = \prod_{i=1}^{M} P(ss_i) \tag{3.20}$$

In the localization stage, the question is given this level of RSS what is the probability for the mobile to be located in each grid? Or as shown in Equation 3.21 [206]:

$$P(L_j|\boldsymbol{ss}') = \frac{P(\boldsymbol{ss}'|L_j)P(L_j)}{P(\boldsymbol{ss})} \tag{3.21}$$

Since the location of the mobile is unknown, then the probability of each grid to be the location where the mobile locates is equal.

$$P(L_j) = \frac{1}{J} \tag{3.22}$$

The algorithm shows precise analysis of the given data; however, it suffers from extensive labour work [15].

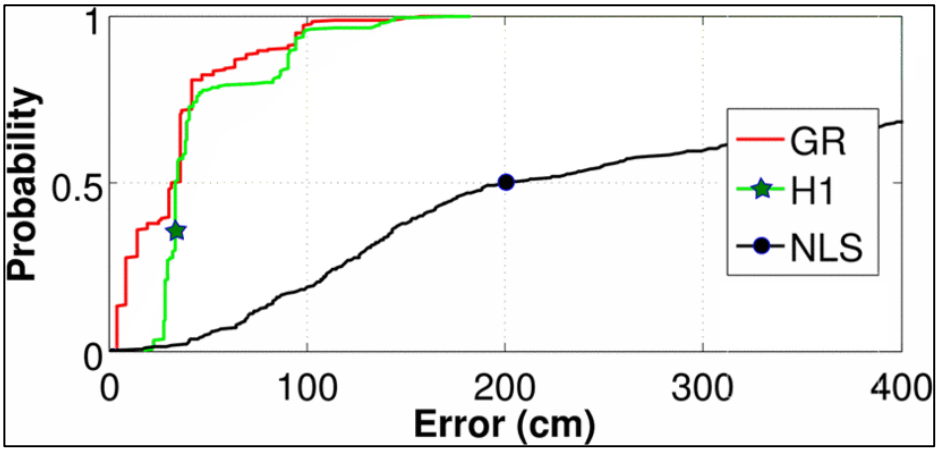

Figure 3.7 Performance comparison between RSS based algorithms [207].

Figure 3.7 and Figure 3.8 give comparisons between RSS based algorithm, including the radar algorithm (*RF-fingerprinting*), GR gridded radar (*RF-fingerprinting*), ABP (*MLE*), H1 (*MLE*), LLS and NLS (*Range based*) using WLAN network [15] [207], as seen in these figures, MLE and RF fingerprinting performance are very similar while for range based algorithms the performance is relatively poor. Also, it can be seen that NLS is more accurate compared to LLS.

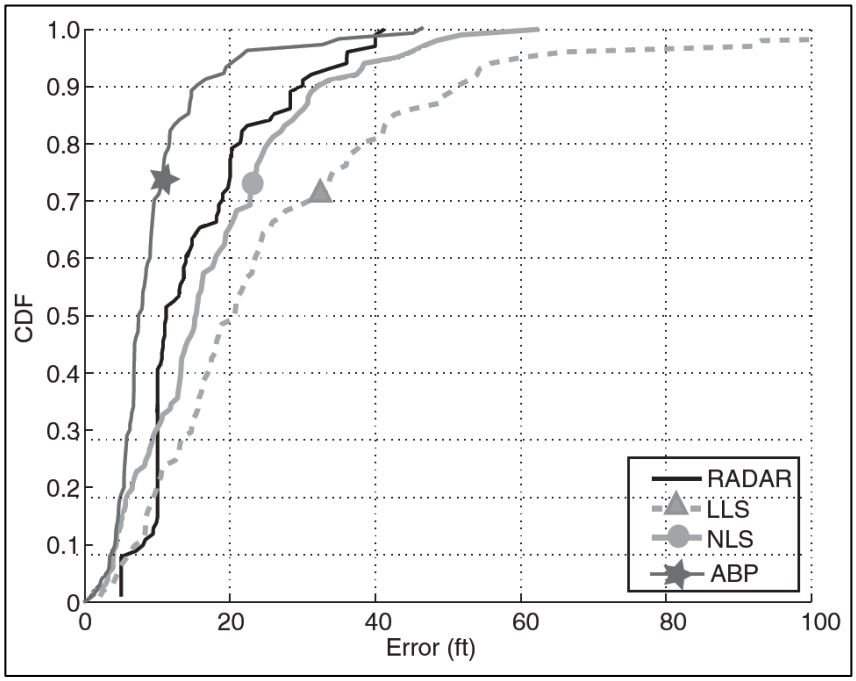

Figure 3.8 Performance comparison between RSS based algorithms [15].

3.3 Time of Arrival Measurements

3.3.1 Introduction

In TOA measurements by using wave velocity the flight time between the AP and the mobile is calculated to estimate the distance between the two sensors [208], waves used for localization include RF signals and acoustic signals [208], the velocity of radio waves is 3×10^8 *m/s* while velocity acoustic waves is 343.59 *m/s* [209]; therefore RF measurements are more prone to errors. A measurement error of $1\,\mu s$ will lead to 300 *m* error using RF waves, where it will lead to 0.00034359 *m* error using acoustic waves [210].

3.3.2 Time of Arrival

The time signal takes to travel between two points is directly related to the distance between them, using this property is helpful to localize the mobile, TOA localization uses the concept of lateration [211]. Assuming the mobile is located at an unknown position (x, y), and the APs are located at known locations (x_i, y_i), the measured time t_i at the mobile from i^{th} AP is:

$$t_i = \tau_i + t_a = \frac{d_i}{v} + t_a \tag{3.23}$$

$$t_i = \frac{\sqrt{(x_i - x)^2 + (y_i - y)^2}}{v} + t_a \tag{3.24}$$

where t_a is the time when the signal was transmitted from the AP, τ_i is the flight time between the two sensors, v is the wave velocity and d_i is the distance to be estimated. In Equation 3.24 there are three unknowns: x, y and t_a. In order to solve these equations it is required to have three equations (i.e. three APs measurements must be used). In a 3D situation (x, y, z) four APs at least must be used to have a unique solution. Rearranging Equation 3.24 gives the equation of

a circle (Equation 3.25). This means that the mobile will be at any point on the circle circumference. With three circles formed by the three APs measurements, the intersection of these circles will determine the mobile's location; however it is required that all APs and the mobile be synchronized in order to have accurate estimation.

$$(\tau_i . v)^2 = (x_i - x)^2 + (y_i - y)^2 \tag{3.25}$$

TOA measurements are transformed into circular equations, by solving these equations the coordinates of the mobile will be inferred [212] TOA circular equations are solved using NLS and LLS similar to RSS range-based positioning as shown in Figure 3.3 TOA circular equations are solved using NLS and LLS similar to RSS range-based positioning. The use of Nonlinear Least Square (NLS) is more complicated and more accurate while LLS is very sensitive to the presence of noise and NLOS [213].

3.3.3 Time Difference of Arrival (TDOA)

Another related time measurement is the time difference of arrival (TDOA), where the time difference between two TOA measurements (t_i, t_j) are used to formulate one equation t_{ij} as shown in Equation 3.26.

$$t_{ij} = t_i - t_j = \tau_i - \tau_j = \frac{d_i}{v} - \frac{d_j}{v} \tag{3.26}$$

$$t_{ij} = \frac{\sqrt{(x_i - x)^2 + (y_i - y)^2} - \sqrt{\left(x_j - x\right)^2 + \left(y_j - y\right)^2}}{v} \tag{3.27}$$

Possessing three TOA measurements (t_i, t_j, t_k) will formulate two TDOA measurements (t_{ij}, t_{ik}); however, the third equation t_{kj} will be dependent on the other equations and hence does not provide new information, in order to have

unique solution four APs measurements are used [212]. Possible locations for the mobile will be located on a hyperbola [212], the intersection of two hyperbola will find the location [212] as shown in Figure 3.4.

3.3.4 TOA vs. TDOA

In TOA all sensors including the mobile must be synchronized, since mobile's clock is not as accurate as the base station's clock [214] [215], as a result, there will be an error in estimating the flight time and thus errors in localization, however, in TDOA only APs are required to be synchronized [214].

On the other hand, TOA makes better use of existing information, one measurement of TOA will confine the possible locations for the mobile to be on a circle, using two measurements the mobile will be located possibly in two locations using TOA, while using TDOA the location will lie on a hyperbola, using three measurements TOA can estimate a unique solution while TDOA will have one or possibly two solutions [216].

Another drawback of using TDOA is the sensitivity LOS existence [217], due to the nature of hyperbole, a small amount of error will lead to a huge change in the curve and the result will be less accurate [218].

3.3.5 Impact of Building material and NLOS on localization

If the LOS path suffered from attenuation and fall below the threshold chosen to reject the noise, then the next path with a power above noise level is considered

as the first arrival path, this will lead to inaccurate TOA estimation and thus inaccurate localization [219].

The wave encountered walls through the propagation, as a result, the propagation time will not be a distance-dependent only, but a material dependent as well [220], The excess delay is given by [220], where ϵ_r is the material relative permittivity, w is the thickness of material and c is the speed of light:

$$\tau_{ex} = (\sqrt{\epsilon_r} - 1)\frac{w}{c} \tag{3.28}$$

3.3.6 Effect of Receiver Bandwidth on TOA Estimation

Receiver's ability to separate closed multipath components depends on its bandwidth. A larger receiver bandwidth BW a better separation for closely multipath components. For example a receiver with BW = 30 MHz will have a time resolution around 33.3 ns, if the incoming signals were separated by less than 33.3 ns, the receiver will consider them as one signal, as a result, delay estimation will be inaccurate.

With the availability of BW, the temporal resolution becomes high and hence better of separation of the closely multipath signals. In Figure 3.9-A due to limited BW, the receiver was not able to distinguish between the two signals, thus the peak is shifted in time more towards the second arriving path, causing an error in TOA estimation. By using larger BW receiver closely multipath components were distinguished as seen in Figure 3.9-B.

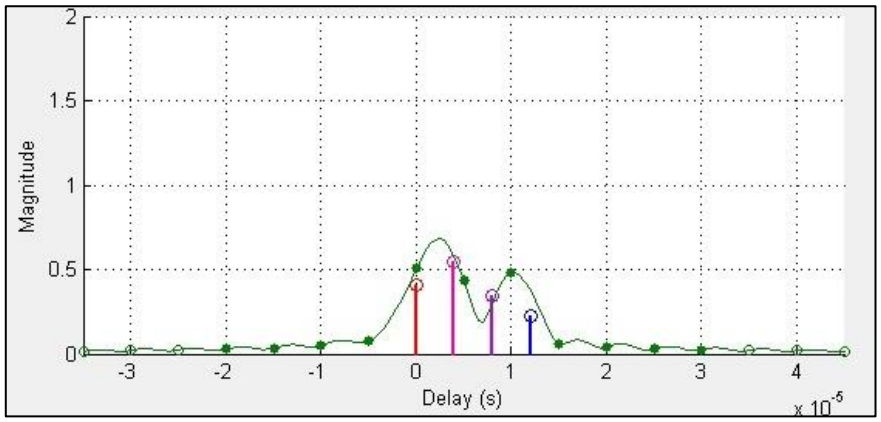

(A)

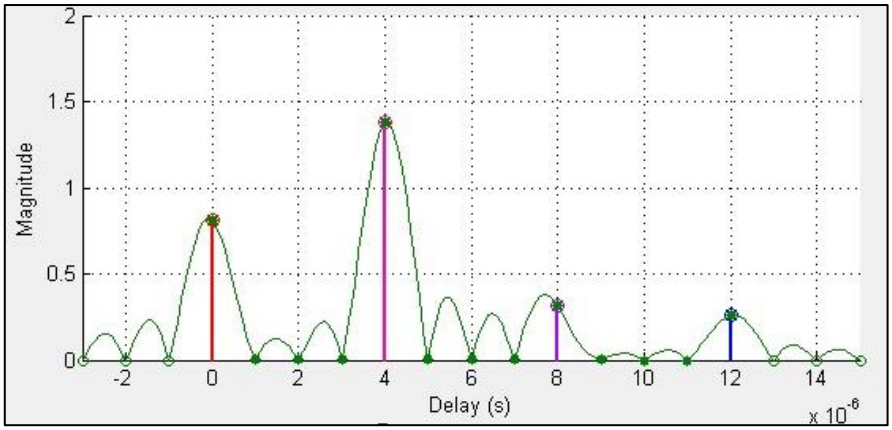

(B)

Figure 3.9 TOA estimation using different receiver BW.

3.3.7 TOA Estimation Techniques

Correlation Based Techniques

Cross-correlation is one of the most widely methods used to estimate TOA [219]. In Figure 3.10 TOA estimation is demonstrated, once the signal arrived, its matched (correlated) to a known template $p(t)$ by a match filter MF. The output of the filter is forwarded to a square law device where the sign of the correlated signal is removed, and then the time instant with the maximum peak value represents the time at which the signal arrived first [220].

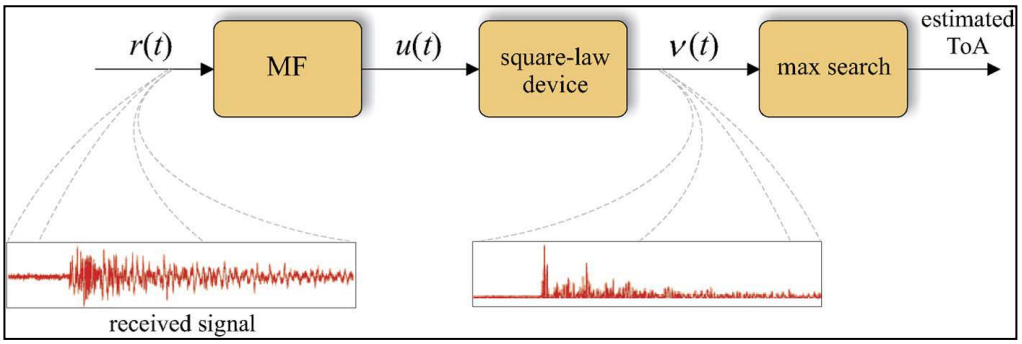

Figure 3.10 TOA estimation using cross-correlation [220].

In multipath propagation adjacent arrival peaks will have comparable amplitudes to the correct one; therefore the selection of the correct peak become ambiguous, which lead to large errors [220]. This method is preferred to its low complexity; however, it's prone to multipath and noise.

Inverse Fourier Transform method (Deconvolution)

This method is based on the fact that the received signal is a convolution of the transmitted signal and the channel, knowing the channel response will give the arrival times of the signals. In the frequency domain the convolution becomes multiplication, thus the channel response can be estimated by dividing the received signal by the transmitted signal [15]. The deconvolution problem is defined as if the output of a convolution process $v(t)$ and the inputs $s(t)$ are given what would be the other input $h(t)$ [221].

The received signal $v(t)$ is expressed as [15]:

$$v(t) = s(t) * h(t) + n(t) \tag{3.29}$$

where $s(t), h(t)$ and $n(t)$ are the transmitted signal, channel response and additive white Gaussian noise (AWGN) respectively. By taking Fourier Transform of Equation 3.29:

$$V(f) = S(f) \cdot H(f) + N(f) \tag{3.30}$$

Channel response in frequency domain is given:

$$H(f) = \frac{V(f)}{S(f)} - \frac{N(f)}{S(f)} \tag{3.31}$$

By taking the inverse Fourier transform of $H(f)$ the channel respose $h(t)$ is estimated and hence TOA. Practically this is done by sweeping the frequency from lowest frequency ($f_c - \frac{B}{2}$) to highest frequency ($f_c + \frac{B}{2}$) by a step of Δf [222]. Where B is the bandwidth, f_c is the center frequency and Δf is the frequency segment. The range of frequencies is shown in Equation 3.32.

$$f(n) = f_0 + (n-1)\Delta f \tag{3.32}$$

where f_0 is the lowest frequency and n is ranges from 1 to K.

For every frequency step different values of $V(f)$, $S(f), H(f)$ and $N(f)$ will be observed. A matrix can be generated to represent channel behaviour over the bandwidth:

$$\boldsymbol{V} = \boldsymbol{S}.\boldsymbol{H} + \boldsymbol{N} \tag{3.33}$$

This method performs better than the convolution-based method for resolving the closely separated multipath, but it suffers from the noise enhancement $\frac{N(f)}{S(f)}$. Another drawback of this method is the size of memory required for computation of the matrices [15].

Subspace techniques

Considering Equation 3.33, if L observations are collected and at each frequency step and M signal delays are received at each observation, then channel $\boldsymbol{H}$ will include information about the frequency segments and time delays. It's possible to view the time delays and the channel behaviour on each individual delay as [222]:

$$\boldsymbol{H}_{K\times 1} = \boldsymbol{U}_{K\times M} \cdot A_{M\times 1} \tag{3.34}$$

where

$$\boldsymbol{U} = \begin{bmatrix} 1 & & 1 \\ e^{-j2\pi\Delta f\tau_1} & & e^{-j2\pi\Delta f\tau_M} \\ \vdots & \cdots & \vdots \\ e^{-j2\pi(K-1)\Delta f\tau_1} & & e^{-j2\pi(K-1)\Delta f\tau_M} \end{bmatrix} = [\boldsymbol{u}(\tau_1) \quad \cdots \quad \boldsymbol{u}(\tau_M)]$$

$$A = \begin{bmatrix} \alpha_1 e^{-j2\pi f_0\tau_1} \\ \vdots \\ \alpha_M e^{-j2\pi f_0\tau_M} \end{bmatrix}$$

where $\boldsymbol{u}(\tau_i)$ is the normalized frequency response at the i^{th} delay and α is the attenuation factor. The n^{th} row of U times A represents the channel response at the n^{th} frequency [223].

$$H(n) = \sum_{m=1}^{M} \alpha_m e^{-j2\pi(f_0+(n-1)\Delta f)\tau_m} \tag{3.35}$$

Multiplying $\boldsymbol{S}^{-1}$ with both sides of Equation 3.33 gives [222]:

$$\boldsymbol{Y} = \boldsymbol{UA} + \boldsymbol{W} \tag{3.36}$$

where ($\boldsymbol{Y} = \boldsymbol{S}^{-1}\boldsymbol{V}$) and ($\boldsymbol{W} = \boldsymbol{S}^{-1}\boldsymbol{N}$).

Covariance matrix can be taken for Equation 3.36 by taking L observations as in [222]:

$$\boldsymbol{R_{YY}} = E\langle \boldsymbol{YY}^H \rangle = \boldsymbol{UAA}^H\boldsymbol{U}^H + \boldsymbol{WW}^H + \boldsymbol{A}^H\boldsymbol{U}^H\boldsymbol{W} + \boldsymbol{WA}^H\boldsymbol{U}^H \quad (3.37)$$

Assuming that both signal delays and noise are orthogonal, then Equation 3.37 becomes [224]:

$$\boldsymbol{R_{YY}} = E\langle \boldsymbol{YY}^H \rangle = \boldsymbol{UAA}^H\boldsymbol{U}^H + \boldsymbol{WW}^H = \boldsymbol{UR_{AA}U}^H + \sigma^2\boldsymbol{I} \quad (3.38)$$

where σ^2 is the noise variance.

Using the concept on eigenvalues and eigenvectors, $\boldsymbol{R_{YY}}$ has K dimensional space which can be decomposed into: M signal delays sub-spaces $\boldsymbol{Q}_S$ and ($K - M$) noise sub-spaces $\boldsymbol{Q}_N$ (i.e. signal delays sub-space will have M eigenvectors and eigenvalues while noise sub-space will have ($K - M$) eigenvectors and eigenvalues) [224].

It's worth mentioning that the signal delays sub-spaces and noise sub-spaces are orthogonal. The signal sub-space is formed from the signal time delays, provided that these delays are independent of each other, MUltiple SIgnal Classification (MUSIC) takes advantage of the covariance matrix decomposition, knowing that the signal sub-space is orthogonal to noise sub-space and that signal sub-space is formed from signal delays, then it's expected that signal delays will be orthogonal to noise sub-space, this information is useful to separate closely separated multipath as shown in Equation 3.39 [224]:

$$S = \frac{1}{\boldsymbol{u}(\tau)^H\boldsymbol{Q}_N^H\boldsymbol{Q}_N\boldsymbol{u}(\tau)} = \frac{1}{|\boldsymbol{Q}_N\boldsymbol{u}(\tau)|^2} \quad (3.39)$$

In Equation 3.39 Euclidean distance is estimated between the signal delay vectors and the noise sub-space, since they are orthogonal, multiplication will lead to zero, dividing by an amount approaching zero will give a large number. In Figure 3.11 a comparison between MUSIC and IF algorithms is presented, MUSIC algorithm outperforms IF algorithm provided by its ability to distinguish closed multipath components. In spite of the advantages of the MUSIC algorithm, however, the number of multipath is a priori information for the algorithm [15].

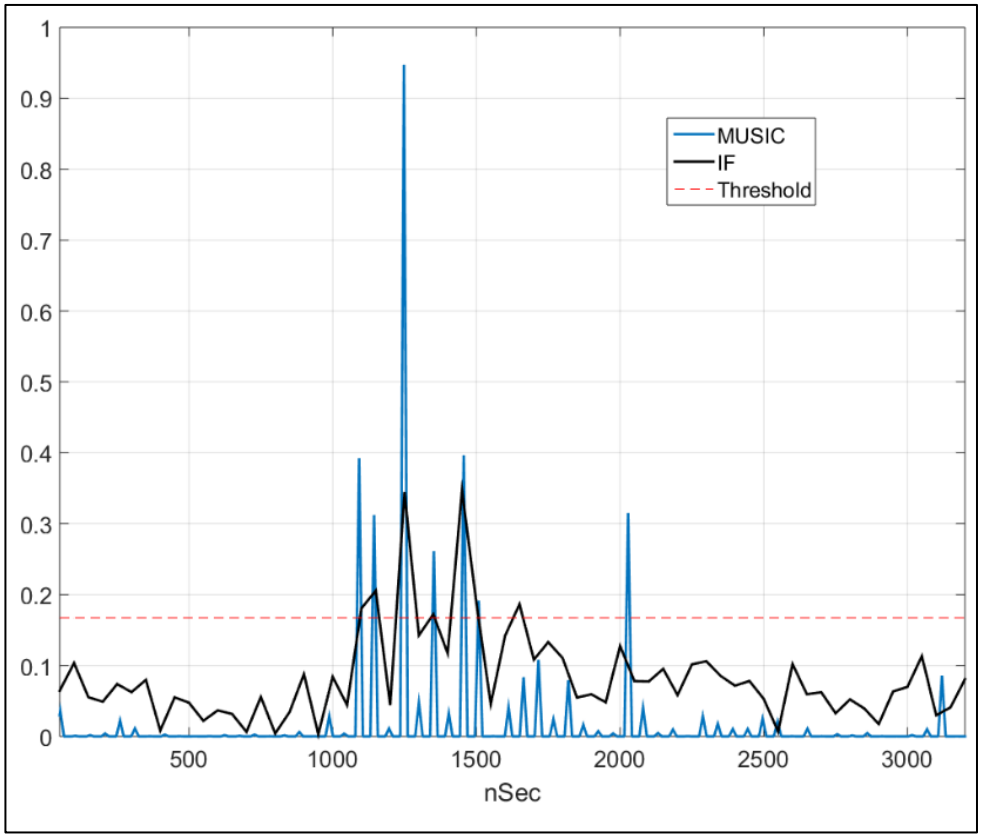

Figure 3.11 TOA estimation comparison between MUSIC and IFT algorithms.

3.4 Angle of Arrival Measurements

3.4.1 Introduction

Antenna arrays are used to detect angle of arrivals, direction of arrival (DOA) is used for many application including beamforming and localization [15], DOA requires the use of antenna arrays which makes the technique more expensive and more power consumption compared to TOA and RSS [219]; however it requires less equipment as only two APs are required to infer mobile's location [225].

3.4.2 Propagation Delay and Narrowband Approximation

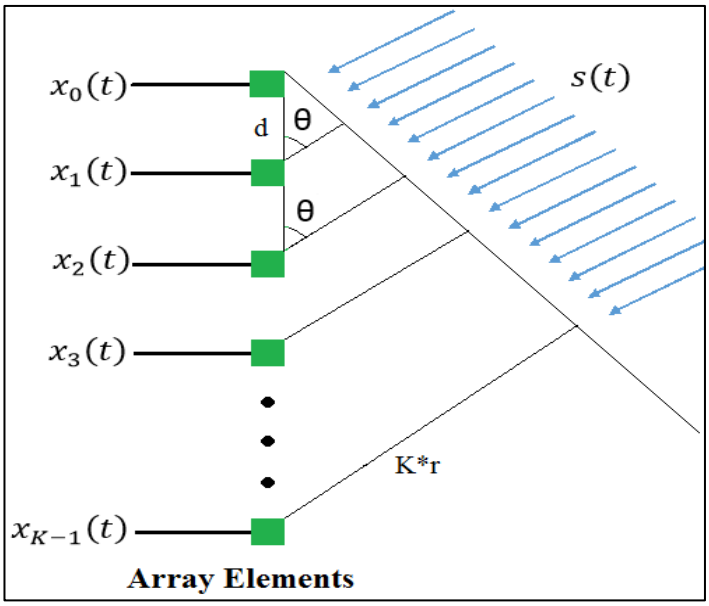

Figure 3.12 Incident signal on Uniform Linear Array (ULA).

Assuming the transmitted signal $s(t)$ is received by the antenna array, array's elements will examine different delays due to spacing and due to the direction to where the signal comes from [226], the latter cause is important to estimate the

angle of arrival (AOA), where the delays are directly related to phase differences from which we can estimate the AOA [227].

Assuming the spaces between the elements are small enough (around $\frac{\lambda}{2}$), the received signals are considered to be correlated [227]. Mutual coupling effects between array elements alter received signals [228], the smaller spacing between array elements the more coupling effect, while the more spacing between elements the less coupling which will create grating lobes [229], a trade off spacing is required, thereby spacing set to be (0.5λ).

As shown in Figure 3.12, incoming signal will arrive elements with different delays, assuming the source of signals is in the far field region of the array, the angle θ will be considered the same for array elements [227]. In the case where the transmitted signal is considered to be narrowband the received signal is given by [30]:

$$\begin{bmatrix} x_0[n] \\ x_1[n] \\ x_2[n] \\ . \\ . \\ . \\ x_{K-1}[n] \end{bmatrix} = \begin{bmatrix} 1 \\ e^{-j\beta\, \mathrm{dcos}(\theta)} \\ e^{-2j\beta\, \mathrm{dcos}(\theta)} \\ . \\ . \\ . \\ e^{-j\beta(K-1)\ \mathrm{dcos}(\theta)} \end{bmatrix} s[n] + \begin{bmatrix} n_0[n] \\ n_1[n] \\ n_2[n] \\ . \\ . \\ . \\ n_{K-1}[n] \end{bmatrix} \tag{3.40}$$

where $\boldsymbol{\beta}$ is the propagation constant and K is the number of array elements. Derivation for the received signal is explained in details in Appendix A. Equation 3.40 can be represented in matrix form:

$$\mathbf{x}[n] = \mathbf{a}(\theta)s[n] + \mathbf{n}[n] \tag{3.41}$$

$\mathbf{x}[n]$ is known as *input data vector* and $\mathbf{a}(\theta)$ is known as *steering vector* [226]. For M signals coming from different angles Equation 3.41 can be modified as:

$$\boldsymbol{x}[n] = \begin{bmatrix} a_0(\theta_0) & a_0(\theta_1) & \cdots & a_0(\theta_{M-1}) \\ a_1(\theta_0) & a_1(\theta_1) & & a_1(\theta_{M-1}) \\ a_2(\theta_0) & a_2(\theta_1) & & a_2(\theta_{M-1}) \\ . & . & & . \\ . & . & & . \\ . & . & & . \\ a_{K-1}(\theta_0) & a_{K-1}(\theta_1) & & a_{K-1}(\theta_{M-1}) \end{bmatrix} \begin{bmatrix} s_0[n] \\ s_1[n] \\ s_2[n] \\ . \\ . \\ . \\ s_{M-1}[n] \end{bmatrix} + \boldsymbol{n}[n] \qquad (3.42)$$

In matrix form:

$$\boldsymbol{x}[n] = [\mathbf{a}(\theta_0)\ \mathbf{a}(\theta_1)\ \ldots\ \mathbf{a}(\theta_{M-1})]\boldsymbol{s}[n] + \boldsymbol{n}[n] = \boldsymbol{A}(\theta)\boldsymbol{s}[n] + \boldsymbol{n}[n] \qquad (3.43)$$

Delays can be expressed as phase shifts, if signals are added as they being received they will add up constructively and destructively in a random manner; weightings are used to compensate for delays to maximize the reception from the desired direction this is accomplished by imposing complex factors (have different amplitudes and phases) on the weighting [230].

For uniformly linear array (ULA) antenna, weightings are complex conjugate to the steering vector in the desired angle, the complex conjugate will cancel the effect of the phases on the arrived signal (due to the delay) [229], the result will be K signals added with no phase shift, which means that the signal will be K times larger [227]. The output of the array is given by Equation 3.44 and Figure 3.13 [231]:

$$y[n] = \sum_{k=0}^{K-1} (w_k \cdot x_k[n]) = \boldsymbol{w}^{\mathrm{T}}.\mathbf{x}[n] \qquad (3.44)$$

$$\boldsymbol{w} = \begin{bmatrix} 1 \\ e^{j\beta \mathrm{dcos}(\theta_d)} \\ e^{2j\beta \mathrm{dcos}(\theta_d)} \\ . \\ . \\ . \\ e^{j\beta(K-1)\,\mathrm{dcos}(\theta_d)} \end{bmatrix} \tag{3.45}$$

It's noteworthy that the steering vector search for all θ ranging from 0^0 to 180^0, while weighting is designed for a specific angle θ_d. The conjunction of weighting and input data vector is called *beamforming* [229].

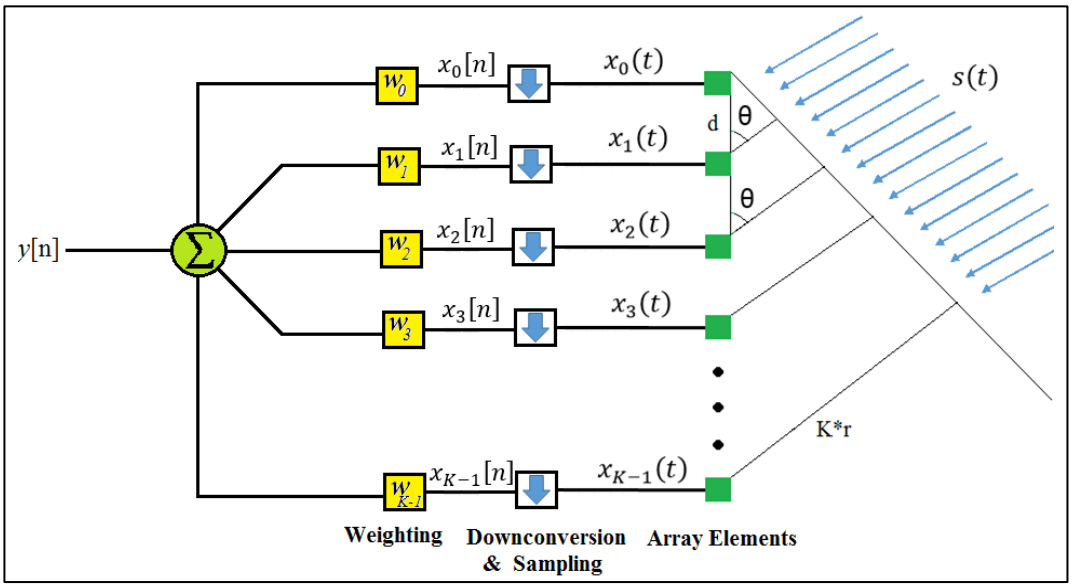

Figure 3.13 Array beamforming system.

If spacing between elements is large, there will be different angles where the array has maximum radiation, as seen in Figure 3.14, when the spacing is λ/2, array's performance shows that there is one main lobe towards the desired angle, while when the spacing is 1.5λ, another two lobes with same radiation power appears at different angles, such lobes are called *Grating lobes* [229]. Mutual coupling between array elements should be minimized to have accurate estimation [228, 232].

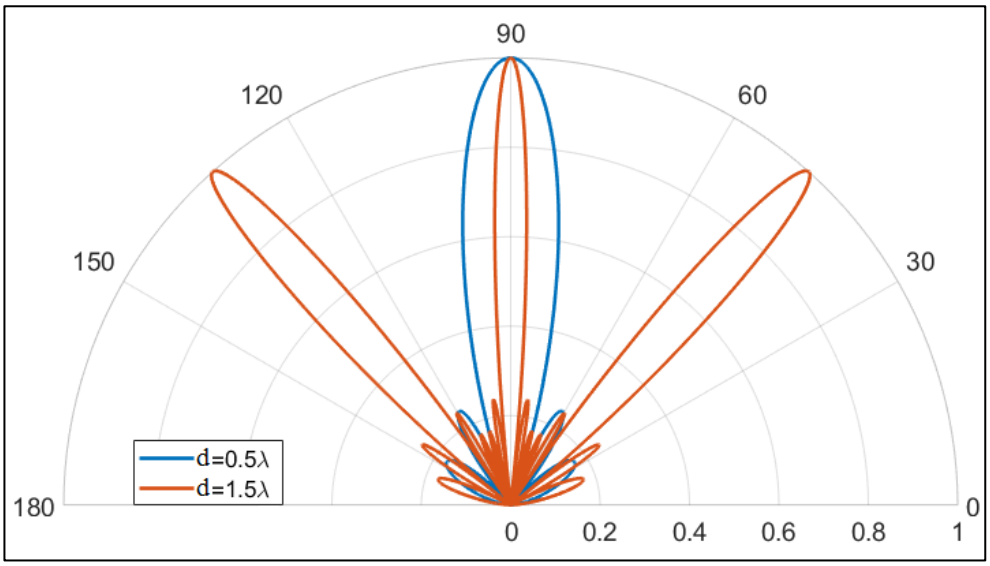

Figure 3.14 Grating lobes due to element's large separation.

Figure 3.15 shows a comparison between two arrays' radiation patterns, the first array has six elements while the second has twelve. Adding more elements will focus the power in the main beam by reducing the beamwidth. The output of each array is normalized with respect to its maximum value.

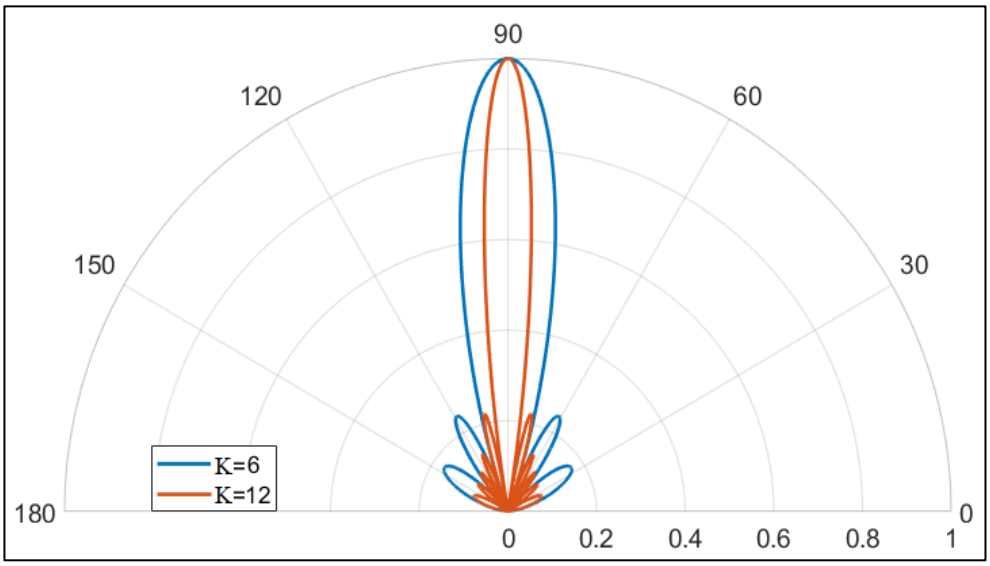

Figure 3.15 Performance comparison between two arrays radiation with a different number of elements.

3.4.3 Covariance Matrix

In statistics, covariance is a multi-dimensional measure of how two random variables change from the mean with respect to each other. A zero covariance means that the two random variables are independent, a negative value means if one variable increases the other will decrease, while a positive value means if one variable increases the other will increase [233], if the covariance is taken for the random variable with itself it gives variance [234].

In antenna array signal processing, if the input data $x[n]$ is taken for a huge number of samples in time ($X[n] = [x_1[n] \quad x_2[n] \quad \dots \quad x_N[n]]$) the covariance matrix $\boldsymbol{R}_{xx}$ is computed as shown in Equation 3.46 [235].

$$\boldsymbol{R}_{xx} = E\left[X[n] \; X^{\mathrm{H}}[n]\right] = \boldsymbol{A}(\theta) R_{ss} \boldsymbol{A}^{\mathrm{H}}(\theta) + \sigma^2 \boldsymbol{I}_{N\times N} \tag{3.46}$$

Derivation of Equation 3.46 is given in Appendix B. In practice, the covariance matrix is estimated as in Equation 3.47 [236]:

$$\boldsymbol{R}_{xx} = \frac{1}{N} \sum_{i=1}^{N} x[n] \; x^{\mathrm{H}}[n] \tag{3.47}$$

where N is the number of observations. The covariance matrix is important in array signal processing, as it can be decomposed into a signal subspace and a noise subspace provided that the number of antenna array elements is larger than the number of arrival signals [227]; those subspaces are used in algorithms which will enhance the localization process [235].

3.4.4 Angle of Arrival Techniques

Delay and Sum (Bartlett Beamformer)

The Bartlett method is considered to be one of the earliest AOA estimation techniques, during the process of making the array manifold the covariance matrix is implemented, accordingly, the output power of the beamformer is estimated, maximum peaks of $P(\theta)$ correspond to AOA [226, 237].

$$P(\theta) = E\{|y[n]|^2\} = \max E\{\boldsymbol{w}^H \boldsymbol{x}[n]\boldsymbol{x}[n]^H \boldsymbol{w}\} = \max E\{\boldsymbol{w}^H \boldsymbol{R}\, \boldsymbol{w}\} = \frac{\boldsymbol{w}^H \boldsymbol{R}\, \boldsymbol{w}}{\boldsymbol{w}^H \boldsymbol{w}} \quad (3.48)$$

For ULA [236]:

$$P(\theta) = \frac{\boldsymbol{w}^H \boldsymbol{R}\, \boldsymbol{w}}{K^2} \quad (3.49)$$

The drawback of using the Bartlett beamformer is the poor resolution as it appears when the impinging signals are very close [236].

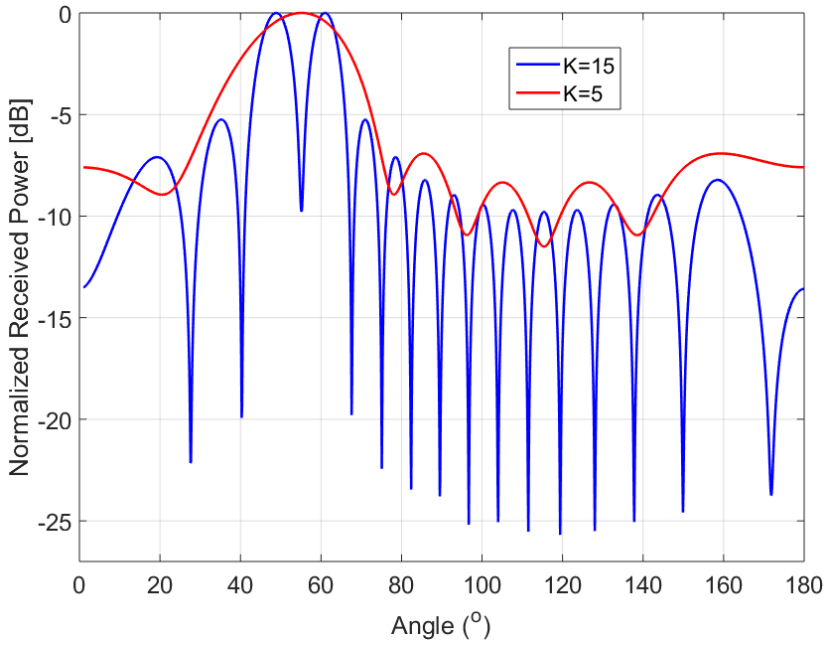

Figure 3.16 Effect of array elements on AOA estimation using the Bartlett Beamformer.

As seen in Figure 3.16, two signals arriving from angles (50^o and 60^o), using five elements array the algorithm failed to distinguish the two signals and thus considered them as one signal coming from angle (55.2^o), level of side lobes and width of the main beam are inversely proportional to the number of array elements, adding more elements with suitable design will compensate for these impairments; however this will add more the cost, size and storage data for calibration [236].

Capon Minimum Variance Method

The Capon method use some of the degrees of freedom to look at the desired signal θ_0 and use the remaining to suppress the interfering signals [226]; in other words, the algorithm has two constraints, minimize the power from noise and interferer signals $\boldsymbol{w}^H.n[n]$ and keeping the gain of the desired signal constant $\boldsymbol{w}^H.\boldsymbol{a}(\hat{\theta}_0) \cong 1$ [226] where $\hat{\theta}_0$ is the estimated angle of arrival. Mathematically array weighting is estimated by [236]:

$$\min_{w}(\boldsymbol{w}^H.\boldsymbol{R}_{xx}.\boldsymbol{w}) \text{ subject to } \boldsymbol{w}^H.\boldsymbol{a}\left(\hat{\theta}_0\right) = 1 \tag{3.50}$$

The weighting vector can be estimated using Lagrange multiplier method:

$$\boldsymbol{w} = \frac{\boldsymbol{R}_{xx}{}^{-1}\boldsymbol{a}\left(\hat{\theta}_0\right)}{\boldsymbol{a}^{\mathrm{H}}\left(\hat{\theta}_0\right)\boldsymbol{R}_{xx}{}^{-1}\boldsymbol{a}\left(\hat{\theta}_0\right)} \tag{3.51}$$

Applying in Equation 3.49 the total power received is:

$$P(\theta) = \frac{1}{\boldsymbol{a}^{\mathrm{H}}\left(\hat{\theta}_0\right)\boldsymbol{R}_{xx}{}^{-1}\boldsymbol{a}\left(\hat{\theta}_0\right)} \tag{3.52}$$

This method shows better performance than the Bartlett beamformer as shown in Figure 3.17.

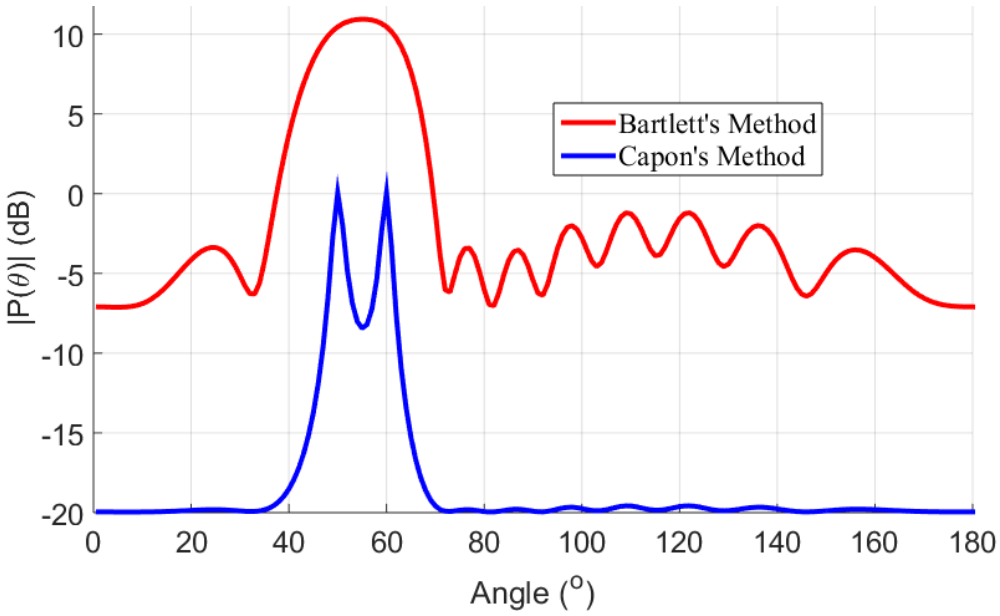

Figure 3.17 Comparison of Capon and Bartlett methods.

The comparison shows that using 10 elements array, the Bartlett beamformer cannot distinguish between (50^o and 60^o), while the Capon beamformer is able to distinguish between them. In addition to this, the Capon method suppressed the side lobes more effectively. One drawback for the Capon method is the expensive calculation for the inverse matrix for large antenna arrays [227].

The Capon beamformer shows acceptable performance in terms of resolution and rejection of interference under the condition that the presumed steering vector of the desired signal is identical to the actual one; however practically it is difficult to let the most accurate steering vector identical to the actual one, as a result, the performance degrades dramatically [238].

The MUSIC Algorithm

Rather than looking at the covariance matrix, MUSIC algorithm looks at the eigenvector decomposition of the covariance matrix (details are given in Appendix B) [239].

The array will scan all possible angles, for an arbitrary steering vector there will be a projection on signal subspace and projection on noise subspace, the projection on a subspace is estimated by finding the Euclidean distance between the vector and the other subspace [239].

$$d^2 = a^H(\theta) Q_{s/n} Q_{s/n}^H \, a(\theta) \tag{3.53}$$

where $Q_{s/n}$ is either the signal subspace or noise subspace.

Among those possible steering vectors, there will M steering vectors related to the arriving signals. Those vectros will be on the signal subspace: in other words, they will be orthogonal to the noise subspace and parallel to the signal subspace. One way to find those angles is to find the maximum Euclidean distance to noise subpace. The AOA estimation based on this method is expressed by the following equation:

$$P_{MU} = \frac{1}{a^H(\theta) Q_n Q_n^H \, a(\theta)} \tag{3.54}$$

On the other hand, using Equation 3.54 for Q_s will give a maximum for the true steering vectors and minimum for the inaccurate ones, but the difference here is that the peak will not be as sharp as in the previous case, due to the fact that the effect of noise is embedded on signal subspace (eigenvalues of signal subspace are ${\sigma_s}^2 + \sigma^2$); therefore the effect of multiplication will go smoothly around the accurate angles.

In Figure 3.18, an antenna array with ten elements received three signals come from angles -30^o, -22^o and 40^o. Both the Bartlett and Capon methods could not resolve the closed multipath, while MUSIC can determine the AOA more efficiently, the sharpness of the peaks reflects the robustness of the algorithm.

On the other hand, we implement the MUSIC algorithm but based on signal subspace, as mentioned before, the performance is very similar to the Bartlett algorithm, as a result, the noise subspace is adopted to estimate the AOA.

MUSIC is prefered for different reasons including its ability to measure more than one signal simultaneously [236], in addition to its highly accurate and precise estimation for closed separated signals; however, the algorithm requires the knowledge of number incoming signals [236].

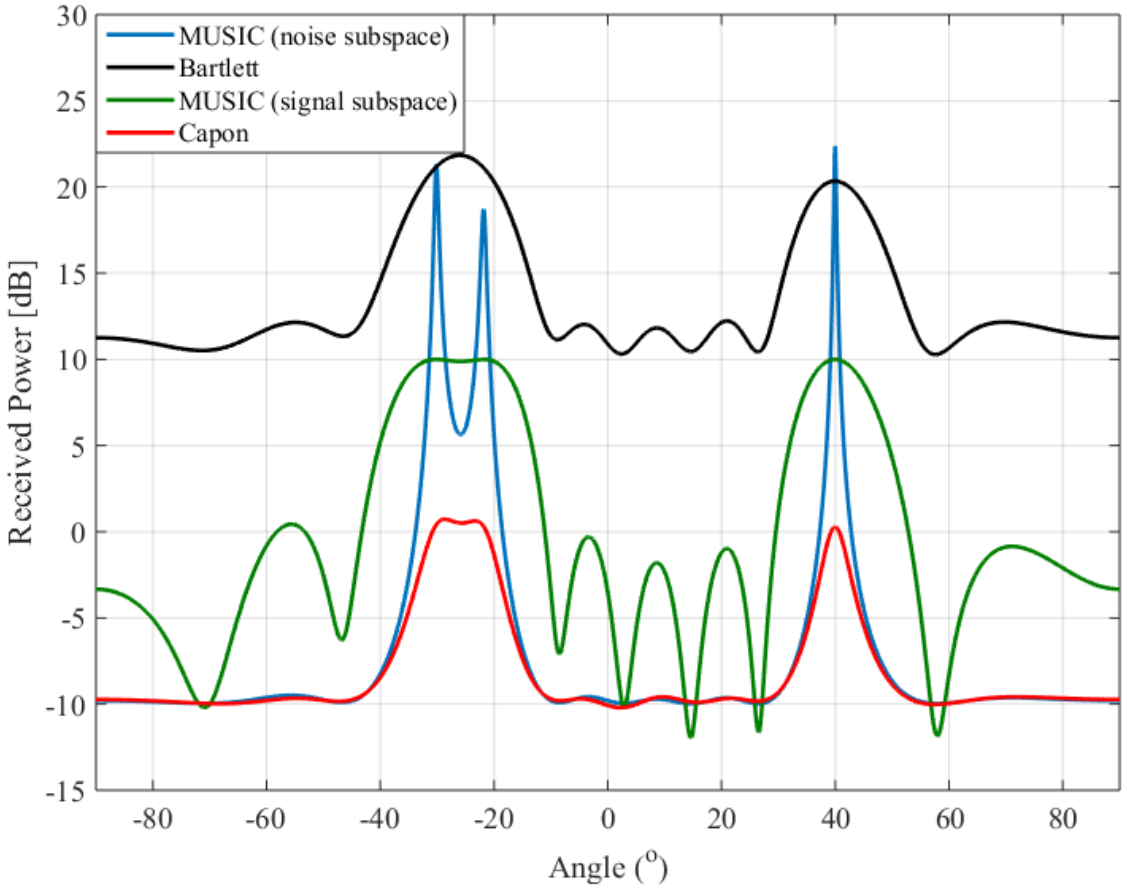

Figure 3.18 Comparison of AOA techniques.

Chapter 4

An Indoor Path Loss Prediction Model using Wall Correction Factors for WLAN and 5G Indoor Networks

4.1 Introduction

Propagation models have been developed and can be broadly categorised as either predicting median signal strength (path loss and shadowing) like Motley Keenan model [10] or channel behaviour (fading across time or frequency) like Saleh-Valenzuela model [17]. Path loss models predict the signal level (averaged over several wavelengths or a wide bandwidth) at a given distance from the transmitter [10], whilst channel models describe the stochastic or non-deterministic variation of the signal level (narrowband) and the time-dispersion (wideband) at that location [17].

Despite the obvious underlying complexity of the indoor channel, [10] looked to provide a straightforward engineering model for path loss. Their approach was to consider the various walls and floors obstructing the straight-line path between transmitter and receiver and to factor in a best-fit loss per wall or floor of each identifiable type, e.g. stud partition (drywall) or concrete block walls, suspended concrete floor beams or wooden floors, etc. When these losses were factored in, they found a residual free-space variation with distance (i.e. power law index of two). A deficiency of their model was its tendency to an over-predict loss where there are many floors or walls (presumably because there is an alternative, lower-loss path around those obstacles).

Other models have been proposed from simple power laws, two-slope or multi-slope models [49] [50] [65] to those that use the Keenan and Motley concept with some added sophistication to reduce the loss per floor as the number of floors increases [72]. Waveguiding, e.g. along corridors can lead to path loss indices approaching one, whilst the presence of clutter within the first Fresnel zone of a ray can lead to indices of 4-6 beyond a break-point as for ground-wave propagation [59].

In this study, several indoor path loss models and their associated parameters are examined and tested. A modified method named Effective Wall Loss Model (EWLM) to estimate the path loss is proposed. The performance of the proposed method was compared to other related methods in terms of various frequency spectrums covering WLAN and millimetre wave frequencies; the effect of antenna polarization was also studied. Simulated and measured test results were presented in which it shows the proposed method outperformed the other tested models.

4.2 Indoor Path Loss Models

Many models have been proposed in literature including one slope model [49], dual slope model [50], linear attenuation model [51], partitioned model [52], Motley Keenan model [10], averaged wall loss model [53], ITU-R P.1238 model [54] COST 231 indoor model [55] and dominant path model [56]. A detailed description of the aforementioned models is presented in Chapter 2.

Effective Wall Loss Model (EWLM)

The Averaged Wall Loss Model (AWM) captures changes in the propagation environment; therefore, wall losses may be positive or negative. In fact, these losses can be considered as correction factors rather than losses. Using the "*average*" will superimpose the effect of all walls and then assume that all walls will contribute equally which is not necessarily true. The main problem with this model is the assumption that the main source of signal fading is the walls; therefore, similar walls will affect the signal similarly. Although this is partially true especially for millimetre waves as will be shown later, there are many other sources that affect the SS level mainly multipath.

The AWM model superimposes the multipath effect; however, the effects of multipath fading give an idea about how waves in specific region behave. Also, the concept of averaging does not reflect a scientific impact as it is unlikely that the last wall loss will affect the measurements at locations much before that wall. Another limitation to the AWM that it does not consider the effect of LOS propagation where path loss exponent will be less than the free space path loss exponent due to wave-guiding effect.

Due to these limitations, AWM was adopted with two modifications: first, the path loss estimated at a point depends on the losses due to the encountered wall only. The second modification includes the effect of path loss exponent in the region between the transmitter and the first wall which may be affected by the waveguiding effect. For NLOS propagation areas the effect of path loss exponents is already embedded with the wall correction factors. In order to distinguish it from

the AWM, the last modification is called Effective Wall Loss Model (EWLM). The path loss at distance *d* can be expressed as:

$$P_r(d) = P_0 - 10n\log_{10}(d) - \sum_{i=1}^{L} W_i \qquad (4.1)$$

where *n* is 2 for NLOS propagation, while for LOS propagation it is estimated by best fitting, and *L* is the number of walls. It is worth mentioning that W_{avg} in Equation 2.11 depends on total wall losses of the same type; therefore, applying Equation 2.11 will consider the effect of walls before and after the point of interest. EWLM considers the effect of walls which are only before the point of interest. Even if the walls are of the same type both models will work differently as shown in the incoming sections; however, they will have similar results after the last encountered wall where ($W_{avg} \cdot v = \sum_{i=1}^{v} W_i$).

4.3 Methodology and Experimental Setup

In the first part of this analysis, different indoor path prediction models were examined and compared to the EWLM using data obtained from ray tracing software called Wireless InSite® which has been extensively validated, especially for the UHF band [240] and for 802.11ac frequencies [241]. The adopted environment for the experiment was the third floor in Chesham building at the University of Bradford. The model for the building was constructed using the software.

Transmitters and receivers implemented in the environment are both omnidirectional, transmitted power was set to 20 dBm, while receiver sensitivity was set to -120 dBm. Five frequencies were examined including (2.4 GHz, 5.3

GHz, 28 GHz, 60 GHz and 73.5 GHz), their corresponding bandwidths are (0.084 GHz [242], 0.12 GHz [243], 0.8 GHz [70], 2.15 GHz [244] and 2 GHz [245] respectively, those frequencies have wide usage for indoor applications. Two types of polarization are investigated: vertical polarisation (VP) and circular polarization (CP), settings for Wireless InSite are given in Table 4-1, where SBR stands for Shooting-and-Bouncing-Rays.

Table 4-1 Wireless InSite settings for the investigated scenario.

Property	Setting
Number of reflections	6
Number of transmissions	4
Number of diffractions	0
Number of reflections before the first diffraction	3
Number of reflections after the last diffraction	3
Number of reflections between diffractions	1
Number of transmissions before the first diffraction	2
Number of transmissions after the last diffraction	2
Number of transmissions between diffractions	1
Ray tracing method	SBR
Propagation model	Full 3D

In the second part of the experiments, real-time measurements have been collected from WLAN access points (AP) distributed in the 3rd floor of Chesham building at the University of Bradford, those APs support Wi-Fi coverage on both 2.4 GHz and 5.3 GHz bands. In these experiments, three APs were considered as shown in Figure 4.1. All APs are similar, this includes the transmitter power, types of antenna used and bandwidth. For each AP, data are collected over two routes, measurements are taken at 1-meter height with 0.5 m spacing between every two measurements. The heights for AP1 is 2.2 m while for AP2 and AP3 the heights are 2.75 m. A WLAN scanner software called *inSSIDer*® was used to

collect the measurements using a laptop, these measurements are averaged to remove the effect of fast fading, the RSS reading is updated every one second.

This experiment was limited for a single floor only; in this case, the comparison includes OSM, DSM, LAM, PM, MKM, AWM and EWLM (DPM is included in the experimental part only). For single floor analysis, the ITU model and the COST-231 model are the same as the OSM and MKM respectively.

A valid comparison between the different modelling approaches requires that each model is applied to the same dataset in order to predict parameters. MATLAB is used to estimate the parameter values which provide the best fit to the data. Typical data are shown in Table 4-2. Table 4-3 summarises the different parameters used in each model.

Having generated the best-fit parameters, these same values are used to predict the RSS along various routes. Model-predicted RSS is calculated for each model using the equations in chapter 2. The model-predicted RSS values for each route and frequency are compared with the data available from measurements and from Wireless InSite ray-tracing simulations.

Error vector distance is estimated between the model-predicted RSS values and the data from Wireless InSite simulations or measurements, then the Root Mean Square Error (RMSE) of this vector is calculated as shown in Equation 4.2 where L is the length of the error vector. The smaller the RMSE the better model performance.

$$RMSE = \sqrt{\sum_{i=1}^{L} \frac{(Predicted_i - Actual_i)^2}{L}} \quad (4.2)$$

In [56] authors formulated a generalised formula for the DPM to be applied for different types of building. Since Ray tracing and DPM are two distinct approaches to estimate SS, analysis for DPM is performed only on data collected from real-time measurements. In the experimental part, DPM results were compared to other models at both investigated frequencies. As recommended by authors in [56], DPM parameter values are taken from [56] and [246].

Table 4-2 Example of data used to predict model parameters

	Distance (m)	RSS (dBm)
1	1	-32.22
2	8	-34.89
3	11	-40.22
4	16	-44.23
5	27	-54.22
6	30	-57.25
7	41	-66.78
8	44	-71.4

Table 4-3 Estimated model parameters

Model	Estimated Parameters
One slope model	Path loss exponent n
Dual slope model	Path loss exponents (n_1,n_2)
Linear Attenuation Model	Attenuation factor (a)
Motley-Keenan model	Wall losses (L_w)
Dominant Path model	Interaction losses
Average wall model	Averaged wall losses ($W_{avg.}$)
Effective wall loss models	Wall correction factors (W_i)

It is worth mentioning that for the EWLM after each wall the model makes a correction factor either by adding gain or adding loss in order to fit the

simulations/measurements. MKM assumes values for wall losses such that it makes the best fit for all simulations (in case of ray tracing) or measurements (in case of actual measurements) from all different routes, these losses are different from correction factors used by AWM and EWLM. OSM, DSM and LAM look for the best fitting for the simulations/measurements (different values for n and a can be used to describe the propagation channels within corridors and rooms. DPM use the cumulated wall losses and interaction losses; this is required to identify all possible direct paths and their corresponding bent angles as mentioned in [56]. After that, cumulated wall losses and interaction losses are calculated using Table 4 and Figure 6 in [56].

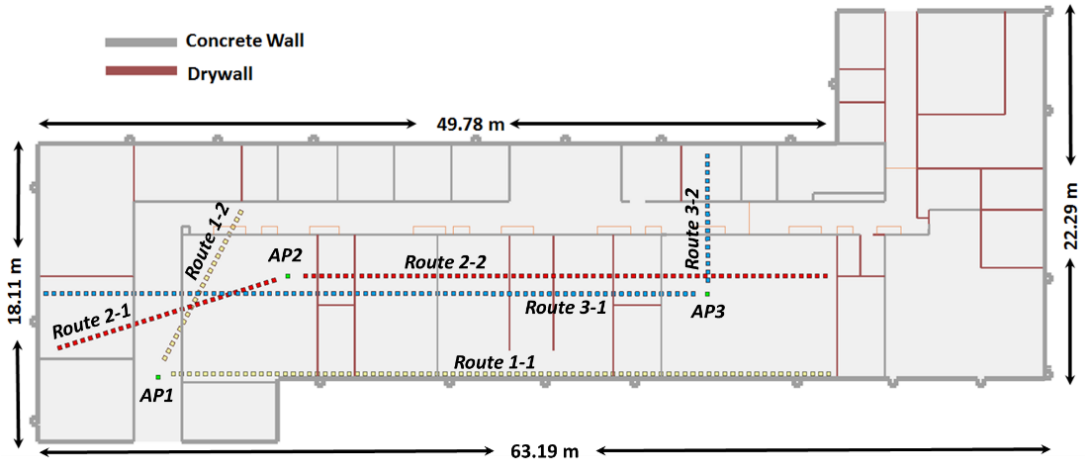

Figure 4.1: Experimental routes in 3rd floor Chesham building at the University of Bradford.

As shown in Figure 4.1, measurements are taken from AP1 on the yellow routes, while they were taken from AP2 and AP3 on the red and blue routes respectively. The simulation includes many routes within the floor to cover different scenarios and to verify the observations.

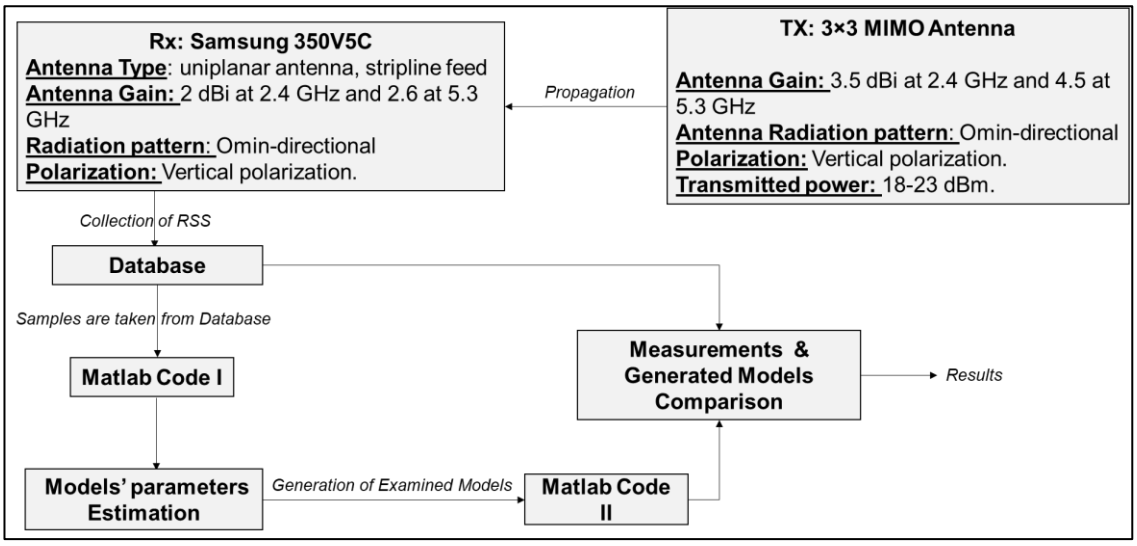

Figure 4.2: Experimental Setup Diagram

Figure 4.2 presents the experimental setup diagram; specifications of AP and the receiver are specified as seen in the figure. Collected RSS at the receiver are used as a radiomap, where samples are taken to generate model's parameters. Given that the models' parameters are estimated, the examined models are then generated. These models are compared to measurements where the model with least error is considered to have best performance.

Figure 4.3 shows a 3D view of the simulated environment; the colours are different for different features. Material dependence on operating frequency plays a major role in determining the radio coverage, as shown in Equation 2.25 and Equations 2.27-2.28. As the operating frequency is changing, the interaction between waves and building material will change accordingly. Table 4-4 shows the values of ε_r and σ adopted in our experiment which are calculated using Equations 4.3 and 4.4.

Table 4-4 Material properties with frequency

Frequency (GHz)	Concrete		Glass		Wood		Drywall	
	ε_r	σ	ε_r	σ	ε_r	σ	ε_r	σ
2.4	5.31	0.0662	6.27	0.0122	1.99	0.0120	2.94	0.0216
5.3	5.31	0.1258	6.27	0.0314	1.99	0.0281	2.94	0.0378
28	5.31	0.4838	6.27	0.2287	1.99	0.1672	2.94	0.1226
60	5.31	0.8967	6.27	0.5674	1.99	0.3784	2.94	0.2102
73.5	5.31	1.0568	6.27	0.7228	1.99	0.4703	2.94	0.2427

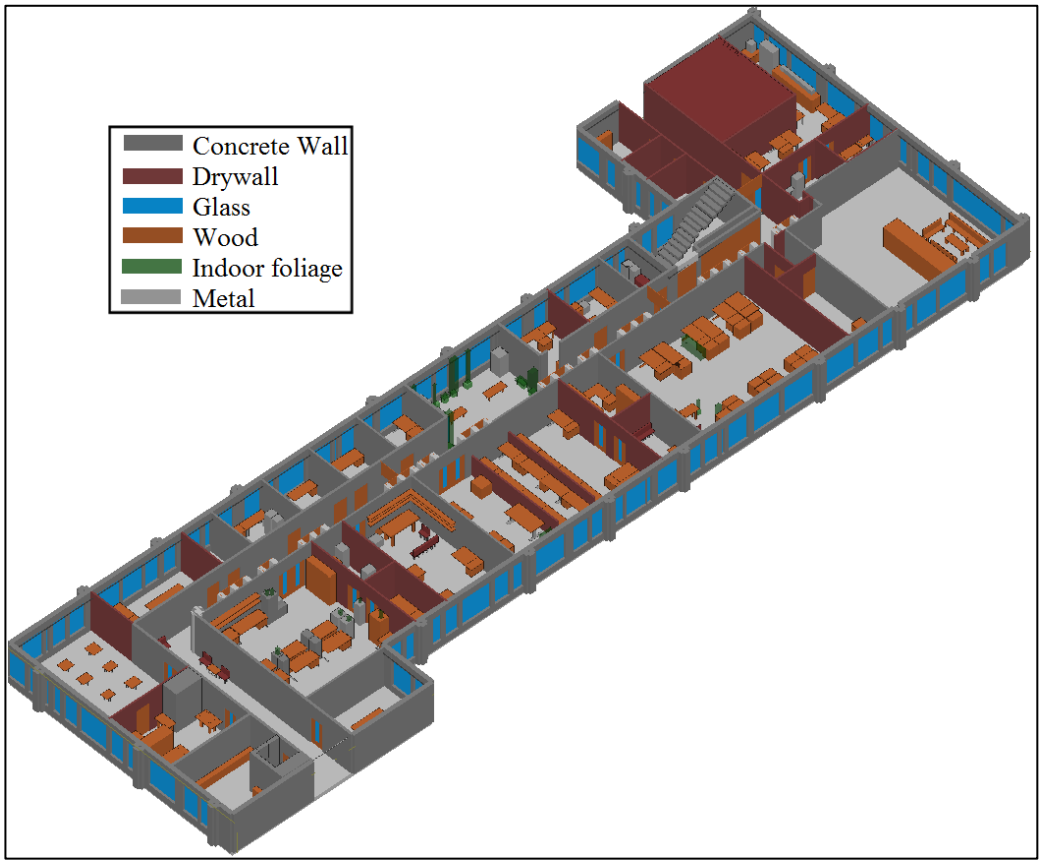

Figure 4.3: The simulated environment for the 3rd floor in Chesham building, University of Bradford.

4.4 Results and Discussion

4.4.1 Simulation Results

Table 4-5 RMSE (in dB) of the examined error (Simulation part)

	EWLM	AWM	OSM	LAM	PM	MKM	DSM
1	7.6	10.4	12.4	10.9	9.8	8.3017	7.8
2	5.3	6.4	5.7	6.4	8.5	6.1118	8.1
3	5.3	6.4	9.2	8.1	7.2	5.549	6.5
4	14.9	15.6	13.1	12.9	12.6	11.2973	14.7

Table 4-5 summarises the simulation results for the examples presented in this chapter, where row 1, 2, 3 and 4 represent RMSE for the examined indoor path loss prediction models of different routes in the environment at 5.3 GHz using VP antenna, 2.4 GHz using VP antenna, 73.5 GHz using CP antenna and 60 GHz using CP antenna respectively.

A comparison between different indoor path loss models at 5.3 GHz using vertically polarized antenna is shown in Figure 4.4; RMSE of the examined models are presented in Table 4.5, row 1. In this scenario, the EWLM outperforms other models as it was able to capture the changes in the environments. After each wall, the model makes a correction factor either adding gain or adding a loss to fit the simulation data. In the AWM, the first two walls loss give positive gain to the averaging, as a result, the model underestimates SS fading. MKM works fine as long as the signal level follows semi-monotonic decrease.

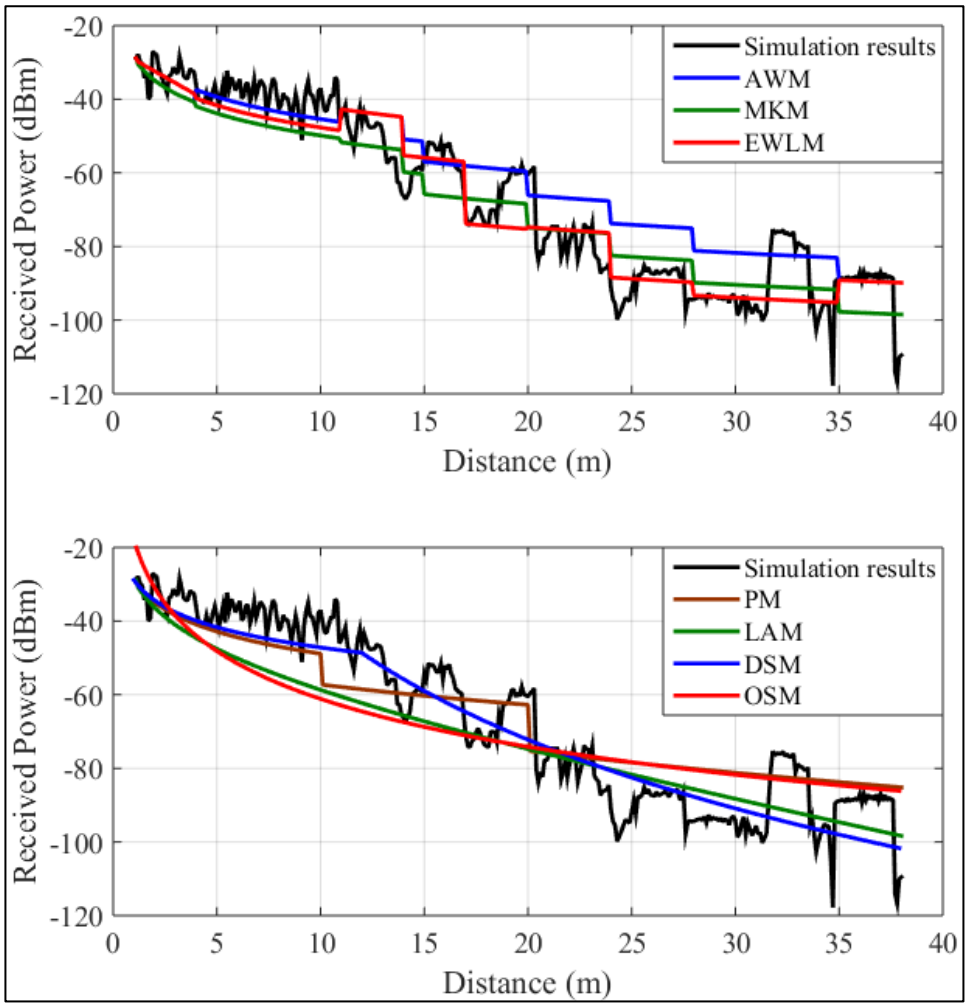

Figure 4.4: Indoor path loss prediction models comparisons for a route in the environment at 5.3 GHz using a vertically polarized antenna.

As provided from the RMSE values, both OSM and LAM models show low performance; this may be due to the difficulty to model the simulation data with a monotonic function. The DSM uses two slopes to describe the changes in the environment. Due to this flexibility, it has better results compared to OSM. Finally, the PM has different path loss exponents; however, it shows good performance if the test environment has similar path loss exponents to the model.

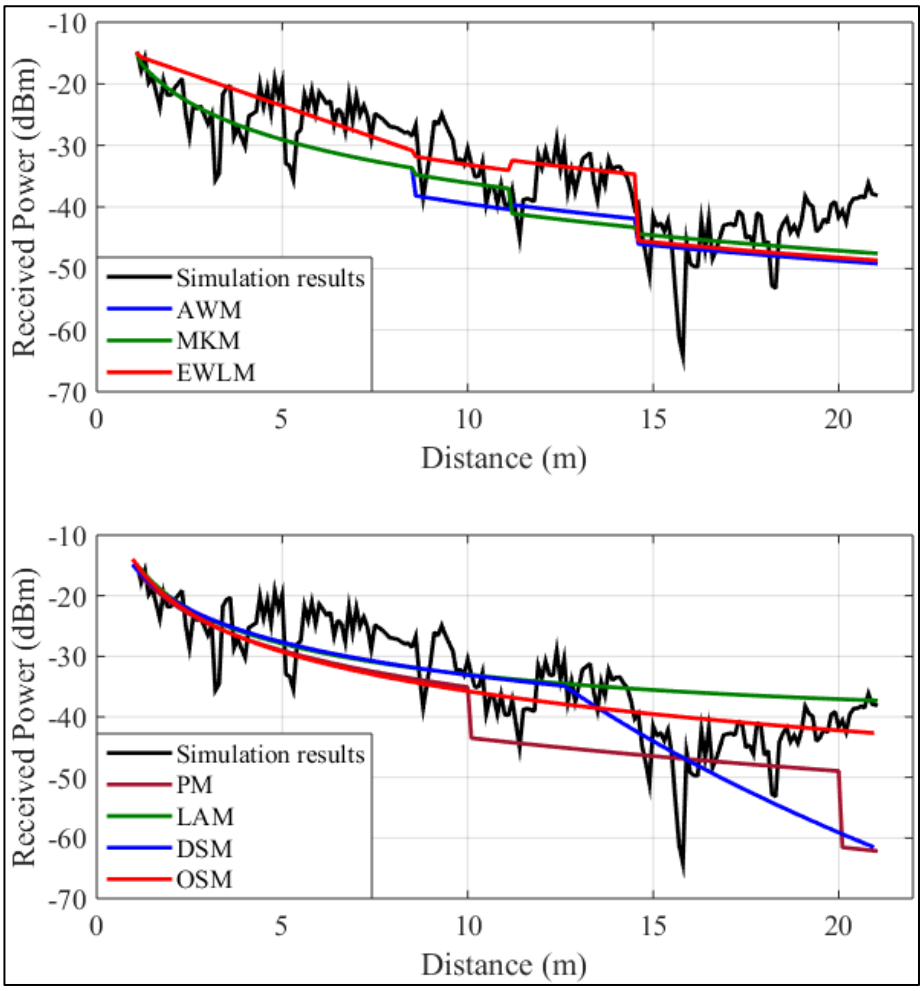

Figure 4.5: Indoor path loss prediction models comparisons for a route in the environment at 2.4 GHz using a vertically polarized antenna.

In Figure 4.5, the mean SS level decays slowly with distance, the RMSE of the examined models are presented in Table 4.5, row 2. EWLM model has the best performance; while OSM has the second best performance as the path loss exponent found to be around 2, this may be regarded due to the wave-guiding effect. The DSM has lower performance compared to OSM, although this model uses two path loss exponents which gives more flexibility, the model requires more data in order to provide accurate prediction. In this scenario and using lower frequencies, there will not be much loss due to propagation through drywalls. As a result, the correction factors will have less significant effect; however, considering the wave-guiding effect gives EWLM advantage over AWM as seen

in Figure 4.5. While at higher frequencies, propagation through these walls will lead to greater losses; therefore, the correction factors will have more impact as shown in Figure 4.6.

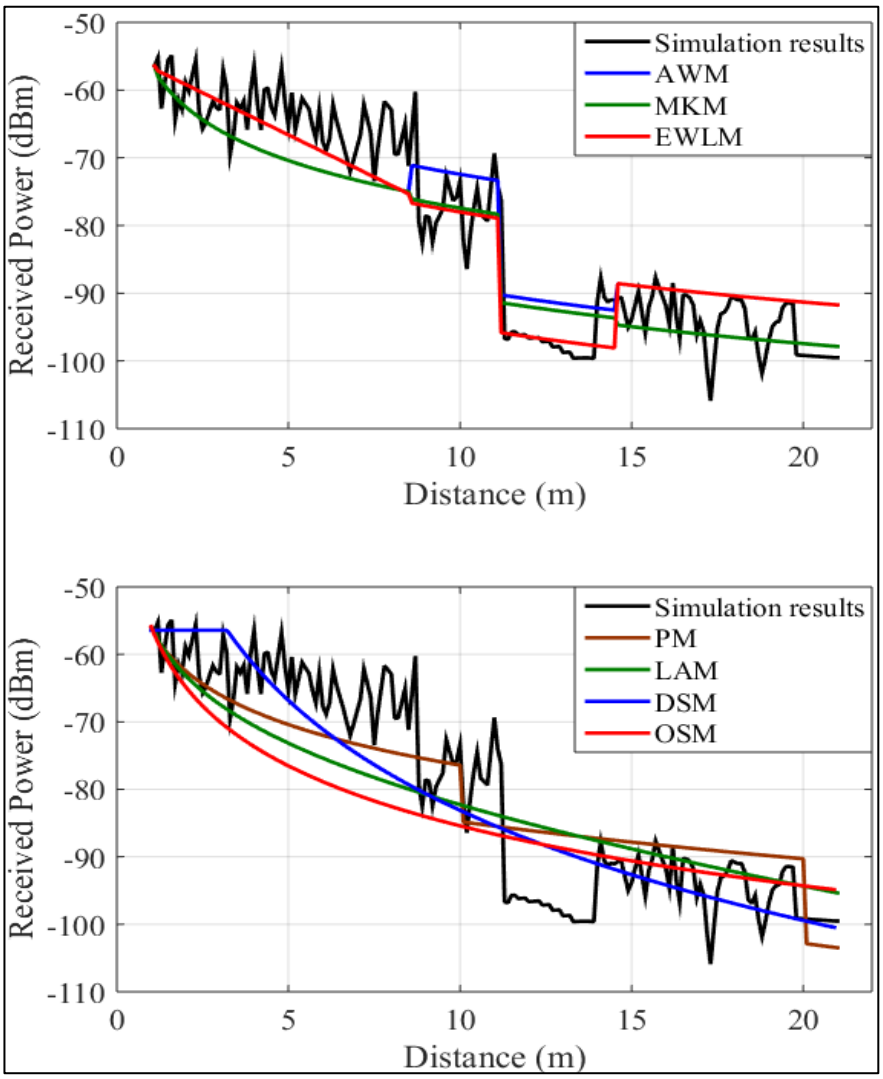

Figure 4.6: Indoor path loss prediction models comparisons at 73.5 GHz and circular polarization for the same route in Figure 4.5.

In Figure 4.6 simulation results are presented for the same route whose results are shown in Figure 4.5 but at a higher frequency. The RMSE of the examined models are presented in Table 4.5, row 3. In comparison, models which use free space path loss exponent (n=2) and add walls losses (i.e. EWLM, AWM and

MKM) or models use fixed values of n like PM are both expected to have better performance, this is due to fact that wall losses tend to be greater as frequency increases as indicated in metrics presented in Table 4.5. At higher frequencies, walls contribute to loss significantly; as a result, the OSM will have less accurate estimation while the DSM has an advantage from having two slopes and hence shows more stability.

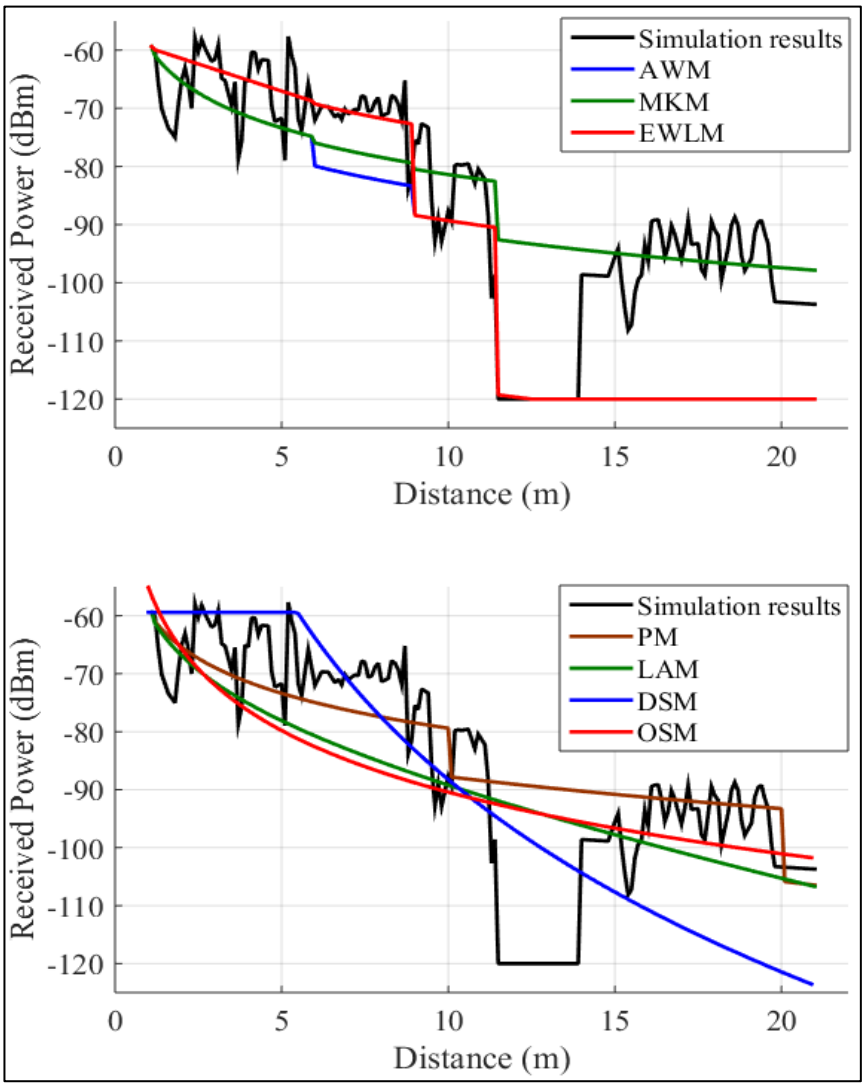

Figure 4.7: Indoor path loss prediction models comparisons at 60 GHz and circular polarization for a route in the environment.

In Figure 4.7 many models predict the SS sufficiently in the first 11 m and in the last 7 m; however SS level follows unpredicted behaviour in the 11-14 m window where most of them find difficulties to capture these changes as provided by their corresponding RMSE values which are presented in Table 4.5, row 4, in this scenario the MKM has the best performance.

Through the experiment, the average RMSE shows an increase as frequency increases as shown in Table 4-6. Almost all models have larger RMSE values at 28 and 60 GHz compared to the 73.5 GHz band. This increase varies from one model to another as shown in the table, in performance comparison for the models using VP antenna CP antenna, the table shows that for AWM, OSM, MKM, LAM and PM have higher RMSE for VP antenna. The EWLM has similar performance for both types of antenna, especially for mm-wave frequencies.

Table 4-6 Average RMSE (in dB) with frequencies for examined models

Model	2.4 GHz		5.3 GHz		28 GHz		60 GHz		73.5 GHz	
	VP	CP	VP	CP	VP	CP	VP	CP	VP	CP
EWLM	5.0	5.6	4.7	6.3	10.8	10.8	10.5	9.7	8.6	8.7
AWM	8.5	7.1	8.4	10.23	15.9	15.6	11.9	10.6	9.6	8.8
OSM	7.6	7.8	9.0	10.0	15.5	13.6	13.7	11.7	13.8	11.1
LAM	8.3	8.4	9.5	10.5	16.7	14.1	13	11.8	13.6	11.1
PM	16.5	15.7	16.9	15.5	16.9	16.2	14.3	12.4	15.3	12.5
MKM	9.8	8.7	10.1	11.1	13.4	12.4	11.3	10.0	9.7	9.1
DSM	5.8	6.1	7.5	8.7	12.6	13.8	11.3	10.1	11.1	9.3

As mentioned earlier, MKM adopts values for wall losses to give the best fit for simulations; Table 4-7 shows the values given for drywall and concrete walls for the used frequencies; losses for concrete walls and drywall tend to increase with frequency. They also tend to be larger in the case of VP compared to CP; this is because when a singly reflected CP signal with angle of incidence is smaller than

Brewster angle it will be orthogonally polarized to the LOS component which leads to reduction in multipath interference [54], moving further away from the transmitter, incidence angles become greater than the Brewster angle.

Table 4-7: Wall losses using MKM

Frequency (GHz)	VP		CP	
	Drywall	Concrete	Drywall	Concrete
2.4	1	4	1	3
5.3	1	6	1	5
28	3	7	1	8
60	1	21	1	10
73.5	3	20	1	13

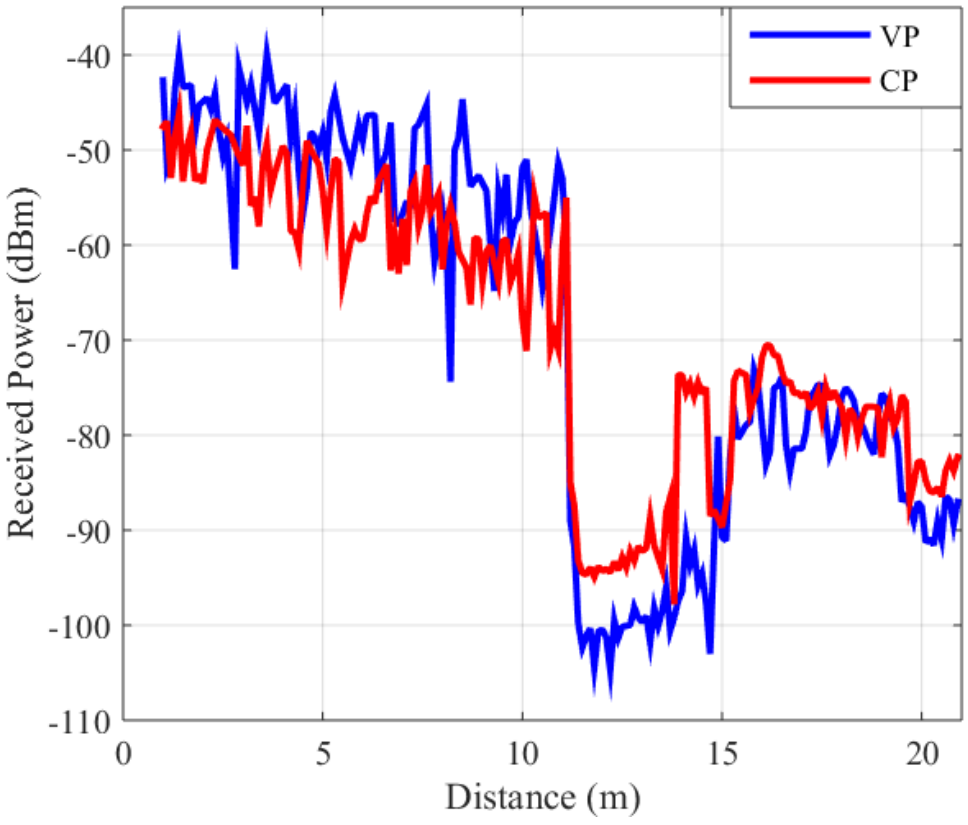

Figure 4.8: Received Power comparison between simulated VP and CP propagation at 28 GHz.

Figure 4.8 presents an RSS comparative behaviour with the distance between VP and CP at 28 GHz, the higher SS in the CP case as the receiver is moving further away from the AP can be explained by the effect of the multipath interference reduction as mentioned above. As shown in the incoming discussion, the examined model parameters are found to have less values in the case of CP.

The average path loss exponent versus operating frequency for OSM is plotted in Figure 4.9; for VP antenna, n tends to increase as frequency increases. However, in the case of CP antenna, the average value of n tends to decrease as frequency exceeds 28 GHz. This is may be explained due to radio coverage reduction occurred as frequency increased; hence, a lower value for n is obtained.

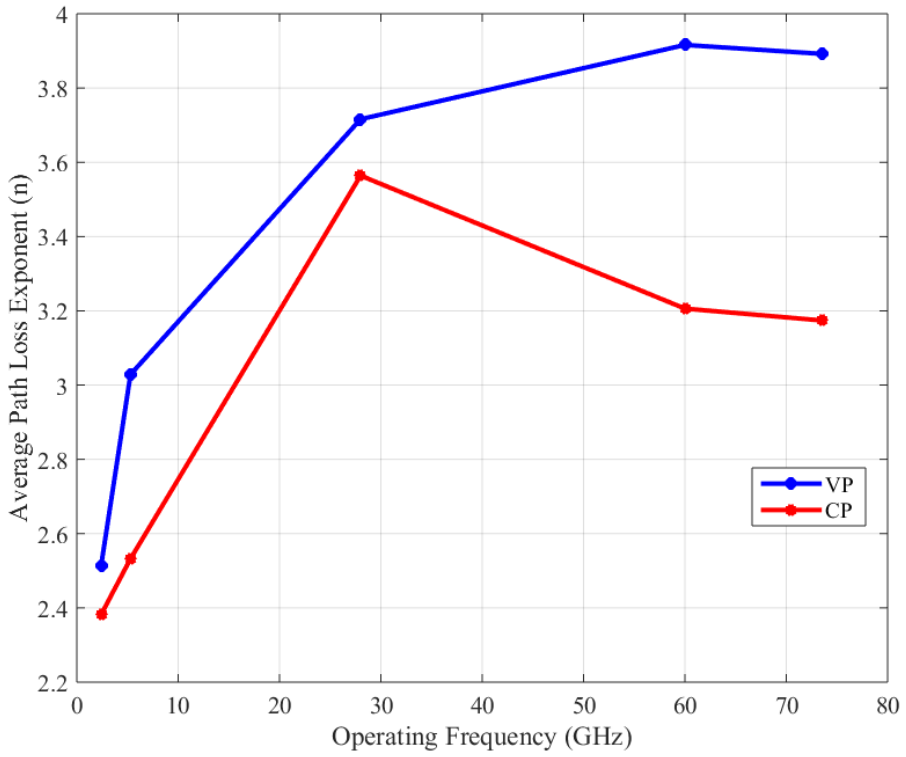

Figure 4.9: OSM path loss exponent relationship with operating frequency.

The value of n for the corridor shown in Figure 4.1 tends to have a slight dependency on the examined frequencies as it has an almost fixed value equivalent to 0.9 in the case of VP and (0.6-0.9) in the case of CP.

Path loss exponent is influenced by changes in frequency, polarization and depending on route location within the floor. For example, using 60 GHz and CP antenna, n in corridor routes due to waveguiding effect found to have a value of 1, while using VP antenna for the same route it has a value of 1.7. In the case where the path is between rooms, where walls are made from concrete, using VP antenna, n reached a value of 5.

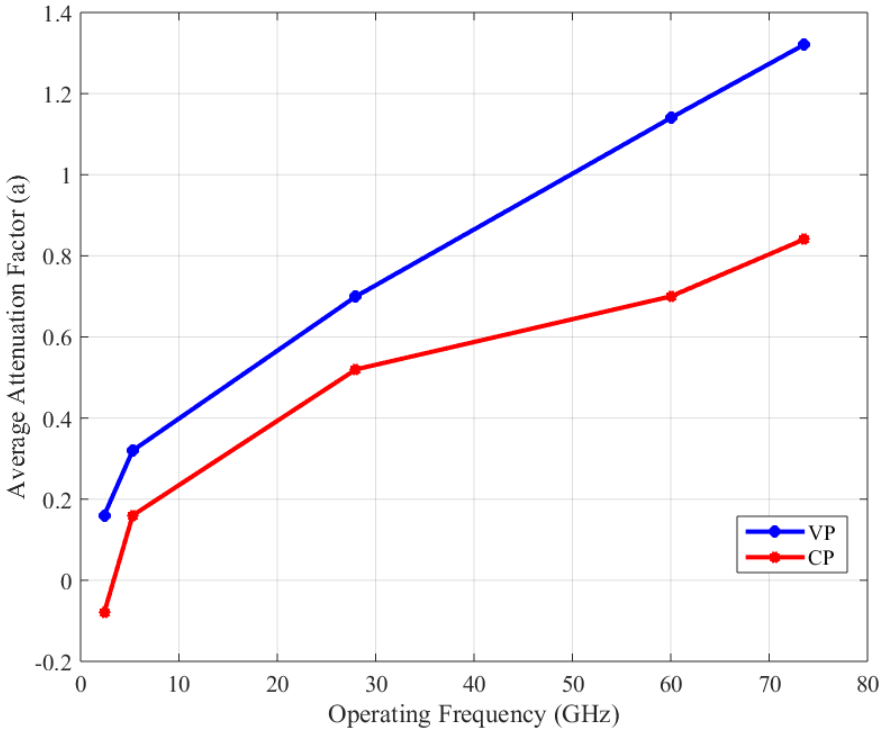

Figure 4.10: Linear attenuation factor relationship with operating frequency.

The relationship between average attenuation factor and frequency for LAM model is shown in Figure 4.10. As expected a increases as frequency increases,

VP antenna has higher attenuation factor than circular polarization antenna. The mean value for a for VP and CP are: 0.67 dB/m and 0.367 dB/m respectively. Considering Figure 4.9 and Figure 4.10, a similarity between OSM and LAM is observed, as the variation of n and a are very similar for many routes on different frequencies and polarization.

This also is proved by Figure 4.11, as shown both models have similar performance provided from their corresponding RMSE for almost 40% of tested scenarios. Whilst OSM has better performance for frequencies 2.4, 5.3 and 28 GHz, LAM has better performance for frequencies over 28 GHz.

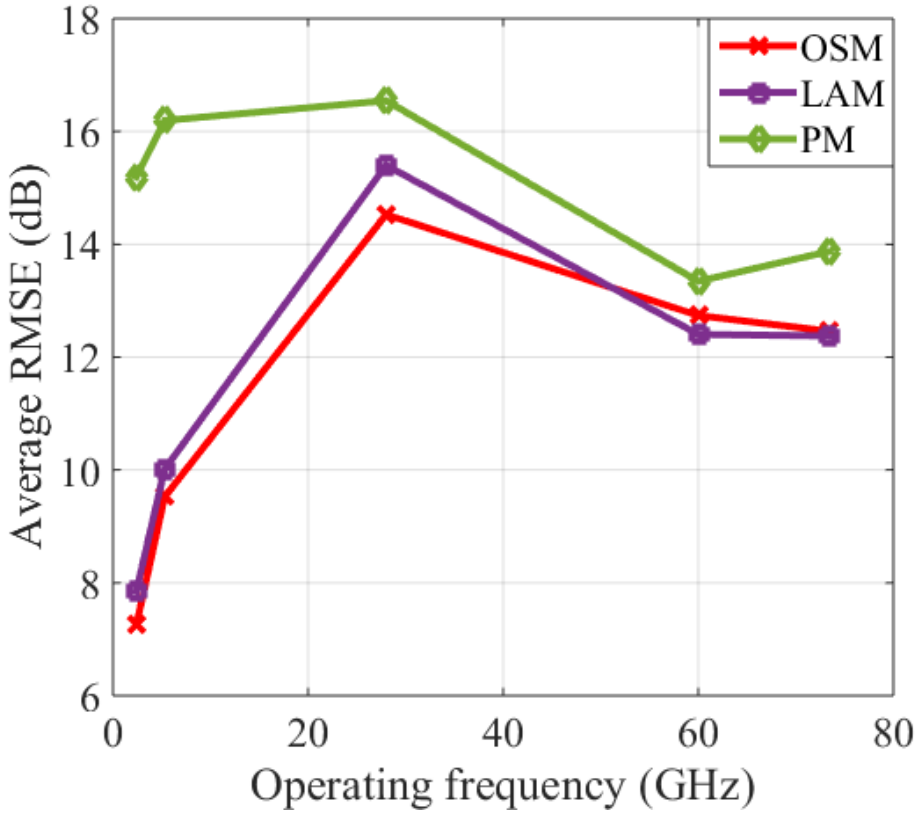

Figure 4.11: Performance comparison between LAM, OSM and PM.

The figure also presents PM performance which shows the poorest performance among all the models due to its limitation by having fixed path loss exponents

over predefined distances; however, the model seems to have better performance for 60 and 73.5 GHz.

A comparison between OSM, DSM and MKM is demonstrated in Figure 4.12. DSM outperforms both OSM and MKM as it has less RMSE compared to OSM for almost 72.5% of tested scenarios and less RMSE compared to MKM for 60.8% of tested scenarios. For lower frequencies range of this experiment, DSM outperforms MKM, while for millimetre waves MKM has better performance. This can be regarded due to the effect of wall losses in SS fading which is considered by MKM. OSM and DSM show a similar pattern with an obvious advantage for the DSM, due to the latter's flexibility as it has two values for n. The model can capture propagation changes in the environment more efficiently; the gap between the two models increases as frequency increases. On the other hand, MKM outperforms OSM as it has less RSME for almost 62.75% of tested scenarios. It can also be observed that for higher frequencies, both DSM and MKM are preferable compared to OSM.

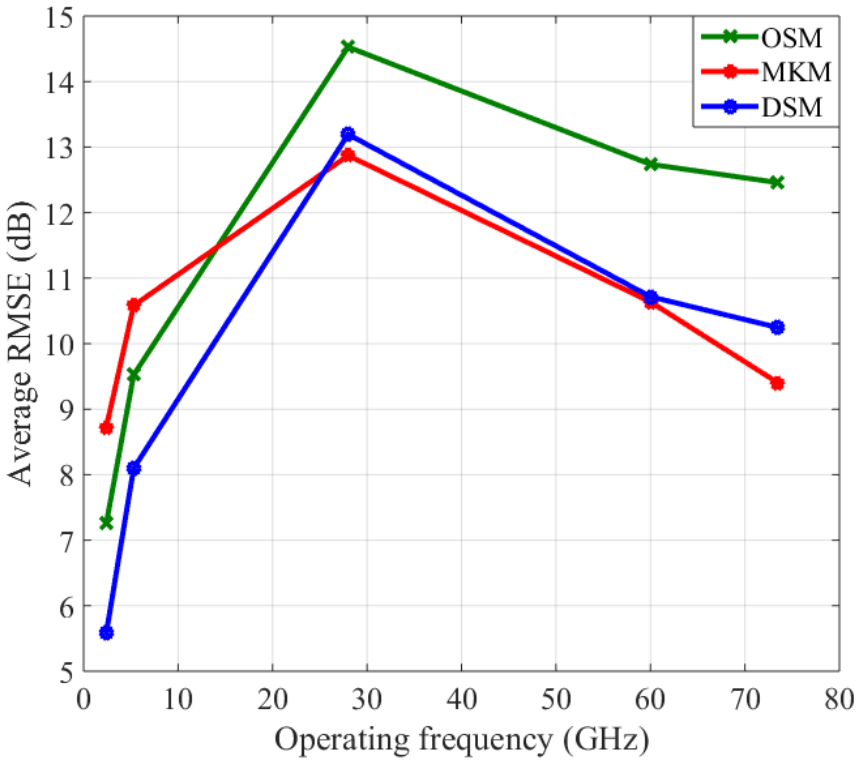

Figure 4.12: Performance comparison between DSM, MKM and OSM.

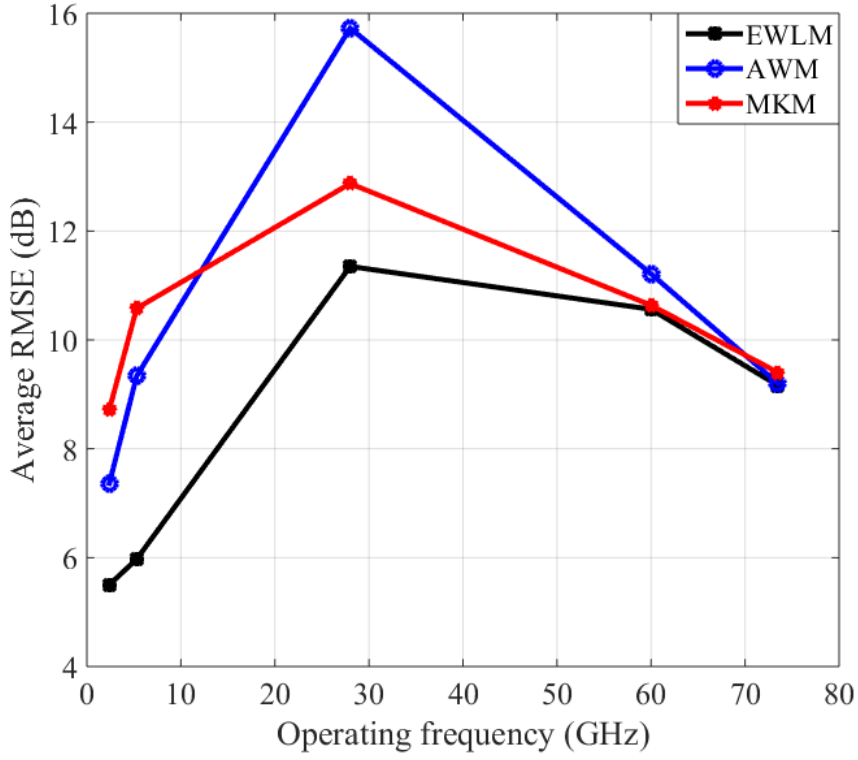

Figure 4.13: Performance comparison between EWLM, AWM and MKM.

A comparison between EWLM, AWM and MKM is shown in Figure 4.13. EWLM shows better performance than MKM and AWM for almost 78.4% and 80.4% of tested scenarios respectively. The model has such advantage because the use of effective wall correction factors enhances SS prediction significantly. When comparing AWM with MKM, the former has less RMSE for almost 56.9% of tested scenarios. The AWM has also better performance in the 2.4, 5.3, 73.5 GHz regions, while it has comparable performance at the 60 GHz. It may be observed that at 28 GHz the AWM has lower performance. This is due to the effect of averaging which makes SS prediction less accurate at higher frequencies; however, as frequency increases the radio wave coverage becomes smaller. Therefore, the encountered walls become less, in such case the AWM works better. It was also observed that when all the walls encountered are of the same type (i.e. either all are concrete or drywall) the performance of AWM is always lower than EWLM.

Considering models performance at all frequencies, DSM shows the second-best performance, a comparison between EWLM and DSM is presented in Figure 4.14; the metrics show better performance for EWLM as it has less RMSE for almost 66.67% of the tested scenarios. At 2.4 GHz DSM has comparable performance with the EWLM; however, as the operating frequency increases, EWLM tends to have better results. This is due to considering effects of wall losses as mentioned earlier.

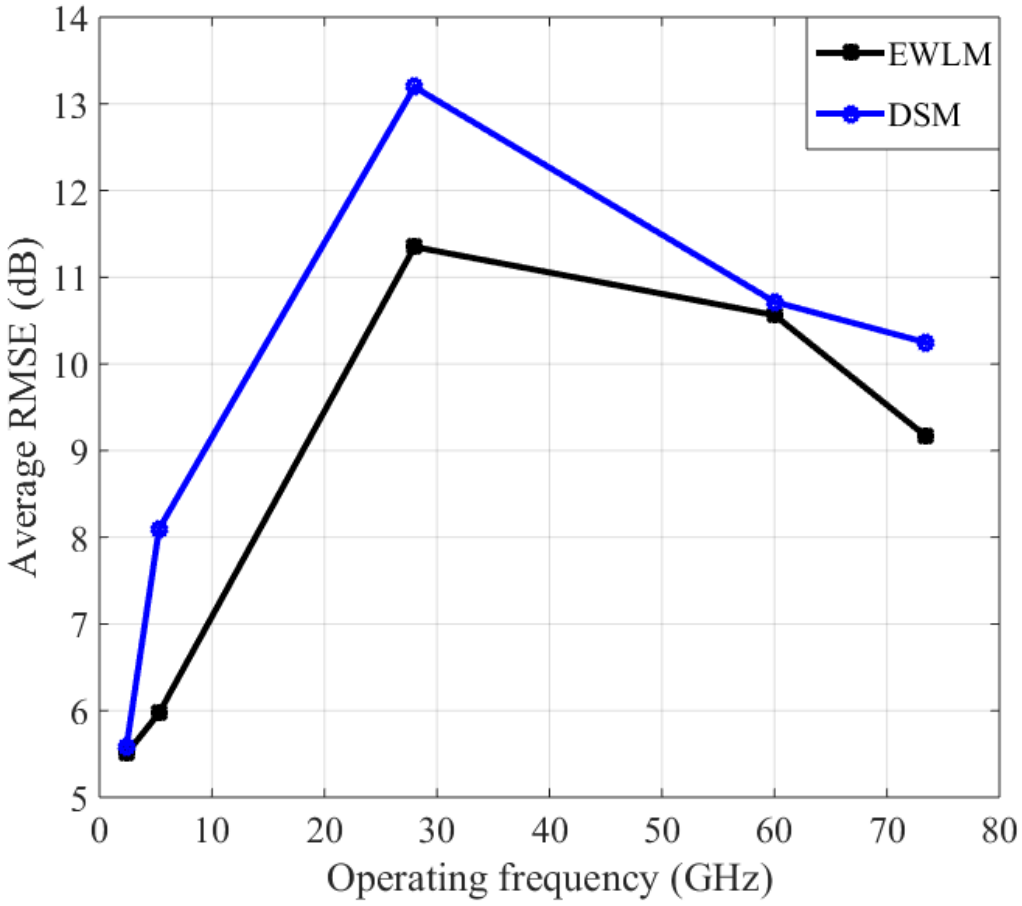

Figure 4.14: Performance comparison between EWLM and DSM.

The average error for most models reaches a maximum at 28 GHz. This can be explained as follow: as the frequency increases the radio coverage tends to become shorter, so it will have less error. Although at 28 GHz the coverage was less compared to 5.3 and 2.4 GHz; however, signal variations tend to be greater; therefore, errors are greater. While at 60 GHz and 73.5 GHz the radio coverage becomes much smaller; thus, errors are less compared to 28 GHz. One interesting observation noted, although both 60 GHz and 73.5 GHz share the same radio coverage, errors at 60 GHz are greater; this might be because the 60 GHz has more fluctuations compared to 73.5 GHz.

Although AWM has the advantage of being fast prediction model, it comes at the expense of accuracy. EWLM combines accuracy and speed. The PM has the lowest performance as it has pre-determined values for n, in comparison to EWLM it has less RMSE for less than 7.8% of tested scenarios.

Table 4-8: Percentage of having the least RMSE (ordered by average RMSE)

Model	Percentage of the least RMSE	Average RMSE (RMSE)
EWLM	51%	7.7
DSM	22%	9.3
AWM	9.5%	10.5
MKM	9.5%	10.5
OSM	6%	11
LAM	0%	11.3
PM	2%	15.4

The order of the best models according to their RMSE values is EWLM, DSM, MKM, AWM, OSM, LAM then PM; their respective average RMSE for all scenarios at all frequencies are shown in Table 4-8. EWLM has the best performance while PM has the worst performance.

Table 4-8 also shows the percentage of having the least RMSE for each model over all scenarios and frequencies; EWLM was considered as the one with the least RMSE for 51% of all scenarios while DSM has a percentage of 22%. Considering these results EWLM is an attractive model, especially for mm-wave frequency usage.

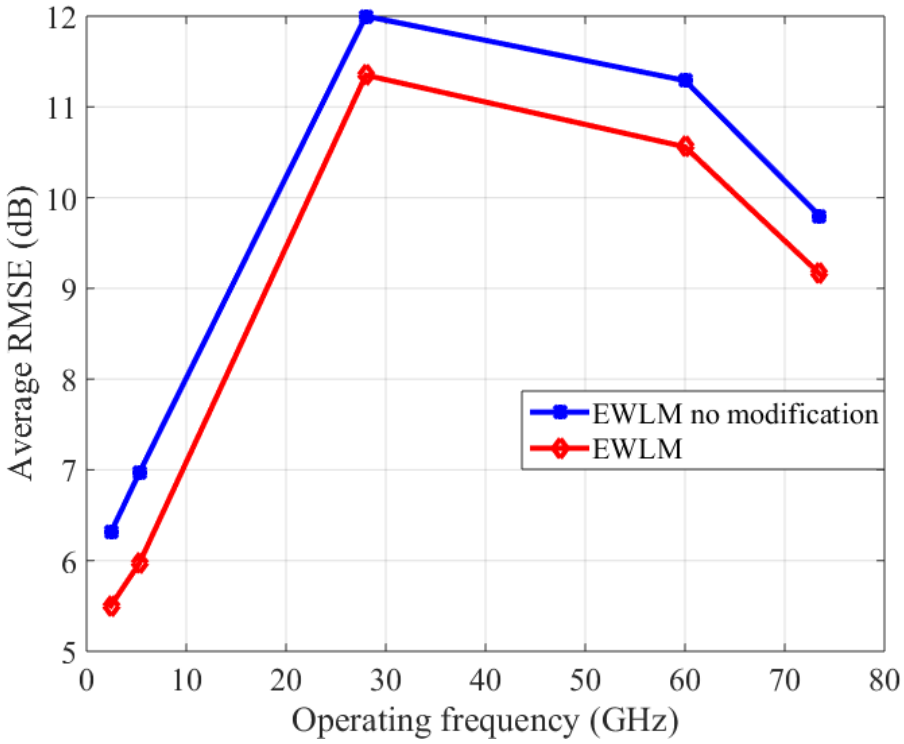

Figure 4.15: Enhancement on EWLM by considering the effect of LOS propagation.

A comparison between the EWLM with no modification (where *n*=2 for all scenarios) and with enhancement (*n* is estimated by best fitting for LOS propagation and 2 for NLOS propagation) is presented in Figure 4.15, on average the RMSE for all frequencies had reduced by about 1 dB. Compared to other models “EWLM with no modification” had the least RMSE for 27.45% of all tested scenarios; however, by considering the effect of LOS and wave guiding effect, the percentage was enhanced to 51% as mentioned above.

In Figure 4.16 correction factor for concrete wall found to increase linearly with increasing the operating frequency in the range of (5.3-60 GHz) for both VP and CP cases. While correction factor for drywall tends to vary linearly with frequency range (5.3-73.5 GHz) for VP and in the range (5.3-60 GHz) for CP. For both types

of wall, mean wall correction factor tends to be larger for VP compared to CP especially at large frequencies.

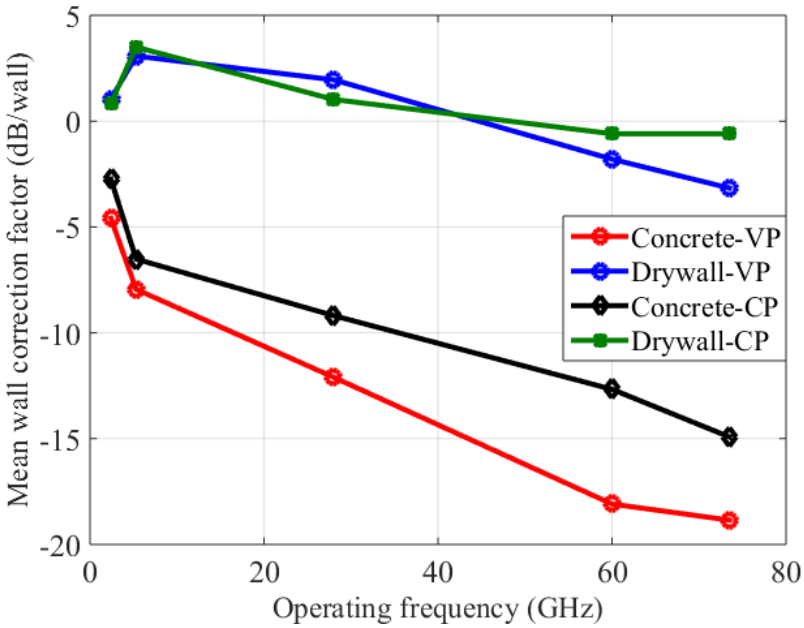

Figure 4.16: Mean wall correction factor relationship with operating frequency for concrete and drywall.

4.2.2 Experimental Results

The experimental study in this chapter includes same models investigated in the simulation part in addition to DPM. Figure 4.1 represents measurements collected in 3rd floor, measurements were taken in different routes to examine more possible scenarios where walls are made from concrete and drywall. It was observed that radio coverage for 5 GHz band is slightly larger than radio coverage for 2.4 GHz band, this can be explained as the former's antenna gain is larger which tends to increase as frequency increases.

A comparison between investigated models is presented in Figure 4.17 where data are collected from route 2-2 (shown in Figure 4.1) at 5.3 GHz. It's expected to have a semi-monotonic RSS decaying. The RMSE for the EWLM, AWM, OSM, LAM, PM, MKM DSM and DPM in dB are 4.3, 5.5, 6.0, 5.5, 7.6, 6.0, 4.9 and 14.2 respectively.

As the first wall is close to the transmitter the correction factor will add more accurate estimation to the results, EWLM has the best performance, the AWM also shows a good resolution; however it shows less performance compared to EWLM, this is due to the effect of last wall loss on averaging which cause the SS prediction to be pessimistic. Since the RSS follows a semi-monotonic decaying OSM, LAM, MKM and DSM show a good performance, the PM use fixed values of n, which underestimate the actual losses in this scenario. DPM uses predefined values for building wall losses; however the performance was pessimistic, this may be due to the wall losses recommended are not for universal use as authors claims; also the model has no difference in performance from other wall loss models if the direct path between the transmitter and the receiver is the path with least losses.

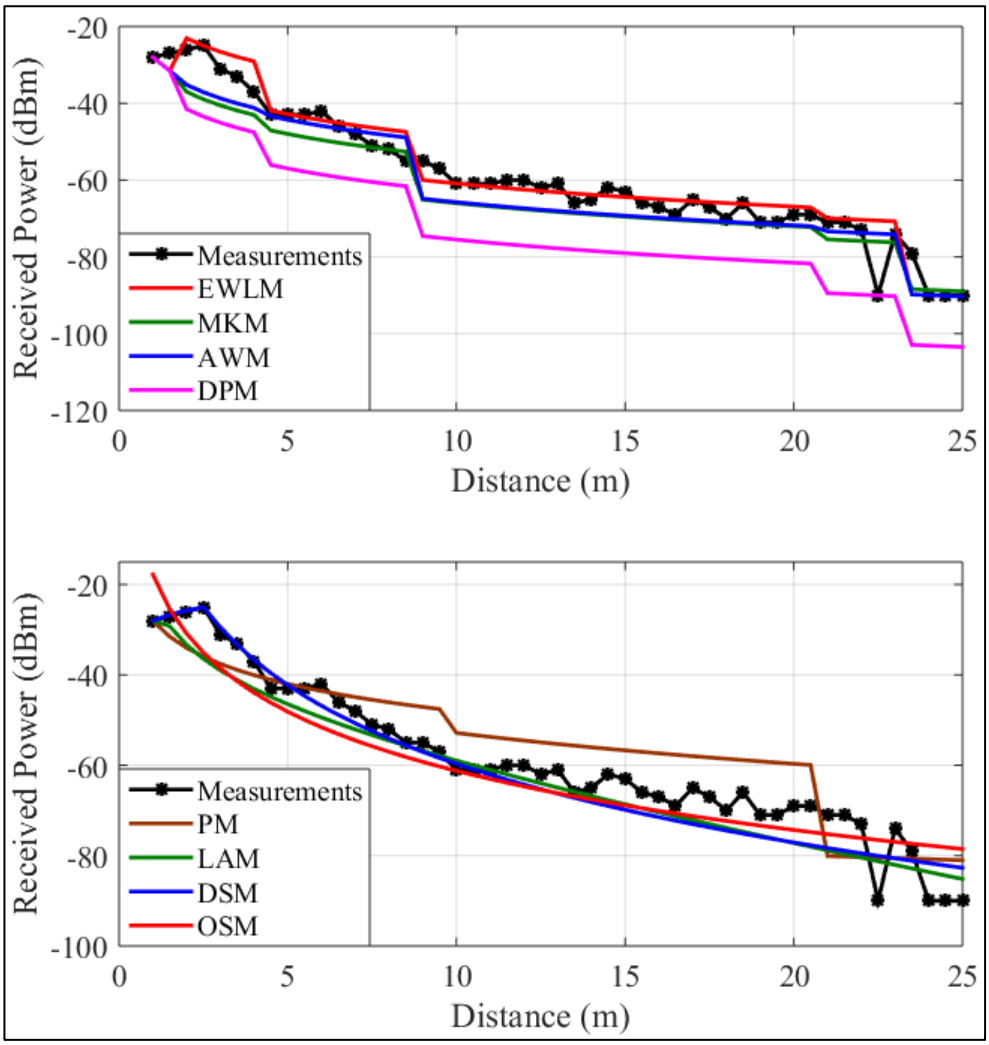

Figure 4.17: Indoor path loss prediction models comparisons at 5.3 GHz for route 2-2 in the environment.

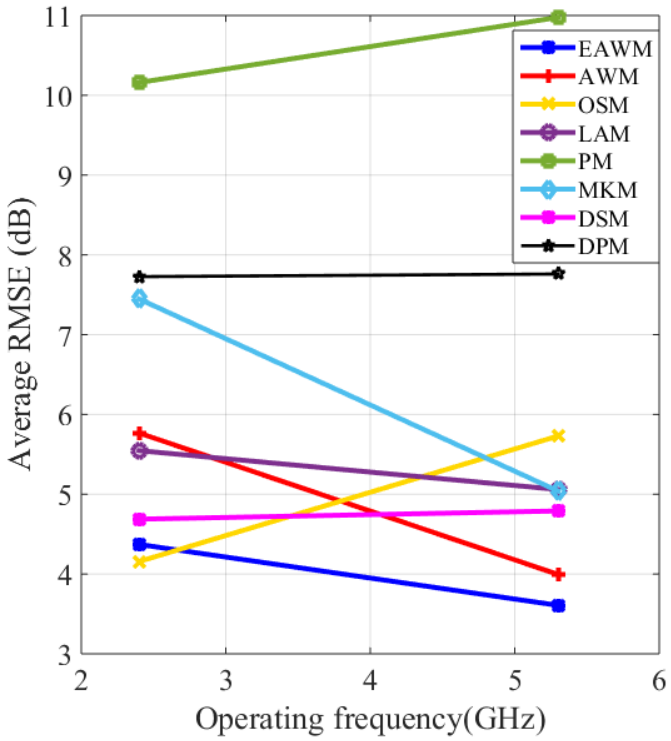

Figure 4.18: Average RMSE for all models.

Table 4-9 Statistical metrics (in dB) between measured and simulated data for the presented models at 2.4 GHz

Model	Max. Error	Min. Error	STD	RMSE
EWLM	6.1	2.9	1.2	4.4
AWM	8.5	3.0	2.1	5.8
OSM	6.6	3.4	1.2	4.2
LAM	8.2	3.9	1.7	5.5
PM	15.4	5.8	3.4	10.2
MKM	11.5	3.7	2.9	7.4
DSM	7.0	3.1	1.41	4.7
DPM	14.3	4.3	4.11	7.7

A comparison between all presented models is introduced in Figure 4.18, the total error for all routes are averaged. For the 2.4 GHz, as shown from the figure and Table 4-9, the OSM, DSM and EWLM have the best performance. Similar to observed results from simulation part, EWLM has the most stable performance as the maximum error did not exceed 6.1 dB and the standard deviation (STD) of errors is around 1.2 dB. PM, DPM and MKM have low accuracy, as the maximum error exceeds 15 dB, 14 dB and 11 dB respectively, while their STD are 3.4 dB, 4.1 dB and 2.9 dB respectively. The LAM and AWM have comparable performance as provided by their metrics.

Similar to PM, DPM uses predefined wall losses; therefore, the performance was poor as seen by the presented metrics. The advantage of using this model is limited to scenarios where the transmitter and receiver are separated by one/multi walls and there is another path which encounters less number of walls; however, in many cases the best path is the shortest in distance between the transmitter and receiver which return this model to be similar to multi-wall models.

Using higher operating frequency, the EWLM has the best performance provided that it has the lowest values for all metrics as shown in Table 4-10; the metrics are consistent with the observed results in the simulation part. The AWM has the second-best performance and still show good results in terms of accuracy and stability. The DSM and LAM show comparable performances. The former performance degraded with increasing frequency; however, it still has a stable and accurate estimation.

Table 4-10 Statistical metrics between measured and simulated data for the presented models at 5.3 GHz

Model	Max. error	Min. error	STD	RMSE
EWLM	4.6941	2.4044	0.7903	3.60744
AWM	5.6672	2.5276	1.2646	3.9943
OSM	8.4177	4.4267	1.3921	5.7298
LAM	6.2044	3.3204	1.121	5.0591
PM	14.1389	7.62	2.2813	10.9763
MKM	9.0968	3.0752	2.1387	5.0392
DSM	6.6239	4.0949	0.973	4.7900
DPM	14.1928	3.9692	3.7557	7.7599

Table 4-11 Wall loss using MKM and DPM*

Frequency	MKM		DPM	
	Drywall	Concrete	Drywall	Concrete
2.4 GHz	4	4	2	10
5.3 GHz	3	12	7.5	12.5

**Wall losses using DPM from [246] [56].*

The OSM suffers from poor accuracy this is because of wall losses at a higher frequency which requires more than one path loss exponent to have an accurate estimation. The MKM still suffer from instability; however, it has better performance at 5.3 GHz this is due to the more effective contribution from the walls at higher frequencies which have larger values as frequency increases as shown in Table 4-11. DPM has similar behaviour to what was observed at 2.4 GHz; typical values used for wall losses using DPM are presented in Table 4-11.

Path loss exponent increases as operating frequency increases. Among all tested routes, measurements provided an evidence of path loss exponent dependency on the operating frequency. As observed from the measurements, n varies in the range of (1.93-3.3) at 2.4 GHz and in the range of (3.37-4.35) at 5.3 GHz. The averaged path loss exponent found to be 2.83, 3.89 at 2.4 GHz and 5.3 GHz respectively. Linear attenuation factor also shows an increase as the operating frequency increases. Among the six tested routes, measurements from five routes provided an evidence of linear dependency of the attenuation on the operating frequency; a varies in the range of (0.4-1.6) at 2.4 GHz and (1.2-2.5) at 5.3 GHz. The average attenuation factor for the 2.4 GHz and 5.3 GHz are 0.8166 and 1.6 respectively.

Table 4-12 Averaged RMSE (in dB) for all models

Model	Average RMSE
EWLM	4.0
AWM	4.9
OSM	4.9
LAM	5.3
PM	10.6
MKM	6.2
DSM	4.7
DPM	6.7

The averaged RMSE for all scenarios and frequencies are given in Table 4-12; among all scenarios, EWLM has the lowest RMSE for almost 50% of tested scenarios, whilst DSM has the lowest RMSE for 16.667% of tested scenarios as seen in Figure 4.19. EWLM tends to have better performance as the frequency increase that seems to be consistent with the simulation results.

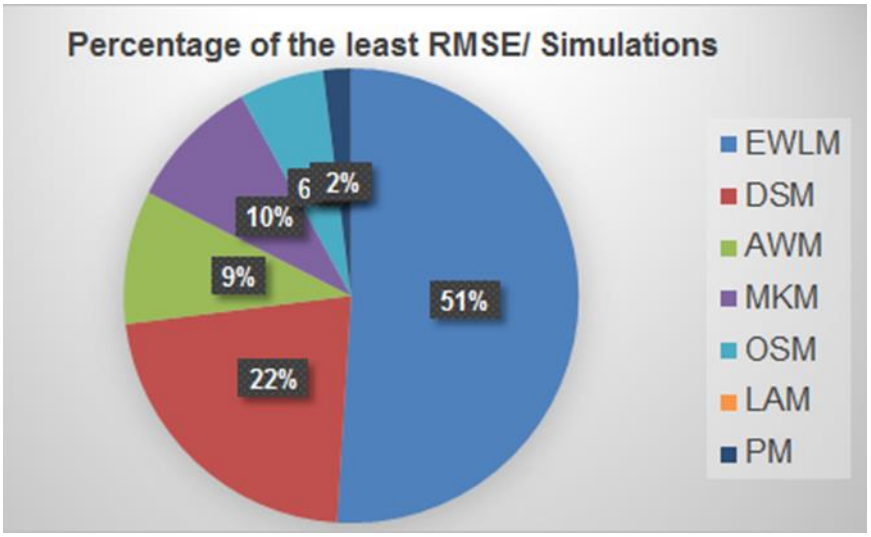

(a)

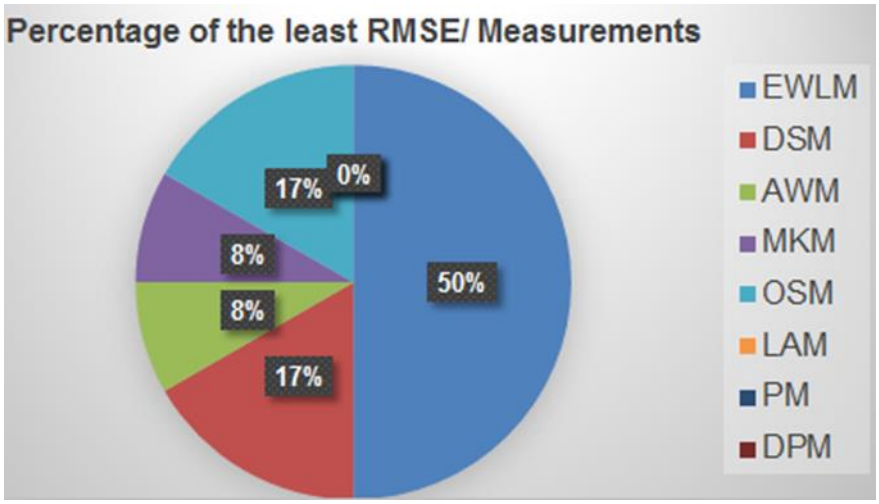

(b)

Figure 4.19: Percentage of the least RMSE

Similar to observations in Figure 4.16, wall correction factor for concrete tends to increase more rapidly as frequency increased while for drywall the steep was smoother.

Wireless InSite Validation with Measurements

So far, in this chapter the proposed model was compare with other models against simulation and measurements, which is the main target. However, comparison between the simulated RSS data and the measured RSS data has not yet been conducted. Therefore, in this section, validation of Wireless InSite

simulated results against the measurements results has been presented. This comparison gives more reliability over the observed results. The comparison was conducted at different routes and frequencies. For both cases (simulation and measurements), similar antenna types, gain, transmitted power and radiation pattern were used. Also, sensors coordinates in the environments for both simulations and measurements were identical.

In Figure 4.20, a comparison is presented between simulation and measurements results for route 1-1 at 2.4 GHz. As seen in the figure, a good agreement between simulation and measurements is observed, as the STD is 3.7 dB.

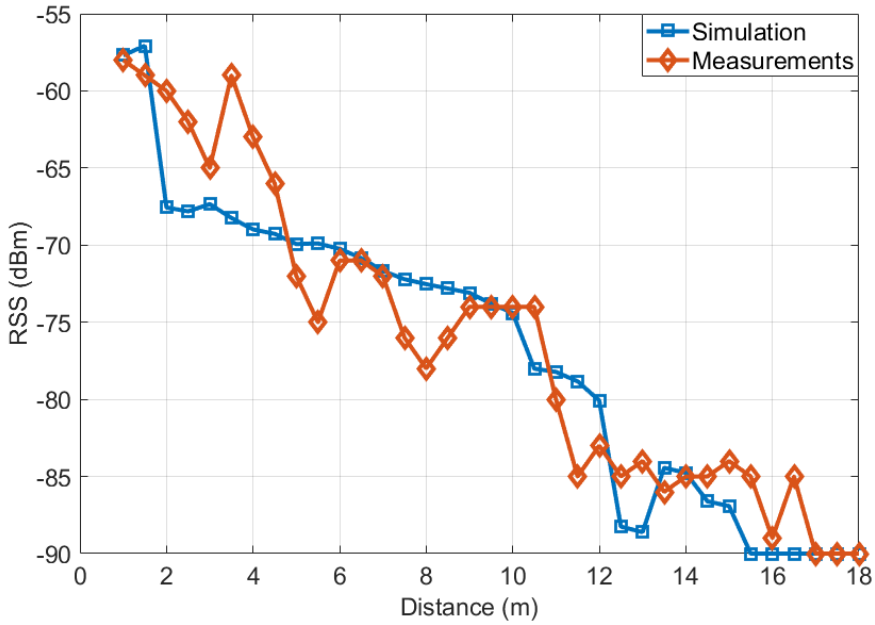

Figure 4.20: Wireless InSite validation against measurements at route 1-1 at 2.4 GHz.

In this scenario, the examined models are generated based on samples taken from the simulation/measurements results, which are later compared to database by estimating RMSE. The RMSE of the examined models for simulation and measurements is shown in Table 4-13. The results shows a good agreement as observed in the table.

Table 4-13: Models RSME comparison between measurements and Simulations for route 1-1 at 2.4 GHz.

Model	Measurement results	Simulation results
EAWM	3.5	4.1
AWM	4.2	5.2
OSM	3.4	4.2
LAM	3.9	4.3
PM	5.8	5.3
MKM	7.7	6.4
DSM	5.7	3.1

Figure 4.21 presents a comparison between simulation and measurements results for route 1-2 at 5.3 GHz. A good agreement between simulation and measurements is observed, as the STD is 4.5 dB.

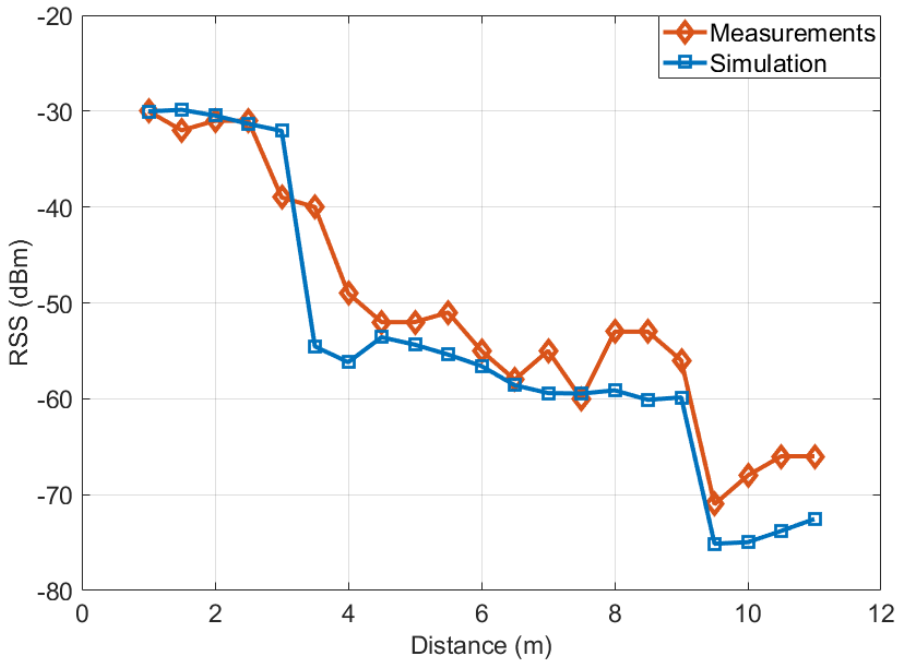

Figure 4.21: Wireless InSite validation with measurements at route 1-2 at 5.3 GHz.

Table 4-14 presents a comparison between the RMSE of the examined models for simulation and measurements, as seen, the results shows a good agreement.

Table 4-14: Models RSME comparison between measurements and Simulations for route 1-2 at 5.3 GHz.

Model	Measurement results	Simulation results
EAWM	3.4	2.2
AWM	3.5	2.9
OSM	6.3	7.7
LAM	4.2	5.3
PM	9.50	11.1
MKM	5.7	2.9
DSM	6.6	6.9

Chapter 5

Local Average Signal Strength Estimation for Indoor Multipath Propagation

5.1 Introduction

Wireless communication engineers frequently experience difficulty with the dynamic behaviour of wireless radio channels. Wireless channels are more susceptible to noise, interference and other hindrances [23]. The challenge, therefore, is to make the channel determinable at any location.

When a signal arrives at a receiver, the signal strength level follows three scales of variations, the largest scale being path loss which is range dependent, where the signal strength level decays exponentially. The second scale is due to shadowing, where the signal strength varies around its mean according to a log-normal distribution, these variations take place over ranges of the order of 10λ-30λ. The smallest scale is due to multipath, where the signal follows a Rayleigh or Rician distribution and variations are of order 0.5λ [247].

Multipath effects can be observed when the mobile terminal moves distances that are short compared to the correlation shadowing distance, hence this is called small-scale fading. Due to these effects, recorded SS at the receiver becomes very sensitive to any small movement. In fact, even if the receiver is stationary, the recorded SS will still vary noticeably; this will make the use of SS in localization impractical and inaccurate.

Researchers have developed techniques to remove the effect of multipath [19] so that the RSS value will be linked to path loss and shadowing only; such integrated representations will make the RSS-distance relationship more tractable. One of the main problems in localization using RSS is the non-monotonic fading of RSS level with distance; such a problem will lead to ambiguity of location estimation.

For example, Figure 5.1 shows the RSS data along a building hallway that was simulated using Wireless InSite ray tracing software: when the mobile's RSS equals -35 dBm there are five possible locations for the mobile; the range of error is around 17 m which is intolerable for localization purposes within indoor environments. The main objective is to make this relationship unambiguous (i.e. monotonically decreasing). A possible way to achieve this is to average over local area to remove the effects of fast fading [19].

5.2 Vector Sum vs. Power Sum Prediction Methods

In ray tracing techniques there are two methods to perform averaging: the first method takes the power sum of all multipath rays, which is known as "*Power sum prediction (PS)"* [19]

$$\langle P_{PS} \rangle = \sum_{M} P_M \tag{5.1}$$

where $\langle P_{PS} \rangle$, M and P_M are the averaged power using the PS method, number of multipath rays and power of each individual ray respectively. The second method takes the average of the squared sum of all electric fields (amplitude and phases), known as "*vector sum prediction (VS)"* [19]:

$$\langle P_{VS} \rangle = \left| \sum_{M} \sqrt{P_M}\, e^{-j\varphi_M} \right|^2 \tag{5.2}$$

where $\langle P_{VS} \rangle$ is the averaged power using the VS method and φ_M is the Mth ray phase in radians.

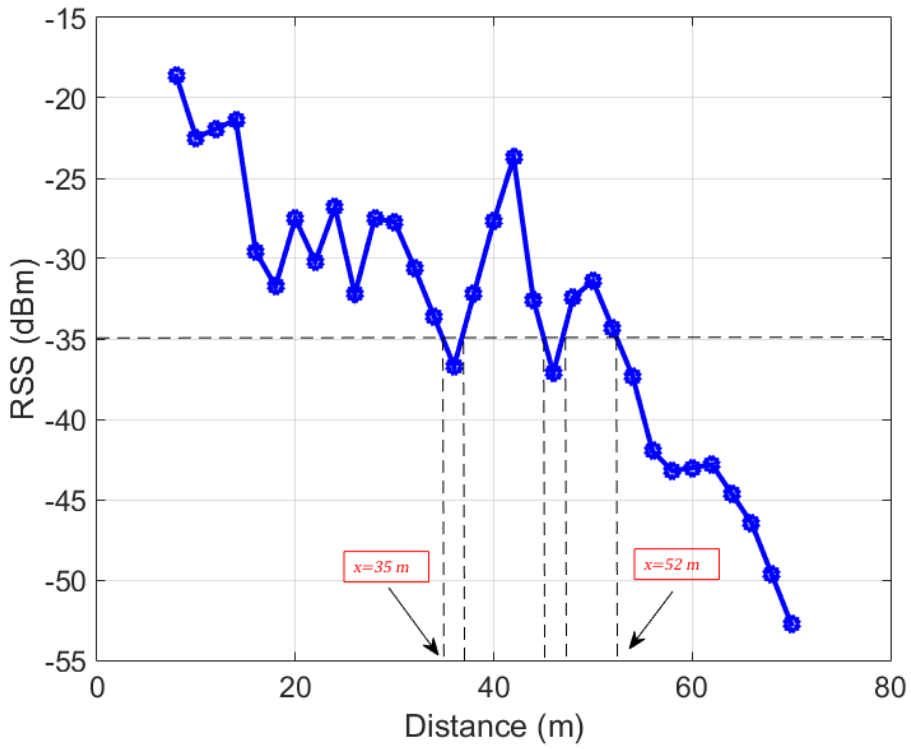

Figure 5.1: RSS-distance ambiguity problem.

In [248] PS is recommended to be used for frequencies higher than 2 GHz, while VS is recommended for lower frequencies. In [19] the PS method is stated to be faster and better; however, it is difficult to implement practically as it requires the receiver to be able to distinguish all incoming rays so that the effect of each ray's phase will be removed; this process requires a huge array antenna to detect arrival angles and also requires very large bandwidth to detect delays.

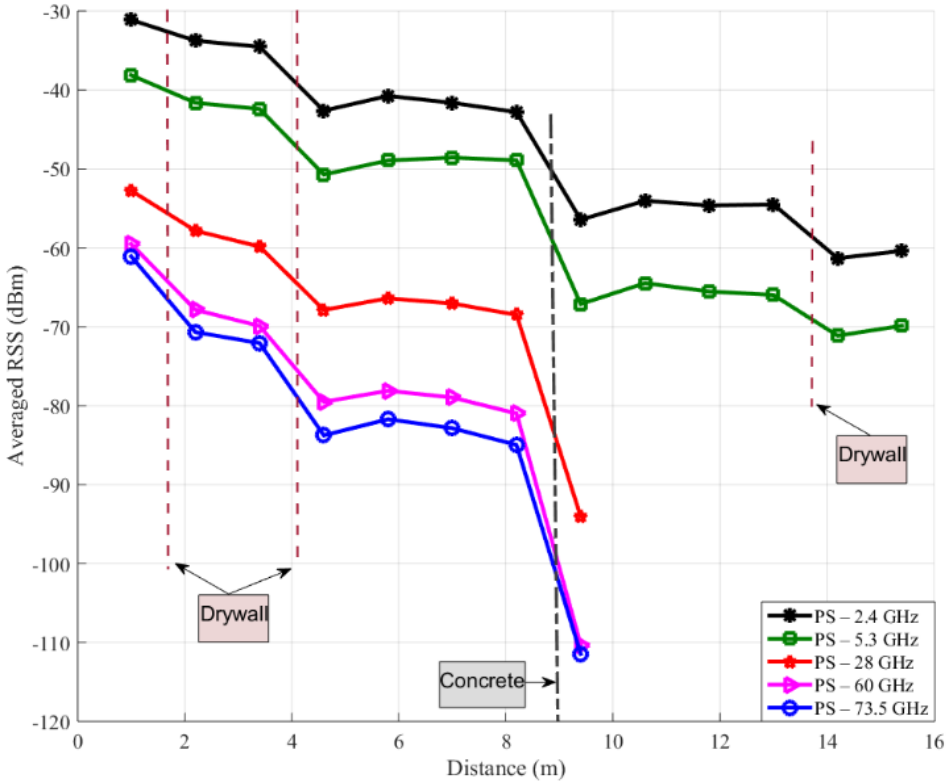

Figure 5.2: PS method performance for a different set of frequencies.

The performance of the above-mentioned methods was investigated over a set of frequencies including 2.4 GHz, 5.3 GHz, 28 GHz, 60 GHz and 73.5 GHz: results are presented in Figure 5.2 and Figure 5.3. It can be seen that averaged RSS using the PS method tends to be similar for all frequencies since this method removes the effect of multipath fading so that the only contributors to SS level are the path loss and shadowing. The reason why these averaged RSS take the form of similar layers is due to two types of losses: path loss with distance and wall losses, both of which are frequency dependent. On the other hand; VS includes the effect of phases which vary significantly due to multipath; therefore, measurements taken after the wall may receive higher power compared to those taken before the wall, as seen in Figure 5.3. This will make the SS-distance relationship less likely to be monotonic and therefore will reduce the localization efficiency.

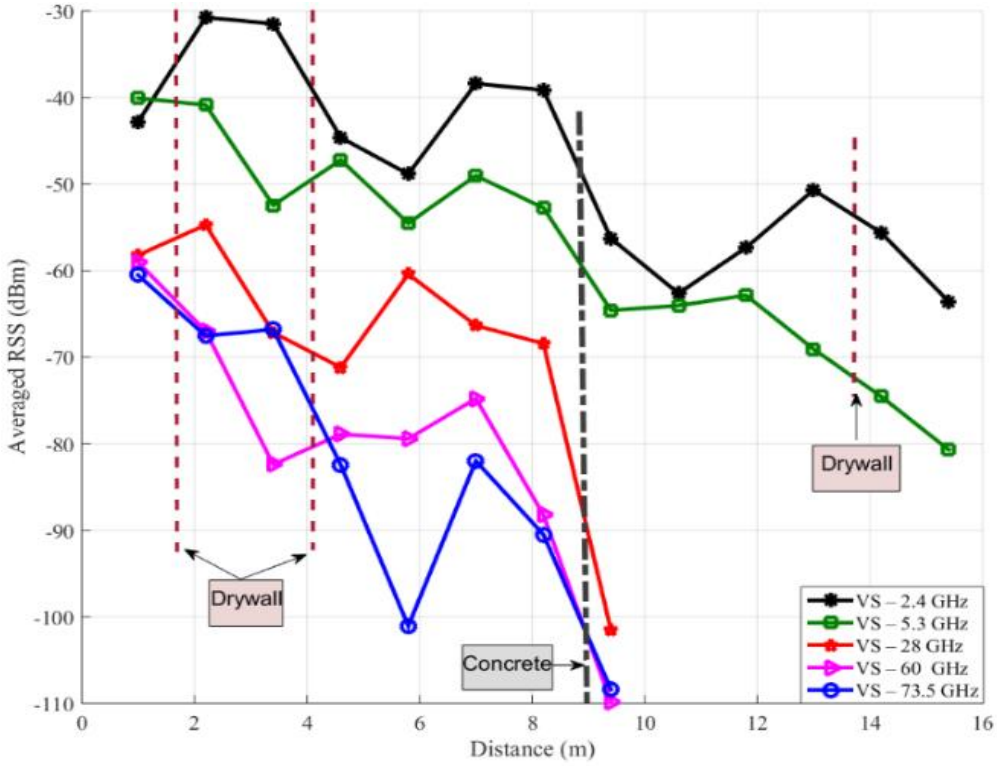

Figure 5.3: VS method performance for a different set of frequencies.

5.3 Previous Related Work

In an averaging estimating process three parameters are considered as shown in Figure 5.4 [249]: the averaging length (*2L*) also known as window size; the number of samples also known as the number of collection points (*N*) and the distance between the samples also known as spacing (*d*). Finding two parameters is sufficient to find the third using (*2L=Nd*). In a study conducted by [250] over the band 1.8 to 5.2 GHz the window size was found to be equal to 1 m or (5λ-15λ), window size was chosen based on shadowing correlation distance in which shadowing was found to be highly correlated at distances less than 1 m (shadowing variations can be neglected within this range) [251].

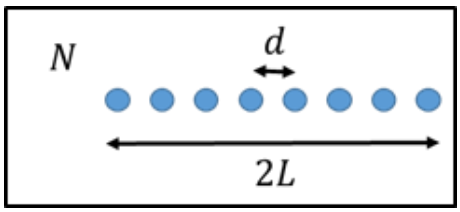

Figure 5.4: Average length, spacing and number of samples.

A set of measurements was conducted by [19] at 0.9 and 2.4 GHz and averaging performed. Two procedures were followed: in the first procedure many measurements were taken on circular paths around the point of interest, also known as the reference point (RP), then averaging was performed. Each circular path had a 0.3 m radius and measurements were taken from 120 points on the circle; the whole process was repeated every 0.6 m.

In the second method, measurements were collected from many points lying on a linear path where the spacing between the measurement points was λ/4 and averaging was performed over a window size of 10λ. This method was claimed to be good for LOS and measurements in corridors [19]. In [252] the authors performed RSS averaging over regions of $(2\lambda)^2$ dimensions. In [253] averaging was performed over regions of $(3\lambda)^2$ dimensions, while in [254] and [255] regions were of $(3\lambda)^3$ size. In [256] averaging was conducted over a 10λ interval while the minimum spacing between every two samples was set to 0.38λ.

Averaging should not distort the large-scale fading; therefore, estimating correlation distance r_c is crucial and this can be determined by estimating 1/e of the normalised shadowing autocorrelation ρ_s. The autocorrelation function is a function of location variability σ_L which is a function of frequency [30]. σ_L tends to increase as frequency increases; therefore, for larger frequencies ρ_s decreases

and hence r_c decreases. In [79] authors considered shadowing correlation distance to be in the range of 1-2 m, as estimated by [257]; they found that using a 10λ spacing window would be too long while using 4λ would be optimum.

In [258] an analysis is reported that aimed to find the best averaging window and spacing; it was found that the best averaging window was within 20λ-40λ with a sample spacing of 1.11λ (36 samples) to ensure that samples were uncorrelated. This procedure was also applied for indoor application at 15 GHz [259]. Work done by [258] was generalised for the medium-frequency band [260]: they found that best window size was 2λ; the optimum distance between samples was 0.17λ and the best number of samples was 8.

A local mean was taken over a rectangular area of 0.1 m^2 at 1.8 GHz, where nine measurements were taken within the grid [261]. For Nakagami propagation channels it is recommended by [251] to use 40 collection points within a 20λ averaging window for channels with a small number of multiple paths $2 \leq m < 4$ (m is the fading parameter), while for multipath channels in the range $4 \leq m \leq 8$ it was recommended to use 20 collection points within a 10λ averaging window. In [262] local mean estimation was conducted in a multi-floor building; measurements were collected through routes in the environment: these environments were gridded and then local mean estimated. The sizes of these grids were (kλ×kλ) where k was from 1 to 15; measurements were conducted at 0.9 GHz and 1.9 GHz.

At 0.9 GHz k was in the range of (6.5-7), while at 1.9 GHz it was in the range (5-12.5). The performance was compared to [258], however, no approach

outperformed the other. In [258] the authors assumed a normal distribution for SS while in [263] the SS distribution was found to be to be left-skewed: skewness is due to the limitation on the maximum achievable RSS at each location.

5.4 Methodology and Simulation Setup

In the scenario of propagation over a flat ground, there will be two rays: a direct ray and a ground reflected ray. The two paths have different lengths and hence different phases, hence for a moving terminal, the received power will follow a constructive and destructive interference every phase difference of π which represents a path difference of λ/2. If the signals are coming from opposite directions then a moving terminal experiences constructive and destructive interference every phase difference of π/2 which represents a path difference of λ/4. Generally; multiple paths tend to be more than two; however, the same concept still applies, therefore, the present work started by averaging over λ/4, and then the arrangement size was increased by λ/4 increments each time.

As seen in Figure 5.5, the objective is to remove the effect of fast fading from the collected SS, therefore a group of collection points (red cubes) are taken around the point of interest (yellow cubes) and then the corresponding RSS at the red points are averaged. The averaging process requires conversion of RSS values from dB scale to linear scale, followed by averaging and then conversion back to dB.

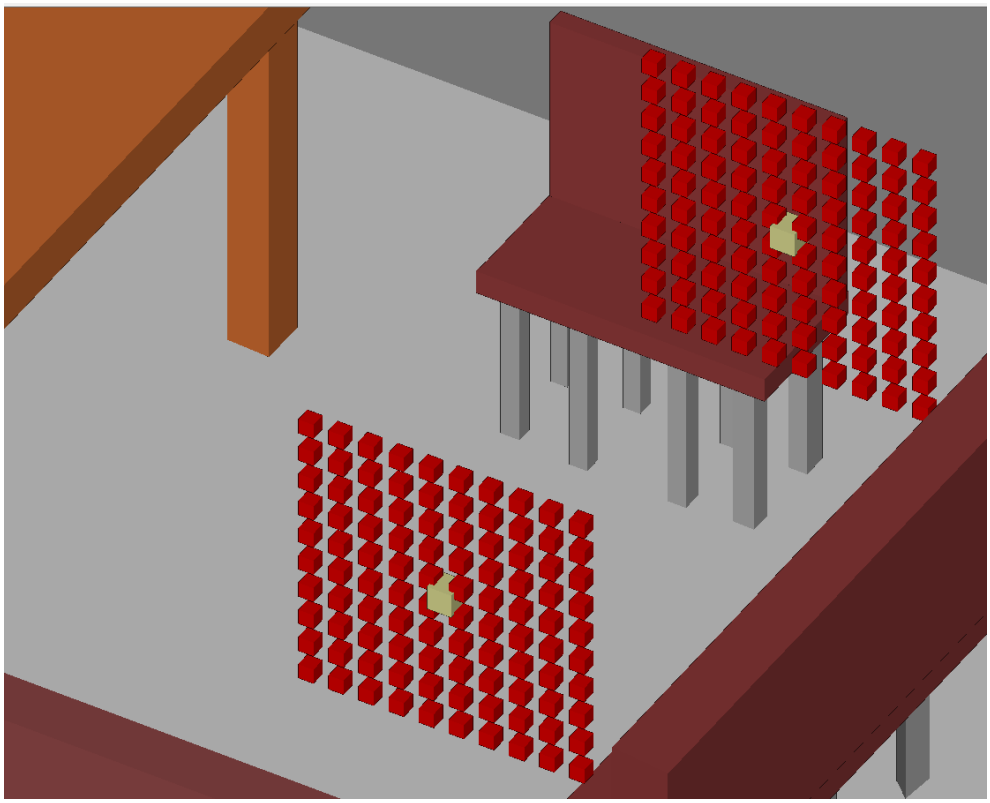

Figure 5.5: SS collection points, red points for averaging, yellow points are the points of interest.

The simulation was conducted using the ray-tracing software Wireless InSite. The operating frequency used in these simulations was 2.45 GHz and the distance between points of interest (yellow points) was 10λ as this has been reported to give the optimum representative data, as stated by [258]. Wireless InSite settings for these simulations are listed in Table 4-1.

Simulations were conducted in a simulated environment for the 3rd floor of a typical modern office-type building (the Chesham Building at the University of Bradford, U.K.). As seen in Figure 4.3, the model considered different types of materials used in the building: these materials have frequency dependent properties [54], therefore, their corresponding electrical parameters (relative permittivity ε_r and conductivity σ) will change as frequency changes. Typical

values for ε_r and σ in Table 5-1 are calculated using Equations 2.27 and 2.28 based on the ITU recommendations.

Table 5-1: Material properties adopted for 2.45 GHz frequency.

Material	ε_r	σ
Concrete	5.31	0.0663
Glass	6.27	0.0122
Wood	1.99	0.012
Drywall	2.94	0.0216
Wet Ground	30	0.4681

In this discussion, three parameters are considered: arrangement size, arrangement type and the distance between collection points (spacing). The total number of conducted scenarios was 406.

A. Arrangement Types

The word *arrangement* as used here refers to the configuration of the overall set of collection points. The shape of the overall set of collection points is termed as *arrangement type*, while the dimension of this configuration is termed as *arrangement size*. In this analysis, different types of arrangement have been studied to validate the best one for averaging.

Seven arrangements have been studied, termed as three-dimensional arrangement (3D), two-dimensional arrangement where the collection points lie on a plane horizontal to the floor (2D-H), two dimensional arrangement where the collection points lie on a plane perpendicular to the floor (2D-V), one-dimensional arrangement perpendicular to the floor (1D-V), one-dimensional arrangement perpendicular to the movement between the points of interest and horizontal to

the floor (1D-P), one-dimensional arrangement parallel (horizontal) to both the movement between the points of interest and the floor (1D-H) and a combination of all one-dimensional averaging loci, termed as hybrid (HYB). In all tested scenarios the collection points were equally spaced.

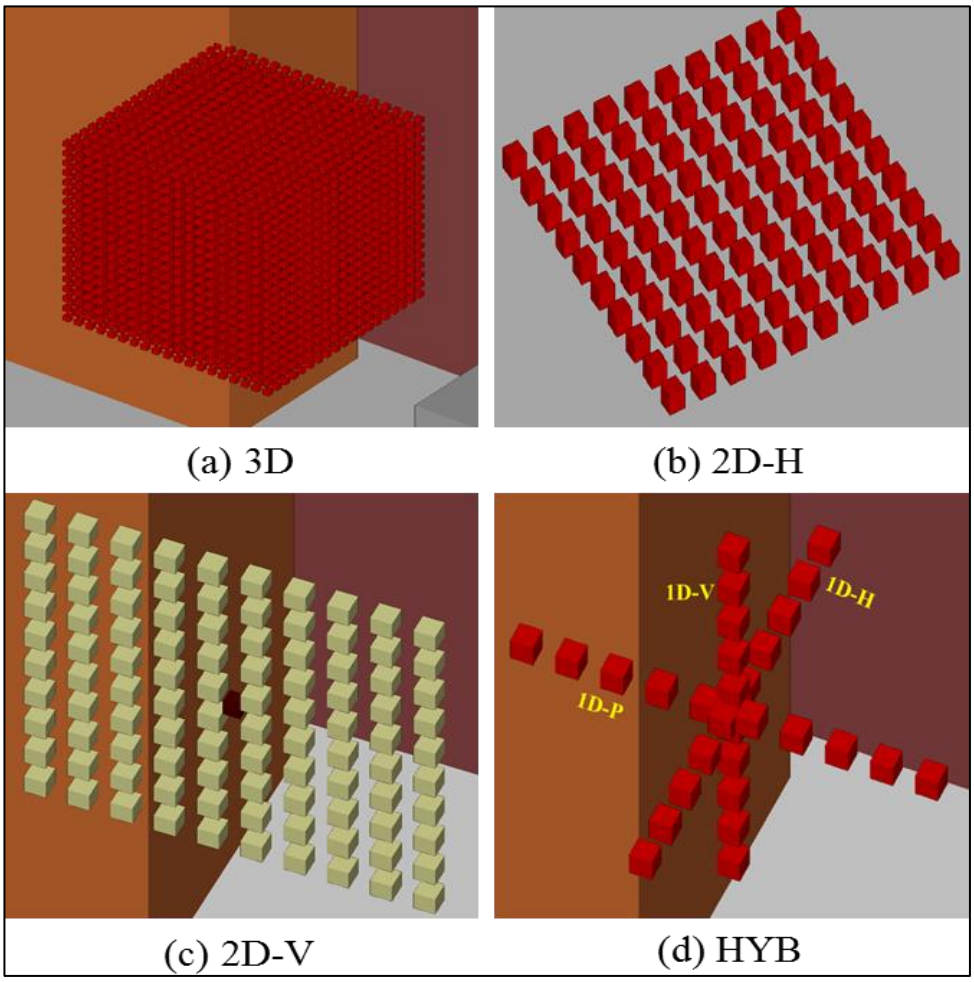

Figure 5.6: Arrangement types used in the simulation.

In the 3D arrangement, a set of measurements was taken with equal spacing, forming a cube as seen in Figure 5.6a, where the point of interest is at the centre of this cube. For example, a $(4.5\lambda)^3$ arrangement is a cube with edge length 4.5λ. For both 2D-H and 2D-V, the collection points form a square which is concentric with the point of interest, as seen in Figure 5.6b and 8c. The 1D-H, 1D-P, 1D-V and HYB are symmetrical about the point of interest, as seen in Figure 5.6d.

B. Arrangement Size

Different arrangement sizes have been investigated, from 0.25λ up to 4.5λ with 0.25λ incremental steps.

C. Spacing Between Points

Initially, for each arrangement size the spacing between the adjacent points was set to be 0.25λ; in order to investigate the effect of spacing between points, the spacing was increased by an increment of 0.25λ each time (i.e. spacings: 0.25λ, 0.5λ, 0.75λ … up to maximum arrangement size).

However not all arrangement sizes can maintain the same size when the spacing is increased (for example if the spacing for the 4.25λ size were incremented by 0.5λ then the resultant arrangement would be either 4.5λ or 4λ; therefore, spacing by this increment cannot be used). Table 5-5 lists the arrangement sizes used in the simulations along with arrangement type and their possible spacing; the table also shows the number of points required for averaging for all 406 scenarios.

As seen in the table, using a 3D arrangement with the size of 4.5λ and spacing of 0.25λ will be computationally expensive as it requires 6859 collection points for averaging. In this analysis, the aim is to find the best arrangement type, size and spacing for estimating the local mean of RSS.

5.5 Results and Discussions

Arrangement size

Averaging over each arrangement size and its behaviour with different spacing between collection points and arrangement types are examined, examples of the results are presented and general observations on the analyses for all arrangements sizes are presented after these examples.

Figure 5.7 presents averaging over a 4.5λ arrangement size for all types and all possible spacings (0.25λ, 0.5λ, 0.75λ, 1.5λ, 2.25λ and 4.5λ). As seen in Table 5-5 the number of points used ranged from 6859 in the 3D/0.25λ (arrangement type/spacing) case to 2 points in the 1D/4.5λ cases. In the figure, it can be seen that using simpler arrangement types with smaller numbers of points gives better results compared to the computationally demanding 3D cases. Averaging over a huge number of points as in the 3D/0.25λ case does not provide significant fast fading reduction; increasing the number of points does not necessarily improve the result. Generally, the results obtained from the 3D arrangement are not satisfactory.

As seen in the figure, all averaging results show enhancement compared to no averaging case (single measurement per location). For this arrangement size, the best arrangement type performance is 2D-H/1.5λ as it has the lowest RMSE; it requires only 16 collection points for averaging. The descending order of RMSE performance for all arrangements types is shown in Table 5-2, row 1. In terms of mean average error (MAE) 2H-D has the best performance while both 1D-H and then 1D-V have the worst performance respectively.

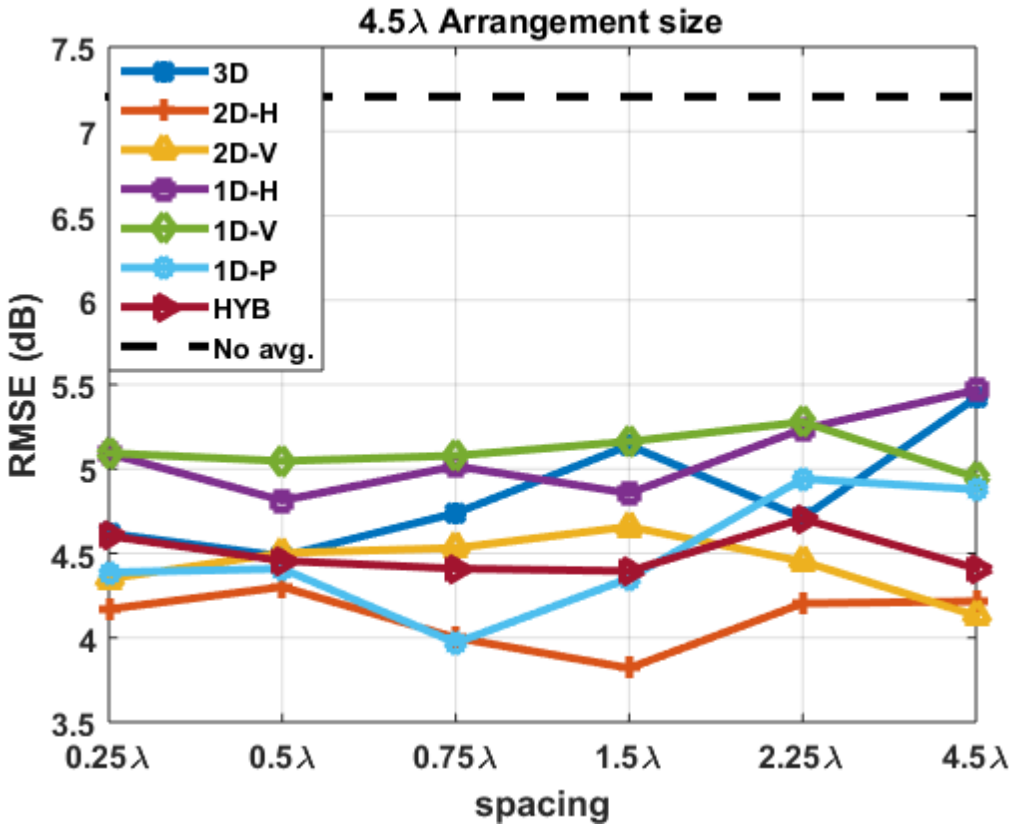

Figure 5.7: 4.5λ arrangement averaging.

A comparison between different arrangement types for 1.25λ arrangement size and spacings of 0.25λ and 1.25λ is shown in Figure 5.8. The number of SS collection points used ranged from 216 points in the 3D/0.25λ case to 2 points in the 1D/1.25λ cases. Averaging over all arrangement types shows good performance except for the 1D-H case where the performance is worse compared to the no averaging case, as depicted in the figure.

The descending order of performance in terms of RMSE for all arrangement types is shown in Table 5-2, row 14. In terms of MAE, 1D-H has the worst performance while the best performances are for 2D-H and 3D. 2D-H/1.25λ gives the best result (in terms of both RMSE and MAE) through all of the investigated scenarios in this experiment.

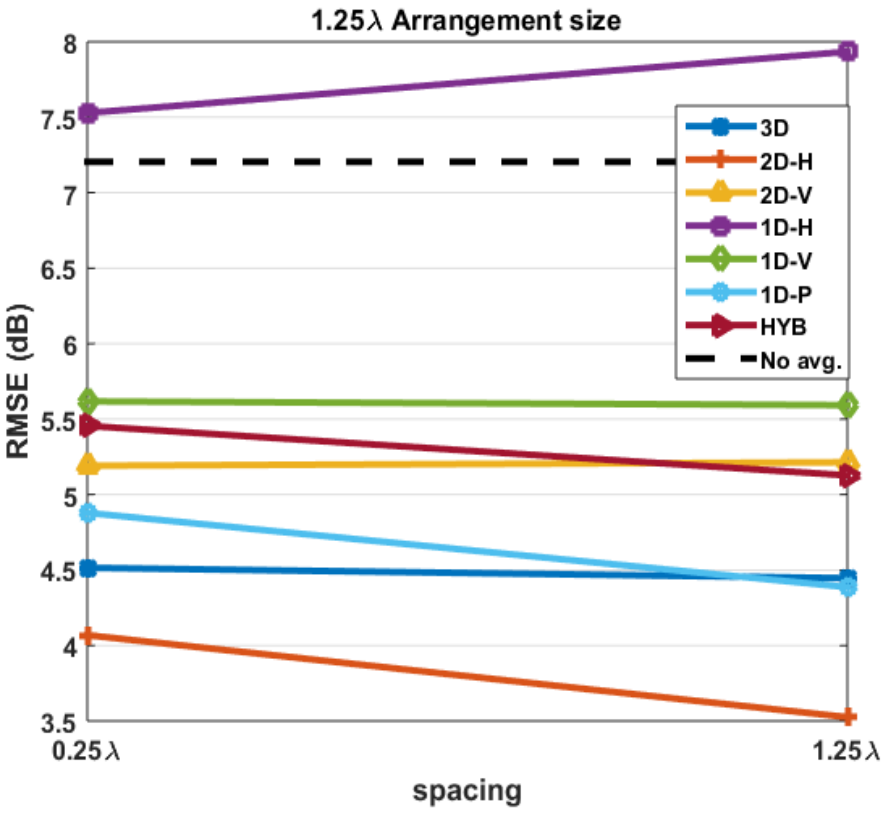

Figure 5.8: 1.25λ arrangement averaging.

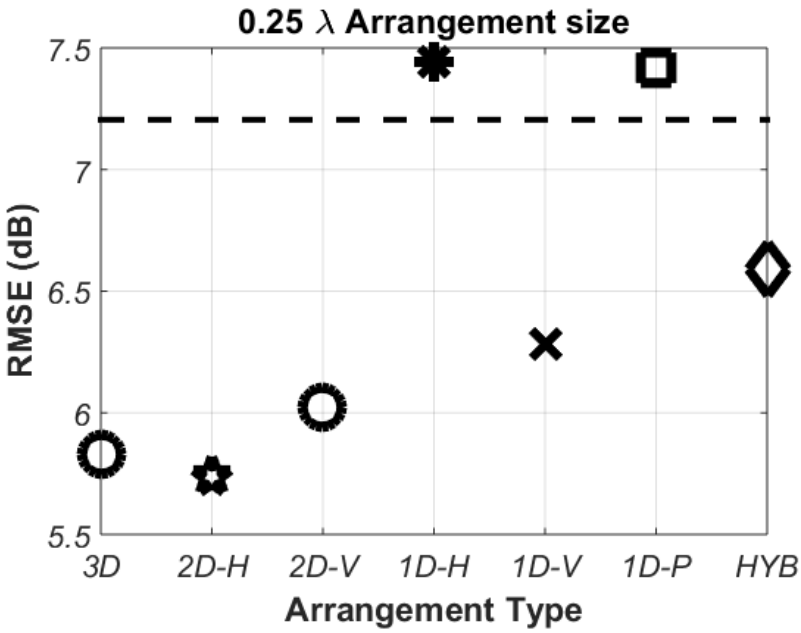

Figure 5.9: 0.25λ arrangement averaging.

Averaging over 0.25λ arrangement size is presented in Figure 5.9, the number of SS collection points ranged from 8 to 2 as seen in Table 5-5. The descending order of performance in terms of RMSE for all arrangement types is shown in Table 5-2, row 18. All arrangements have poor performance as their RMSE values are more than 5.5 dB; however, 1D-H and 1D-P have results that are worse than the no averaging case. It can be concluded that averaging with this arrangement size is not recommended.

Table 5-2: Ranking of best arrangement types by RMSE performance for all arrangement sizes and possible spacings.

	size	1st	2nd	3rd	4th	5th	6th	7th
1	4.5λ	2D-H	2D-V	1D-P	HYB	3D	1D-H	1D-V
2	4.25λ	2D-H	2D-V	HYB	1D-P	3D	1D-V	1D-H
3	4λ	2D-V	HYB	1D-P	3D	1D-V	2D-H	1D-H
4	3.75λ	HYB	2D-V	2D-H	3D	1D-V	1D-H	1D-P
5	3.5λ	2D-H	HYB	2D-V	3D	1D-P	1D-V	1D-H
6	3.25λ	2D-H	3D	2D-V	HYB	1D-V	1D-P	1D-H
7	3λ	2D-H	2D-V	3D	HYB	1D-V	1D-P	1D-H
8	2.75λ	2D-H	2D-V	3D	HYB	1D-V	1D-H	1D-P
9	2.5λ	2D-H	2D-V	3D	HYB	1D-V	1D-P	1D-H
10	2.25λ	2D-V	2D-H	3D	HYB	1D-P	1D-V	1D-H
11	2λ	2D-H	3D	2D-V	HYB	1D-P	1D-V	1D-H
12	1.75λ	2D-H	1D-P	2D-V	3D	HYB	1D-V	1D-H
13	1.5λ	2D-H	3D	1D-P	2D-V	HYB	1D-V	1D-H
14	1.25λ	2D-H	3D	1D-P	2D-V	HYB	1D-V	1D-H
15	λ	2D-H	3D	1D-P	2D-V	HYB	1D-V	1D-H
16	0.75λ	2D-H	3D	1D-P	2D-V	HYB	1D-V	1D-H
17	0.5λ	3D	2D-H	2D-V	HYB	1D-V	1D-P	1D-H
18	0.25λ	2D-H	3D	2D-V	1D-V	HYB	1D-P	1D-H

Observations recorded in this study during the simulations suggest the use of a grid size larger than 0.75λ as the RMSE tends to be large for smaller arrangement sizes. On the other hand, the results show that using a large arrangement size (larger than 2λ) does not guarantee good performance. Moreover, large-sized arrangements are computationally expensive due to the huge number of points used. Arrangements in the size range 1.25λ-1.75λ may be an optimum choice as they provide good results and require manageable numbers of collection points.

Table 5-3: Ten best arrangement results.

Ranking	Arrangement type	Arrangement size/Spacing	No. of points	RMSE (dB)
1	2D-H	1.25λ/1.25λ	4	3.5
2	2D-H	1.5λ/1.5λ	4	3.7
3	2D-H	4.5λ/1.5λ	16	3.8
4	2D-H	3.5λ/1.75λ	9	3.8
5	2D-H	3.75λ/0.25λ	256	3.8
6	2D-H	1.5λ/0.75λ	9	3.9
7	1D-P	4.5λ/0.75λ	7	3.96
8	2D-H	4.5λ/0.75λ	49	3.99
9	HYB	3.75λ/3.75λ	6	4.00
10	2D-H	1.75λ/0.25λ	64	4.06

Table 5-3 shows the best 10 averaging results found in the whole experiment; among these, 8 of them are the 2D-H type. Among the top 20 arrangements 13 are 2D-H and among the best 50 arrangements, 26 are 2D-H. On the other hand, the 2D-H arrangement type had only 4 poor results amongst the worst 100 results. Therefore, it’s highly recommended that this arrangement type to be used for averaging.

Table 5-4: Occurrence of arrangement types for best and worst RMSE results.

Arrangement type	Occurrence for Best Result	Occurrence for 2nd Best Result
2D-H	14	2
2D-V	2	6
HYB	1	2
3D	1	7
	Occurrence for Worst Result	Occurrence for 2nd Worst Result
1D-H	15	3
1D-V	1	9
1D-P	2	5

In Table 5-4 the occurrence of best, 2nd best, worst and 2nd worst arrangement type performance is presented. By exploring the presented numbers, it can be concluded that the 2D-H arrangement type is the best for averaging, while the 1D-H arrangement tends to have the worst performance. The descending order of performance for all arrangements types and for all arrangement sizes is 2D-H, 3D, 2D-V, HYB, 1D-P, 1D-V then 1D-H.

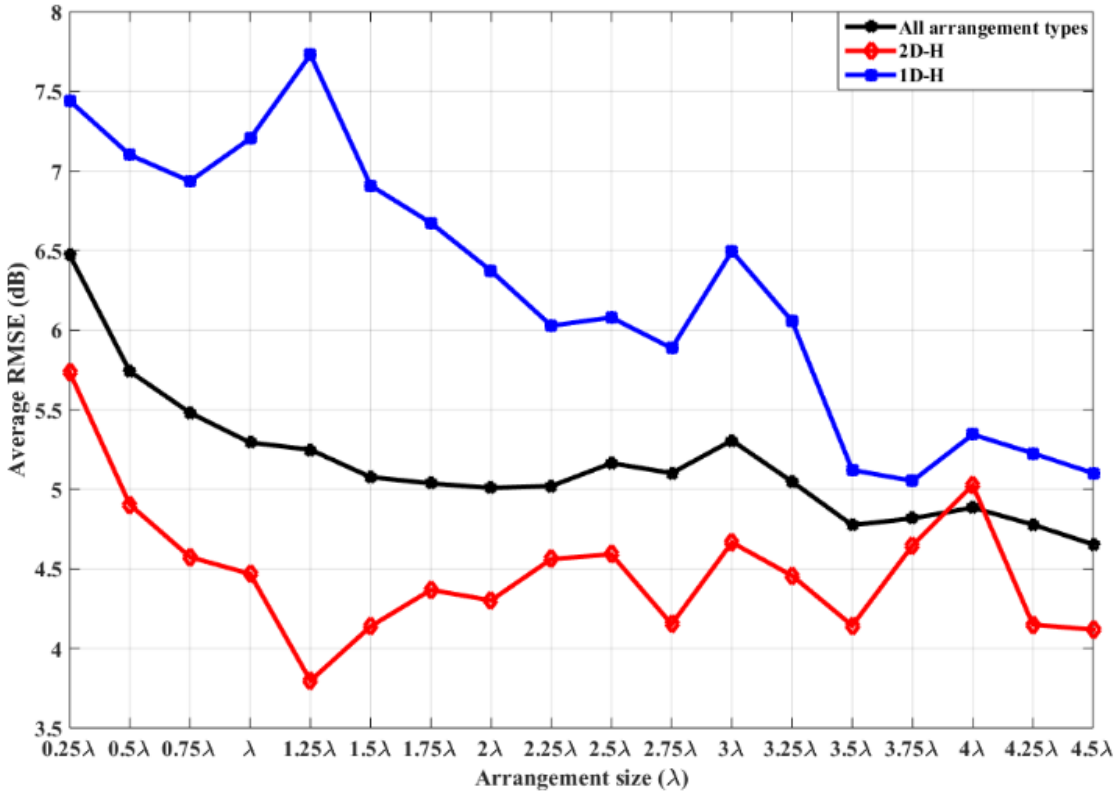

Figure 5.10: Averaged RMSE for all arrangement types and spacings compared with the best (2D-H) and worst (1D-H) arrangements.

For overall performance, the averaged RMSE for all spacings and arrangement types are shown in Figure 5.10, together with the best and worst arrangements, for comparison. It can be seen that as the size increases averaging tend to be enhanced; however, this does not mean that larger size guarantees better performance for all types of arrangement. This is evidenced in the same figure where 2D-H has its best result at 1.25λ and tends to have similar good performance for larger arrangement sizes. On the other hand, 1D-H has improving results as size increases: this explains why the results for all sizes improve as size increases. For all grid sizes larger than 0.75λ the worst averaging performance is at 3λ; therefore, it is recommended not to use this size for averaging.

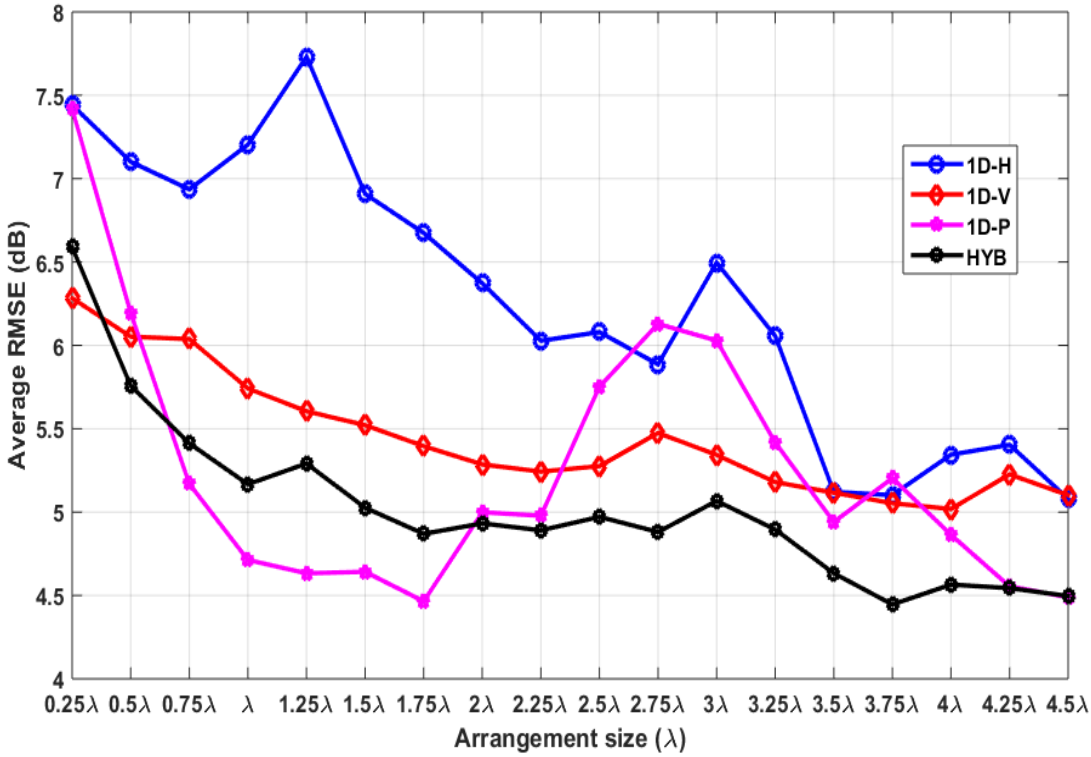

Figure 5.11: Averaged RMSE for 1D and HYB at all spacing for each arrangements size.

The overall performance of 1D and HYB arrangement types for all spacings and all arrangement sizes is presented in Figure 5.11. 1D-H has the worst performance for the majority of the examined sizes, while the HYB tends to have the best performance for the majority of the arrangement sizes. Although HYB shows better performance in general, averaging with the 1D-P arrangement tends to have the lowest average RMSE for arrangement sizes from 0.75λ to 2λ; therefore, it may be better to use this arrangement type as it needs a lower number of collection points. It should be noted that these values are averaged over all spacings, therefore when choosing any arrangement type for averaging it is recommended to check the individual averaging result for each spacing at each arrangement size.

A comparison between arrangement type performances for all spacings at each arrangement size is presented in Figure 5.12. 2D-H has the best overall performance for almost all of the arrangement sizes. Also, it can be seen that both 2D-H and 3D performance was not enhanced significantly after a certain size; hence it may be better to use arrangements with the smaller size as they need less points.

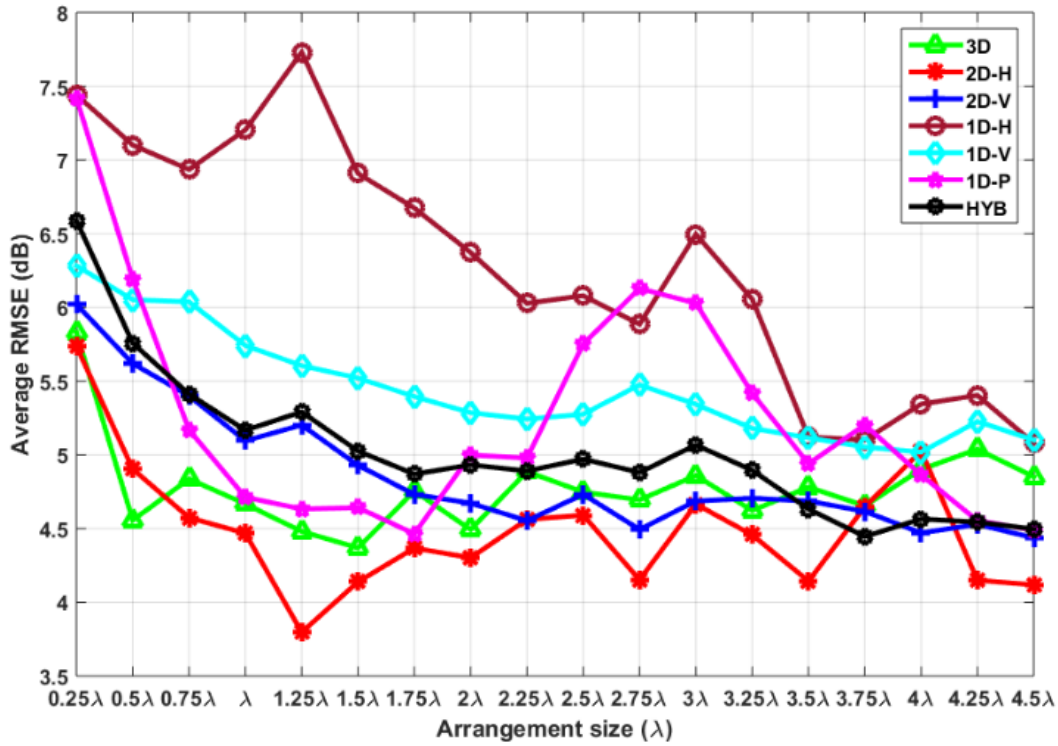

Figure 5.12: Averaged RMSE for the investigated arrangement types at all spacings for each arrangement size.

Number of Points

Several arrangement configurations have the same number of collection points, for example, arrangement types at 4.5λ/1.5λ and 3.75λ/1.25λ have the same number of points (see Table 5-5). These results will suggest the optimum arrangement to be adopted as those with the same number of points will require the same effort. In order to distinguish between different studied cases, each

scenario (having the same number of points) is termed according to the number of layers in the 3D case.

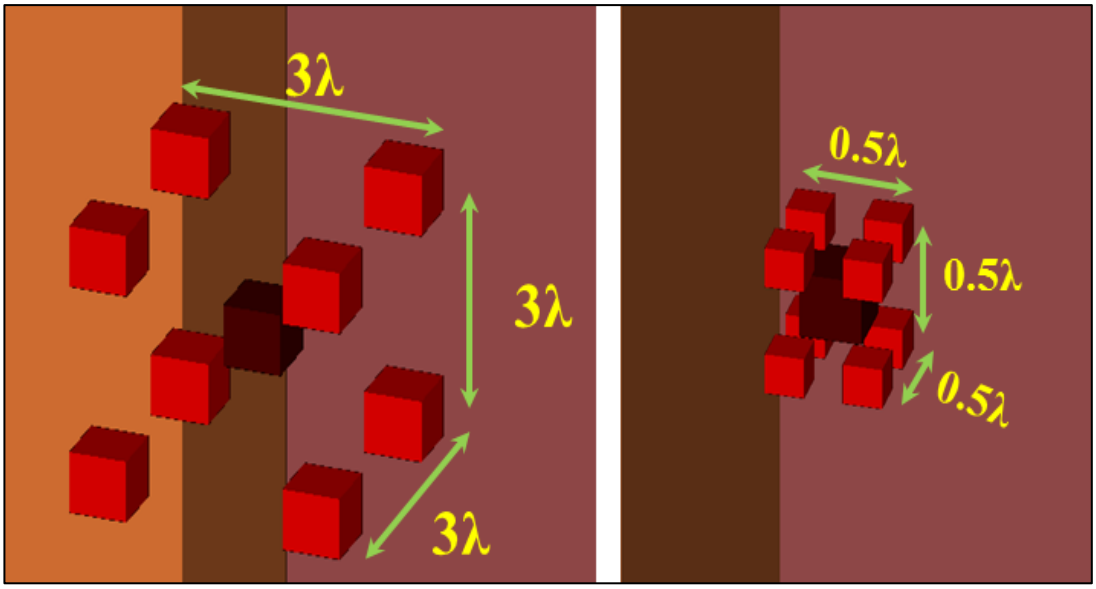

Figure 5.13: Example on arrangements sizes which have the same number of points (two layers) using different spacing.

When averaging over the maximum possible spacing then the same arrangement type will have the same number of points for all arrangements size (e.g. 3λ/3λ and 0.5λ/0.5λ) as seen in Table 5-5 and Figure 5.13. The number of points for 3λ/3λ and 0.5λ/0.5λ are mentioned in Table 5-5 rows 29 and 57 respectively. For the cases shown in Figure 5.14, the same number of points was used for each arrangement type: as the arrangement size increased averaging enhanced; this is provided as the mean of the RMSE for all arrangement types was reduced by around 1.7 dB. It can be concluded that for a small number of points it is better to use a large arrangement size rather than a small one for most of the arrangement types.

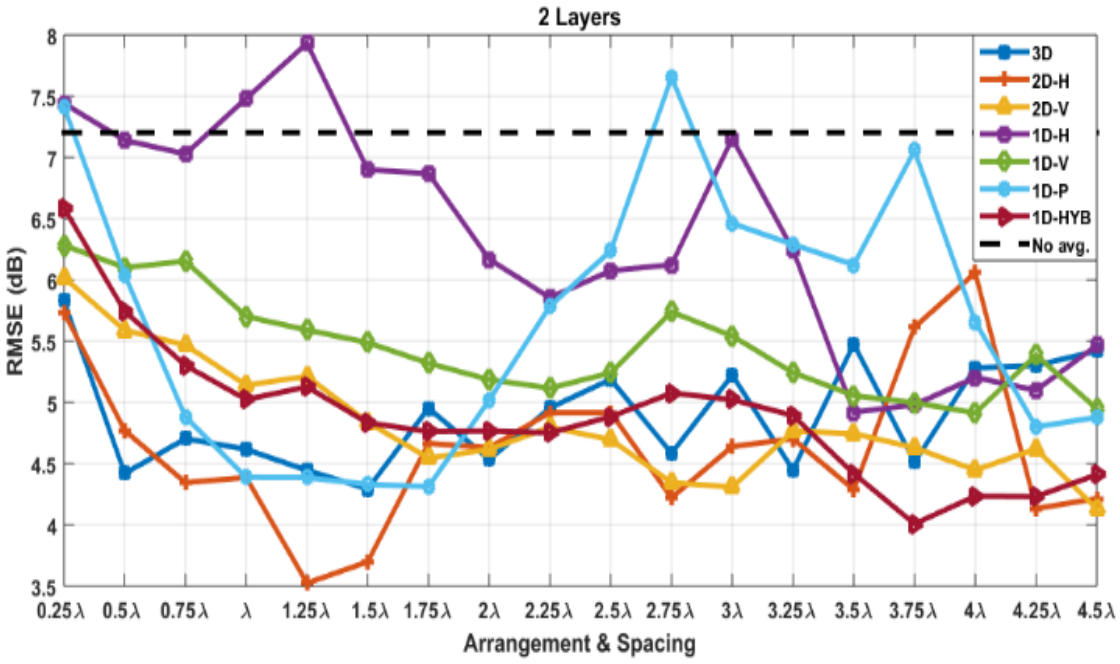

Figure 5.14: Performance comparison for two-layer arrangements.

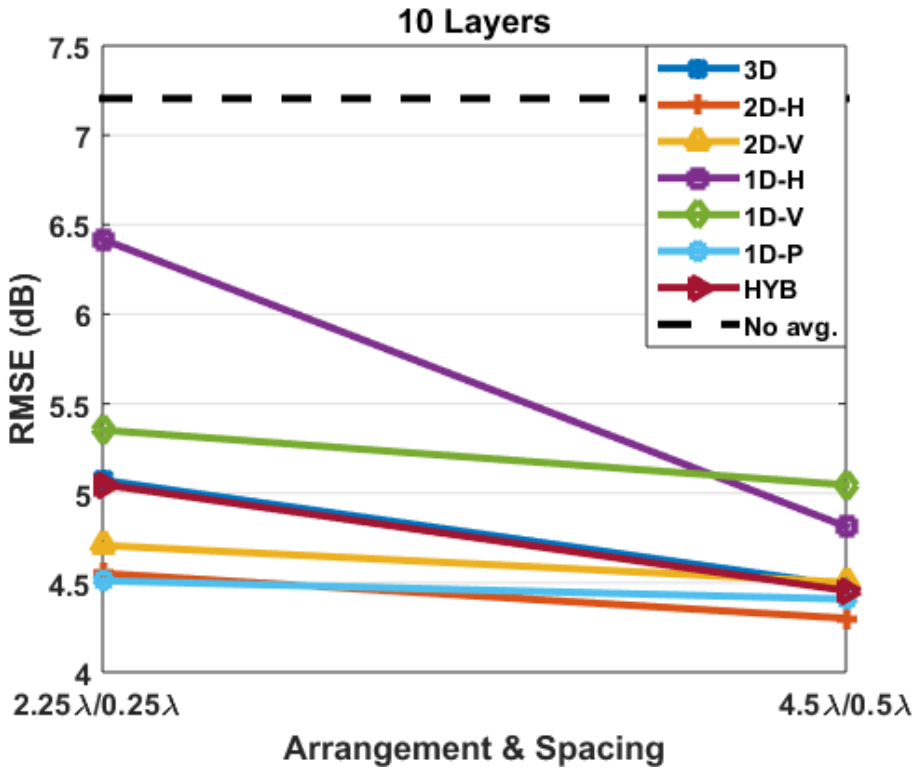

Figure 5.15: Performance comparison for 10 layers arrangements.

This is also confirmed for a large arrangement with a large number of points, as shown in Figure 5.15 where the RMSE was reduced by 0.6 dB. Data in Table 5-5

rows 2 and 36 are presented in Figure 5.15, these data have the same number of points but, by increasing the spacing between the points, the RMSE tends to decrease.

Fixing the number of points and changing the spacing does not improve 3D and 2D-H significantly but it does give an improvement for 2D-V, 1D-V, 1D-H and HYB, and in some cases, 1D-P also tends to have better performance as mentioned earlier.

Arrangement Type

Since 2D-H gives the best results it is worthy to investigate the arrangements type relationship with spacing and size and its effect on RMSE. Figure 5.16 presents RMSE relationship with spacing for 2D-H arrangement type at all arrangements size. It was found that for small arrangement size (≤ 1.5λ) RMSE decreases as spacing increases. For large (≥ 3.25λ) and medium arrangements no spacing relationship between spacing and RMSE was found, therefore it's recommended to use 2D-H arrangement with smaller size and larger spacing.

Generally, for the 3D, 2D-H, 1D-V and 1D-P arrangements smaller arrangement sizes have better results as spacing increases. The 2D-V and 1D-H type have better results for large arrangements as spacing increases. The 1D-V type has better results for most medium arrangement sizes as spacing increases. The HYB type tends to have good results as spacing increases for most of the arrangements.

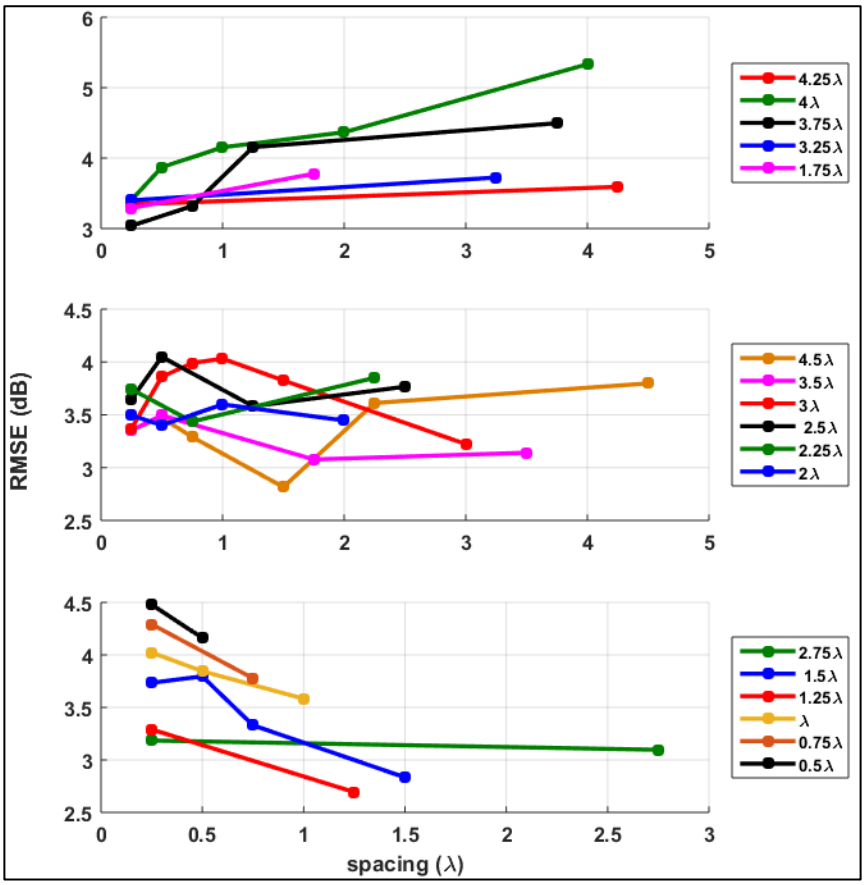

Figure 5.16: RMSE relationship with spacing for 2D-H arrangement type.

Table 5-5: Arrangement sizes and their possible spacings, with the required number of points for averaging.

	Size	*Spacing*	3D	2D-H	2D-V	1D-H	1D-V	1D-P	HYB
1	4.5λ	0.25λ	6859	361	361	19	19	19	57
2		0.5λ	1000	100	100	10	10	10	30
3		0.75λ	343	49	49	7	7	7	21
4		1.5λ	64	16	16	4	4	4	12
5		2.25λ	27	9	9	3	3	3	9
6		4.5λ	8	4	4	2	2	2	6
7	4.25λ	0.25λ	5832	324	324	18	18	18	54
8		4.25λ	8	4	4	2	2	2	6
9	4λ	0.25λ	4913	289	289	17	17	17	51
10		0.5λ	729	81	81	9	9	9	27
11		λ	125	25	25	5	5	5	15
12		2λ	27	9	9	3	3	3	9
13		4λ	8	4	4	2	2	2	6
14	3.75λ	0.25λ	4096	256	256	16	16	16	48
15		0.75λ	216	36	36	6	6	6	18
16		1.25λ	64	16	16	4	4	4	12
17		3.75λ	8	4	4	2	2	2	6

18	3.5λ	0.25λ	3375	225	225	15	15	15	45
19		0.5λ	512	64	64	8	8	8	24
20		1.75λ	27	9	9	3	3	3	9
21		3.5λ	8	4	4	2	2	2	6
22	3.25λ	0.25λ	2744	196	196	14	14	14	42
23		3.25λ	8	4	4	2	2	2	6
24	3λ	0.25λ	2197	169	169	13	13	13	39
25		0.5λ	343	49	49	7	7	7	21
26		0.75λ	125	25	25	5	5	5	15
27		λ	64	16	16	4	4	4	12
28		1.5λ	27	9	9	3	3	3	9
29		3λ	8	4	4	2	2	2	6
30	2.75λ	0.25λ	1728	144	144	12	12	12	36
31		2.25λ	8	4	4	2	2	2	6
32	2.5λ	0.25λ	1331	121	121	11	11	11	33
33		0.5λ	216	36	36	6	6	6	18
34		1.25λ	27	9	9	3	3	3	9
35		2.5λ	8	4	4	2	2	2	6
36	2.25λ	0.25λ	1000	100	100	10	10	10	30
37		0.75λ	64	16	16	4	4	4	12
38		2.25λ	8	4	4	2	2	2	6
39	2λ	0.25λ	729	81	81	9	9	9	27
40		0.5λ	125	25	25	5	5	5	15
41		λ	27	9	9	3	3	3	9
42		2λ	8	4	4	2	2	2	6
43	1.75λ	0.25λ	512	64	64	8	8	8	24
44		1.75λ	8	4	4	2	2	2	6
45	1.5λ	0.25λ	343	49	49	7	7	7	21
46		0.5λ	64	16	16	4	4	4	12
47		0.75λ	27	9	9	3	3	3	9
48		1.5λ	8	4	4	2	2	2	6
49	1.25λ	0.25λ	216	36	36	6	6	6	18
50		1.25λ	8	4	4	2	2	2	6
51	λ	0.25λ	125	25	25	5	5	5	15
52		0.5λ	27	9	9	3	3	3	9
53		λ	8	4	4	2	2	2	6
54	0.75λ	0.25λ	64	16	16	4	4	4	12
55		0.75λ	8	4	4	2	2	2	6
56	0.5λ	0.25λ	27	9	9	3	3	3	9
57		0.5λ	8	4	4	2	2	2	6
58	0.25λ	0.25λ	8	4	4	2	2	2	6

Chapter 6

Channel Measurements and Simulation Validation at Millimetre-wave Frequencies

6.1 Introduction

Ray-tracing software is used to predict channel parameters within indoor and outdoor environments. These programs are used to save time, cost and effort compared to real-time measurements. However, precise and accurate use of these software is required in order to get representative channel parameters.

Wireless InSite is a commercial software which is widely used especially in WLAN applications. Validation for these software at different frequencies and environments is required to make the software widely applicable. The purpose of this study is to examine how accurate can Wireless InSite simulate the real-time propagation at millimetre-wave frequencies especially at 60 GHz which is attractive for 5G systems [264].

6.2 Channel Sounder

Channel sounder is used to measure channel impulse response $h(\tau)$ or its frequency response $H(f)$ in the frequency domain. Since the channel is dependent on frequency, time and position, a channel can be identified by delay spread, angle of arrival/departure, Doppler shift and received signal strength. Figure 6.1 and Figure 6.2 show the architecture of the channel sounder.

The message signal is implemented using Altera FPGA board (Figure 6.2-c) which is programmed to provide a pseudo-random binary sequence of 2^m-1 sequence, where m ranges from 6 to 10. CO2201A converter evaluation board (Figure 6.2-b) controls the transmitter (Tx) and receiver (Rx) converter modules. It also has power detectors, power amplifier, automatic gain control and USB interface to control the modules. The CO2201A evaluation board architecture is shown in Figure 6.3.

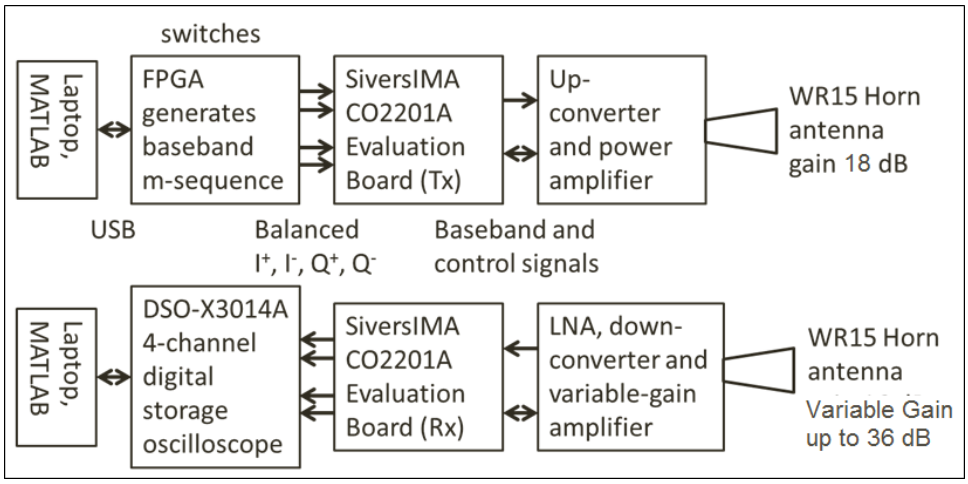

Figure 6.1: Channel Sounder architecture

Keysight digital storage oscilloscope (DSO) X-3014A (Figure 6.2- a) has four channels, each channel has 200 MHz BW which is equivalent to 400 MHz bandwidth (±200 MHz). This is sufficient in indoor applications for 1 m path difference. Both the CO2201A and the DSO are connected to PC via USB that can generate commands. The sounder can be integrated with MATLAB which also can be used to generate commands. Table 6-1 illustrates the channel sounder characteristics.

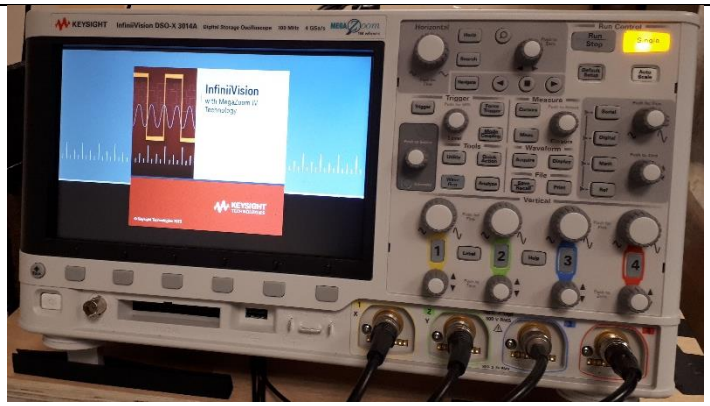

(a)

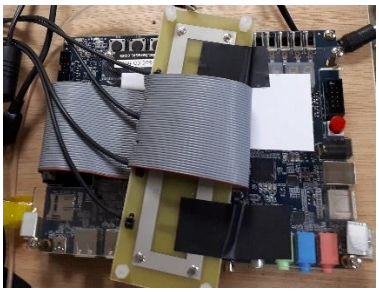

(b) (c)

Figure 6.2: Channel sounder: (a) Keysight's DSO, (b) COST2201A evaluation board, (c) Altera FPGA board.

Table 6-1: Channel Sounder characteristics.

Item	Value
Internal pulse amplitude	5 V peak
Bit period	4 ns
Bandwidth of operation	400 MHz
Transmitter antenna gain	18 dBi
Transmitted Power	30 dBm
Data rate	250 Mb/s
sampling interval	2 ns
Sweep speed	10 µs/div

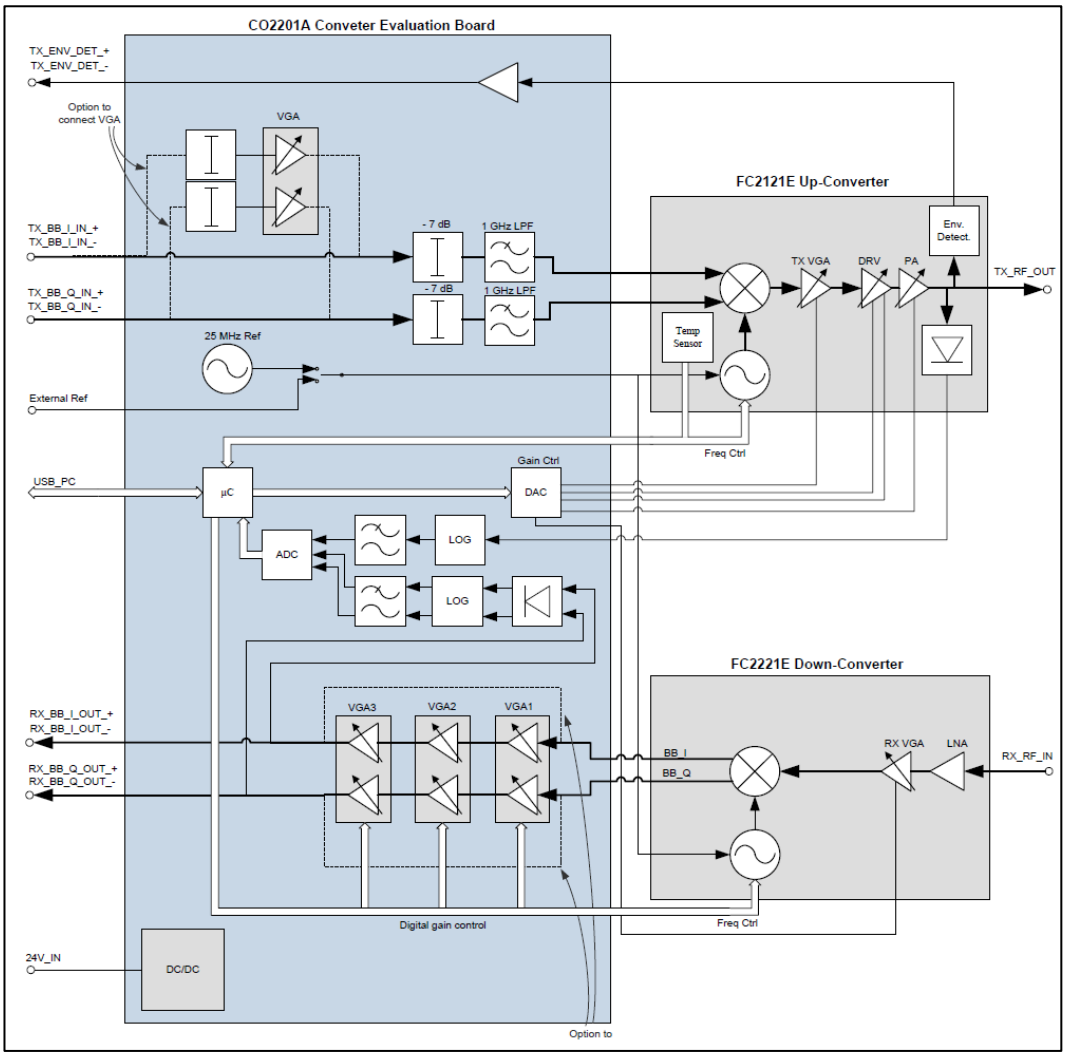

Figure 6.3: COST2201A Evaluation board.

6.3 Simulation and Experimental Analysis.

Validation of Wireless InSite is performed in two indoor scenarios, LOS and NLOS. Both scenarios are conducted in the 3rd floor of Chesham Building, University of Bradford. The simulated environment took into account fine details of the building for accurate validation.

6.3.1 Direct LOS Simulation and Measurement Validation:

The first step of this validation is the direct LOS propagation which was investigated in B3.26 lab in the 3rd floor of Chesham building at the University of

Bradford. A transmitter Tx and receiver Rx with vertically polarized horn antenna were placed in the lab room in LOS at 1.5 m height and separated by 5 m as shown in Figure 6.4.

Simulation setup is presented in Table 4-1. Wireless InSite considers the effects of material electrical properties. It also allows the user to configure waveform, antenna types and transmitter and receivers' properties. In this scenario, a sinusoidal waveform is used for simulation at 60 GHz frequency with an input power of 30 dBm. The propagation paths for this scenario is presented in Figure 6.5, where the loudest seven paths are shown; the colour of each path represents its strength as shown in the legend. As shown, the direct path is the one with the strongest signal level.

Figure 6.4: Simulated LOS Scenario in B3.26 lab.

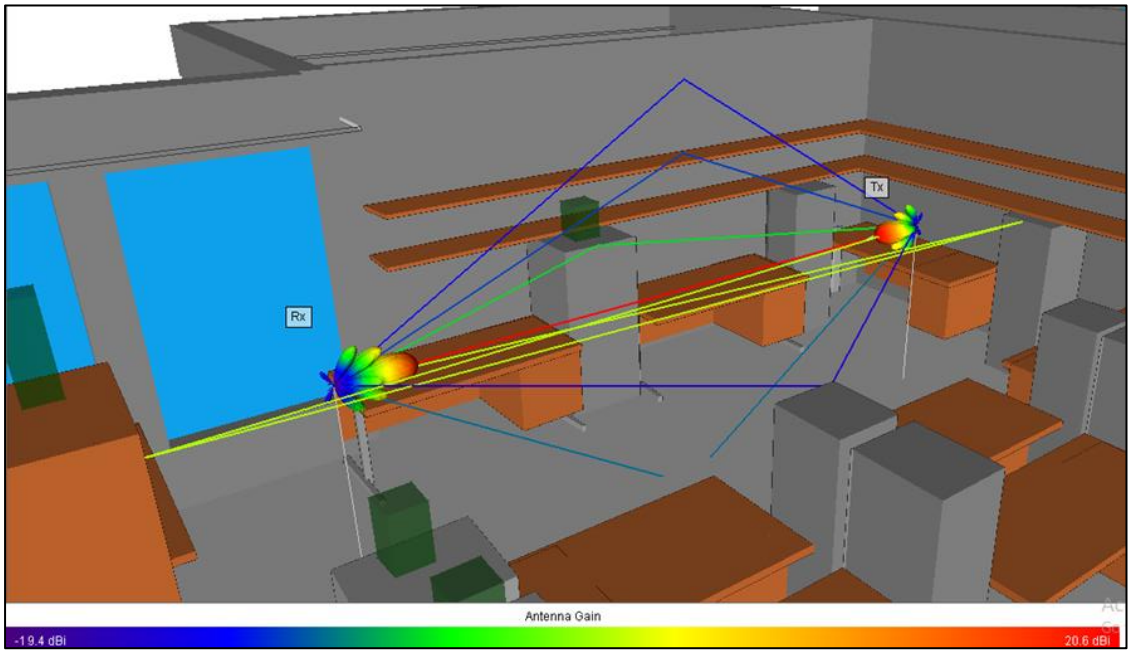

Figure 6.5: Strongest Propagation paths for the LOS experiment.

The 60 GHz band channel sounder can be used for back-back measurements and radar measurements; however, calibration for both mode of measurements is required. The calibration was performed in an anechoic chamber in B3.19 at the University of Bradford as seen in Figure 6.6; the radar calibration setup includes reflections from a flat reflector and corner reflectors.

After calibration, measurements were performed using the 60 GHz band channel sounder in the B3.26 lab, where the adopted scenario is exact to the simulation part, as shown in Figure 6.7.

(a)

(b)

Figure 6.6: Calibration in the anechoic chamber, (a) Back-back mode and (b) radar mode.

(a)

(b) Transmitter

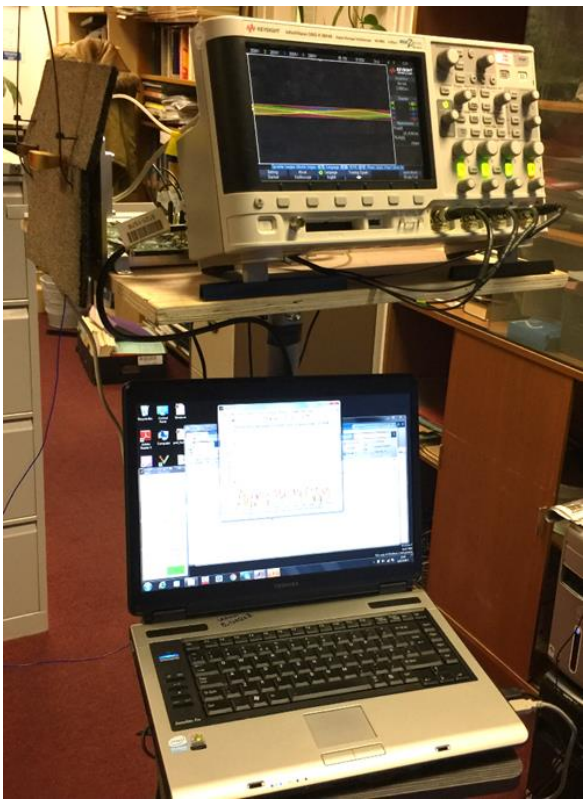

(c) Receiver

Figure 6.7: 60 GHz Channel Sounder in Lab B3.26, (a) LOS scenario, (b) Transmitter, (c) Receiver.

Figure 6.8 shows a comparison between the simulation and measurements for the LOS scenario, both results show good matching as the direct path received power in the measurements was -14.57 dBm while it was -16.07 dBm in the simulations.

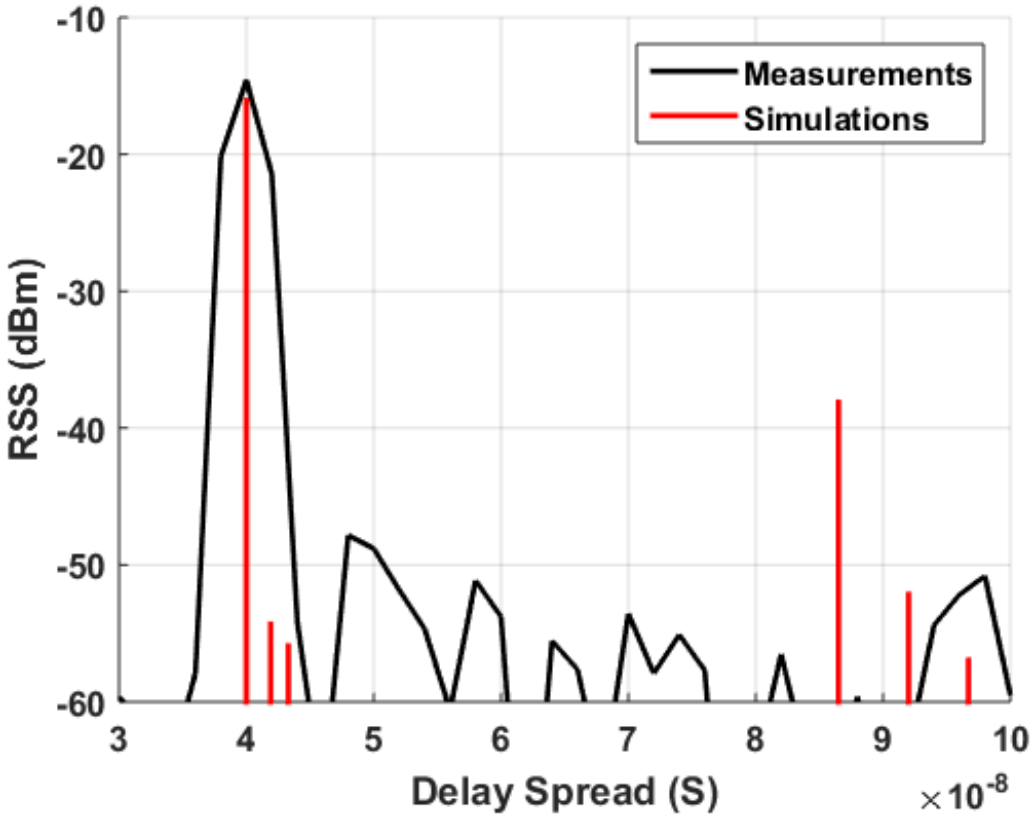

Figure 6.8: Comparison between simulations and measurements.

6.3.2 NLOS Simulation and Measurement Validation:

Measurements were conducted at three positions distributed in the 3rd floor of Chesham building while rotating the receiver about the Z-axis. The same instruments that have been used in the LOS experiment are used in the NLOS experiment part. The transmitter was placed in the printer room of the corridor at height of 2m while the receiver was set to 1.5 m at all receiver points as shown in Figure 6.9.

Figure 6.9: NLOS experiment at receiver position 1.

In NLOS propagation, the effect of building materials are more evident; many studies tried to investigate the effect of the material on propagation through knowing the relative permittivity and conductivity of these materials. In this study, two materials had been investigated: concrete and wood. Concrete is a composite material made from adding water to fine aggregate (sand), coarse aggregate and cement, which hardens over time. Concrete mix is defined based on water/cement ratio, cement/sand/aggregate ratio and the cement/total-aggregate ratio [265, 266]. Electric conductivity tends to increase as water content increases [267].

Reinforced concrete are different from concrete as it has longitudinal reinforcement and stirrup, which are made from steel. Therefore, electrical constitutive parameters are different from concrete, reinforced concrete are used

in columns, slaps, ceilings and floors. It was found that relative permittivity at 0.9 and 1.8 GHz is about 7 while conductivity found to be 0.015 S/m and 0.03 S/m respectively [265].

Literature suggests that concrete complex permittivity changes with the type of concrete sample (i.e. aerated, lightweight or hardened) rather than changing the operating frequency for the same type of materials [265].

Complex permittivity of wood depends on the type of wood species, wood density, water content, temperature, the electric field orientation with respect to the grain, operating frequency and if the wood was chemically treated [265]. Therefore, chipboard, plywood, floorboard, Beechwood, Sipo and plain wood are expected to have different values for electrical constitutive parameters. It was found that dielectric constant increases as temperature increases [268] while conductivity increases as water content increases [265].

Table 6-2: Electrical constitutive parameters values for concrete and wood at 60 GHz.

Material	Reference	Description	ε_r	σ	Notes
Concrete	[54] (a)	ITU-A	5.31	0.8967	Table 9
	[54] (b)	ITU-B	6.5	0.2283	Table 8
	[267]	Fares	7 - 13	-	
	[269]	Fakharzadeh	6.1326	1.0047	
	[270]	Lu	3.3	1.2667	
	[271] (a)	Correia-A	6.14	1.005	Table I
	[271] (b)	Correia-B	6.5	1.4278	Table II
	[272]	Pinhasi	11.47	0.988	
Wood	[54]	ITU	1.99	0.3784	Table 9
	[268]	Torgovnikov	2.1	0.2	
	[269]	Fakharzadeh	1.5671	0.3207	

	[273]	Affum	3.3	-	
	[270]	Lu	2.8	0.0013	
	[271] (a)	Correia-A	1.57	0.3214	
	[271] (b)	Correia-B	1.54	0.1181	Table II
	[274]	Salous	2.4	0.4	
	[272] (a)	Pinhasi-A	1.64	3.7173	Table 2
	[272] (b)	Pinhasi-B	2.068	1.38	Table 2

Typical values from literature for relative permittivity and conductivity of concrete and wood at 60 GHz are presented in Table 6-2. These values will be used by the Wireless InSite to predict channel impulse response which will be compared to the channel sounder results.

The Wireless InSite software allows the user to set the number of paths; the more paths are considered the more accurate the results, while more processing time is required. We found that having more than 10 paths will not improve the accuracy of the results; therefore, the maximum number of paths was set to 10.

The receiver was placed in three locations along the printer room and corridor in the floor with different angle rotations. Among these locations and rotations, the receiver was successful to receive a signal from 20 receiver points. In the first position, measurements were observed successfully with rotations: 0^o, 10^o, 20^o, 30^o, 50^o and 70^o. Second position measurements were observed successfully with rotations: 120^o-180^o and 210^o-250^o, In the third positions only two rotations have decent results; the simulated scenario was only for rotations 150^o and 160^o.

Table 6-3 gives examples of simulated ray paths between the transmitter and some receiver points using Wireless InSite, where Tx, Rx, R and T represent

transmitter, receiver, reflection and transmission respectively. Rays arrive in clusters; the main RSS cluster is considered as a reference to justify the Wireless InSite performance with measurements by changing ε_r and σ presented in Table 6-2**.**

Table 6-3: Ray paths and interactions.

Paths No.	Interactions at Rx1_0	Interactions at Rx2_120	Interactions at Rx2_170	Interactions at Rx2_250	Interactions at Rx3_150
1	Tx-R-Rx	Tx-Rx	Tx-R-R-Rx	Tx-R-Rx	Tx-R-R-Rx
2	Tx-R-R-Rx	Tx-R-Rx	Tx-Rx	Tx-Rx	Tx-R-T-T-T-R-Rx
3	Tx-R-R -Rx	Tx-R-R-Rx	Tx-R-Rx	Tx-R-R-Rx	Tx-R-T-T-Rx
4	Tx-T-R-T-R-Rx	Tx-R-Rx	Tx-R-Rx	Tx-T-R-T-Rx	Tx-T-T-R-Rx
5	Tx-R-R-Rx	Tx-R-R-Rx	Tx-R-Rx	Tx-R-R-Rx	Tx-T-T-R-T-R-Rx
6	Tx-R-R-Rx	Tx-R-R-Rx	Tx-R-Rx	Tx-R-R-Rx	Tx-R-R-T-T-Rx
7	Tx-T-T-R-R-T-T-Rx	Tx-R-Rx	Tx-R-R-Rx	Tx-R-Rx	Tx-R-T-T-R-Rx
8	Tx-T-T-R-T-R-T-Rx	Tx-T-R-T-Rx	Tx-R-Rx	Tx-R-R-Rx	Tx-T-T-T-R-Rx
9	Tx-Rx	Tx-R-R-T-Rx	Tx-T-R-T-Rx	Tx-R-T-R-T-Rx	Tx-T-T-R-T-T-R-Rx
10	Tx-R-Rx	Tx-R-Rx	Tx-R-R-Rx	Tx-R-Rx	Tx-R-T-T-T-Rx

Position 1*: Main Ray is reflected from one concrete wall.*

For all rotations in “position one” it was found that the main ray is reflected from one concrete wall. Figure 6.10 shows the propagation paths between the

transmitter and receiver Rx1_20º (receiver at first position with 20º rotation). Path's colour represents the strength of the ray. The strongest ray is the one with red colour which results from reflection of the indoor concrete wall.

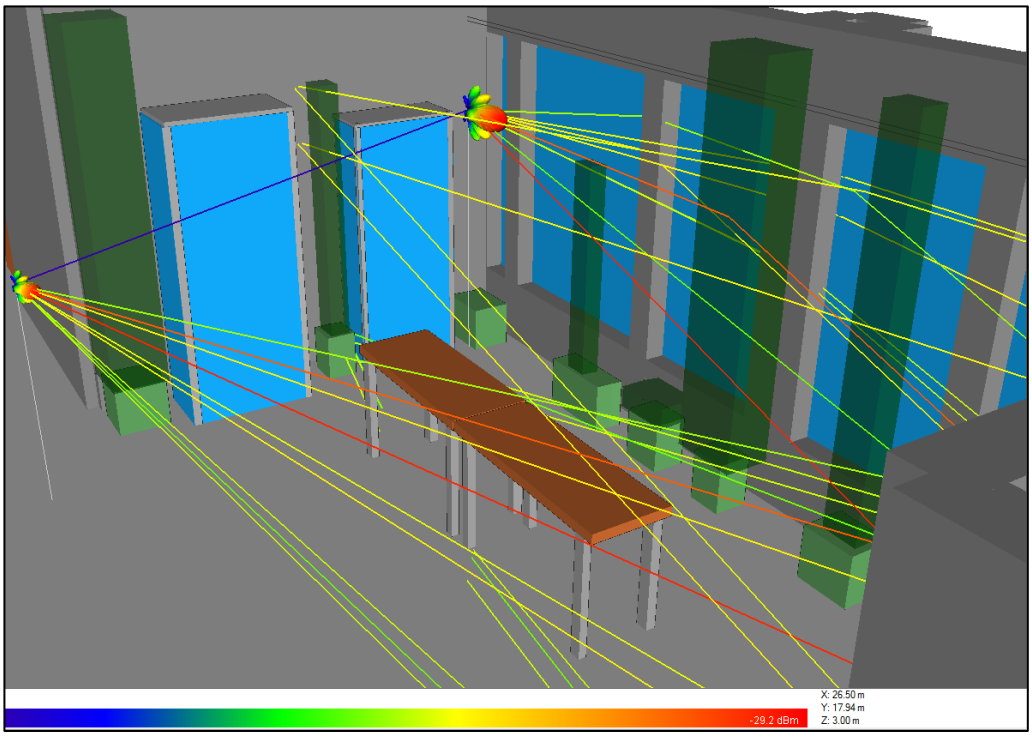

Figure 6.10: Reflection from the concrete wall (strongest path for all Rx1 points).

Figure 6.11 displays power delay profile at receiver Rx1_20º for both measurements and simulations. Concrete relative permittivity is set to be 13 as in [267] and conductivity is set to be 0.8967 S/m as in [54]. The main cluster at 40 ns is due to reflection from the concrete wall as shown in Figure 6.10. The figure shows good agreement between simulations and measurements; the measured RSS was -23.91 dBm while the simulated value was -25.63 dBm.

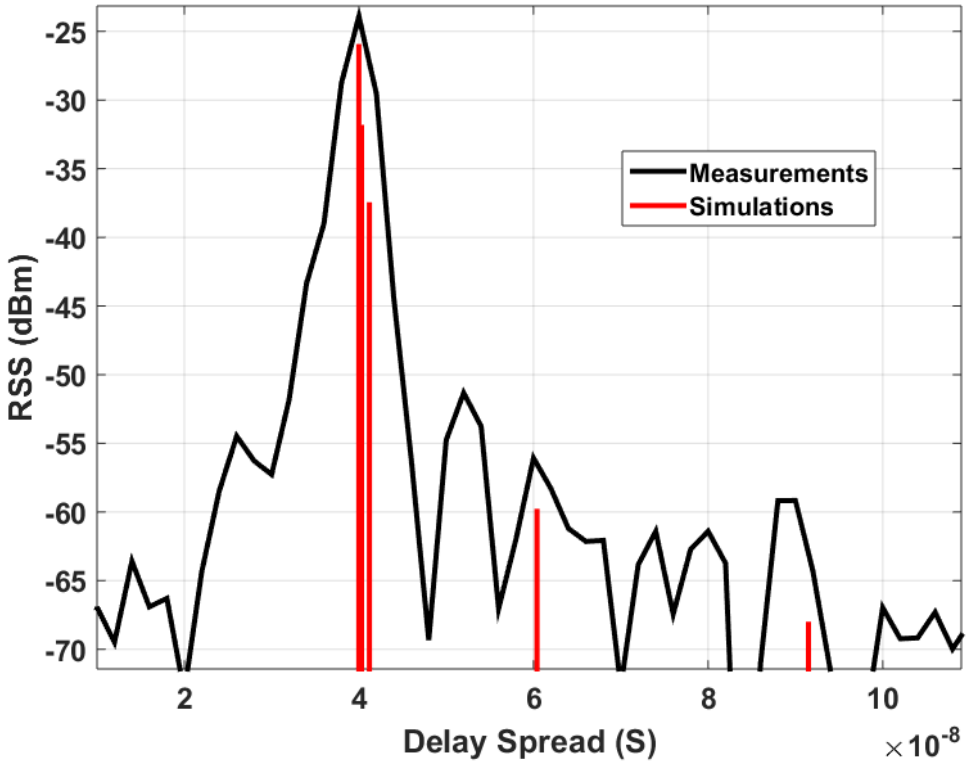

Figure 6.11: Power delay profile at Rx1_20°.

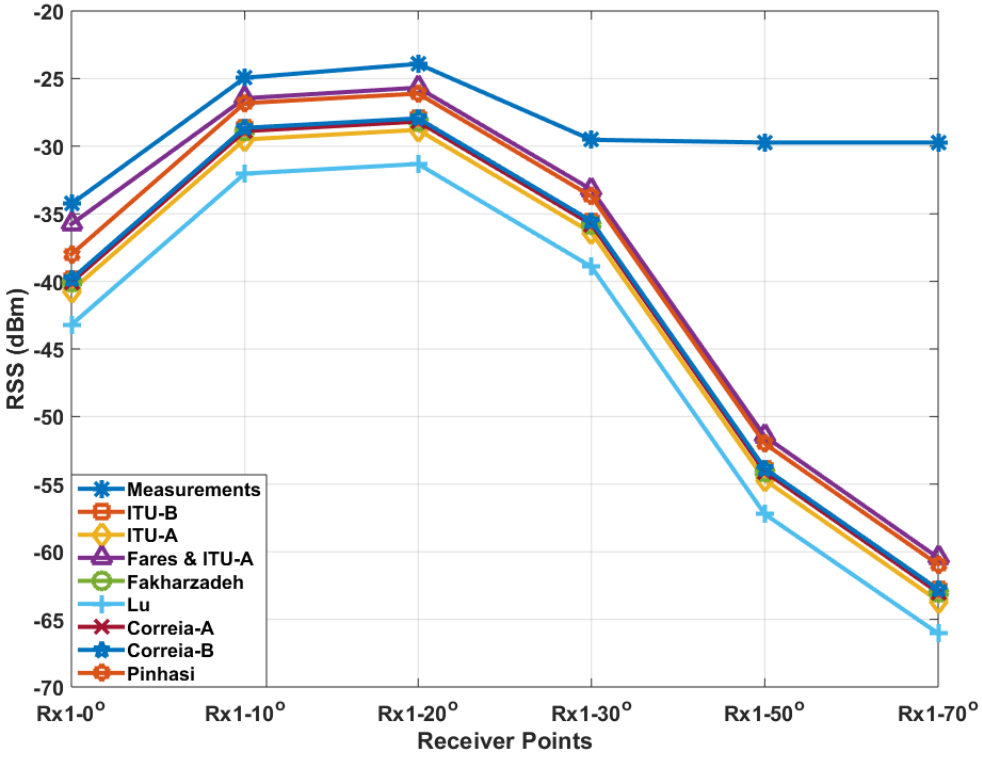

Figure 6.12: Performance comparison between measurements and data taken from references at Rx1.

Figure 6.12 shows a performance comparison for all Rx1 rotations between measurements and simulated results whose complex permittivity values are taken from Table 6-2. Using different complex permittivity values for concrete can vary the results around 3.36 dB as seen in the figure. In comparison with measurements, the best-simulated results for the first four rotations have a mean error of 4.82 dB; however, all simulated results at rotations 50^{o} and 70^{o} have pessimist estimation for RSS as the average difference between measurements and simulations are around 22 dB and 32 dB respectively; while it was around 5 dB for the first four rotations.

This is maybe explained due to two possible reasons: the first reason is due to the location/or the alignment of the transmitter and receiver are not exactly the same as in the measurements, despite the detailed preparation of the procedure, it's difficult to match the locations with 100% accuracy. Therefore, receiver's location in the software was replaced within ± 4 cm in all dimensions. The results were almost the same; the receiver also has been rotated ± 2^{o} and almost no significant difference was observed.

The second possibility is due to the effect of antenna radiation pattern, which is found to be very sensitive to antenna's dimensions, although the receiver antenna used in the measurements is horn antenna; however, there is slight difference between this antenna and the typical horn antenna build-in the Wireless InSite, adjusting the dimensions of the antenna around 1 cm can change the simulated results more than 2 dB.

Position 2:

In the second position, when the receiver is rotated with angles 120º-180º, the main cluster found to be in LOS with the transmitter, while for 210º-250º rotations, the main cluster is reflected from a wooden board.

Case 1: LOS for (120º-180º) rotation

As seen in Figure 6.13, both Tx and Rx are in LOS while bore-sight for both antennae is not in direct contact. Since it is a LOS propagation, changing complex permittivity values for building material will have no effect on RSS of the main cluster.

Figure 6.13 shows the LOS and two reflected ray propagation paths from the transmitter to the receiver at the second position with 150º rotation. The strongest path is the direct LOS between the transmitter and the receiver, while the second one is reflected from two concrete walls. The power of these rays are presented in Figure 6.14.

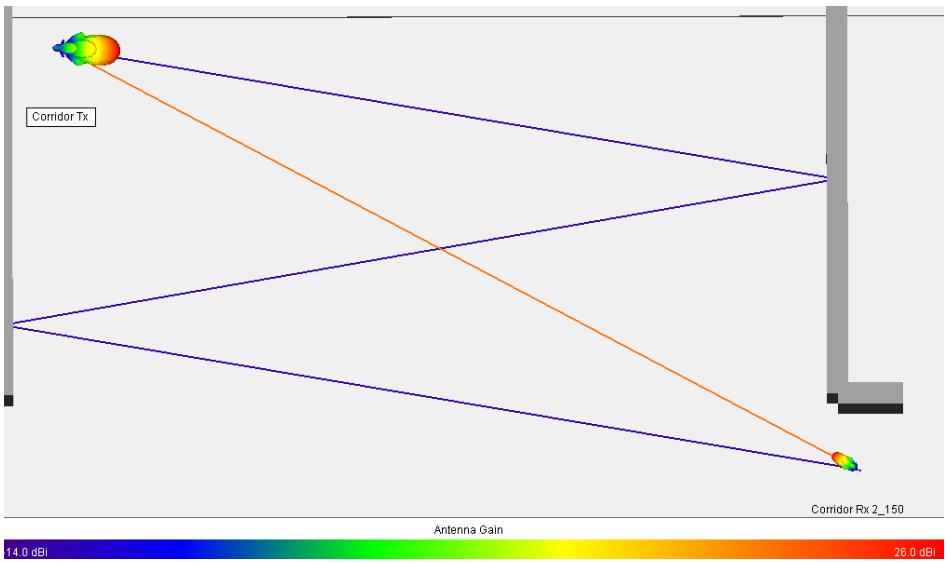

Figure 6.13: LOS and two reflected ray propagation paths from the transmitter to Rx2_150º.

The RSS of the LOS measurement is -24.16 dBm while the simulated results are -28.31 dBm; this may be regarded due to the slight difference in the receiver antenna pattern for simulation and measurements. The second ray reflected from two concrete walls, the measured value is -40.34 dBm while the simulated one is -48.39 dB. Such significant difference may be regarded to reflection from two walls in addition to the slight difference of the receiver antenna patterns.

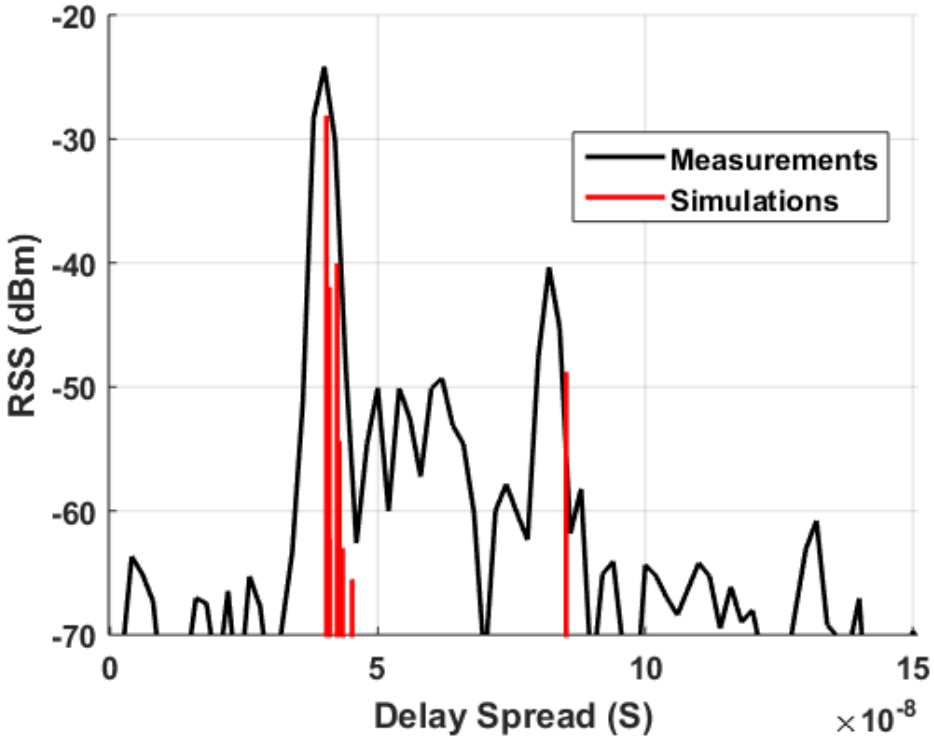

Figure 6.14: Power delay profile at Rx2_150^{o}.

Table 6-4 presents the difference in comparison between the simulation and measurements at Rx2 (120^{o}-180^{o}). As seen in the table, the mean difference is around 7.78 dB. Similar to above observation this may be regarded due to the slight difference in the receiver antenna pattern for simulation and measurements.

Table 6-4: Performance comparison between simulation and measurements at Rx2 (120º-180º) for LOS component.

Receiver	Measured	Simulated
Rx2_120	-42.89	-51.742
Rx2_130	-33.82	-46.533
Rx2_140	-23.86	-34.464
Rx2_150	-24.16	-28.308
Rx2_160	-25.78	-30.812
Rx2_170	-52.46	-41.34
Rx2_180	-50.37	-48.37

Table 6-5: Performance comparison between simulation and measurements at Rx2 (120º-180º) for two wall reflection components.

	Meas.	[267]+[54]	[54] (a)	[54] (b)	[269]	[270]	[271] (a)	[271] (b)	[272]
Rx2_120	-58.53	-63.45	-69.61	-67.9	-68.36	-74.76	-68.35	-67.87	-64.12
Rx2_130	-54.3	-63.97	-70.13	-68.42	-68.88	-75.28	-68.87	-68.39	-64.64
Rx2_140	-54.98	-53.36	-59.51	-57.81	-58.26	-64.66	-58.25	-57.78	-54.02
Rx2_150	-40.34	-48.39	-54.6	-52.89	-53.35	-59.75	-53.34	-52.86	-49.11
Rx2_160	-37.92	-35.65	-41.81	-40.1	-40.56	-46.96	-40.55	-40.07	-36.32
Rx2_170	-39.38	-31.34	-37.5	-35.79	-36.24	-42.65	-36.23	-35.76	-32.01
Rx2_180	-46.2	-35.01	-35.5	-39.44	-39.89	-46.3	-39.88	-39.41	-35.66

Simulated results for the ray reflected from two concrete walls reflected are presented in Table 6-5. The RMSE for the examined references in the table are 7.37, 10.21, 8.59, 8.83, 13.45, 8.82, 8.57, 7.40 dB respectively. Values taken from [267] and [54] give the best result while data taken from [270] give the worst results.

Case 2: Reflection from wooden board for (210º-250º) rotations.

The paths with strongest SS received at the second location with rotations (210º-250º) were reflected from the wooden board as shown in Figure 6.15. As seen, the ray is not from the bore-sight; therefore, the simulated values may be slightly different from measurements.

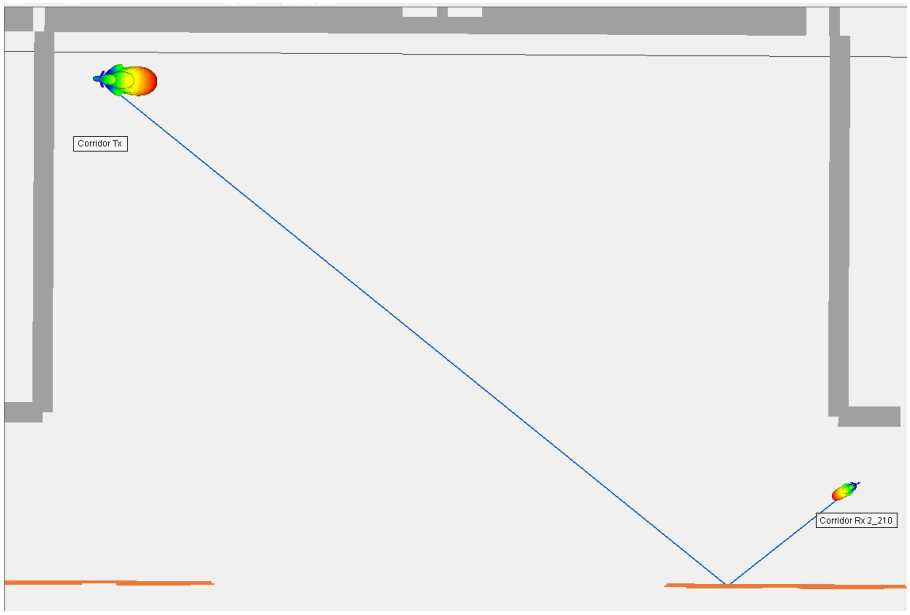

Figure 6.15: Reflection from the wooden wall (strongest paths for all Rx2 (210º-250º)).

Figure 6.16 shows performance comparison between references at Rx2, the closest performance is obtained by using values from [270] while the worst performance is obtained by using values from [272]-(b) where the mean difference between simulation results is around 5.26 dB. The mean RSS difference between the best results and measurements is around 11.7 dB, which is relatively high value, specially at 240º and 250º rotations as the error differences were around 24 dB and 20 dB respectively. Similar to above observation this may be regarded due to the slight difference in the receiver antenna pattern for simulation and measurements.

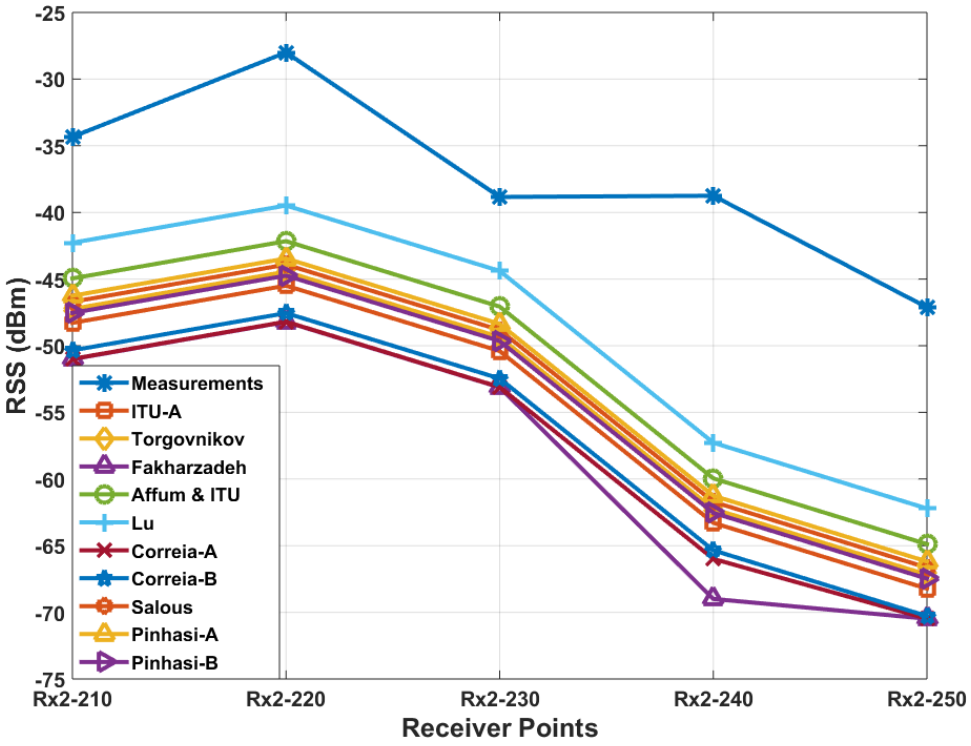

Figure 6.16: Performance comparison between references at Rx2 (210º-250º).

***Position 3**: Reflection from two wooden surfaces.*

Figure 6.17 presents the strongest path between the transmitter and the receiver at the third position with 150º rotation. As seen in the figure the strongest ray is reflected from two wooden surfaces.

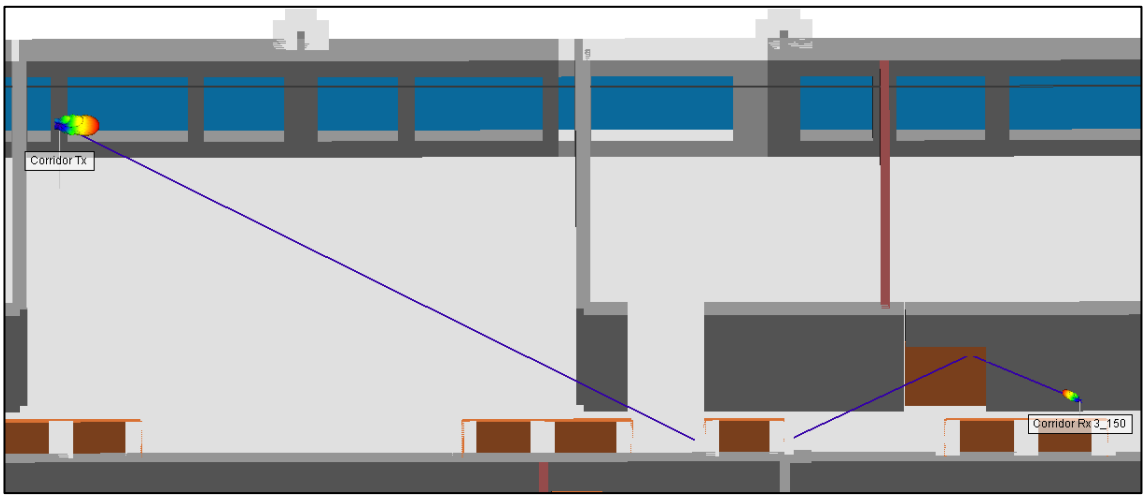

Figure 6.17: Reflection from two wooden surfaces strongest paths for all Rx3.

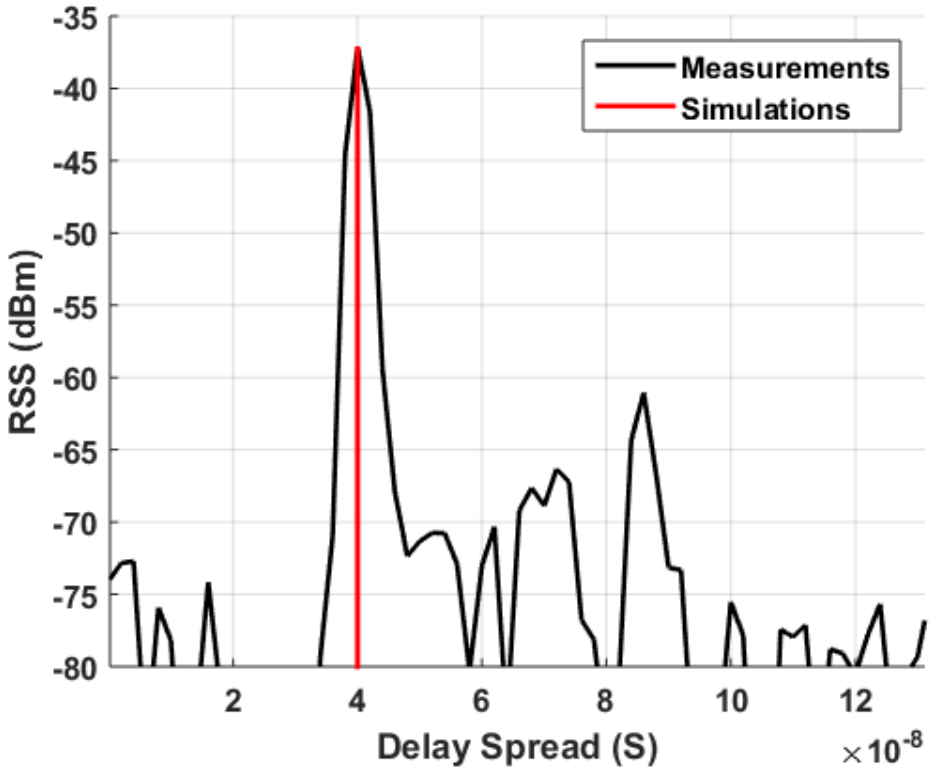

Figure 6.18: Power delay profile at Rx3_150.

The PDP is presented in Figure 6.18; the RSS of the strongest path in the measurements is -37.11 dBm while the simulation results is -37.25 dBm which shows perfect agreement; however, another three measurements have RSS bigger than -70 dBm in which the Wireless InSite overestimated the transmission losses and thus the results were pessimistic.

Table 6-6 presents a performance comparison between references from the literature and measurements at the third receiver positions. As seen from the table, rotating 10 degrees made the measured value to be less more than 20 dB. This exemplifies how much the channel is sensitive and unpredictable. This sudden change may be due to change in propagation paths or due to the presence of a human in the time of making measurements. For all data are taken from the literature, such a sudden change could not be observed by just changing the complex permittivity values.

Table 6-6: Performance comparison between references from literature and measurements at the third receiver position.

	Rotations	
	Rx3_150^{o}	Rx3_160^{o}
Measured	-37.11	-58.14
[54]-(a)	-50.05	-49.03
[268]	-48.73	-47.72
[269]	-54.60	-53.60
[273]+ [54]-(a)	-44.70	-43.70
[270]	-37.25	-39.77
[271]-(a)	-54.55	-53.54
[271]-(b)	-56.93	-55.91
[274]	-47.70	-46.69
[272]-(a)	-46.80	-45.79
[272]-(b)	-48.94	-47.93

In general, for wooden surfaces complex permittivity values from reference [270] tend to have better values, while for concrete best results obtained when relative permittivity is 13 as in [267] and when conductivity is 0.8967 as in [54](a).

The obtained results suggest that building material in references [267] and [54] for concrete and in [270] for wood may be more similar to the material used in our environment compared to other references. Therefore, values in other references are not necessarily inaccurate and may be suitable for other environments.

Wireless InSite software is sensitive to complex permittivity values, antenna pattern, dimensions of the environment and the exact locations of transmitters

and receivers. As long the user takes into account these factors results can be considered as representative.

Chapter 7

Conclusions and Recommendations for Future Work

7.1 Conclusions

The objective of this work is to enhance the awareness of the indoor propagation behaviour, by a set of investigations including simulations and measurements being conducted. These investigations include indoor propagation behaviour, local mean power estimation, proposing new indoor path loss model and introducing a study on 60 GHz propagation in the indoor environment using ray tracing and measurements.

- A survey of indoor propagation mechanisms and manifestations has been presented. It has been aimed at helping to achieve a better understanding of indoor service applications: the study explores the major differences between outdoor and indoor propagation and provides current frequency allocations for many indoor applications. Channel modelling, including empirical and deterministic approaches, has been introduced. Building material properties with frequency have also been investigated with a comparison of current research outcomes. Many models for propagation through buildings were introduced and compared.

- A study on indoor localization techniques was introduced using channel inferred parameters including angle of arrival (AOA), time of arrival (TOA) and received signal strength (RSS). A set of comparisons between the applied techniques were suggested and investigated.

- A comprehensive study on estimating local average signal strength (SS) for indoor multipath propagation has been conducted. The study covered the effect of the required number of the SS collected points samples, the distance between these sample points and the distribution of them. It was found that the effect of fast fading was reduced sufficiently using two-dimensional horizontal configuration samples and using the same number of samples with larger spacing compared to a small spacing. It was also noticed that using larger configuration averaging improved results for some arrangement types.

- A modified indoor path loss prediction model has been presented using ray tracing software and then verified experimentally for 2.4 GHz and 5.3 GHz WLAN frequency bands. In the simulation part, the model was examined and compared to other indoor path loss models at 2.4, 5.3, 28, 60, and 73.5 GHz with different antenna polarization. In the experimental part, the model was compared to similar models at 2.4 and 5.3 GHz. In the simulation part, EWLM shows the best performance as it outperforms the dual-slope model by a factor of two. Similar observations were recorded from the experimental results. DSM showed the second best performance provided that it is equipped with sufficient data points. OSM and LAM have similar behaviour, and the two models showed dependency on operating frequency and antenna polarization. The PM showed the poorest performance as it has fixed path loss exponents.

- Finally, a detailed study on indoor propagation environment at 60 GHz is conducted. The collected measurements were compared to Wireless

InSite simulation results. The study includes LOS and NLOS propagation, the effect of using different electrical parameters values recorded in literature are investigated for different materials.

7.2 Recommendation for future work

Market demands on localization are growing as there is always a margin for improvement. This can be achieved by enhancing understanding of propagation in indoor environments and by proposing robust localization algorithms. Some of the topics that can be of interest for further research are listed as follows:

- A similar analysis to that conducted in Chapter 5 can be performed for 5 GHz band and the mm-wave bands since 5 GHz is already implemented in WLAN systems and the trend for the 5G systems is targeting the mm-wave frequencies.

- Further validation for Wireless InSite can be performed by estimating electrical parameters values at 60 GHz using Friss reflection and transmission equations and then apply them in the software for validation.

- Multi-radio maps can be used to mitigate the effect of using single radio map for the RF-fingerprinting technique, the maps suggested considering the effect of absence and presence of people and the effect of having out of service APs.

- Localization could be improved by having hybrid algorithm between proximity and RF-fingerprinting, radio maps can be divided into sub-radio maps based on proximity which will reduce computation process while the RF fingerprinting will operate in the sub-radio maps.

Bibliography

1. Fernández-Madrigal, J.-A., *Simultaneous Localization and Mapping for Mobile Robots: Introduction and Methods: Introduction and Methods*. 2012: IGI Global.
2. Pace, S., et al., *The global positioning system: assessing national policies*. 1995, DTIC Document.
3. GPS.fov. *GPS Accuracy*. 24/ May /2016]; Available from: http://www.gps.gov/systems/gps/performance/accuracy/.
4. Ladd, A.M., et al., *On the feasibility of using wireless ethernet for indoor localization.* IEEE Transactions on Robotics and Automation, 2004. **20**(3): p. 555-559.
5. Gu, Y., A. Lo, and I. Niemegeers, *A survey of indoor positioning systems for wireless personal networks.* Communications Surveys & Tutorials, IEEE, 2009. **11**(1): p. 13-32.
6. Suits, J.I., et al., *Personal alert safety system localization field tests with firefighters.* The Journal of the Acoustical Society of America, 2014. **136**(4): p. 2166-2166.
7. Pierleoni, P., et al. *Indoor localization system for AAL over IPv6 WSN*. in *2016 IEEE 27th Annual International Symposium on Personal, Indoor, and Mobile Radio Communications (PIMRC)*. 2016. Valencia, Spain.
8. Zhang, R., F. Hoflinger, and L. Reindl, *Inertial sensor based indoor localization and monitoring system for emergency responders.* IEEE Sensors Journal, 2013. **13**(2): p. 838-848.
9. Obeidat, H.A., et al., *A Comparison between Vector Algorithm and CRSS Algorithms for Indoor Localization using Received Signal Strength.* The Applied Computational Electromagnetics Society (ACES), 2016. **31**: p. 868-876.
10. Keenan, J. and A. Motley, *Radio coverage in buildings.* British telecom technology Journal, 1990. **8**(1): p. 19-24.
11. Borrelli, A., et al. *Channel models for IEEE 802.11 b indoor system design*. in *Communications, 2004 IEEE International Conference on*. 2004. IEEE.
12. Crow, B.P., et al., *IEEE 802.11 wireless local area networks.* IEEE Communications magazine, 1997. **35**(9): p. 116-126.
13. Kong, Z.-n., et al., *Performance analysis of IEEE 802.11 e contention-based channel access.* IEEE Journal on selected areas in communications, 2004. **22**(10): p. 2095-2106.
14. Damosso, E. and L. Correia, *Digital Mobile Radio Towards Future Generation Systems Communications. COST 231 Final Report.* CEC, Brussels, Belgium, 1999.
15. Zekavat, R. and R.M. Buehrer, *Handbook of position location: Theory, practice and advances*. Vol. 27. 2011: John Wiley & Sons.
16. Moraitis, N. and P. Constantinou, *Indoor channel measurements and characterization at 60 GHz for wireless local area network applications.* IEEE Transactions on Antennas and Propagation, 2004. **52**(12): p. 3180-3189.
17. Saleh, A.A. and R.A. Valenzuela, *A statistical model for indoor multipath propagation.* Selected Areas in Communications, IEEE Journal on, 1987. **5**(2): p. 128-137.
18. Remcom. *Wireless Insite*. 2017 05 Jan 2017; Available from: http://www.remcom.com/wireless-insite.

19. Valenzuela, R.A., O. Landron, and D. Jacobs, *Estimating local mean signal strength of indoor multipath propagation.* IEEE transactions on vehicular technology, 1997. **46**(1): p. 203-212.
20. REMCOM, *Wireless InSite Reference Manual*. 2017, REMCOM: State College, Pennsylvania.
21. Hashemi, H., *The indoor radio propagation channel.* Proceedings of the IEEE, 1993. **81**(7): p. 943-968.
22. Spencer, Q.H., et al., *Modeling the statistical time and angle of arrival characteristics of an indoor multipath channel.* IEEE Journal on Selected Areas in Communications, 2000. **18**(3): p. 347-360.
23. Goldsmith, A., *Wireless communications*. 2005: Cambridge university press.
24. Yassin, A., et al., *Recent Advances in Indoor Localization: A Survey on Theoretical Approaches and Applications.* IEEE Communications Surveys & Tutorials, 2016.
25. Chowdhary, N., S. Kaur, and S. Mahajan, *Study and Analysis of LTE-Advanced Systems at 2.6 GHz for Indoor Large Hall.* 2016.
26. Blaunstein, N. and C. Christodoulou, *Indoor radio propagation.* Radio Propagation and Adaptive Antennas for Wireless Communication Links: Terrestrial, Atmospheric and Ionospheric, 2014: p. 302-334.
27. Cao, Z., et al., *38-GHz Millimeter Wave Beam Steered Fiber Wireless Systems for 5G Indoor Coverage: Architectures, Devices and Links.* IEEE Journal of Quantum Electronics, 2016.
28. Chen, S. and J. Zhao, *The requirements, challenges, and technologies for 5G of terrestrial mobile telecommunication.* IEEE Communications Magazine, 2014. **52**(5): p. 36-43.
29. Chai, P. and L. Zhang. *Indoor radio propagation models and wireless network planning*. in *Computer Science and Automation Engineering (CSAE), 2012 IEEE International Conference on*. 2012. IEEE.
30. Saunders, S. and A. Aragón-Zavala, *Antennas and Propagation for Wireless Communication Systems: 2nd Edition*. 2007: John Wiley & Sons.
31. Sheikhsofla, M. and K. Sarabandi. *Indoor wave propagation simulations at HF using rayleigh-gans approximation*. in *Radio Science Meeting (Joint with AP-S Symposium), 2013 USNC-URSI*. 2013. IEEE.
32. Zhu, Y., et al. *Demystifying 60GHz outdoor picocells*. in *Proceedings of the 20th annual international conference on Mobile computing and networking*. 2014. ACM.
33. Kutty, S. and D. Sen. *An improved numerical optimization method for efficient beam search in 60 GHz indoor millimeter wave wireless networks*. in *Advanced Networks and Telecommuncations Systems (ANTS), 2015 IEEE International Conference on*. 2015. IEEE.
34. Alippi, C., et al., *RTI goes wild: Radio tomographic imaging for outdoor people detection and localization.* IEEE Transactions on Mobile Computing, 2016. **15**(10): p. 2585-2598.
35. Sun, S., G.R. MacCartney, and T.S. Rappaport. *Millimeter-wave distance-dependent large-scale propagation measurements and path loss models for outdoor and indoor 5G systems*. in *Antennas and Propagation (EuCAP), 2016 10th European Conference on*. 2016. IEEE.
36. Awad, M.K., K.T. Wong, and Z.-b. Li, *An integrated overview of the open literature's empirical data on the indoor radiowave channel's delay properties.* Antennas and Propagation, IEEE Transactions on, 2008. **56**(5): p. 1451-1468.

37. Saha, S.K., A. Garg, and D. Koutsonikolas. *A first look at TCP performance in indoor IEEE 802.11 ad WLANs*. in *Computer Communications Workshops (INFOCOM WKSHPS), 2015 IEEE Conference on*. 2015. IEEE.
38. Qadar, N., et al. *Investigating the Effects of Microwave Oven on the Performance of Wi-Fi Network*. in *Frontiers of Information Technology (FIT), 2014 12th International Conference on*. 2014. IEEE.
39. Samimi, M.K. and T.S. Rappaport, *Characterization of the 28 GHz millimeter-wave dense urban channel for future 5g mobile cellular.* Technical Report, TR 2014-001, 2014.
40. Mautz, R., *Indoor positioning technologies*. 2012, Habilitationsschrift ETH Zürich, 2012.
41. Kim, M.-D., et al. *Path loss measurements and modeling for indoor office scenario at 28 and 38 GHz*. in *Antennas and Propagation (ISAP), 2016 International Symposium on*. 2016. IEEE.
42. Bocquet, M., et al. *Millimeter-wave broadband positioning system for indoor applications*. in *Microwave Symposium Digest (MTT), 2012 IEEE MTT-S International*. 2012.
43. Loyez, C., N. Rolland, and M. Bocquet. *UWB technology applied to millimeter-wave indoor location systems*. in *Radar Conference (Radar), 2014 International*. 2014. IEEE.
44. Zvanovec, S., P. Pechac, and M. Klepal, *Wireless LAN networks design: site survey or propagation modeling?* Radioengineering, 2003. **12**(4): p. 42-49.
45. Alhamoud, A., et al. *Empirical investigation of the effect of the door's state on received signal strength in indoor environments at 2.4 GHz*. in *Local Computer Networks Workshops (LCN Workshops), 2014 IEEE 39th Conference on*. 2014. IEEE.
46. Andersen, J.B., T.S. Rappaport, and S. Yoshida, *Propagation measurements and models for wireless communications channels.* Communications Magazine, IEEE, 1995. **33**(1): p. 42-49.
47. Rappaport, T.S., S.Y. Seidel, and K. Takamizawa, *Statistical channel impulse response models for factory and open plan building radio communicate system design.* Communications, IEEE Transactions on, 1991. **39**(5): p. 794-807.
48. Seidel, S.Y. and T.S. Rappaport, *914 MHz path loss prediction models for indoor wireless communications in multifloored buildings.* IEEE transactions on Antennas and Propagation, 1992. **40**(2): p. 207-217.
49. Lott, M. and I. Forkel. *A multi-wall-and-floor model for indoor radio propagation*. in *Vehicular Technology Conference, 2001. VTC 2001 Spring. IEEE VTS 53rd*. 2001. Rhodes, Greece, Greece: IEEE.
50. Andrade, C.B. and R.P.F. Hoefel. *IEEE 802.11 WLANs: A comparison on indoor coverage models*. in *Electrical and Computer Engineering (CCECE), 2010 23rd Canadian Conference on*. 2010. Calgary, AB, Canada: IEEE.
51. Davies, R., A. Simpson, and J. Mcgreehan, *Propagation measurements at 1.7 GHz for microcellular urban communications.* Electronics letters, 1990. **26**(14): p. 1053-1055.
52. Alsindi, N.A., B. Alavi, and K. Pahlavan, *Measurement and Modeling of Ultrawideband TOA-Based Ranging in Indoor Multipath Environments.* IEEE Transactions on Vehicular Technology, 2009. **58**(3): p. 1046-1058.

53. Lloret, J., et al. *A fast design model for indoor radio coverage in the 2.4 GHz wireless LAN*. in *Wireless Communication Systems, 2004, 1st International Symposium on*. 2004. Mauritius, Mauritius: IEEE.
54. ITU, I.T.U., *Propagation data and prediction methods for the planning of indoor radiocommunication systems and radio local area networks in the frequency range 900 MHz to 100 GHz*, in *Recommendation ITU-R P.1238-7*. 2012, ITU: Geneva.
55. Pedersen, G.F., *COST 231-Digital mobile radio towards future generation systems*. 1999: European Commission.
56. Plets, D., et al., *Coverage prediction and optimization algorithms for indoor environments.* EURASIP Journal on Wireless Communications and Networking, 2012. **2012**(1): p. 123.
57. Zvanovec, S., M. Valek, and P. Pechac. *Results of indoor propagation measurement campaign for WLAN systems operating in 2.4 GHz ISM band*. in *Antennas and Propagation, 2003.(ICAP 2003). Twelfth International Conference on (Conf. Publ. No. 491)*. 2003. Exeter, UK,: IET.
58. Alexander, S. and G. Pugliese, *Cordless communication within buildings: Results of measurements at 900 MHz and 60 GHz.* British Telecom Technology Journal, 1983. **1**(1): p. 99-105.
59. Rappaort, T.S., *Wireless communications: principles and practice*. 2 edition ed. 2002, Upper Saddle River, NJ, USA: Prentice Hall.
60. Devasirvathan, D. *Multi-frequency propagation measurements and models in a large metropolitan commercial building for personal communications*. in *Personal, Indoor and Mobile Radio Communications., IEEE International Symposium on*. 1991. UK: IEEE.
61. Karlsson, P., *Indoor radio propagation for personal communications services*. 1995.
62. Nuangwongsa, K., et al. *Path loss modeling in durian orchard for wireless network at 5.8 GHz*. in *Electrical Engineering/Electronics, Computer, Telecommunications and Information Technology, 2009. ECTI-CON 2009. 6th International Conference on*. 2009. Pattaya, Chonburi, Thailand: IEEE.
63. Cheung, K., et al. *Indoor propagation prediction utilizing a new empirical model*. in *Singapore ICCS'94. Conference Proceedings.* 1994. IEEE.
64. Zhao, Y., M. Li, and F. Shi, *Indoor radio propagation model based on dominant path.* International Journal of Communications, Network and System Sciences, 2010. **3**(3): p. 330.
65. Pahlavan, K. and A.H. Levesque, *Wireless information networks*. Vol. 93. 2005: John Wiley & Sons.
66. Lima, A.G. and L.F. Menezes. *Motley-Keenan model adjusted to the thickness of the wall*. in *SBMO/IEEE MTT-S International Conference on Microwave and Optoelectronics, 2005.* 2005. Brasilia, Brazil: IEEE.
67. Sah, N., et al. *Optimizing the Path Loss of Wireless Indoor Propagation Models Using CSP Algorithms*. in *Computer and Network Technology (ICCNT), 2010 Second International Conference on*. 2010.
68. Sayidmarie, K., A.H. Aboud, and M.S. Salim. *Estimation of wall penetration loss for indoor WLAN systems*. in *Sciences of Electronics, Technologies of Information and Telecommunications (SETIT), 2012 6th International Conference on*. 2012.
69. Lafortune, J.-F. and M. Lecours, *Measurement and modeling of propagation losses in a building at 900 MHz.* Vehicular Technology, IEEE Transactions on, 1990. **39**(2): p. 101-108.

70. Maccartney, G.R., et al., *Indoor Office Wideband Millimeter-Wave Propagation Measurements and Channel Models at 28 and 73 GHz for Ultra-Dense 5G Wireless Networks.* IEEE Access, 2015. **3**: p. 2388-2424.
71. Motley, A. and J. Keenan, *Personal communication radio coverage in buildings at 900 MHz and 1700 MHz.* Electronics Letters, 1988. **24**(12): p. 763-764.
72. Serôdio, C., et al. *A lightweight indoor localization model based on motley-keenan and cost*. in *Proceedings of The World Congress on Engineering 2012, WCE 2012*. 2012. London, U.K.: International Association of Engineers.
73. Chaibi, H., M. Belkasmi, and Z. Mohammadi. *UWB outdoor channel characterization and modeling based on measurements*. in *Wireless Networks and Mobile Communications (WINCOM), 2015 International Conference on*. 2015.
74. Perez-Vega, C. and J. Garcia, *Frequency behavior of a power-law path loss model.* Proc. 10th Microcoll. Budapest, 1999: p. 413-416.
75. Cepeda, R., et al. *On the measurement and simulations of the frequency dependent path loss and MB-OFDM*. in *Ultra-Wideband, 2009. ICUWB 2009. IEEE International Conference on*. 2009.
76. Pajusco, P. and P. Pagani. *Frequency Dependence of the UWB Indoor Propagation Channel*. in *Antennas and Propagation, 2007. EuCAP 2007. The Second European Conference on*. 2007.
77. Wang, Y., et al. *An empirical path loss model in the indoor stairwell at 2.6 GHz*. in *Wireless Symposium (IWS), 2014 IEEE International*. 2014.
78. Turkmani, A. and A. De Toledo. *Radio transmission at 1800 MHz into, and within, multistory buildings*. in *Communications, Speech and Vision, IEE Proceedings I*. 1991. IET.
79. Dey, I., G.G. Messier, and S. Magierowski, *Joint Fading and Shadowing Model for Large Office Indoor WLAN Environments.* IEEE Transactions on Antennas and Propagation, 2014. **62**(4): p. 2209-2222.
80. Bultitude, R., *Measurement, characterization and modeling of indoor 800/900 MHz radio channels for digital communications.* IEEE Communications Magazine, 1987. **25**(6): p. 5-12.
81. Hashemi, H., *Impulse response modeling of indoor radio propagation channels.* Selected Areas in Communications, IEEE Journal on, 1993. **11**(7): p. 967-978.
82. Molina-Garcia, M., A. Fernandez-Duran, and J.I. Alonso. *Application of extreme value distribution to model propagation fading in indoor mobile radio environments*. in *Radio and Wireless Symposium, 2008 IEEE*. 2008.
83. Diaz, N.R. and J.E.J. Esquitino. *Wideband channel characterization for wireless communications inside a short haul aircraft*. in *Vehicular Technology Conference, 2004. VTC 2004-Spring. 2004 IEEE 59th*. 2004.
84. Eluma, G. and K. Arshad. *Indoor statistical channel modelling using Agilent 8960*. in *Current Trends in Information Technology (CTIT), 2013 International Conference on*. 2013.
85. Jiang, L. and S.Y. Tan, *Geometrically Based Statistical Channel Models for Outdoor and Indoor Propagation Environments.* IEEE Transactions on Vehicular Technology, 2007. **56**(6): p. 3587-3593.
86. Hashemi, H. and D. Tholl, *Statistical modeling and simulation of the RMS delay spread of indoor radio propagation channels.* Vehicular Technology, IEEE Transactions on, 1994. **43**(1): p. 110-120.

87. Suzuki, H., *A statistical model for urban radio propogation.* Communications, IEEE Transactions on, 1977. **25**(7): p. 673-680.
88. Bhaskar, V. and P.A. Devi, *Performance of multiband orthogonal frequency division multiplexing network in ultra wideband channels incorporating people shadowing and channel fading.* IET Communications, 2013. **7**(15): p. 1665-1675.
89. Poon, A.S. and M. Ho. *Indoor multiple-antenna channel characterization from 2 to 8 GHz*. in *ICC*. 2003.
90. Chong, C.-C., et al., *A new statistical wideband spatio-temporal channel model for 5-GHz band WLAN systems.* IEEE Journal on selected areas in Communications, 2003. **21**(2): p. 139-150.
91. Molisch, A.F., et al., *A Comprehensive Standardized Model for Ultrawideband Propagation Channels.* IEEE Transactions on Antennas and Propagation, 2006. **54**(11): p. 3151-3166.
92. Meijerink, A. and A.F. Molisch, *On the Physical Interpretation of the Saleh–Valenzuela Model and the Definition of Its Power Delay Profiles.* IEEE Transactions on Antennas and Propagation, 2014. **62**(9): p. 4780-4793.
93. Hashemi, H. and D. Tholl. *Analysis of the RMS delay spread of indoor radio propagation channels*. in *Communications, 1992. ICC '92, Conference record, SUPERCOMM/ICC '92, Discovering a New World of Communications., IEEE International Conference on*. 1992.
94. Wang, Y., W.-J. Lu, and H.-B. Zhu, *Propagation characteristics of the LTE indoor radio channel with persons at 2.6 GHz.* IEEE Antennas and Wireless Propagation Letters, 2013. **12**: p. 991-994.
95. Ghassemzadeh, S.S., et al., *Measurement and modeling of an ultra-wide bandwidth indoor channel.* IEEE Transactions on Communications, 2004. **52**(10): p. 1786-1796.
96. De la Roche, G., A. Alayón-Glazunov, and B. Allen, *LTE-advanced and next generation wireless networks: channel modelling and propagation*. 2012: John Wiley & Sons.
97. Nobles, P., D. Ashworth, and F. Halsall. *Propagation measurements in an indoor radio environment at 2, 5 and 17 GHz*. in *High Bit Rate UHF/SHF Channel Sounders-Technology and Measurement, IEE Colloquium on*. 1993. IET.
98. Takamizawa, K., S. Seidel, and T. Rappaport. *Indoor radio channel models for manufacturing environments*. in *Southeastcon'89. Proceedings. Energy and Information Technologies in the Southeast., IEEE*. 1989. IEEE.
99. Heidari-Bateni, G. and C.D. McGillem. *Performance Limitations Of The Indoor Radio Channel*. in *Personal, Indoor and Mobile Radio Communications., IEEE International Symposium on*. 1991.
100. Rappaport, T.S. and C.D. McGillem, *UHF fading in factories.* Selected Areas in Communications, IEEE Journal on, 1989. **7**(1): p. 40-48.
101. Hashemi, H., D. Lee, and D. Ehman. *Statistical modeling of the indoor radio propagation channel. II*. in *Vehicular Technology Conference, 1992, IEEE 42nd*. 1992. IEEE.
102. Howard, S.J. and K. Pahlavan, *Doppler spread measurements of indoor radio channel.* Electronics Letters, 1990. **26**(2): p. 107-109.
103. Hanssens, B., et al. *Measurement-based analysis of doppler characteristics for Ultra-Wideband radio channels in an office*

environment. in *Antennas and Propagation Society International Symposium (APSURSI), 2014 IEEE*. 2014. IEEE.
104. Renaudin, V., Z. He, and M. Petovello. *Characterization of the impact of indoor Doppler errors on Pedestrian Dead Reckoning*. in *Position Location and Navigation Symposium (PLANS), 2012 IEEE/ION*. 2012.
105. Va, V. and R.W. Heath. *Basic relationship between channel coherence time and beamwidth in vehicular channels*. in *Vehicular Technology Conference (VTC Fall), 2015 IEEE 82nd*. 2015. IEEE.
106. Meinilä, J., et al., *WINNER II channel models.* Radio Technologies and Concepts for IMT-Advanced, 2009: p. 39-92.
107. Wang, Y., S. Safavi-Naeini, and S.K. Chaudhuri, *A hybrid technique based on combining ray tracing and FDTD methods for site-specific modeling of indoor radio wave propagation.* Antennas and Propagation, IEEE Transactions on, 2000. **48**(5): p. 743-754.
108. Wölfle, G., et al. *Dominant path prediction model for indoor scenarios*. in *German Microwave Conference (GeMIC)*. 2005.
109. Austin, A.C.M., M.J. Neve, and G.B. Rowe, *Modeling Propagation in Multifloor Buildings Using the FDTD Method.* IEEE Transactions on Antennas and Propagation, 2011. **59**(11): p. 4239-4246.
110. Pozar, D.M., *Microwave engineering*, ed. t. Edition. 2012: John Wiley & Sons.
111. Nagy, L., R. Dady, and A. Farkasvolgyi. *Algorithmic complexity of FDTD and ray tracing method for indoor propagation modelling*. in *2009 3rd European Conference on Antennas and Propagation*. 2009. IEEE.
112. Tirkas, P.A., et al., *Finite-difference time-domain method for electromagnetic radiation, interference, and interaction with complex structures.* Electromagnetic Compatibility, IEEE Transactions on, 1993. **35**(2): p. 192-203.
113. Hao, Y. and R. Mittra, *FDTD modeling of metamaterials: Theory and applications*. 2008: Artech house.
114. Remley, C.A., *Time domain modeling of electromagnetic radiation with application to ultrafast electronic and wireless communications systems*. 1999.
115. Nagy, L. *Indoor propagation modeling for short range devices*. in *Antennas and Propagation, 2007. EuCAP 2007. The Second European Conference on*. 2007. IET.
116. Virk, U., et al. *Full-wave characterization of indoor office environment for accurate coverage analysis*. in *Electromagnetics in Advanced Applications (ICEAA), 2013 International Conference on*. 2013. IEEE.
117. Remley, K.A., R. Anderson, and A. Weisshar, *Improving the accuracy of ray-tracing techniques for indoor propagation modeling.* Vehicular Technology, IEEE Transactions on, 2000. **49**(6): p. 2350-2358.
118. Gschwendtner, B., et al., *Ray tracing vs. ray launching in 3-D microcell modelling.* 1995.
119. Lawton, M.C. and J. McGeehan, *The application of a deterministic ray launching algorithm for the prediction of radio channel characteristics in small-cell environments.* Vehicular Technology, IEEE Transactions on, 1994. **43**(4): p. 955-969.
120. Lee, B., A. Nix, and J. McGeehan. *Indoor space-time propagation modelling using a ray launching technique*. in *Antennas and Propagation, 2001. Eleventh International Conference on (IEE Conf. Publ. No. 480)*. 2001. IET.

121. Athanasiadou, G., A. Nix, and J. McGeehan. *A ray tracing algorithm for microcellular and indoor propagation modelling*. in *Antennas and Propagation, 1995., Ninth International Conference on (Conf. Publ. No. 407)*. 1995. IET.
122. Liu, Z.-Y., et al., *Sensitivity of power and RMS delay spread predictions of a 3D indoor ray tracing model.* Optics Express, 2016. **24**(12): p. 13179-13193.
123. Yun, Z. and M.F. Iskander, *Ray tracing for radio propagation modeling: principles and applications.* IEEE Access, 2015. **3**: p. 1089-1100.
124. HyperWorks, A. *WinProp*. 2017 10 Jan 2018; Available from: http://www.altairhyperworks.com/product/FEKO/WinProp-Propagation-Modeling.
125. Wireless, E. *EDX Signal Pro*. 2017 15 Jan 2018; Available from: http://edx.com/products/indoor/.
126. iBWAVE. *iBWAVE Wi-Fi*. 2018 20 Jan 2018]; Available from: http://www.ibwave.com/ibwave-wi-fi.
127. Yoon, Y.-K., M.-W. Jung, and J. Kim. *Intelligent ray tracing for the propagaiton prediction*. in *Proceedings of the 2012 IEEE International Symposium on Antennas and Propagation*. 2012.
128. Communications, A. *Indoor Ray Optical Propagation Models, Highly accurate ray optical prediction models*. AWE Communications, Wave Propagation and Radio Network Planning 2016 10/May/2018; Available from: http://awe-communications.com/Propagation/Indoor/RayOptical/index.htm.
129. Porebska, M., T. Kayser, and W. Wiesbeck. *Verification of a hybrid ray-tracing/FDTD model for indoor ultra-wideband channels*. in *Wireless Technologies, 2007 European Conference on*. 2007. IEEE.
130. Nagy, L. *Comparison and application of FDTD and ray optical method for indoor wave propagation modeling*. in *Proceedings of the Fourth European Conference on Antennas and Propagation*. 2010. IEEE.
131. Nagy, L., *FDTD and ray optical methods for indoor wave propagation modeling.* Mikrotalasna revija, 2010.
132. Thiel, M. and K. Sarabandi, *A hybrid method for indoor wave propagation modeling.* IEEE transactions on antennas and propagation, 2008. **56**(8): p. 2703-2709.
133. Kim, H., B. Kim, and Y. Lee. *An accurate indoor propagation analysis for Wi-Fi antenna embedded in a commercial TV set*. in *The 8th European Conference on Antennas and Propagation (EuCAP 2014)*. 2014. IEEE.
134. Zakharov, P., et al. *Finite Integration Technique capabilities for indoor propagation prediction*. in *Antennas & Propagation Conference, 2009. LAPC 2009. Loughborough*. 2009. IEEE.
135. Wolfle, G. and F. Landstorfer. *Field strength prediction in indoor environments with neural networks*. in *Vehicular Technology Conference, 1997, IEEE 47th*. 1997. IEEE.
136. Plets, D., et al., *Coverage prediction and optimization algorithms for indoor environments.* EURASIP Journal on Wireless Communications and Networking, 2012. **2012**(1): p. 1-23.
137. Wahl, R., et al., *Dominant path prediction model for urban scenarios.* 14th IST Mobile and Wireless Communications Summit, Dresden (Germany), 2005.

138. Wölfle, G., G. Wol, and F. Landstorfer, *Field Strength Prediction With Dominant Paths And Neural Networks For Indoor Mobile Communication.* 1997.
139. Wolfle, G. and F. Landstorfer. *Dominant paths for the field strength prediction*. in *Vehicular Technology Conference, 1998. VTC 98. 48th IEEE*. 1998. IEEE.
140. Woelfe, G., et al., *Extensions to the field strength prediction technique based on dominant paths between transmitter and receiver in indoor wireless communications.* ITG FACHBERICHT, 1997: p. 29-36.
141. ITU, I.T.U., *Effects of building materials and structures on radiowave propagation above about 100 MHz*, in *Recommendation ITU-R P.2040-1*. 2015, Electronic Publication: Geneva.
142. Ulaby, F.T. and U. Ravaioli, *Fundamentals of Applied Electromagnetics 7e*. 2015: Prentice Hall.
143. Stavrou, S. and S. Saunders. *Review of constitutive parameters of building materials*. in *Antennas and Propagation, 2003.(ICAP 2003). Twelfth International Conference on (Conf. Publ. No. 491)*. IET.
144. Safaai-Jazi, A., et al., *Ultra-wideband propagation measurements and channel modeling.* DARPA NETEX Time Domain and RF Measurement Laboratory, Virginia, 2002.
145. Sagnard, F. and G.E. Zein, *In situ characterization of building materials for propagation modeling: Frequency and time responses.* IEEE transactions on antennas and propagation, 2005. **53**(10): p. 3166-3173.
146. Jemai, J., et al. *Determination of the permittivity of building materials through WLAN measurements at 2.4 GHz*. in *2005 IEEE 16th International Symposium on Personal, Indoor and Mobile Radio Communications*. 2005. IEEE.
147. Cuiñas, I. and M.G. Sánchez, *Permittivity and conductivity measurements of building materials at 5.8 GHz and 41.5 GHz.* Wireless Personal Communications, 2002. **20**(1): p. 93-100.
148. Kakar, F.A.K., K.A. Sani, and F. Elahi. *Essential factors influencing building penetration loss*. in *Communication Technology, 2008. ICCT 2008. 11th IEEE International Conference on*. 2008.
149. Celik, S., et al. *Indoor to outdoor propagation model improvement for GSM900/GSM1800/CDMA-2100*. in *2011 XXXth URSI General Assembly and Scientific Symposium*. 2011.
150. Okamoto, H., K. Kitao, and S. Ichitsubo, *Outdoor-to-Indoor Propagation Loss Prediction in 800-MHz to 8-GHz Band for an Urban Area.* IEEE Transactions on Vehicular Technology, 2009. **58**(3): p. 1059-1067.
151. Miura, Y., Y. Oda, and T. Taga. *Outdoor-to-indoor propagation modelling with the identification of path passing through wall openings*. in *Personal, Indoor and Mobile Radio Communications, 2002. The 13th IEEE International Symposium on*. 2002. IEEE.
152. Suikkanen, E., A. Tölli, and M. Latva-aho. *Characterization of propagation in an outdoor-to-indoor scenario at 780 MHz*. in *21st Annual IEEE International Symposium on Personal, Indoor and Mobile Radio Communications*. 2010. IEEE.
153. Alatossava, M., et al. *Extension of COST 231 path loss model in outdoor-to-indoor environment to 3.7 ghz and 5.25 ghz*. in *11th International Symposium on Wireless Personal Multimedia Communications (WPMC)*. 2008.

154. Hägerling, C., C. Ide, and C. Wietfeld. *Coverage and capacity analysis of wireless M2M technologies for smart distribution grid services*. in *Smart Grid Communications (SmartGridComm), 2014 IEEE International Conference on*. 2014. IEEE.
155. Müller, C., et al. *Performance analysis of radio propagation models for smart grid applications*. in *Smart Grid Communications (SmartGridComm), 2011 IEEE International Conference on*. 2011. IEEE.
156. Aguirre, S., L.H. Loew, and Y. Lo. *Radio propagation into buildings at 912, 1920, and 5990 MHz using microcells*. in *Universal Personal Communications, 1994. Record., 1994 Third Annual International Conference on*. 1994. IEEE.
157. Wells, P.I., *The attenuation of UHF radio signals by houses.* Vehicular Technology, IEEE Transactions on, 1977. **26**(4): p. 358-362.
158. Ferreira, L., et al. *Characterisation of Signal Penetration into Buildings for GSM and UMTS*. in *Wireless Communication Systems, 2006. ISWCS'06. 3rd International Symposium on*. 2006. IEEE.
159. Schwengler, T. and M. Glbert. *Propagation models at 5.8 GHz-path loss and building penetration*. in *Radio and Wireless Conference, 2000. RAWCON 2000. 2000 IEEE*. 2000. IEEE.
160. Gahleitner, R. and E. Bonek. *Radio wave penetration into urban buildings in small cells and microcells*. in *Vehicular Technology Conference, 1994 IEEE 44th*. 1994. IEEE.
161. Medbo, J., et al. *Multi-frequency path loss in an outdoor to indoor macrocellular scenario*. in *Antennas and Propagation, 2009. EuCAP 2009. 3rd European Conference on*. 2009. IEEE.
162. Gibson, T.B. and D.C. Jenn, *Prediction and measurement of wall insertion loss.* 1999.
163. Rose, D.M. and T. Kürner. *Outdoor-to-indoor propagation—Accurate measuring and modelling of indoor environments at 900 and 1800 MHz*. in *Antennas and Propagation (EUCAP), 2012 6th European Conference on*. 2012. IEEE.
164. Elgannas, H. and I. Kostanic. *Outdoor-to-indoor propagation characteristics of 850 MHz and 1900 MHz bands in macro cellular environments*. in *Proceedings of the World Congress on Engineering and Computer Science (WCECS'14)*. 2014.
165. Rodriguez, I., et al. *Path loss validation for urban micro cell scenarios at 3.5 GHz compared to 1.9 GHz*. in *Global Communications Conference (GLOBECOM), 2013 IEEE*. 2013. IEEE.
166. De Toledo, A. and A. Turkmani. *Propagation into and within buildings at 900, 1800 and 2300 MHz*. in *Vehicular Technology Conference, 1992, IEEE 42nd*. 1992. IEEE.
167. Davidson, A. and C. Hill, *Measurement of building penetration into medium buildings at 900 and 1500 MHz.* IEEE Transactions on Vehicular Technology, 1997. **46**(1): p. 161-168.
168. Tanis, W.J. and G.J. Pilato. *Building penetration characteristics of 880 MHz and 1922 MHz radio waves*. in *Vehicular Technology Conference, 1993., 43rd IEEE*. 1993. IEEE.
169. LaSorte, N.J., W.J. Barnes, and H.H. Refai, *Experimental Characterization of Building Penetration Loss of a Hospital from 55-1950MHz.* studies, 2009. **649**(050): p. 135.

170. Rodriguez, I., et al. *Radio propagation into modern buildings: Attenuation measurements in the range from 800 MHz to 18 GHz*. in *Vehicular Technology Conference (VTC Fall), 2014 IEEE 80th*. 2014. IEEE.
171. Backer, B.D., et al. *The study of wave-propagation through a windowed wall at 1.8 GHz*. in *Vehicular Technology Conference, 1996. Mobile Technology for the Human Race., IEEE 46th*. 1996. IEEE.
172. Kvicera, M. and P. Pechac, *Building Penetration Loss for Satellite Services at L-, S- and C-band: Measurement and Modeling.* IEEE Transactions on Antennas and Propagation, 2011. **59**(8): p. 3013-3021.
173. Kvicera, M., et al. *Building penetration loss measurements for satellite-to-indoor systems: Preliminary results*. in *Antennas and Propagation (EuCAP), 2010 Proceedings of the Fourth European Conference on*. 2010.
174. Axiotis, D.I. and M.E. Theologou. *Building penetration loss at 2 GHz for mobile communications at high elevation angles by HAPS*. in *Wireless Personal Multimedia Communications, 2002. The 5th International Symposium on*. 2002.
175. Chee, K.L., et al. *Outdoor-to-indoor propagation loss measurements for broadband wireless access in rural areas*. in *Antennas and Propagation (EUCAP), Proceedings of the 5th European Conference on*. 2011. IEEE.
176. Zhang, M., S. Zhang, and J. Cao. *Fusing received signal strength from multiple access points for WLAN user location estimation*. in *Internet Computing in Science and Engineering, 2008. ICICSE'08. International Conference on*. 2008. IEEE.
177. Ji, Y., et al. *Impact of building environment on the performance of dynamic indoor localization*. in *Wireless and Microwave Technology Conference, 2006. WAMICON'06. IEEE Annual*. 2006. IEEE.
178. Li, X., K. Pahlavan, and J. Beneat. *Performance of TOA estimation techniques in indoor multipath channels*. in *Proceedings of IEEE international symposium on personal, indoor and mobile radio communications*. 2002.
179. Liu, Y. and Z. Yang, *Location, localization, and localizability: location-awareness technology for wireless networks*. 2010: Springer Science & Business Media.
180. Sayrafian-Pour, K. and D. Kaspar. *A robust model-based approach to indoor positioning using signal strength*. in *Personal, Indoor and Mobile Radio Communications, 2008. PIMRC 2008. IEEE 19th International Symposium on*. 2008. IEEE.
181. Chapre, Y., et al. *Received signal strength indicator and its analysis in a typical WLAN system (short paper)*. in *Local Computer Networks (LCN), 2013 IEEE 38th Conference on*. 2013. IEEE.
182. Xu, L., et al. *Variation of received signal strength in wireless sensor network*. in *Advanced Computer Control (ICACC), 2011 3rd International Conference on*. 2011. IEEE.
183. Ullah, K., et al. *An Experimental Study on the Behavior of Received Signal Strength in Indoor Environment*. in *Frontiers of Information Technology (FIT), 2013 11th International Conference on*. 2013. IEEE.
184. Obeidat, H., et al. *Indoor localization using received signal strength*. in *Design and Test Symposium (IDT), 2013 8th International*. 2013. IEEE.
185. Ahn, H.-S. and W. Yu, *Environmental-adaptive RSSI-based indoor localization.* Automation Science and Engineering, IEEE Transactions on, 2009. **6**(4): p. 626-633.

186. Bouchereau, F. and D. Brady. *Bounds on range-resolution degradation using RSSI measurements*. in *Communications, 2004 IEEE International Conference on*. 2004. IEEE.
187. Munoz, D., et al., *Position location techniques and applications*. 2009: Academic Press.
188. Hatami, A., et al. *On RSS and TOA based indoor geolocation-a comparative performance evaluation*. in *Wireless Communications and Networking Conference, 2006. WCNC 2006. IEEE*. 2006. IEEE.
189. Savvides, A., H. Park, and M.B. Srivastava, *The n-hop multilateration primitive for node localization problems.* Mobile Networks and Applications, 2003. **8**(4): p. 443-451.
190. Zanca, G., et al. *Experimental comparison of RSSI-based localization algorithms for indoor wireless sensor networks*. in *Proceedings of the workshop on Real-world wireless sensor networks*. 2008. ACM.
191. Priyantha, N.B., A. Chakraborty, and H. Balakrishnan. *The cricket location-support system*. in *Proceedings of the 6th annual international conference on Mobile computing and networking*. 2000. ACM.
192. Langendoen, K. and N. Reijers, *Distributed localization in wireless sensor networks: a quantitative comparison.* Computer Networks, 2003. **43**(4): p. 499-518.
193. Mehdi Dehghan, S., H. Moradi, and S.A. Asghar Shahidian. *Optimal path planning for DRSSI based localization of an RF source by multiple UAVs*. in *Robotics and Mechatronics (ICRoM), 2014 Second RSI/ISM International Conference on*. 2014. IEEE.
194. Wagner, D. *Resilient aggregation in sensor networks*. in *Proceedings of the 2nd ACM workshop on Security of ad hoc and sensor networks*. 2004. ACM.
195. Lin, L., H.-C. So, and Y.T. Chan, *Accurate and simple source localization using differential received signal strength.* Digital Signal Processing, 2013. **23**(3): p. 736-743.
196. Chang, N., R. Rashidzadeh, and M. Ahmadi, *Robust indoor positioning using differential Wi-Fi access points.* Consumer Electronics, IEEE Transactions on, 2010. **56**(3): p. 1860-1867.
197. Liu, B.-C. and K.-H. Lin, *Distance difference error correction by least square for stationary signal-strength-difference-based hyperbolic location in cellular communications.* Vehicular Technology, IEEE Transactions on, 2008. **57**(1): p. 227-238.
198. Alkasi, U., M.A. Shayokh, and H.P. Partal. *An experimental comparison study on indoor localization: RF fingerprinting and Multilateration methods*. in *Electronics, Computer and Computation (ICECCO), 2013 International Conference on*. 2013.
199. Khanbashi, N.A., et al. *Real time evaluation of RF fingerprints in wireless LAN localization systems*. in *Positioning Navigation and Communication (WPNC), 2013 10th Workshop on*. 2013.
200. Xie, L., Y. Wang, and X. Xue. *A new indoor localization method based on inversion propagation model*. in *Wireless Communications Networking and Mobile Computing (WiCOM), 2010 6th International Conference on*. 2010. IEEE.
201. Bahl, P. and V.N. Padmanabhan. *RADAR: An in-building RF-based user location and tracking system*. in *INFOCOM 2000. Nineteenth Annual Joint Conference of the IEEE Computer and Communications Societies. Proceedings. IEEE*. 2000. Ieee.

202. Li, D., et al. *A feature scaling based k-nearest neighbor algorithm for indoor positioning system*. in *2014 IEEE Global Communications Conference*. 2014.
203. Feng, C., et al., *Received-signal-strength-based indoor positioning using compressive sensing.* Mobile Computing, IEEE Transactions on, 2012. **11**(12): p. 1983-1993.
204. Patwari, N. and A.O. Hero III. *Using proximity and quantized RSS for sensor localization in wireless networks*. in *Proceedings of the 2nd ACM international conference on Wireless sensor networks and applications*. 2003. ACM.
205. Küpper, A., *Location-based services: fundamentals and operation*. 2005: John Wiley & Sons.
206. Elnahrawy, E., X. Li, and R.P. Martin. *The limits of localization using signal strength: A comparative study*. in *Sensor and Ad Hoc Communications and Networks, 2004. IEEE SECON 2004. 2004 First Annual IEEE Communications Society Conference on*. 2004. IEEE.
207. Chandrasekaran, G., et al. *Empirical evaluation of the limits on localization using signal strength*. in *Sensor, Mesh and Ad Hoc Communications and Networks, 2009. SECON'09. 6th Annual IEEE Communications Society Conference on*. 2009. IEEE.
208. Savvides, A., C.-C. Han, and M.B. Strivastava. *Dynamic fine-grained localization in ad-hoc networks of sensors*. in *Proceedings of the 7th annual international conference on Mobile computing and networking*. 2001. ACM.
209. wikipedia. *Speed of sound*. 2016 [cited 2016 12/May/2016]; Available from: https://en.wikipedia.org/wiki/Speed_of_sound.
210. Ash, J.N. and R.L. Moses, *Acoustic time delay estimation and sensor network self-localization: Experimental results.* The Journal of the Acoustical Society of America, 2005. **118**(2): p. 841-850.
211. Sertatıl, C., M.A. Altınkaya, and K. Raoof, *A novel acoustic indoor localization system employing CDMA.* Digital Signal Processing, 2012. **22**(3): p. 506-517.
212. Wang, S., J. Min, and B.K. Yi. *Location based services for mobiles: Technologies and standards*. in *IEEE international conference on communication (ICC)*. 2008.
213. Go, S., S. Kim, and J.-W. Chong. *An efficient non-line-of-sight error mitigation method for TOA measurement in indoor environments*. in *Proceedings of the 8th International Conference on Ubiquitous Information Management and Communication*. 2014. ACM.
214. Shin, D.-H. and T.-K. Sung, *Comparisons of error characteristics between TOA and TDOA positioning.* Aerospace and Electronic Systems, IEEE Transactions on, 2002. **38**(1): p. 307-311.
215. Jagoe, A., *Mobile location services: The definitive guide*. Vol. 1. 2003: Prentice Hall Professional.
216. Güvenç, İ. and C.-C. Chong, *A survey on TOA based wireless localization and NLOS mitigation techniques.* Communications Surveys & Tutorials, IEEE, 2009. **11**(3): p. 107-124.
217. Cong, L. and W. Zhuang. *Non-line-of-sight error mitigation in TDOA mobile location*. in *Global Telecommunications Conference, 2001. GLOBECOM'01. IEEE*. 2001. IEEE.

218. Mailaender, L. *Comparing geo-location bounds for TOA, TDOA, and round-trip TOA*. in *Personal, Indoor and Mobile Radio Communications, 2007. PIMRC 2007. IEEE 18th International Symposium on*. 2007. IEEE.
219. Patwari, N., et al., *Locating the nodes: cooperative localization in wireless sensor networks.* Signal Processing Magazine, IEEE, 2005. **22**(4): p. 54-69.
220. Dardari, D., et al., *Ranging with ultrawide bandwidth signals in multipath environments.* Proceedings of the IEEE, 2009. **97**(2): p. 404-426.
221. Hahm, M.D., Z.I. Mitrovski, and E.L. Titlebaum, *Deconvolution in the presence of Doppler with application to specular multipath parameter estimation.* Signal Processing, IEEE Transactions on, 1997. **45**(9): p. 2203-2219.
222. Li, X. and K. Pahlavan, *Super-resolution TOA estimation with diversity for indoor geolocation.* Wireless Communications, IEEE Transactions on, 2004. **3**(1): p. 224-234.
223. Ali, A.A. and A. Omar. *Time of Arrival estimation for WLAN indoor positioning systems using Matrix Pencil Super Resolution Algorithm*. in *Proceedings of the 2nd Workshop on Positioning, Navigation and Communication, WPNC*. 2005.
224. Alsindi, N., X. Li, and K. Pahlavan. *Performance of TOA estimation algorithms in different indoor multipath conditions*. in *Wireless Communications and Networking Conference, 2004. WCNC. 2004 IEEE*. 2004. IEEE.
225. Chen, H.-C., et al. *Determining RF angle of arrival using COTS antenna arrays: a field evaluation*. in *MILITARY COMMUNICATIONS CONFERENCE, 2012-MILCOM 2012*. 2012. IEEE.
226. Muhamed, R., *Direction of arrival estimation using antenna arrays*. 1996, Virginia Polytechnic Institute and State University.
227. Foutz, J., A. Spanias, and M.K. Banavar, *Narrowband direction of arrival estimation for antenna arrays.* Synthesis Lectures on Antennas, 2008. **3**(1): p. 1-76.
228. Stutzman, W.L. and G.A. Thiele, *Antenna theory and design*. 2012: John Wiley & Sons.
229. antenna-theory.com. 17/May/2016]; Available from: http://www.antenna-theory.com/arrays/main.php.
230. Allen, B. and M. Ghavami, *Adaptive array systems: fundamentals and applications*. 2006: John Wiley & Sons.
231. Bevelacqua, P.J., *Antenna arrays: Performance limits and geometry optimization*. 2008: ProQuest.
232. Orfanidis, S.J., *Electromagnetic waves and antennas*. 2002: Rutgers University New Brunswick, NJ.
233. Wasserman, L., *All of statistics: a concise course in statistical inference*. 2013: Springer Science & Business Media.
234. Wikipedia. *Covariance Matrix*. 19/May/2016]; Available from: https://en.wikipedia.org/wiki/Covariance_matrix.
235. Godara, L.C., *Smart antennas*. 2004: CRC press.
236. Krim, H. and M. Viberg, *Two decades of array signal processing research: the parametric approach.* Signal Processing Magazine, IEEE, 1996. **13**(4): p. 67-94.
237. Godara, L.C., *Application of antenna arrays to mobile communications. II. Beam-forming and direction-of-arrival considerations.* Proceedings of the IEEE, 1997. **85**(8): p. 1195-1245.

238. Jiang, Y., et al. *Capon beamforming in the presence of steering vector errors and coherent signals*. in *11th Annual Workshop on Adaptive Sensor Array Processing (ASAP 2003), MIT Lincoln Laboratory, Lexington, MA*. 2003.
239. Schmidt, R.O., *Multiple emitter location and signal parameter estimation.* Antennas and Propagation, IEEE Transactions on, 1986. **34**(3): p. 276-280.
240. Medeđović, P., M. Veletić, and Ž. Blagojević. *Wireless insite software verification via analysis and comparison of simulation and measurement results*. in *MIPRO, 2012 Proceedings of the 35th International Convention*. 2012. Opatija, Croatia: IEEE.
241. Dama, Y., et al. *Indoor Channel Measurement and Prediction for 802.11 n System*. in *Vehicular Technology Conference (VTC Fall), 2011 IEEE*. 2011. IEEE.
242. Wu, J.-W., et al., *Dual broadband design of rectangular slot antenna for 2.4 and 5 GHz wireless communication.* Electronics Letters, 2004. **40**(23): p. 1461-1463.
243. Koivunen, J., et al., *Dynamic multi-link indoor MIMO measurements at 5.3 GHz.* 2007.
244. Technologies, A., *Wireless LAN at 60 GHz - IEEE 80211ad-Explained-Agilent-White-Paper*. 2017.
245. Instruments, N. *mmWave: The Battle of the Bands*. 2016 25/10/2016]; Available from: http://www.ni.com/white-paper/53096/en/.
246. Zhang, Y. and Y. Hwang. *Measurements of the characteristics of indoor penetration loss*. in *Vehicular Technology Conference, 1994 IEEE 44th*. 1994. IEEE.
247. Turin, G.L., et al., *A statistical model of urban multipath propagation.* IEEE Transactions on Vehicular Technology, 1972. **21**(1): p. 1-9.
248. Erceg, V., A.J. Rustako, and R.S. Roman, *Diffraction around corners and its effects on the microcell coverage area in urban and suburban environments at 900 MHz, 2 GHz, and 4 GHz.* IEEE Transactions on Vehicular Technology, 1994. **43**(3): p. 762-766.
249. Njemcevic, P. and V. Lipovac. *Estimation of radio signal spatial local mean*. in *Software, Telecommunications and Computer Networks (SoftCOM), 2016 24th International Conference on*. 2016. IEEE.
250. Njemcevic, P., *A Novel Approach in Determination of the Appropriate Spatial Averaging Signal Length.* Wireless Personal Communications, 2015. **82**(3): p. 1851-1861.
251. Pamela, N. *Local average signal estimation in Nakagami-m channels*. in *Communications, Control and Signal Processing (ISCCSP), 2014 6th International Symposium on*. 2014. IEEE.
252. Austin, A.C., *Wireless Channel Characterization in Burning Buildings Over 100–1000 MHz.* IEEE Transactions on Antennas and Propagation, 2016. **64**(7): p. 3265-3269.
253. Austin, A.C., et al., *Application of polynomial chaos to quantify uncertainty in deterministic channel models.* IEEE Transactions on Antennas and Propagation, 2013. **61**(11): p. 5754-5761.
254. Austin, A., *Performance estimation for indoor wireless systems using FDTD method.* Electronics Letters, 2015. **51**(17): p. 1376-1378.
255. Austin, A.C., M.J. Neve, and G.B. Rowe, *Modeling propagation in multifloor buildings using the FDTD method.* IEEE Transactions on Antennas and Propagation, 2011. **59**(11): p. 4239-4246.

256. Lindhé, M., K.H. Johansson, and A. Bicchi. *An experimental study of exploiting multipath fading for robot communications*. in *3rd International Conference on Robotics Science and Systems, RSS 2007, 27-30 June 2007, Atlanta, GA, USA*. 2008.
257. Jaldén, N., et al. *Correlation properties of large scale fading based on indoor measurements*. in *Wireless Communications and Networking Conference, 2007. WCNC 2007. IEEE*. 2007. IEEE.
258. Lee, W.C., *Estimate of local average power of a mobile radio signal.* IEEE Transactions on Vehicular Technology, 1985. **34**(1): p. 22-27.
259. Wang, Q., et al., *Ray-based statistical propagation modeling for indoor corridor scenarios at 15 GHz.* International Journal of Antennas and Propagation, 2016. **2016**.
260. de la Vega, D., et al., *Generalization of the Lee Method for the Analysis of the Signal Variability.* IEEE transactions on vehicular technology, 2009. **58**(2): p. 506-516.
261. Marinović, I. and D. Čoko, *Inter-Floor Wide Band Radio Channel Measurements and Simulation Applying Saleh-Valenzuela Model.* automatika, 2015. **56**(1): p. 91-99.
262. Seseña-Osorio, J., I. Zaldivar-Huerta, and A. Aragón-Zavala. *Experimental estimation of the large-scale fading in an indoor environment and its impact on the planning of wireless networks*. in *Microwave & Optoelectronics Conference (IMOC), 2013 SBMO/IEEE MTT-S International*. 2013. IEEE.
263. Kaemarungsi, K. and P. Krishnamurthy. *Properties of indoor received signal strength for WLAN location fingerprinting*. in *Mobile and Ubiquitous Systems: Networking and Services, 2004. MOBIQUITOUS 2004. The First Annual International Conference on*. 2004. IEEE.
264. Yilmaz, T., E. Fadel, and O.B. Akan. *Employing 60 GHz ISM band for 5G wireless communications*. in *Communications and Networking (BlackSeaCom), 2014 IEEE International Black Sea Conference on*. 2014. IEEE.
265. Stavrou, S. and S. Saunders, *Review of constitutive parameters of building materials.* 2003.
266. Ferreira, D., et al. *A review on the electromagnetic characterisation of building materials at micro-and millimetre wave frequencies*. in *Antennas and Propagation (EuCAP), 2014 8th European Conference on*. 2014. IEEE.
267. Fares, M., et al., *Determining the permittivity profile inside reinforced concrete using capacitive probes.* NDT & E International, 2016. **79**: p. 150-161.
268. Torgovnikov, G.I., *Dielectric properties of wood and wood-based materials*. 2012: Springer Science & Business Media.
269. Fakharzadeh, M., et al., *CMOS phased array transceiver technology for 60 GHz wireless applications.* IEEE Transactions on Antennas and Propagation, 2010. **58**(4): p. 1093-1104.
270. Lu, J., et al. *Propagation characterization of an office building in the 60 GHz band*. in *Antennas and Propagation (EuCAP), 2014 8th European Conference on*. 2014. IEEE.
271. Correia, L.M. and P.O. Frances. *Estimation of materials characteristics from power measurements at 60 GHz*. in *Personal, Indoor and Mobile Radio Communications, 1994. Wireless Networks-Catching the Mobile Future., 5th IEEE International Symposium on*. 1994. IEEE.

272. Pinhasi, Y., A. Yahalom, and S. Petnev. *Propagation of ultra wide-band signals in lossy dispersive media*. in *Microwaves, Communications, Antennas and Electronic Systems, 2008. COMCAS 2008. IEEE International Conference on*. 2008. IEEE.
273. Affum, E., et al., *Wideband Parameters Analysis and Validation for Indoor radio Channel at 60/70/80GHz for Gigabit Wireless Communication employing Isotropic, Horn and Omni directional Antenna.* arXiv preprint arXiv:1312.5109, 2013.
274. Salous, S., et al., *Millimeter-wave propagation: characterization and modeling toward fifth-generation systems.[Wireless Corner].* IEEE Antennas and Propagation Magazine, 2016. **58**(6): p. 115-127.
275. Strang, G. and W.-C. Press, *Introduction to linear algebra*. 5th ed. Vol. 3. 2016: Wellesley-Cambridge Press Wellesley, MA.

Appendix A: Narrowband Approximation

$$s(t) = Re\{s_l(t)e^{j\omega t}\} = Re\{A(t)e^{jB(t)} \cdot e^{j\omega t}\} \quad \text{(A.1)}$$

$$s_l(t) = A(t)e^{jB(t)} \quad \text{(A.2)}$$

Where $s_l(t)$ is the lowpass equivalent representation of $s(t)$. $A(t)$ and $B(t)$ are the amplitude and phase respectively, the linear array is assumed to be uniform (i.e. the spacing between the elements are the same), with K elements used the received signal by the k^{th} element will be [227]:

$$x_k(t) = s(t - \tau_k) + n_k(t) = Re\{A(t - \tau_k)e^{jB(t-\tau_k)}e^{-j\omega\tau_k}e^{j\omega t}\} + n_k(t) \quad \text{(A.3)}$$

Where $n_k(t)$ is the Additive White Gaussian Noise. Given that the signal is narrowband, $A(t)$ and $B(t)$ are slowly varying with time, thus:

$$x_k(t) = Re\{s_l(t) \cdot e^{-j\omega\tau_k} \cdot e^{j\omega t}\} + n_k(t) \quad \text{(A.4)}$$

The received signal will be down-converted to the baseband (or to Intermediate frequency IF band) to make signal processing easier [226]:

$$x_k(t) = s(t) \cdot e^{-j2\pi f\tau_k} + n_k(t) \quad \text{(A.5)}$$

Substituting with $f = \frac{c}{\lambda}$; and $\beta = \frac{2\pi}{\lambda}$

$$x_k(t) = s(t) \cdot e^{-j\beta c\tau_k} + n_k(t) \quad \text{(A.6)}$$

As shown in Figure 3.11 phase at element k can be estimated using time delay (τ_k):

$$r_k = d_k \cdot \cos(\theta) \quad \text{(A.7)}$$

Given that

$$c = \frac{r_k}{\tau_k} \tag{A.8}$$

And substitute in Equation A.7 gives

$$c.\tau_k = d_k.\cos(\theta) \tag{A.9}$$

And assuming that the spacing between the elements is equal [226]:

$$d_k = k\,.d \tag{A.10}$$

Equation A.5 becomes:

$$x_k(t) = s(t).e^{-j\beta k\, d\cos(\theta)} + n_k(t) \tag{A.11}$$

After the down-conversion process, the signal is being sampled:

$$x_k[n] = s[n] \cdot e^{-j\beta k\, \mathrm{d}\cos(\theta)} + n_k[n] \tag{A.12}$$

In more general case, the incident signals will be from different angles, spherical coordinates are used to relate the delay τ_k with the corresponding phases [226]:

$$\tau_k = \frac{x_k \cos\varphi \sin\theta + y_k \sin\varphi \sin\theta + z_k \cos\theta}{c} \tag{A.13}$$

Each element in the array has different directional gain (φ,θ) and frequency response (ω); thus:

$$\boldsymbol{a}(\omega,\varphi,\theta) = \begin{bmatrix} g_0(\omega,\varphi,\theta) \\ g_1(\omega,\varphi,\theta)e^{-j\beta(x_1\cos\varphi\sin\theta + y_1\sin\varphi\sin\theta + z_1\cos\theta)} \\ g_2(\omega,\varphi,\theta)e^{-j\beta(x_2\cos\varphi\sin\theta + y_2\sin\varphi\sin\theta + z_2\cos\theta)} \\ . \\ . \\ . \\ g_{K-1}(\omega,\varphi,\theta)e^{-j\beta(x_{K-1}\cos\varphi\sin\theta + y_{K-1}\sin\varphi\sin\theta + z_{K-1}\cos\theta)} \end{bmatrix} \tag{A.14}$$

Appendix B: Covariance Matrix Derivation:

$$\boldsymbol{R}_{xx} = E\left[X[n]\ X^{\mathrm{H}}[n]\right] = E[(\boldsymbol{A}(\theta)\boldsymbol{s}[n] + \boldsymbol{n}[n]) \cdot (\boldsymbol{s}^{\mathrm{H}}[n]\boldsymbol{A}^{\mathrm{H}}(\theta) + \boldsymbol{n}^{\mathrm{H}}[n])] \quad \text{(B.1)}$$

Provided that both the imagining signals and noise have zero correlation:

$$E[\boldsymbol{A}(\theta)\boldsymbol{s}[n]\boldsymbol{n}^{\mathrm{H}}[n]] + E[\boldsymbol{A}(\theta)\boldsymbol{s}[n]\boldsymbol{n}^{\mathrm{H}}[n]] = 0 \quad \text{(B.2)}$$

Equation B.1 is reduced to [235]:

$$\begin{aligned}\boldsymbol{R}_{xx} &= \boldsymbol{A}(\theta)E\left[\boldsymbol{s}[n]\boldsymbol{s}^{\mathrm{H}}[n]\right]\boldsymbol{A}^{\mathrm{H}}(\theta) + E\left[\boldsymbol{n}[n]\boldsymbol{n}^{\mathrm{H}}[n]\right] \\ &= \boldsymbol{A}(\theta)R_{ss}\boldsymbol{A}^{\mathrm{H}}(\theta) + \sigma^2\boldsymbol{I}_{N\times N}\end{aligned} \quad \text{(B.3)}$$

where $R_{ss} = \boldsymbol{s}[n]\boldsymbol{s}^{\mathrm{H}}[n]$.

The covariance of the noise is its variance times the identity matrix, this is due to the assumption that the noise signals are not correlated, as a result, the non-diagonal elements are close to zero, while the diagonal elements are the variance of the noise signals [227].

<u>Covariance matrix Decomposition:</u>

For a square matrix $\boldsymbol{P}$, recalling the condition for an eigenvector x and eigenvalue λ [275]:

$$\boldsymbol{P}\boldsymbol{x} = \lambda\boldsymbol{x} \quad \text{(B.4)}$$

The eigenvectors give the availability of decomposing the covariance matrix into K spaces: signal space and noise space, signal space and noise space are orthogonal to each other [275].

A vector which is in the noise space $\boldsymbol{q}_n$ will be orthogonal to the signal subspace (i.e. orthogonal on $\boldsymbol{A}$), multiplying $\boldsymbol{q}_n$ with $\boldsymbol{R}_{xx}$ gives:

$$\boldsymbol{R}_{xx}\boldsymbol{q}_n = \boldsymbol{A}(\theta)R_{ss}\boldsymbol{A}^{\mathrm{H}}(\theta)\boldsymbol{q}_n + \sigma^2\boldsymbol{I}_{N\times N}\boldsymbol{q}_n = \sigma^2\boldsymbol{q}_n \qquad \text{(B.5)}$$

σ^2 is an eigenvalue for the eigenvector $\boldsymbol{q}_n$. Since there are M arrival signals to the array, the signal space will be M dimensional (provided that ($\boldsymbol{A}(\theta)R_{ss}\boldsymbol{A}^{\mathrm{H}}(\theta)$) is singular (i.e. det. =0)) while noise space will be ($K-M$) dimensional space [227].

$$\boldsymbol{R}_{xx}\boldsymbol{q}_s = \boldsymbol{A}(\theta)R_{ss}\boldsymbol{A}^{\mathrm{H}}(\theta)\boldsymbol{q}_s + \sigma^2\boldsymbol{I}_{N\times N}\boldsymbol{q}_s = {\sigma_s}^2\boldsymbol{q}_s + \sigma^2\boldsymbol{q}_s = ({\sigma_s}^2 + \sigma^2)\boldsymbol{q}_s \qquad \text{(B.6)}$$

As seen the noise variance is part of all signal space eigenvalues, the eigenvalues ${\sigma_s}^2$ values are related to the strength of incoming signals, the stronger signal the larger eigenvalue, whereas the noise eigenvalues are same [236].

Author's Publication Record

JOURNAL PAPERS

1. **H.A. Obeidat**, et al., "An Indoor Path Loss Prediction Model using Wall Correction Factors for WLAN and 5G Indoor Networks" *Radio Science*, April. 2018.
2. **H. A. Obeidat**, Omar A. Obeidat, Stephen M. Jones et al, "Local Average Signal Strength Estimation for Indoor Multipath Propagation", under Review by *IEEE Transactions on Antennas and Propagation, 2018*.
3. **H.A. Obeidat**, S.M.R. Jones, O.A. Obeidat, W. Suhaib, R.A. Abd-Alhameed. "Indoor Environment Propagation Review*", under review by IEEE Access, 2018.*
4. **H.A. Obeidat**, Y.A.S. Dama, R.A. Abd-Alhameed, J.M. Noras, S.M.R. Jones, A Comparison between Vector Algorithm and CRSS Algorithms for Indoor Localization using Received Signal Strength, ACES Journal, Vol. 31, No.8, pp.868-876. August 2016.
5. W. Manan, **H. Obeidat**, A. Al-Abdullah, R. Abd-Alhameedand F. Hu, "Indoor To Indoor And Indoor To Outdoor Millimeter Wave Propagation Channel Simulations At 26 GHz, 28 GHz And 60 GHz For 5G Mobile Networks" in The International Journal of Engineering and Science, March 2018.
6. W. Shuaieb, **H. Obeidat**, R. A. Abd-Alhameed, G. T.A. El Sanousi, S.M.R.Jones "Implementation Scheme for a Wideband Transmission and Direction Finding System in a Ricean Channel with High Level of Noise" Submitted to IEEE Transactions on Communications, 2018.

7. Wafa Shuaieb, George Oguntala, **Huthaifa Obeidat**, Rameez Asif, Steve Jones, Raed Abd-Alhameed “Distributed Wearable RFID System for Indoor Patient Tracking and Monitoring”, under review by MDPI Journal, Future Internet, 2018.

INTERNATIONAL CONFERENCES

1. **H.A. Obeidat**, W. Shuaieb, H Alhassan, K. Samarah, M. Abousitta, R.A. Abd-Alhameed, S.M.R. Jones, J.M. Noras "Location Based Services using Received Signal Strength Algorithms," in Sixth International Conference on Internet Technologies & Applications 4th International Workshop on Energy Efficient and Reconfigurable Transceivers, Wrexham, 8-11 Sept, 2015, pp.409-411
2. **H. Obeidat**, O. Obeidat, M. Bomhara *et al*., "Performance comparative study between vector and ECOLOCATION algorithms for indoor positioning," *2017 Internet Technologies and Applications (ITA)*, Wrexham, 2017, pp. 230-234.
3. HSO Migdadi, **H Obeidat**, KO Anoh, NN Khatib, JM Noras, R Qahwaji, RA Abd-Alhameed, “Channel Estimation for OFDM FFT/DWT in Multi-carrier Modulation Used in Wireless Telemedicine,” in IEEE International Conference on Computer and Information Technology; Ubiquitous Computing and Communications; Dependable, Autonomic and Secure Computing; Pervasive Intelligence and Computing (CIT/IUCC/DASC/PICOM), 2015.
4. G. Oguntala, **H. Obeidat** et al, "Design framework for unobtrusive patient location recognition using passive RFID and particle filtering," 2017

Internet Technologies and Applications (ITA), Wrexham, 2017, pp. 212-217.

5. W. S. Shuaieb, S. M. Jones, **H. A. Obeidat**, G. T. A. E. Sanousi and R. A. Abd-Alhameed, "Radio-location techniques under adverse channel conditions," 2017 Internet Technologies and Applications (ITA), Wrexham, 2017, pp. 270-274.
6. HSO Migdadi, RA Abd-Alhameed, **HA Obeidat**, JM Noras, EAA Qaralleh, MJ Ngala, “FIR implementation on FPGA: Investigate the FIR order on SDA and PDA algorithms,” in Sixth International Conference on Internet Technologies & Applications 4th International Workshop on Energy Efficient and Reconfigurable Transceivers, Wrexham, 8-11 Sept, 2015, pp. 409-411.
7. MA Bomhara, JG Gardiner, **HA Obeidat**, RA Abd-Alhameed, “CP-QFSK modem for TDMA short range communications systems,” in Sixth International Conference on Internet Technologies & Applications 4th International Workshop on Energy Efficient and Reconfigurable Transceivers, Wrexham, 8-11 Sept 2015, pp. 409-411
8. MA Bomhara, JG Gardiner, **HA Obeidat**, RA Abd-Alhameed, “On the elegibilty grounds of CP-QFSK for mobile radio systems,” in Sixth International Conference on Internet Technologies & Applications 4th International Workshop on Energy Efficient and Reconfigurable Transceivers, Wrexham, 8-11 Sept 2015, pp. 409-411
9. A. A. AlAbdullah, N. Ali, **H. Obeidat**, R. A. Abd-Alhameed and S. Jones, "Indoor millimetre-wave propagation channel simulations at 28, 39, 60 and 73 GHz for 5G wireless networks," 2017 Internet Technologies and Applications (ITA), Wrexham, 2017, pp. 235-239.

10. Y.Dama, A. Masri, H. Ghannam, W. Shuaieb, H. Alhassan, **H.A. Obeidat**, R.A. Abd-Alhameed, “RSSI evaluation for multi-story building,” in Sixth International Conference on Internet Technologies & Applications 4th International Workshop on Energy Efficient and Reconfigurable Transceivers, Wrexham, 8-11 Sept 2015, pp. 409-411
11. A AbouAlmal, H Alhassan, **H Obeidat**, MM Abusitta, RA Abd-Alhameed, SMR Jones, H Al-Ahmad, “Surface refractivity profile and validation of measurements in Arabian Gulf region,” Antennas & Propagation Conference (LAPC), 2-3 Nov 2015, pp. 240-243, DOI: 978-1-4799-8943-0/15/ ©2015 IEEE.
12. B. A. Mohammed, A. S. Hussaini, R. Abd-Alhameed, N. A. Abduljabbar, **H. A. Obeidat**, I. T. E. Elfergani, J. Rodriguez, M. Fonkam, C. Nche and B. M. Mustapha"A load-pull approach to design an optimum load impedance and matching network for class-F RF power amplifier," *2017 Internet Technologies and Applications (ITA)*, Wrexham, 2017, pp. 280-283.

List of Publications

AGU100 ADVANCING EARTH AND SPACE SCIENCE

Radio Science

RESEARCH ARTICLE
10.1002/2018RS006536

Key Points:
- A modified effective wall loss model (EWLM) for indoor environment is presented
- Real-time measurements and simulations for various indoor path loss models are used
- Several frequency spectrum band were considered for evaluation purposes

Correspondence to:
R. A. Abd-Alhameed,
r.a.a.abd@bradford.ac.uk

Citation:
Obeidat, H. A., Asif, R., Ali, N. T., Dama, Y. A., Obeidat, O. A., Jones, S. M. R., et al. (2018). An indoor path loss prediction model using wall correction factors for wireless local area network and 5G indoor networks. *Radio Science*, *53*. https://doi.org/10.1002/2018RS006536

Received 24 JAN 2018
Accepted 22 MAR 2018
Accepted article online 2 APR 2018

An Indoor Path Loss Prediction Model Using Wall Correction Factors for Wireless Local Area Network and 5G Indoor Networks

H. A. Obeidat[1], R. Asif[1], N. T. Ali[2], Y. A. Dama[3], O. A. Obeidat[4], S. M. R. Jones[1], W. S. Shuaieb[1], M. A. Al-Sadoon[1], K. W. Hameed[1], A. A. Alabdullah[1], and R. A. Abd-Alhameed[1,5]

[1]School of Engineering and Informatics, University of Bradford, Bradford, UK, [2]Department of Electrical and Computer Engineering, Khalifa University, Abu Dhabi, United Arab Emirates, [3]Department of Telecommunications Engineering, An Najah National University, Nablus, Palestine, [4]College of Engineering, Wayne State University, Detroit, USA, [5]Department of Communication and Informatics Engineering, Basra University College of Science and Technology, Basra, Iraq

Abstract A modified indoor path loss prediction model is presented, namely, effective wall loss model. The modified model is compared to other indoor path loss prediction models using simulation data and real-time measurements. Different operating frequencies and antenna polarizations are considered to verify the observations. In the simulation part, effective wall loss model shows the best performance among other models as it outperforms 2 times the dual-slope model, which is the second best performance. Similar observations were recorded from the experimental results. Linear attenuation and one-slope models have similar behavior, the two models parameters show dependency on operating frequency and antenna polarization.

1. Introduction

The ability to locate a target object in an indoor environment has many potential applications: for example, in security, emergency services, and health care and commercial fields (Pierleoni et al., 2016; Suits et al., 2014; R. Zhang et al., 2013). However, it is difficult to provide accurate location by radio means because of the complex multipath propagation within buildings (Obeidat et al., 2016).

Multipath propagation of wireless signals within buildings has been extensively studied in the context of the deployment of cordless phones (Keenan & Motley, 1990) and wireless local area networks (WLANs) (Borrelli et al., 2004; Crow et al., 1997; Kong et al., 2004). Propagation from outdoors to indoors has been studied in the context of cellular networks (Damosso & Correia, 1999). More recently, there has been significant interest in developing indoor location technologies, in many cases relying on the opportunistic exploitation of available WLAN signals (Zekavat & Buehrer, 2011) and deploying WLAN in the millimeter-wave band (Moraitis & Constantinou, 2004).

Propagation models have been developed and can be broadly categorized as predicting either median signal strength (path loss and shadowing) like Motley-Keenan model (MKM; Keenan & Motley, 1990) or channel behavior (fading across time or frequency) like Saleh-Valenzuela model (Saleh & Valenzuela, 1987). Path loss models predict the signal level (averaged over several wavelengths or a wide bandwidth) at a given distance from the transmitter (Keenan & Motley, 1990), while channel models describe the stochastic or deterministic variation of the signal level (narrow band) and the time dispersion (wideband) at that location (Saleh & Valenzuela, 1987). With the advent of multiple input, multiple output systems, spatial channel models have been introduced. The 3-D indoor environment comprises walls and floors, windows and doors, corridors, stairwells and lift shafts, and fixtures and furniture, which can be regarded (using radar parlance) as clutter (Remcom, 2017a).

Radio propagation through this segmented and cluttered environment can usefully be visualized by a ray optical model (Saunders & Aragón-Zavala, 2007). A complete physical spatial channel model describes the angles of departure and arrival of rays, the amplitude, delay, phase, and polarization between transmitting and receiving system. Rays include the direct path, which may or may not be obstructed, together with paths suffering combinations of specular and diffuse reflection, diffraction, scattering, and transmission through walls, floors, or other obstacles. Adjacent buildings can provide additional reflected paths.

The delay on each raypath is related to the path length, while the amplitude, phase, and polarization depend on the combination of spreading losses and losses due to transmission through, reflection from or diffraction around obstacles, which in turn depends on their structure and material electrical properties (Saunders & Aragón-Zavala, 2007). At frequencies above the ultrahigh-frequency band, penetration and diffraction losses tend to increase (Wells, 1977). In the millimeter-wave band surface roughness becomes more significant, leading to an increase in diffuse reflected components. However, the essential ray optical geometry remains the same, so that multipath components have the same delay, even if they are more attenuated (Haneda et al., 2016; Pascual-García et al., 2016).

This highly complex channel behavior is captured by ray tracing software. However, there are practical limits on the accuracy with which the detail of building structures or clutter can be characterized or the extent to which the material electrical properties can be accurately known (Obeidat et al., 2016). There are also compromises made in the number of raypaths that can be found by the software within the constraints of a reasonable run time and memory requirement (Remcom, 2017b).

The ray optical view of the propagation mechanisms leads naturally to a description of the channel in terms of its impulse response as given by Hashemi (1993). In the indoor channel, rays have been observed to arrive in clusters, as modeled by Saleh and Valenzuela (1987). The clusters can be associated with angles of arrival and departure in developing spatial channel models (Spencer et al., 2000). The impulse response will vary with position, and if the terminal (or clutter) is moving, this translates into time variation.

Despite the obvious underlying complexity of the indoor channel, Keenan and Motley (1990) looked to provide a straightforward engineering model for path loss. Their approach was to consider the various walls and floors obstructing the straight-line path between transmitter and receiver and to factor in a best fit loss per wall or floor of each identifiable type, for example, stud partition (drywall) or concrete block walls and suspended concrete floor beams or wooden floors. When these losses were factored in, they found a residual free space variation with distance (i.e., power law index of 2). A deficiency of their model was its tendency to overpredict loss where there are many floors or walls (presumably because there is an alternative, lower-loss path around those obstacles).

Other models have been proposed from simple power laws, two-slope or multislope models (Andrade & Hoefel, 2010; Lott & Forkel, 2001; Pahlavan & Levesque, 2005) to those that use the Keenan and Motley concept with some added sophistication to reduce the loss per floor as the number of floors increase (Serôdio et al., 2012). Waveguiding, for example, along corridors can lead to path loss indices approaching one, while the presence of clutter within the first Fresnel zone of a ray can lead to indices of 4–6 beyond a breakpoint as for ground wave propagation (Rappaort, 2002).

In this paper, several indoor path loss models and their associated parameters are examined and tested. A modified method named effective wall loss model (EWLM) to estimate the path loss is proposed. The performance of the proposed method was compared to other related methods in terms of various frequency spectrums covering WLAN and millimeter-wave frequencies; the effect of antenna polarization was also studied. Simulated and measured test results were presented in which it shows the proposed method outperformed the other tested models. The organization of this paper is as follow: section 2 investigates different indoor path loss prediction models, and section 3 describes the experimental setup of the simulations and measurements and the procedure followed to estimate model parameters. Section 4 presents simulation and experimental results and a comparison between indoor path loss models and the modified model, and finally, conclusion is drawn.

2. Indoor Path Loss Models

Many models have been proposed in literature including one-slope model (OSM; Lott & Forkel, 2001), dual-slope model (DSM) (Andrade & Hoefel, 2010), linear attenuation model (LAM) (Davies et al., 1990), partitioned model (PM; Alsindi et al., 2009), MKM (Keenan & Motley, 1990), averaged wall model (Lloret et al., 2004), ITU-R P.1238 model (International Telecommunication Union, ITU, 2012), COST 231 indoor model (Pedersen, 1999), and dominant path model (DPM; Plets et al., 2012).

2.1. One-Slope Model

A fast and simple model is also termed as simplified path loss model where the received power at a point is given by (Lott & Forkel, 2001)

$$P_r(dB) = P_0(dB) - 10n\log_{10}(d) \tag{1}$$

where P_0 is the received power at a 1 m away from the transmitter, which can be estimated using free space formula or experimentally (Goldsmith, 2005), n is the path loss exponent, which is calculated using interpolation (Zvanovec et al., 2003), and d is the distance from transmitter. Path loss is dependent on range (distance) and path loss exponent (Goldsmith, 2005). In Alexander and Pugliese (1983) various values of decay index n are presented, the values ranging from 1.2 due to waveguiding effects in corridors to 6.1 for dense office environment (Rappaort, 2002). In outdoor to indoor propagation at 1.7 GHz, decay index n found to be 1.495 for corridor single floor; 1.524 through corridors in that building and 3.25 for rooms single floor and 3.31 in rooms through building (Davies et al., 1990).

2.2. Linear Attenuation Model

Devasirvathan (1991) proposed another approach, the experiments were carried out on range of frequencies (0.85, 1.9, 4, and 5.8 GHz), and it was concluded that total loss L is the sum of free space loss L_{FS} and loss factor a in the range of (0.3 to 0.6 dB/m) depending on frequency and building (Devasirvathan, 1991).

$$P_r(dB) = P_0(dB) - 20\log_{10}(d) - a \cdot d \tag{2}$$

where d represents distance in meter.

2.3. Dual-Slope Model

Propagation within indoor environment was categorized depending on the first Fresnel zone clearance, the "near transmitter propagation," where no obstruction in the first Fresnel zone and the path loss exponent is less than 2 due to waveguiding, and "breakpoint propagation" when the furniture falls in the first Fresnel zone where path loss exponent becomes larger than 2, the model is shown in equation (3) (Andrade & Hoefel, 2010).

$$P_r = P_0 - 10\begin{cases} n_1\log_{10}(d) & d < d_{bp} \\ n_1\log_{10}(d_{bp}) + n_2\log_{10}\left(\dfrac{d}{d_{bp}}\right) & d > d_{bp} \end{cases} \tag{3}$$

where n_1, n_2 are the path loss exponents and d_{bp} is the breakpoint distance. Calculation of the breakpoint distance is done either theoretically as in Andrade and Hoefel (2010) or experimentally as in Nuangwongsa et al. (2009).

2.4. Partitioned Model

In this model, path loss is estimated based on predetermined values of n and distance between transmitter and receiver (Pahlavan & Levesque, 2005):

$$P_r = P_0 - \begin{cases} 20\log_{10}d, & 1m < d \le 10\text{ m} \\ 20 + 30\log_{10}\dfrac{d}{10}, & 10m < d \le 20\text{ m} \\ 29 + 60\log_{10}\dfrac{d}{20}, & 20m < d \le 40\text{ m} \\ 47 + 120\log_{10}\dfrac{d}{40}, & d > 40\text{ m} \end{cases} \tag{4}$$

2.5. ITU-R P.1238 Indoor Model

An empirical model accounts the losses due to penetration through floors within the same building (ITU, 2012):

$$L = 20\log_{10}f_{MHz} + 10n\log_{10}\frac{d}{d_0} + L_f(N(F)) - 28 \tag{5}$$

where $L_f(N(F))$ is the floor penetration loss, which varies with frequency, type of floor, and number of floors between the transmitter and receiver ($N(F)$). Based on enormous measurements, the model gives typical

values for n and $L_f(N(F))$ for different indoor environments, which are available in ITU (2012), in the case both the transmitter and receiver are in the same floor then $L_f = 0$.

2.6. Motley-Keenan Model

The wide range of n makes the use of OSM insufficient (Keenan & Motley, 1990); MKM considers the effect of walls and floors, including their types and numbers (Keenan & Motley, 1990; Lima & Menezes, 2005).

$$L = L_{FS} + L_C + \sum_{i=1}^{I} N_{wi} L_{wi} + \sum_{j=1}^{J} N_{fj} L_{fj} \tag{6}$$

where L_{FS}, L_C, N_w, N_f, L_w, L_f, i, and j are the free space loss, constant term (loss at $d_0 = 1$ m), number of walls, number of floors, wall loss factor, floor loss factor, type of wall, and type of floor, respectively.

2.7. COST231 Indoor Model

A more sophisticated model is given by COST231, which adopts the concept of Keenan and Motley model (Pedersen, 1999). The model assumes a linear increase of loss as the number of walls increase, and nonlinear increase of loss with respect to the number of floors as the average floor losses tend to decrease when the number of floors increase; the model is given in equation (7) (Pedersen, 1999; Serôdio et al., 2012):

$$L = L_{FS} + L_C + \sum_{i=1}^{I} N_{wi} L_{wi} + L_f n_f^{\left(\frac{(n_f+2)}{(n_f+1)} - b\right)} \tag{7}$$

where L_C is the resultant wall losses obtained by applying multiple linear regression to the measurements, n_f is the number of encountered floors, b is an empirical constant, L_{wi} is wall losses of type i, and L_f is the floor loss. An extension has been made so that individual wall losses decrease as the number of walls increases which gives better performance (Serôdio et al., 2012).

2.8. Dominant Path Model

DPM is similar to Motley and Keenan method; however, instead of considering the direct ray, the dominant rays are considered instead (Wölfle et al., 1997). It considers the main rays that contribute most of the energy; using this model will reduce the dependency of having a fine detailed simulated environment, and it also reduces the computational time as it considers less rays (Wolfle & Landstorfer, 1998). Minimum losses for DPM are computed as in equation (8) (Plets et al., 2012):

$$L = L_{FS} + \sum_{i=1}^{k} \mathrm{WL}_j + \sum_{j=1}^{p} w_l \tag{8}$$

where L_{FS} is the free space loss, WL is cumulated wall losses, and w_l is interaction loss, which depends on type of wall, operating frequency, and the angle of bend made by the propagation.

2.9. Average Wall Model

Average wall model (AWM) was proposed by Lloret et al. (2004) as a fast design model for indoor radio coverage where few measurements are required as they are collected 1 m away from the transmitter and each wall in the facility. This model is similar to MKM; however, the way losses are calculated is different, losses from the same type of walls are averaged, and the total loss after each wall is the result of multiplication of the average losses with total number of encountered walls. The first wall loss is estimated at 1 m away from the wall by finding the difference between the path loss estimated from measurements and the losses due to free space propagation as shown in equation (9) (Lloret et al., 2004):

$$W_1 = P_{r1} - P_0 + 20\log_{10}(d_1) \tag{9}$$

where P_{r1} is the received signal strength (RSS) 1 m from the first wall and d_1 is the distance between the transmitter and the point, which is located 1 m from the first wall. Losses of following walls are estimated similarly after excluding previous wall losses (Lloret et al., 2004). In order to exclude the multipath effect, the mean value for the losses of the same type of walls is given by the following:

$$W_{avg} = \frac{\sum_{i=1}^{v} W_i}{v} \tag{10}$$

Table 1
Wireless Insite Settings for the Investigated Scenario

Property	Setting
Number of reflections	6
Number of transmissions	4
Number of diffractions	1
Number of reflections before first diffraction	3
Number of reflections after last diffraction	3
Number of reflections between diffractions	1
Number of transmissions before first diffraction	2
Number of transmissions after last diffraction	2
Number of transmissions between diffractions	1
Ray tracing method	SBR
Propagation model	Full 3-D

Note. SBR = Shooting-and–Bouncing-Rays.

where v is the total number of encountered walls. The path loss at distance d can be expressed as shown in equation (11), where L is the number of encountered walls.

$$P_r(d) = P_0 - 20\log_{10}(d) - W_{\text{avg}} \cdot L \tag{11}$$

2.10. Effective Wall Loss Model

The AWM captures the changes in the propagation environment; therefore, wall losses may be positive or negative. In fact, these losses can be considered as correction factors rather than losses. Using the "average" will superimpose the effect of all walls and then assume that all walls will contribute equally, which is not necessarily true. The main problem with this model is the assumption that the main source of signal fading are the walls; therefore, similar walls will affect the signal similarly. Although this is partially true especially for millimeter waves as will be shown later, there are many other sources that affect the signal strength (SS) level mainly multipath.

The AWM superimposes the multipath effect; however, the effects of multipath fading give a fingerprint about how waves in specific region behave. Also, the concept of averaging does not reflect a scientific impact as it is unlikely that the last wall loss will affect the measurements at locations much before that wall. Another limitation to the AWM is that it does not consider the effect of line-of-sight (LOS) propagation where path loss exponent will be less than the free space path loss exponent due to waveguiding effect.

Due to these limitations, we adopt the AWM with two modifications: first, the path loss estimated at a point depends on the losses due to the encountered wall only rather than using the concept of averaging. The second modification includes the effect of path loss exponent in the region between the transmitter and the first wall, which may be affected by waveguiding effect. For non-line-of-sight (NLOS) propagation areas the effect of path loss exponents is already embedded with the wall correction factors. In order to distinguish it from the AWM, we refer to the last modification as EWLM. The path loss at distance d can be expressed as follows:

$$P_r(d) = P_0 - 10n\log_{10}(d) - \sum_{i=1}^{L} W_i \tag{12}$$

where n is 2 for NLOS propagation, while for LOS propagation it is estimated by best fitting, L is the number of encountered walls. It is worth mentioning that W_{avg} in equation (11) depends on total wall losses of the same type; therefore, applying equation (11) will consider the effect of walls before and after the point of interest. Walls after the point of interest are unlikely to contribute significantly to the RSS compared to those before the point; therefore, EWLM considers the effect of walls, which are only before the point of interest. Even if the walls are of the same type, both models will work differently as shown in the incoming sections; however, they will have similar results after the last encountered wall where $(W_{\text{avg}} \cdot v = \sum_{i=1}^{v} W_i)$.

3. Methodology and Experimental Setup

In the first part of our analysis, different indoor path prediction models were examined and compared to the EWLM using data obtained from ray tracing software called Wireless Insite®, which has been extensively

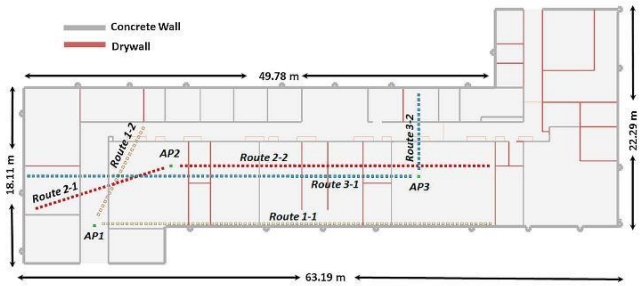

Figure 1. Experimental routes in third floor Chesham building at the University of Bradford.

validated, especially for the ultrahigh frequency band (Medeđović et al., 2012) and for 802.11 ac frequencies (Dama et al., 2011). The adopted environment for the experiment was the third floor in Chesham building in Bradford University. The model for the building was constructed using the software.

Transmitter and receivers implemented in the environment are both omnidirectional, transmitted power was set to 20 dBm, while receiver sensitivity was set to −120 dBm. Five frequencies were examined, including 2.4, 5.3, 28, 60, and 73.5 GHz, and their corresponding bandwidths are 0.084 GHz (Wu et al., 2004), 0.12 GHz (Koivunen et al., 2007), 0.8 GHz (Maccartney et al., 2015), 2.15 GHz (Technologies, 2017), and 2 GHz (Instruments, 2016), respectively; those frequencies have wide usage for indoor applications. We also investigated two types of polarization: vertical polarization (VP) and circular polarization (CP); settings for Wireless Insite are given in Table 1.

In the second part of the experiments, real-time measurements have been collected from WLAN access points (AP) distributed in the third floor of Chesham building at the University of Bradford; those APs support Wi-Fi coverage on both 2.4- and 5.3-GHz bands. In these experiments, three APs were considered as shown in Figure 1. All APs are similar; this includes the transmitter power, types of antenna used, and bandwidth. For each AP, data are collected over two routes; measurements are taken at 1-m height with 0.5-m spacing between each two measurements. The heights for AP1 is 2.2 m, while for AP2 and AP3 the heights are 2.75 m. A WLAN scanner software called *inSSIDer®* was used to collect the measurements using a laptop with a calibrated 802.11a/b/g/ac card adapter, these measurements are averaged to remove the effect of fast fading, and the RSS reading is updated every 1 s.

This experiment was limited for a single floor only; in this case the comparison includes OSM, DSM, LAM, PM, MKM, AWM, and EWLM. (DPM is included in the experimental part only.) For single floor analysis, the ITU model and the COST-231 model are the same as the OSM and MKM, respectively; further analysis for multifloor propagation is subject for further publication.

A valid comparison between the different modeling approaches requires that each model is applied to the same data set in order to predict parameters. MATLAB is used to estimate the parameter values, which

Table 2
Example of Data Used to Predict Model Parameters

Distance (m)	Received signal strength (dBm)
1	−32.22
8	−34.89
11	−40.22
16	−44.23
27	−54.22
30	−57.25
41	−66.78
44	−71.4

Table 3
Estimated Model Parameters

Model	Estimated parameters
One-slope model	Path loss exponent n
Dual-slope model	Path loss exponents (n_1,n_2)
Linear attenuation model	Attenuation factor (a)
Motley-Keenan model	Wall losses (L_W)
Dominant path model	Interaction losses
Average wall model	Average wall losses ($W_{avg.}$)
Effective wall loss models	Wall correction factors (W_i)

provide the best fit to the data. Typical data are shown in Table 2. Table 3 summarizes the different parameters used in each model.

Having generated the best fit parameters, these same values are used to predict the RSS along various routes. Model predicted RSS is calculated for each model using the equations in section 2. The model-predicted RSS values for each route and frequency are compared with the data available from measurements and from Wireless InSite ray tracing simulations.

Error vector distance is estimated between the model-predicted RSS values and the data from Wireless Insite simulations or measurements, then the root-mean-square error (RMSE) of this vector is calculated. The smaller the RMSE, the better model performance.

In Plets et al. (2012) authors formulate a generalized formula for the DPM to be applied for different types of building. Since ray tracing and DPM are two distinct approaches to estimate SS, analysis for DPM is performed only on data collected from real-time measurements. In the experimental part DPM results were compared to other models at both investigated frequencies. As recommended by authors in Plets et al. (2012), DPM parameter values are taken from Plets et al. (2012) and Y. Zhang and Hwang (1994).

It is worth mentioning that for the EWLM after each wall the model makes a correction factor either by adding gain or adding loss in order to fit the simulations/measurements. MKM assumes values for wall losses such that it makes the best fit for all simulations (in case of ray tracing) or measurements (in case of actual measurements) from all different routes; these losses are different from correction factors used by AWM and EWLM. OSM, DSM, and LAM look for the best fitting for the simulations/measurements (different values for n and a can be used to describe the propagation channels within corridors and rooms. DPM uses the cumulated wall losses and interaction losses; this is required to identify all possible direct paths and their

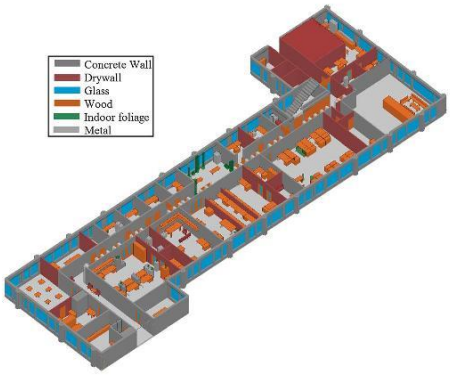

Figure 2. Simulated environment for third floor in Chesham building, University of Bradford.

Table 4
Material Properties With Frequency

	Concrete		Glass		Wood		Drywall	
Frequency (GHz)	ε_r	σ	ε_r	σ	ε_r	σ	ε_r	σ
2.4	5.31	0.0662	6.27	0.0122	1.99	0.0120	2.94	0.0216
5.3	5.31	0.1258	6.27	0.0314	1.99	0.0281	2.94	0.0378
28	5.31	0.4838	6.27	0.2287	1.99	0.1672	2.94	0.1226
60	5.31	0.8967	6.27	0.5674	1.99	0.3784	2.94	0.2102
73.5	5.31	1.0568	6.27	0.7228	1.99	0.4703	2.94	0.2427

corresponding bent angles as mentioned in Plets et al. (2012). After that, cumulated wall losses and interaction losses are calculated using Table 4 and Figure 6 in Plets et al. (2012).

As shown in Figure 1, measurements are taken from AP1 on the yellow routes, while they were taken from AP2 and AP3 on the red and blue routes, respectively. The simulation includes many routes within the floor to cover different scenario and to verify the observations. Figure 2 shows a 3-D view for the simulated environment; the colors are different for different features. Material dependence on operating frequency plays a major role in determining the radio coverage, as shown in equation (13); the attenuation rate A (dB/m) is a function of conductivity σ and relative permittivity ε_r (ITU, 2015).

$$A = \begin{cases} 1636\dfrac{\sigma}{\sqrt{\varepsilon_r}} & \text{Dielectric} \\ 545.8\sqrt{\sigma f_{\text{GHz}}} & \text{Conductor} \end{cases} \tag{13}$$

However, both ε_r and σ are functions of the operating frequency as shown in equations (14) and (15), respectively (ITU, 2015):

$$\varepsilon_r = \alpha f_{\text{GHz}}^{\beta} \tag{14}$$

$$\sigma = \gamma f_{\text{GHz}}^{\delta} \tag{15}$$

where α, β, γ, and δ are given by ITU (2015). As the operating frequency is changing, the interaction between waves and building material will change accordingly. Table 4 shows the values of ε_r and σ adopted in our experiment, which are calculated using equations (14) and (15).

4. Results and Discussion

4.1. Simulation Results

Table 5 summarizes the simulation results for the examples presented in this paper, where row 1, 2, 3, and 4 represent RMSE for the examined indoor path loss prediction models of different routes in the environment at 5.3 GHz using VP antenna, 2.4 GHz using VP antenna, 73.5 GHz using CP antenna, and 60 GHz using CP antenna, respectively.

Table 5
RMSE (in dB) of the Examined Error (Simulation Part)

EWLM	AWM	OSM	LAM	PM	MKM	DSM
7.5665	10.4207	12.4458	10.8654	9.849	8.3017	7.8459
5.2859	6.4431	5.6997	6.4315	8.5297	6.1118	8.1126
5.2702	6.3659	9.1779	8.118	7.2313	5.549	6.5214
14.9072	15.6219	13.115	12.9068	12.5806	11.2973	14.746

Note. RMSE = root-mean-square error; EWLM = effective wall loss model; AWM = average wall model; OSM = one-slope model; LAM = linear attenuation model; PM = partitioned model; MKM = Motley-Keenan model; DSM = dual-slope model.

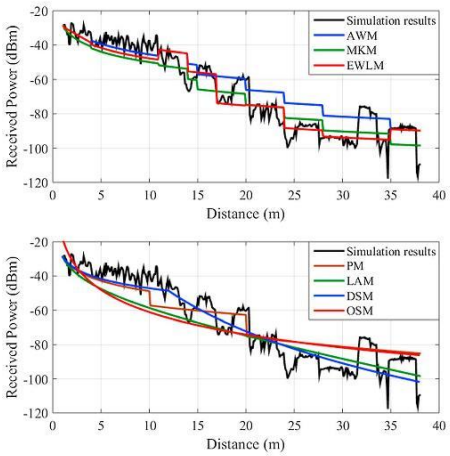

Figure 3. Indoor path loss prediction models comparisons for a route in the environment at 5.3 GHz using vertical polarized antenna. AWM = average wall model; MKM = Motley-Keenan model; EWLM = effective wall loss model; PM = partitioned model; LAM = linear attenuation model; DSM = dual-slope model; OSM = one-slope model.

A comparison between different indoor path loss models at 5.3 GHz using vertical polarized antenna is shown in Figure 3; RMSEs of the examined models are presented in Table 5, row 1. In this scenario, the EWLM outperforms other models as it was able to capture the changes in the environments. After each wall, the model makes a correction factor either adding gain or adding loss to fit the simulation data. In the AWM, the first two

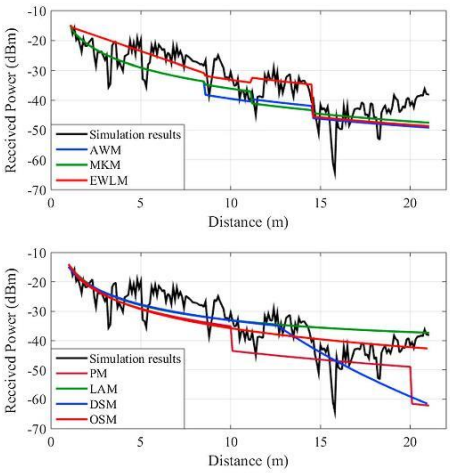

Figure 4. Indoor path loss prediction models comparisons for a route in the environment at 2.4 GHz using vertical polarized antenna. AWM = average wall model; MKM = Motley-Keenan model; EWLM = effective wall loss model; PM = partitioned model; LAM = linear attenuation model; DSM = dual-slope model; OSM = one-slope model.

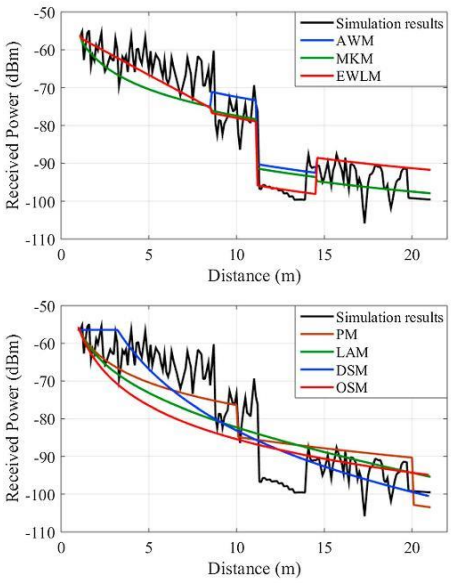

Figure 5. Indoor path loss prediction models comparisons at 73.5 GHz and circular polarization for the same route in Figure 4. AWM = average wall model; MKM = Motley-Keenan model; EWLM = effective wall loss model; PM = partitioned model; LAM = linear attenuation model; DSM = dual-slope model; OSM = one-slope model.

walls loss give positive gain to the averaging, and as a result the model underestimates SS fading. MKM works fine as long the signal level follows semimonotonic decrease.

As provided from the RMSE values, both OSM and LAM show low performance; this may be due the difficulty to model the simulation data with a monotonic function. The DSM uses two slopes to describe the changes in the environment. Due to this flexibility, it has better results than OSM. Finally, the PM has different path loss exponents; however, it shows good performance if the test environment has similar path loss exponents to the model.

In Figure 4, the mean SS level decays slowly with distance; the RMSEs of the examined models are presented in Table 5, row 2. EWLM has the best performance, while OSM has the second best performance as the path loss exponent found to be around 2; this may be regarded due to waveguiding effect. The DSM has lower performance than OSM, although this model uses two path loss exponents, which gives more flexibility; the model requires more data in order to provide accurate prediction. In this scenario and using lower frequencies, there will not be much losses due to propagation through drywall. As a result, the correction factors will have less significant effect; however, considering the waveguiding effect gives EWLM advantage over AWM as seen in Figure 4. While at higher frequencies, propagation through these walls will lead to greater losses; therefore, the correction factors will have more impact as shown in Figure 5.

In Figure 5 simulation results are presented for the same route whose results are shown in Figure 4, but at higher frequency. The RMSEs of the examined models are presented in Table 5, row 3. In comparison, models that use free space path loss exponent ($n = 2$) and add walls losses (i.e., EWLM, AWM, and MKM) or models use fixed values of n like PM are both expected to have better performance; this is due to the fact that wall losses tend to be greater as frequency increases as indicated in the metrics in Table 5. At higher frequencies, walls

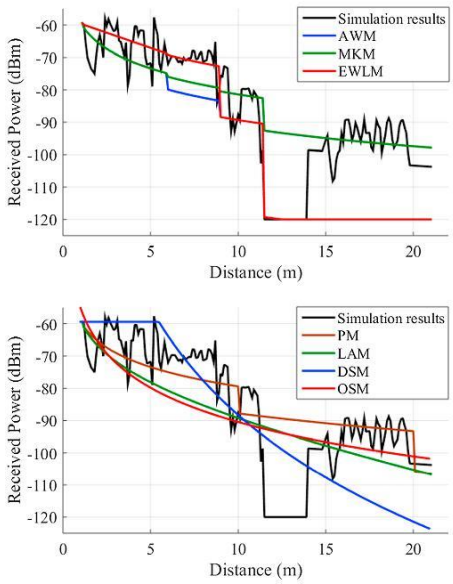

Figure 6. Indoor path loss prediction models comparisons at 60 GHz and circular polarization for a route in the environment. AWM = average wall model; MKM = Motley-Keenan model; EWLM = effective wall loss model; PM = partitioned model; LAM = linear attenuation model; DSM = dual-slope model; OSM = one-slope model

contribute to loss significantly; as a result, the OSM will have less accurate estimation, while the DSM has advantage from having two slopes and hence shows more stability.

In Figure 6 many models predicts the SS sufficiently in the first 11 m and in the last 7 m; however, SS level follows unpredicted behavior in the 11–14-m window where most of them find difficulty to capture these changes as provided by their corresponding RMSE values, which are presented in Table 5, row 4; in this scenario the MKM has the best performance.

Through the experiment, the average RMSE shows an increase as frequency increases as shown in Table 6. Almost all models have larger RMSE values at 28- and 60-GHz band than those at 73.5-GHz band. This

Table 6
Average RMSE (in dB) With Frequencies for Examined Models

	2.4 GHz		5.3 GHz		28 GHz		60 GHz		73.5 GHz	
Model	VP	CP	VP	CP	VP	CP	VP	CP	VP	CP
EWLM	**5.0722**	**5.6069**	**4.6899**	**6.25176**	**10.844**	**10.845**	**10.458**	**9.6559**	**8.6377**	**8.6780**
AWM	8.4641	7.1195	8.4319	10.2344	15.856	15.585	11.860	10.555	9.5655	8.8229
OSM	7.6314	7.811	9.0169	10.0235	15.451	13.589	13.741	11.72	13.811	11.089
LAM	8.2767	8.4406	9.5144	10.5070	16.672	14.114	12.976	11.815	13.596	11.141
PM	16.527	15.743	16.886	15.4893	16.91	16.165	14.288	12.386	15.266	12.471
MKM	9.8295	8.6542	10.093	11.0623	13.383	12.35	11.260	10.002	9.6996	9.0939
DSM	5.752	6.1476	7.4956	8.6941	12.593	13.785	11.342	10.078	11.137	9.3423

Note. As depicted in the table it is clear from the provided metrics that EWLM (in bold) outperforms other models for all examined frequencies and antenna polarization. RMSE = root-mean-square error; EWLM = effective wall loss model; AWM = average wall model; OSM = one-slope model; LAM = linear attenuation model; PM = partitioned model; MKM = Motley-Keenan model; DSM = dual-slope model. VP = vertical polarization; CP = circular polarization.

Table 7
Wall Losses Using Motley-Keenan Model

	Vertical polarization		Circular polarization	
Frequency (GHz)	Drywall	Concrete	Drywall	Concrete
2.4	1	4	1	3
5.3	1	6	1	5
28	3	7	1	8
60	1	21	1	10
73.5	3	20	1	13

increase varies from one model to another as shown in the table; in performance comparison for the models using VP antenna CP antenna, the table shows that AWM, OSM, MKM, LAM and PM have higher RMSE for VP antenna. The EWLM has similar performance for both types of antenna especially for millimeter-wave frequencies.

As mentioned earlier, MKM adopts values for wall losses to give best fit for simulations; Table 7 shows the values given for drywalls and concrete walls for the used frequencies; losses for concrete walls and drywall tend to increase with frequency. They also tend to be larger in the case of VP than CP; this is because when a singly reflected CP signal with angle of incidence is greater than Brewster angle, it will be orthogonal to the LOS component, which leads to reduction in multipath interference (ITU, 2012), moving further away from the transmitter incidence angles become greater than the Brewster angle.

Figure 7 presents a RSS comparative behavior with distance between VP and CP at 28 GHz; the higher SS in the CP case as receiver is moving further away from the AP can be explained by the effect of the multipath interference reduction as mentioned above. As shown in the incoming discussion, the examined model parameters are found to have less values in the case of CP.

The average path loss exponent versus operating frequency for OSM is plotted in Figure 8; for VP antenna, n tends to increase as frequency increases. However, in the case of CP antenna average value of n tends to decrease as frequency exceeds 28 GHz. This is may be explained due to radio coverage reduction occurred as frequency increased; hence, a lower value for n is obtained.

The value of n for the corridor shown in Figure 1 tends to have slight dependency on the examined frequencies as it has almost fixed value equivalent to 0.9 in the case of VP and (0.6–0.9) in the case of CP.

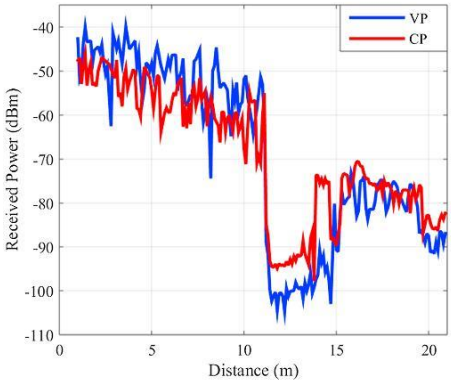

Figure 7. Received power comparison between simulated vertical polarization (VP) and circular polarization (CP) propagation at 28 GHz.

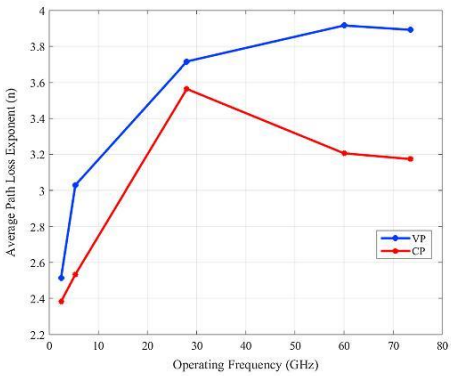

Figure 8. One-slope model path loss exponent relationship with operating frequency. VP = vertical polarization; CP = circular polarization.

Path loss exponent is influenced by changes in frequency and polarization and depending on route location within the floor. For example, using 60 GHz and CP antenna, *n* in corridor routes due to waveguiding effect is found to have a value of 1, while using VP antenna for the same route, it has a value of 1.7. In the case where path is between rooms, where walls are made from concrete, using VP antenna, *n* reached a value of 5.

The relationship between average attenuation factor and frequency for LAM is shown in Figure 9. As expected *a* increases as frequency increases, and VP antenna has higher attenuation factor than CP antenna. The mean value for *a* for VP and CP is 0.67 dB/m and 0.367 dB/m, respectively. Considering Figures 8 and 9, a similarity between OSM and LAM is observed, as the variation of *n* and *a* is very similar for many routes on different frequencies and polarization.

This also is proved in Figure 10; as shown both models have similar performance provided from their corresponding RMSE for almost 40% of tested scenarios. While OSM has better performance for frequencies 2.4, 5.3, and 28 GHz, LAM has better performance for frequencies over 28 GHz. The figure also presents PM

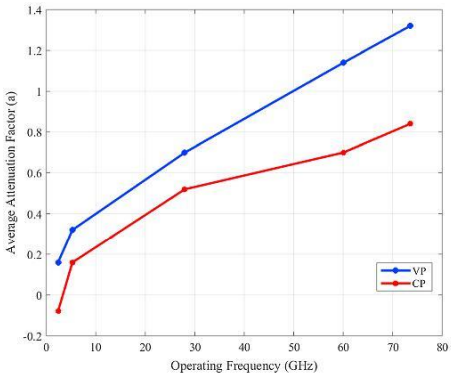

Figure 9. Linear attenuation factor relationship with operating frequency. VP = vertical polarization; CP = circular polarization.

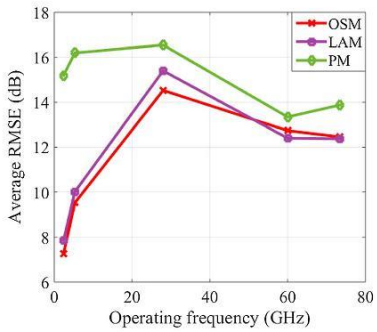

Figure 10. Performance comparison between linear attenuation model (LAM), one-slope model (OSM), and partitioned model (PM). RMSE = root-mean-square error.

performance that shows the poorest performance among all the models due to its limitation by having fixed path loss exponents over predefined distances; however, the model seems to have better performance for 60 and 73.5 GHz.

A comparison between OSM, DSM, and MKM is demonstrated in Figure 11. DSM outperforms both OSM and MKM as it has less RMSE than OSM for almost 72.5% of tested scenarios and less RMSE than MKM for 60.8% of tested scenarios. For low frequencies range of this experiment DSM outperforms MKM, while for millimeter waves MKM has better performance. This can be regarded to the effect of wall losses in SS fading, which is considered by MKM. OSM and DSM show similar pattern with obvious advantage for the DSM, due to the latter flexibility as it has two values for n. The model can capture propagation changes in the environment more efficiently; the gap between the two models increases as frequency increases. On the other hand, MKM outperforms OSM as it has less RMSE for almost 62.75% of tested scenarios. It can also be observed that for higher frequencies, both DSM and MKM are preferable compared to OSM.

A comparison between EWLM, AWM, and MKM is shown in Figure 12. EWLM shows better performance than MKM and AWM for almost 78.4% and 80.4% of tested scenarios, respectively. The model has such advantage because the use of effective wall correction factors enhances SS prediction significantly. When comparing AWM with MKM, the former has less RMSE for almost 56.9% of tested scenarios. The AWM has also better

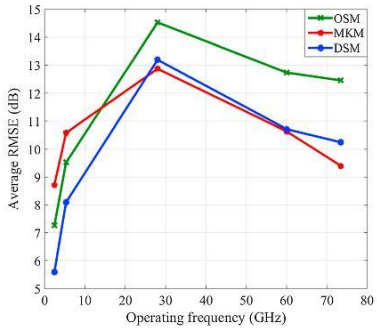

Figure 11. Performance comparison between dual-slope model (DSM), Motley-Keenan model (MKM), and one-slope model (OSM). RMSE = root-mean-square error.

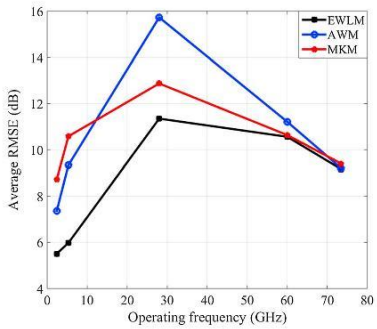

Figure 12. Performance comparison between effective wall loss model (EWLM), average wall model (AWM), and Motley-Keenan model (MKM). RMSE = root-mean-square error.

performance in the 2.4-, 5.3-, and 73.5-GHz regions, while it has comparable performance at the 60 GHz. It may be observed that at 28 GHz the AWM has lower performance. This is due to the effect of averaging with makes SS prediction less accurate at higher frequencies; however, as frequency increases the radio wave coverage becomes smaller. Therefore, the encountered walls become less, in such case the AWM works better. It was also observed that when all the walls encountered are from the same type (i.e., either all are concrete or drywall), the performance of AWM is always lower than EWLM.

Considering models performance at all frequencies, DSM shows the second best performance, a comparison between EWLM and DSM is presented in Figure 13; the metrics show better performance for EWLM as it has less RMSE for almost 66.67% of the tested scenarios. At 2.4 GHz DSM has comparable performance with the EWLM; however, as the operating frequency increases EWLM tends to have better results. This is due to considering effects of wall losses as mentioned earlier.

The average error for most models reaches maximum at 28 GHz. This can be explained as follow: as the frequency increases the radio coverage tends to become shorter, so it will have less error. Although at 28 GHz the coverage was less than 5.3 and 2.4 GHz; however, signal variations tend to be greater; therefore, errors are greater. While at 60 and 73.5 GHz the radio coverage becomes much smaller; thus, errors are less than 28 GHz.

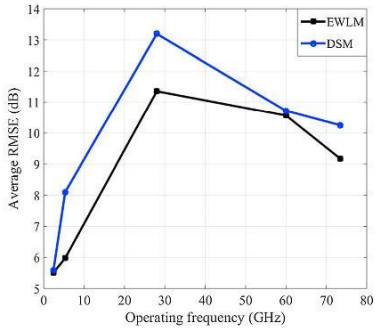

Figure 13. Performance comparison between effective wall loss model (EWLM) and dual-slope model (DSM). RMSE = root-mean-square error.

Table 8
Percentage of Having the Least RMSE (Ordered by Average RMSE)

Model	Percentage of the least RMSE (%)	Average RMSE
EWLM	51	7.6793
DSM	22	9.26586
AWM	9.5	10.4518
MKM	9.5	10.5112
OSM	6	10.9781
LAM	0	11.3626
PM	2	15.4435

Note. RMSE = root-mean-square error; EWLM = effective wall loss model; DSM = dual-slope model; AWM = average wall model; MKM = Motley-Keenan model; OSM = one-slope model; LAM = linear attenuation model; PM = partitioned model.

One interesting observation noted that although both 60 and 73.5 GHz share the same radio coverage, errors at 60 GHz are greater; this might be because the 60 GHz has more fluctuations than 73.5 GHz.

Although AWM has the advantage for being fast prediction model, it comes at the expense of accuracy. EWLM combines accuracy and speed. The PM has the lowest performance as it has predetermined values for n; in comparison to EWLM it has less RMSE for less than 7.8% of tested scenarios.

The order of the best models according to their RMSE values is EWLM, DSM, MKM, AWM, OSM, LAM, then PM; their respective average RMSEs for all scenarios at all frequencies are shown in Table 8. EWLM has the best performance, while PM has the worst performance.

Table 8 also shows the percentage of having the least RMSE for each model over all scenarios and frequencies; EWLM was considered as the one with the least RMSE for 51% of all scenarios, while DSM has a percentage of 22%. Considering these results EWLM is an attractive model especially for millimeter-wave frequency usage.

A comparison between the EWLM with no modification (where $n = 2$ for all scenarios) and with enhancement (n is estimated by best fitting for LOS propagation and 2 for NLOS propagation) is presented in Figure 14; on average the RMSE for all frequencies had reduced by about 1 dB. Compared to other models "EWLM with no modification" had the least RMSE for 27.45% of all tested scenarios; however, by considering the effect of LOS and waveguiding effect the percentage was enhanced to 51% as mentioned above.

In Figure 15 correction factor for concrete wall was found to increase linearly with increasing the operating frequency in the range of (5.3–60 GHz) for both VP and CP cases. While correction factor for drywall tend

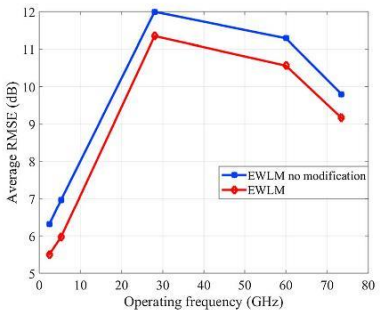

Figure 14. Enhancement on effective wall loss model (EWLM) by considering effect of line-of-sight propagation. RMSE = root-mean-square error.

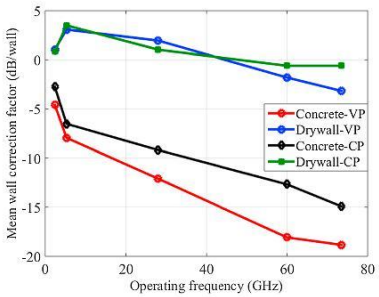

Figure 15. Mean wall correction factor relationship with operating frequency for concrete and drywall. VP = vertical polarization; CP = circular polarization.

to vary linearly with frequency range (2.4–73.5 GHz) for VP and in the range (5.3–60 GHz) for CP. For both types of wall, mean wall correction factor tends to be larger for VP than for CP especially for large frequencies.

4.2. Experimental Results

The experimental study in this paper includes same models investigated in the simulation part in addition to DPM. Figure 1 represents measurements collected in third floor; measurements were taken in different routes to examine more possible scenarios where walls are made from concrete and drywalls. It was observed that radio coverage for 5 GHz band is slightly larger than radio coverage for 2.4-GHz band; this can be explained as the former's effective radiated power is much larger.

A comparison between investigated models is presented in Figure 16 where data are collected from route 2-2 (shown in Figure 1) at 5.3 GHz. It is expected to have a semimonotonic RSS decaying. The RMSEs for the

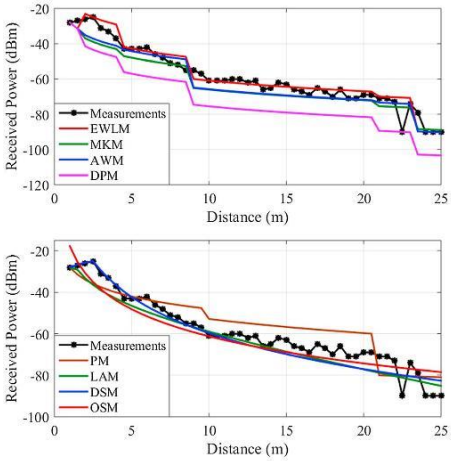

Figure 16. Indoor path loss prediction models comparisons at 5.3 GHz for route 2-2 in the environment. EWLM = effective wall loss model; MKM = Motley-Keenan model; AWM = average wall model; DPM = dominant path model; PM = partitioned model; LAM = linear attenuation model; DSM = dual-slope model; OSM = one-slope model.

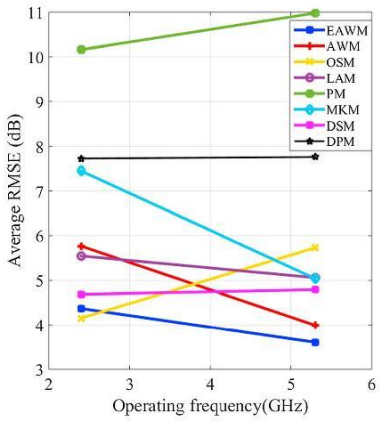

Figure 17. Average root-mean-square error (RMSE) for all models. EWLM = effective wall loss model; AWM = average wall model; OSM = one-slope model; LAM = linear attenuation model; PM = partitioned model; MKM = Motley-Keenan model; DSM = dual-slope model; DPM = dominant path model.

EWLM, AWM, OSM, LAM, PM, MKM DSM, and DPM in decibel are 4.2892, 5.52, 6.067, 5.4572, 7.62, 5.978, 4.9378, and 14.1928 respectively.

As the first wall is close to the transmitter the correction factor will add more accurate estimation to the results, EWLM has the best performance, and the AWM also shows a good resolution; however, it shows less performance than EWLM; this is due to the effect of last wall loss on averaging, which cause the SS prediction to be pessimistic. Since the RSS follows a semimonotonic decaying, OSM, LAM, MKM, and DSM show a good performance, and the PM use fixed values for *n*, which underestimate the actual losses in this scenario. DPM uses predefined values for building wall losses; however, the performance was pessimistic; this may be due to that the wall losses recommended are not for universal use as authors claim; also, the model has no difference in performance from other wall loss models if the direct path between the transmitter and the receiver is the path with least losses.

A comparison between all presented models is introduced in Figure 17; the total error for all routes are averaged. For the 2.4 GHz, as shown from the figure and Table 9, the OSM, DSM, and EWLM have the best performance. Similar to observed results from simulation part, EWLM has the most stable performance as the maximum error did not exceed 6.1102 dB and the standard deviation of errors is around 1.156 dB. PM,

Table 9
Statistical Metrics (in dB) Between Measured and Simulated Data for the Presented Models at 2.4 GHz

Model	Maximum error	Minimum error	STD	RMSE
EWLM	6.1102	2.9334	1.1560	4.3707
AWM	8.4596	3.0472	2.0748	5.7672
OSM	6.5999	3.4202	1.2227	4.1568
LAM	8.1856	3.8566	1.7045	5.54635
PM	15.4375	5.7927	3.4306	10.159
MKM	11.4639	3.7119	2.9566	7.4469
DSM	7.0396	3.123	1.4079	4.6875
DPM	14.3069	4.3167	4.1256	7.7433

Note. STD = standard deviation; RMSE = root-mean-square error; EWLM = effective wall loss model; AWM = average wall model; OSM = one-slope model; LAM = linear attenuation model; PM = partitioned model; MKM = Motley-Keenan model; DSM = dual-slope model; DPM = dominant path model.

Table 10
Statistical Metrics Between Measured and Simulated Data for the Presented Models at 5.3 GHz

Model	Maximum error	Minimum error	STD	RMSE
EWLM	4.6941	2.4044	0.7903	3.60744
AWM	5.6672	2.5276	1.2646	3.9943
OSM	8.4177	4.4267	1.3921	5.7298
LAM	6.2044	3.3204	1.121	5.0591
PM	14.1389	7.62	2.2813	10.9763
MKM	9.0968	3.0752	2.1387	5.0392
DSM	6.6239	4.0949	0.973	4.7900
DPM	14.1928	3.9692	3.7557	7.7599

Note. STD = standard deviation; RMSE = root-mean-square error; EWLM = effective wall loss model; AWM = average wall model; OSM = one-slope model; LAM = linear attenuation model; PM = partitioned model; MKM = Motley-Keenan model; DSM = dual-slope model; DPM = dominant path model.

DPM, and MKM have low accuracy, as the maximum error exceeds 15, 14, and 11 dB respectively, while their standard deviations are 3.4306, 4.1256, and 2.9566 dB, respectively. The LAM and AWM have comparable performance as provided by their metrics.

Similar to PM, DPM uses predefined wall losses; therefore, the performance was poor as seen by the presented metrics. The advantage of using this model is limited to the scenarios where the transmitter and receiver are separated by one/multiwalls and there is another path, which encounters less number of walls; however, in many cases the best path is the shortest in distance between the transmitter and receiver, which return this model to be similar to multiwall models.

Using higher operating frequency, the EWLM has the best performance provided that it has the lowest values for all metrics as shown in Table 10; the metrics are consistent with the observed results in the simulation part. The AWM has the second best performance and still shows good results in terms of accuracy and stability. The DSM and LAM show comparable performances. The former performance degraded with increasing frequency; however, it still have stable and accurate estimation.

The OSM suffers from poor accuracy; this is because of wall losses at higher frequency, which requires more than one path loss exponent to have accurate estimation. The MKM still suffers from instability; however, it has better performance at 5.3 GHz; this is due to the more effect contribution from the walls at higher frequencies, which have larger values as frequency increases as shown in Table 11. DPM has similar behavior to what was observed at 2.4 GHz; typical values used for wall losses using DPM are presented in Table 11.

Path loss exponent increases as operating frequency increases. Among all tested routes, measurements provided an evidence of path loss exponent dependency on the operating frequency. As observed from the measurements, n varies in the range of (1.93–3.3) at 2.4 GHz and in the range of (3.37–4.35) at 5.3 GHz. The averaged path loss exponent is found to be 2.83 and 3.89 at 2.4 and 5.3 GHz, respectively. Linear attenuation factor also shows an increase as the operating frequency increases. Among the six tested routes, measurements from five routes provided an evidence of linear dependency of the attenuation on the operating frequency; a varies in the range of (0.4–1.6) at 2.4 GHz and (1.2–2.5) at 5.3 GHz. The average attenuation factor for the 2.4 and 5.3 GHz are 0.8166 and 1.6, respectively.

Table 11
Wall Loss Using MKM and DPM

	MKM		DPM	
Frequency (GHz)	Drywall	Concrete	Drywall	Concrete
2.4	4	4	2	10
5.3	3	12	7.5	12.5

Note. Wall losses using dominant path model (DPM) from (Plets et al., 2012; Y. Zhang & Hwang, 1994). MKM = Motley-Keenan model.

Table 12
Averaged RMSE (in dB) for All Models

Model	Average RMSE
EWLM	3.9890
AWM	4.8808
OSM	4.9433
LAM	5.3027
PM	10.5681
MKM	6.2431
DSM	4.7388
DPM	6.7379

Note. RMSE = root-mean-square error; EWLM = effective wall loss model; AWM = average wall model; OSM = one-slope model; LAM = linear attenuation model; PM = partitioned model; MKM = Motley-Keenan model; DSM = dual-slope model; DPM = dominant path model.

The averaged RMSEs for all scenarios and frequencies are given in Table 12; among all scenarios, EWLM has the lowest RMSE for almost 50% of tested scenarios, while DSM has the lowest RMSE for 16.667% of tested scenarios. EWLM tends to have better performance as the frequency increase that seems to be consistent with the simulation results. Similar to observations in Figure 15, wall correction factor for concrete tends to increase more rapidly as frequency increased, while for drywall the steep was smoother.

5. Conclusions

A modified indoor path loss prediction model has been presented using ray tracing software and then verified experimentally for 2.4- and 5.3-GHz WLAN frequency bands. In the simulation part, the model was examined and compared to other indoor path loss models at 2.4, 5.3, 28, 60, and 73.5 GHz with different antenna polarization. In the experimental part, the model was compared to same models at 2.4 and 5.3 GHz. In the simulation part EWLM shows the best performance among other models for almost 2 times the second best model. Similar observations were recorded from the experimental results. DSM showed the second best performance provided that it is equipped with sufficient data points. OSM and LAM have similar behavior, and the two models showed dependency on operating frequency and antenna polarization. The PM showed the poorest performance as it has fixed path loss exponents.

Acknowledgments
This work is partially supported by innovation programme under grant agreement H2020-MSCA-ITN-2016 SECRET-722424 and the financial support from the UK Engineering and Physical Sciences Research Council (EPSRC) under grant EP/E022936/1. All measured and simulated data will be available from the following link: https://drive.google.com/file/d/14KhlYxKKObD0p4Nch7PtKJ_TJ97d8XI/view?usp=sharing.

References

Alexander, S., & Pugliese, G. (1983). Cordless communication within buildings: Results of measurements at 900 MHz and 60 GHz. *British Telecom Technology Journal, 1*(1), 99–105.

Alsindi, N. A., Alavi, B., & Pahlavan, K. (2009). Measurement and modeling of ultrawideband TOA-based ranging in indoor multipath environments. *IEEE Transactions on Vehicular Technology, 58*(3), 1046–1058. https://doi.org/10.1109/TVT.2008.926071

Andrade, C. B., & Hoefel, R. P. F. (2010). *IEEE 802.11 WLANs: A comparison on indoor coverage models*. Paper presented at the Electrical and Computer Engineering (CCECE), 2010 23rd Canadian Conference on, Calgary, AB, Canada.

Borrelli, A., Monti, C., Vari, M., & Mazzenga, F. (2004). *Channel models for IEEE 802.11 b indoor system design*. Paper presented at the Communications, 2004 IEEE International Conference on.

Crow, B. P., Widjaja, I., Kim, L., & Sakai, P. T. (1997). IEEE 802.11 wireless local area networks. *IEEE Communications Magazine, 35*(9), 116–126. https://doi.org/10.1109/35.620533

Dama, Y., Abd-Alhameed, R., Salazar-Quinonez, F., Jones, S. M., & Gardiner, J. (2011). *Indoor channel measurement and prediction for 802.11 n system*. Paper presented at the Vehicular Technology Conference (VTC Fall), 2011 IEEE.

Damosso, E., & Correia, L. (1999). Digital mobile radio towards future generation systems communications. COST 231 Final Report. *CEC, Brussels, Belgium*.

Davies, R., Simpson, A., & Mcgreehan, J. (1990). Propagation measurements at 1.7 GHz for microcellular urban communications. *Electronics Letters, 26*(14), 1053–1055. https://doi.org/10.1049/el:19900682

Devasirvathan, D. (1991). *Multi-frequency propagation measurements and models in a large metropolitan commercial building for personal communications*. Paper presented at the Personal, Indoor and Mobile Radio Communications, IEEE International Symposium on, UK.

Goldsmith, A. (2005). *Wireless communications*. New York: Cambridge University Press. https://doi.org/10.1017/CBO9780511841224

Haneda, K., Tian, L., Asplund, H., Li, J., Wang, Y., Steer, D., et al. (2016). *Indoor 5G 3GPP-like channel models for office and shopping mall environments*. Paper presented at the Communications Workshops (ICC), 2016 IEEE International Conference on, Kuala Lumpur, Malaysia.

Hashemi, H. (1993). The indoor radio propagation channel. *Proceedings of the IEEE, 81*(7), 943–968. https://doi.org/10.1109/5.231342

Instruments, N. (2016). mmWave: The battle of the bands. Retrieved 25/10/2016, from http://www.ni.com/white-paper/53096/en/

International Telecommunication Union (ITU) (2012). *Propagation data and prediction methods for the planning of indoor radiocommunication systems and radio local area networks in the frequency range 900 MHz to 100 GHz recommendation ITU-R P* (pp. 1238–1237). Geneva: ITU.

International Telecommunication Union (ITU) (2015). *Effects of building materials and structures on radiowave propagation above about 100 MHz Recommendation ITU-R* (pp. 2040–2041). Geneva: Electronic Publication.
Keenan, J., & Motley, A. (1990). Radio coverage in buildings. *British Telecom Technology Journal*, *8*(1), 19–24.
Koivunen, J., Almers, P., Kolmonen, V.-M., Salmi, J., Richter, A., Tufvesson, F., et al. (2007). Dynamic multi-link indoor MIMO measurements at 5.3 GHz.
Kong, Z.-n., Tsang, D. H., Bensaou, B., & Gao, D. (2004). Performance analysis of IEEE 802.11 e contention-based channel access. *IEEE Journal on Selected Areas in Communications*, *22*(10), 2095–2106. https://doi.org/10.1109/JSAC.2004.836019
Lima, A. G., & Menezes, L. F. (2005). *Motley-Keenan model adjusted to the thickness of the wall*. Paper presented at the SBMO/IEEE MTT-S international conference on microwave and optoelectronics, 2005, Brasilia, Brazil.
Lloret, J., López, J. J., Turró, C., & Flores, S. (2004). *A fast design model for indoor radio coverage in the 2.4 GHz wireless LAN*. Paper presented at the wireless communication systems, 2004, 1st International Symposium on, Mauritius, Mauritius.
Lott, M., & Forkel, I. (2001). *A multi-wall-and-floor model for indoor radio propagation*. Paper presented at the Vehicular Technology Conference, 2001. VTC 2001 Spring. IEEE VTS 53rd, Rhodes, Greece, Greece.
Maccartney, G. R., Rappaport, T. S., Sun, S., & Deng, S. (2015). Indoor office wideband millimeter-wave propagation measurements and channel models at 28 and 73 GHz for ultra-dense 5G wireless networks. *IEEE Access*, *3*, 2388–2424. https://doi.org/10.1109/ACCESS.2015.2486778
Medeđović, P., Veletić, M., & Blagojević, Ž. (2012). *Wireless insite software verification via analysis and comparison of simulation and measurement results*. Paper presented at the MIPRO, 2012 Proceedings of the 35th International Convention, Opatija, Croatia.
Moraitis, N., & Constantinou, P. (2004). Indoor channel measurements and characterization at 60 GHz for wireless local area network applications. *IEEE Transactions on Antennas and Propagation*, *52*(12), 3180–3189. https://doi.org/10.1109/TAP.2004.836422
Nuangwongsa, K., Phaebua, K., Lertwiriyaprapa, T., Phongcharoenpanich, C., & Krairiksh, M. (2009). *Path loss modeling in durian orchard for wireless network at 5.8 GHz*. Paper presented at the Electrical Engineering/Electronics, Computer, Telecommunications and Information Technology, 2009. ECTI-CON 2009. 6th International Conference on, Pattaya, Chonburi, Thailand.
Obeidat, H. A., Dama, Y. A., Abd-Alhameed, R. A., Hu, Y.-F., Qahwaji, R. S., Noras, J. M., & Jones, S. M. (2016). A comparison between vector algorithm and CRSS algorithms for indoor localization using received signal strength. *The Applied Computational Electromagnetics Society (ACES)*, *31*, 868–876.
Pahlavan, K., & Levesque, A. H. (2005). *Wireless information networks* (Vol. 93). Hoboken, NJ: John Wiley.
Pascual-García, J., Molina-García-Pardo, J.-M., Martínez-Inglés, M.-T., Rodríguez, J.-V., & Saurín-Serrano, N. (2016). On the importance of diffuse scattering model parameterization in indoor wireless channels at mm-wave frequencies. *IEEE Access*, *4*, 688–701. https://doi.org/10.1109/ACCESS.2016.2526600
Pedersen, G. F. (1999). *COST 231-Digital mobile radio towards future generation systems*. European Commission.
Pierleoni, P., Pernini, L., Belli, A., Palma, L., Maurizi, L., & Valenti, S. (2016). *Indoor localization system for AAL over IPv6 WSN*. Paper Presented at the 2016 IEEE 27th Annual International Symposium on Personal, Indoor, and Mobile Radio Communications (PIMRC), Valencia, Spain.
Plets, D., Joseph, W., Vanhecke, K., Tanghe, E., & Martens, L. (2012). Coverage prediction and optimization algorithms for indoor environments. *EURASIP Journal on Wireless Communications and Networking*, *2012*(1), 123. https://doi.org/10.1186/1687-1499-2012-123
Rappaort, T. S. (2002). *Wireless communications: Principles and practice* (2nd ed.). Upper Saddle River, NJ: Prentice Hall.
Remcom (2017a). Wireless Insite. Retrieved from http://www.remcom.com/wireless-insite
Remcom (2017b). *Wireless InSite reference manual* (3.1.0 ed.). State College, PA: REMCOM.
Saleh, A. A., & Valenzuela, R. A. (1987). A statistical model for indoor multipath propagation. *IEEE Journal on Selected Areas in Communications*, *5*(2), 128–137. https://doi.org/10.1109/JSAC.1987.1146527
Saunders, S., & Aragón-Zavala, A. (2007). *Antennas and propagation for wireless communication systems* (2nd ed.). Chichester UK: John Wiley.
Serôdio, C., Coutinho, L., Reigoto, L., Matias, J., Correia, A., & Mestre, P. (2012). *A lightweight indoor localization model based on motley-keenan and cost*. Paper Presented at the Proceedings of the World Congress on Engineering 2012, WCE 2012, London, U.K.
Spencer, Q. H., Jeffs, B. D., Jensen, M. A., & Swindlehurst, A. L. (2000). Modeling the statistical time and angle of arrival characteristics of an indoor multipath channel. *IEEE Journal on Selected Areas in Communications*, *18*(3), 347–360. https://doi.org/10.1109/49.840194
Suits, J. I., Farmer, C. M., Ezekoye, O. A., Abbasi, M. Z., & Wilson, P. S. (2014). Personal alert safety system localization field tests with firefighters. *The Journal of the Acoustical Society of America*, *136*(4), 2166–2166. https://doi.org/10.1121/1.4899839
Technologies, A. (2017). Wireless LAN at 60 GHz - IEEE 80211ad-Explained-Agilent-White-Paper.
Wells, P. I. (1977). The attenuation of UHF radio signals by houses. *IEEE Transactions on Vehicular Technology*, *26*(4), 358–362. https://doi.org/10.1109/T-VT.1977.23708
Wolfle, G., & Landstorfer, F. (1998). *Dominant paths for the field strength prediction*. Paper presented at the Vehicular Technology Conference, 1998. VTC 98. 48th IEEE.
Wölfle, G., Wol, G., & Landstorfer, F. (1997). Field strength prediction with dominant paths and neural networks for indoor mobile communication.
Wu, J.-W., Hsiao, H.-M., Lu, J.-H., & Chang, S.-H. (2004). Dual broadband design of rectangular slot antenna for 2.4 and 5 GHz wireless communication. *Electronics Letters*, *40*(23), 1461–1463. https://doi.org/10.1049/el:20046873
Zekavat, R., & Buehrer, R. M. (2011). *Handbook of position location: Theory, practice and advances* (Vol. 27). Piscataway, NJ: John Wiley.
Zhang, R., Hoflinger, F., & Reindl, L. (2013). Inertial sensor based indoor localization and monitoring system for emergency responders. *IEEE Sensors Journal*, *13*(2), 838–848. https://doi.org/10.1109/JSEN.2012.2227593
Zhang, Y., & Hwang, Y. (1994). *Measurements of the characteristics of indoor penetration loss*. Paper presented at the Vehicular Technology Conference, 1994 IEEE 44th.
Zvanovec, S., Valek, M., & Pechac, P. (2003). *Results of indoor propagation measurement campaign for WLAN systems operating in 2.4 GHz ISM band*. Paper presented at the Antennas and Propagation, 2003.(ICAP 2003). Twelfth International Conference on (Conf. Publ. No. 491), Exeter, UK,.

A Comparison between Vector Algorithm and CRSS Algorithms for Indoor Localization using Received Signal Strength

Huthifa A. Obeidat[1], Yousif A.S. Dama[1,2], Raed A. Abd-Alhameed[1], Yim F. Hu[1], Rami Qahwaji[1], James M. Noras[1], Steven M.R. Jones[1]

[1] School of Engineering and Informatics
University of Bradford, Bradford, UK, BD7 1DP
H.A.Obeidat@student.bradford.ac.uk, r.a.a.abd@Bradford.ac.uk, R.S.R.Qahwaji@bradford.ac.uk, j.m.noras@Bradford.ac.uk, s.m.r.Jones@Bradford.ac.uk
[2] Department of Telecommunication Engineering, An Najah National University, Nablus, Palestine
yasdama@najah.edu

Abstract — A comparison is presented between two indoor localization algorithms using received signal strength, namely the vector algorithm and the Comparative Received Signal Strength (CRSS) algorithm. Signal values were obtained using ray tracing software and processed with MATLAB to ascertain the effects on localization accuracy of radio map resolution, number of access points and operating frequency. The vector algorithm outperforms the CRSS algorithm, which suffers from ambiguity, although that can be reduced by using more access points and a higher operating frequency. Ambiguity is worsened by the addition of more reference points. The vector algorithm performance is enhanced by adding more access points and reference points while it degrades with increasing frequency provided that the statistical mean of error increased to about 60 cm for most studied cases.

Index Terms - CRSS, Indoor localization, Ray tracing, RSS.

I. INTRODUCTION

Indoor localization is the process of locating an object within a building, ideally with high accuracy and low computational effort [1]. Localization using Received Signal Strength (RSS) aims to establish a one-to-one relationship between the target location and the measured data [2]: as the distance between the target node and the receiver increases, the signal generally becomes weaker. Knowledge of the radio attenuation helps to establish the relationship between distance and RSS, a process known as radio mapping [2].

RSS-based localization techniques offer low cost, and low sensitivity to the bandwidth and undetected paths [3, 4]. On the other hand, they are sensitive to shadowing, low SNR, and non-line-of-sight propagation, with errors increasing with resulting rapid power attenuation [5].

It is noteworthy that actual distance does not always scale linearly with the RSS value, especially in indoor environments, where obstacles may reduce the strength of the signal, thus giving a false indication that the target is far away from the transmitter [6 - 8]. Deployment of AP, taking into account environmental features, enhances the localization accuracy [9]. The variability of RSS measurements is due to many factors [10, 11]:

- the orientation of the receiver
- temporal factors - readings differ throughout the day because of the people movements
- human factors since 50% of the human body is water
- interference factors due to having devices operating in the same channel, although by using different channels the correlation becomes trivial.

Using wireless sensor networks for localization purposes brings the advantages of continuous monitoring, low cost, and a capability to work unattended, even for years [12]. However, some problems can arise as those devices operate at 2.4 GHz, and may experience interference with devices such as microwave ovens and Bluetooth devices, with a resulting increase in error probability [6].

There are many different RSS–based algorithms used for indoor localization, including radio frequency (RF) fingerprinting, one of the best-known algorithms [12, 14]. This has two phases. In the off-line or training phase, predetermined points are chosen. At each location, the system collects RSS values from the access points, either experimentally which will consume effort, time and cost, or using ray-tracing software, whereby the system builds a database of RSS with locations. This database is called a radio map [15]. The software takes account only of approximate building information, and details are ignored. This introduces more error in comparison with measurement data.

In the on-line phase, RSS measurements are collected from unknown locations, and then values are compared with the existing radio map. The closest match to the database is taken as the best estimate of the target location [15].

The present research work compares two indoor localization algorithms based on RF-fingerprinting, the vector algorithm and the Comparative Received Signal Strength (CRSS) algorithm. It extends previous work [16, 17]: here we have adopted lower operating frequencies. Section II offers a brief explanation of the methodology, and then Section III sets out the environment and specifications of the study. Finally, Section IV presents a discussion of the results.

II. VECTOR AND CRSS ALGORITHMS

In our investigation, the relative benefits and drawbacks of two localization algorithms were investigated. The first algorithm, the vector algorithm, uses a vector of received signal strength readings measured at the reference point from the different access points within the facility. The readings are arranged according to the access point order.

Vectors from the reference points are stored in the database, and the test node vector is compared with the database, by calculating the Euclidean distance between the test vector and the database vectors. The smallest Euclidean distance represents the closest reference point to the test node.

The second algorithm is the CRSS algorithm. We extend the work done by authors in [18], whereby the vectors of the previous approach are converted into constraint matrices, which comprise the database of the radio map. Test node readings also are converted into a matrix, and then the Euclidean distance between this test node matrix and the database matrices is calculated, where again the smallest distance indicates the closest reference location to the test node.

In the initial off-line phase, $R_i(x, y)$ is the RSS from the transmitter or access point i at tag location (x, y). The elements of this matrix depend on RSS values, as shown:

$$M_\alpha(x,y) = [c_{ij}(x,y)].\ \ i,j = 1,2,\dots,\alpha \quad (1)$$

$$c_{ij}(x,y) = \begin{cases} +1 & R_i(x,y) > R_j(x,y). \\ -1 & R_i(x,y) < R_j(x,y). \\ 0 & R_i(x,y) = R_j(x,y). \end{cases} \quad (2)$$

$$c_{ij}(x,y) = 0 \ \ for\ all\ i = j. \quad (3)$$

where $M_\alpha(x, y)$ is the constructed matrix, and $c_{ij}(x, y)$ compares the RSS access point for access point i with that for access point j. (x, y) is the location for the mobile which is considered to be known. The following example illustrates the method: assuming there are three APs, the RSS values received at the RP located at (x, y) are [-20 dBm, -12 dBm, -14 dBm]. The first row compares the power received from the first AP with the other AP readings as explained in equation (2), the second row compares the power received from the second AP with the RSS values from the other APs, etc. The resultant matrix is

$$M_3(x,y) = \begin{bmatrix} 0 & -1 & -1 \\ 1 & 0 & 1 \\ 1 & -1 & 0 \end{bmatrix} \quad (4)$$

In the on-line phase, the radio map is constructed just as in the off-line phase, except that the location of the test devices is estimated by comparing the constraint matrix of a tag with those in the radio map. The closest matrix is the one with the smallest Euclidean distance, thus the corresponding location for the closest matrix is taken to be the closest location to the tag.

The inherent redundancy that exists in each constraint matrix (i.e. insensitivity to the absolute RSS values) gives rise to an acceptable performance for the positioning algorithm and makes the system more robust.

In this work, we assume that the tags operate a protocol that avoids collision, so that in the case of multiple tags there will be no cross talk

This study is based on a simple scenario without clutter, in order to clarify the relative merits of the proposed algorithms. We initially investigate a single room without clutter; further studies will examine the multipath fading arising from clutter.

III. SIMULATION AND RESULTS

A. THE CRSS Algorithm

A severe drawback of the CRSS algorithm was exposed during the analysis of the results obtained in the project, termed "the ambiguity problem".

While generating the CRSS radio map, it was noted that some RPs have identical same constraint matrices, in that although each RP is likely to have unique power readings, the relative power readings are found frequently to coincide.

The generated matrix does not depend on the absolute RSS readings only, but also on the descending order of the received power readings of the APs. Thus, a test area may divide into regions in which all the RPs located in that region can be represented by identical matrices.

Consider a test area with three APs with RSS values: [x dBm, y dBm, z dBm]: we sort them according to these values, giving 13 possible arrangements as shown in the table.

Table 1: Possible arrangements for RRS data from three Aps.

1	$x > y > z$	7	$y > x > z$
2	$x > z > y$	8	$y > z > x$
3	$x > y = z$	9	$y > x = z$
4	$x = y > z$	10	$y = z > x$
5	$x = z > y$	11	$z > x > y$
6	$x = y = z$	12	$z > y > x$
13	$z > x = y$		

This means that if this test area has 20 RPs, then in the best case the area can be represented by 13 matrices, or even fewer. As shown above, this algorithm is dependent on the number of RPs and APs.

In the localization process, a test point will create a matrix based on its RSS readings, using which the Euclidean distance is calculated. Because we are interested in the elements with the same matrix indices the Euclidean distance is estimated as in following:

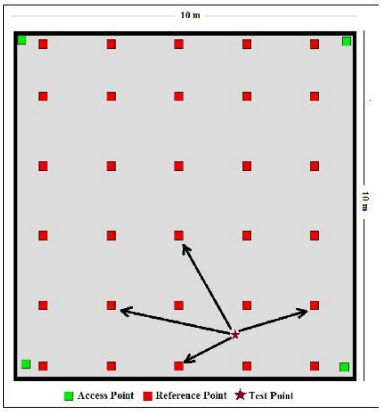

Fig. 1. Ambiguity example for a test area.

$$e = \sqrt{\sum_{i=1}^{N}\sum_{j=1}^{N}(c_{ij} - t_{ij})^2}. \quad (5)$$

where c_{ij} represents the elements in a radio map matrix c in row i and column j, and t_{ij} represents the corresponding element in the on-line matrix t.

Some RPs have identical matrices, and consequently, more than one RP will appear as closest to the test point. This problem is termed *ambiguity*. Fig. 1 illustrates an example; four RPs appear equally closest to the test point, as their corresponding matrices have the same Euclidean distance to the test point matrix.

The effect of the ambiguity problem becomes worse if closest matrix is the same matrix for more than one RP. This can arise when RPs have similar propagation environments: when more than one RP has the same matrix, the phenomenon is called similarity.

Table 2: Similarity in CRSS matrices for three APs at 200 MHz.

No. of RPs	**4**	**9**	**20**	**30**
Unique Matrices	4	3	0	0
Matrix for 2 RPs	0	0	2	0
Matrix for 3 RPs	0	2	2	0
Matrix for 4 RPs	0	0	0	1
Matrix for 5 RPs	0	0	2	4
Matrix for 6 RPs	0	0	0	1

Table 3: Similarity in CRSS matrices for four APs at 200 MHz.

No. of RPs	4	9	20	30
Unique Matrices	4	7	11	8
Matrix for 2 RPs	0	1	3	5
Matrix for 3 RPs	0	0	1	4

The example in Fig. 2 helps more clearly explain the tables. Consider the similarity in the CRSS matrices for twenty RPs, four APs and 200 MHz as in Table 3: among the RPs, 11 of them have distinct matrices, while in 3 pairs of RPs each shares the same matrix. Finally, another 3 RPs generate the same matrix.

Inspection of the identical matrices shows them to be in adjacent location in groups of 2, 3, 4… etc. as also shown in the tables.

Increasing the number of RPs tends to worsen the effect of ambiguity, with more RPs having the same constraint matrix. Table 3 below shows the effect of increasing RPs in a test area with four APs and an operating frequency of 200 MHz. With only four RPs, all four generated matrices are unique, but with nine RPs two RPs share the same matrix while the other seven have unique matrices. With twenty RPs, three pairs of RPs share the same matrix, with a further triplet of three RPs having one matrix in common. The thirty RP case is even worse, with ten RPs sharing five matrices in pairs and twelve RPs sharing four matrices, i.e. four sets of triplet RPs with a matrix in common.

Table 4: Similarity in the CRSS matrices for three APs at 400 MHz.

No. of RPs	4	9	20	30
Unique Matrices	4	4	0	0
Matrix for 2 RPs	0	1	2	1
for 3 RPs	0	1	1	0
for 4 RPs	0	0	2	1
for 5 RPs	0	0	1	2
for 6 RPs	0	0	0	1
for 7 RPs	0	0	0	0
for 8 RPs	0	0	0	1

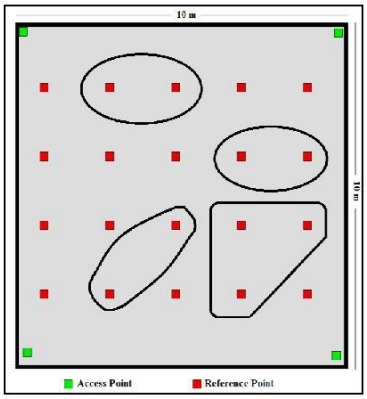

Fig. 2. Example of similarity.

Table 5: Similarity in the CRSS matrices for four APs at 400 MHz.

No. of RPs	4	9	20	30
Unique Matrices	4	7	10	15
Matrix for 2 RPs	0	1	5	7
Matrix for 3 RPs	0	0	0	1

Similarity in CRSS matrices is affected by the number of APs used in the system, as the matrix size will correspondingly increase. Table 3 shows the similarity in the generated matrices using four APs for the same test area and the same operating frequency.

The difference between the cases of four APs and three APs is obvious; adding more APs reduces the similarity in the generated matrices. From the previous tables, it can seen that adding more APs will reduce similarity, while adding more RPs will increase similarity.

Results obtained when changing the frequency from 200 MHz to 400 MHz are shown in Tables 4 and 5, which show that the similarity is reduced as the frequency increased.

Ambiguity need not always have negative consequences, namely if the estimated locations surrounded the test point. Rather than identifying the test point as close to a certain RP, it would be located within a specific area.

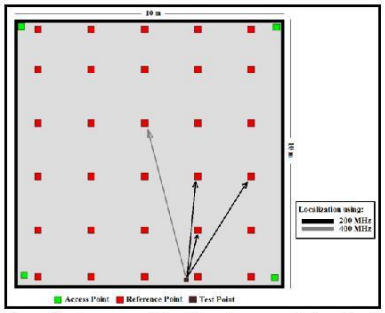

Fig. 3. Less ambiguity does not imply better localization.

However, throughout all the experiments such a thing rarely happened. It is true that with increasing frequency, the similarity in the generated matrices will be less, but this does not mean that localization performance is thereby improved: a test point considered to be close to fewer RPs using 400 MHz does not mean that these RPs are closer than those estimated at 200 MHz, as shown in Fig. 3.

The localization process includes the calculation of the Euclidean distance between all the matrices in the database and choosing the one representing the least error. As a result, more matrices may have the same Euclidean distance, therefore, more RPs will be considered as the closest RP. There have been sincere efforts to characterize the effect of the ambiguity analytically, however, the results show randomness in the number of the linked RPs to the test point as Fig. 4 shows. Based on results obtained from one experiment, this shows the number of the closest RPs using different radio map resolution. The similarity in the twenty RPs is less relatively when compared to the system with thirty RPs, but still this does not necessarily mean that the ambiguity effect will be less. Moreover, even if the number of the estimated "closest locations" is less, this does mean that an estimated location lies closest to the test point, as depicted previously in Fig. 3.

The ambiguity problem is a severe drawback of the CRSS algorithm, which jeopardizes the system's credibility, despite claims that it outperforms the vector algorithm due to the redundancy in the information embedded within the matrix [2]. A similar analysis was conducted for a more elaborate scenario including a number of rooms adjoining a corridor on a single floor of the author's recent work [19] as shown in Fig. 5, and similar conclusions have been drawn.

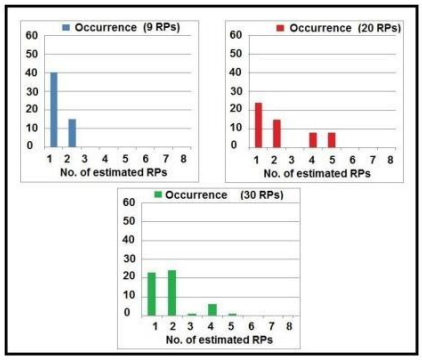

Fig. 4. The number of estimated RPs in the CRSS using different sets of radio maps.

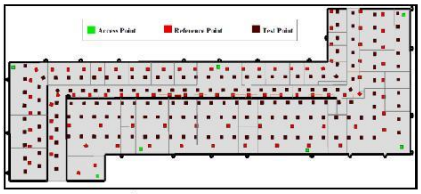
Fig. 5. The 3rd floor of the Chesham Building, University of Bradford.

As the present work shows that the CRSS algorithm is unreliable, in the following we consider the vector algorithm only.

B. THE Vector Algorithm

This algorithm is deemed successful as long as the estimated location is the closest to the actual location of the mobile terminal. When the estimated RP is not closest to the actual location of the mobile terminal, then the algorithm is said to have failed. The percentage of correctly estimated locations gives the *success rate*.

Fig. 6 shows the localization performance for the vector algorithm using three APs and different radio map resolutions. The performance is enhanced as the number of the RPs increases; e.g. P(Error $\leq$ 2m) was about 0.26 for the four RP

system, and increased gradually up to 0.8 for the thirty RP system.

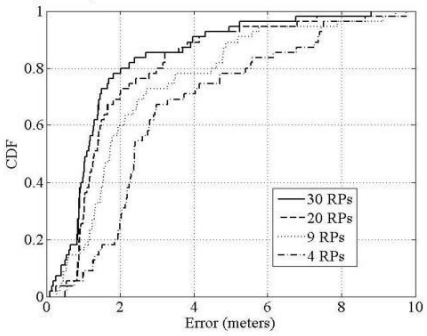

Fig. 6. Localization error for the vector algorithm using three APs, at 200 MHz

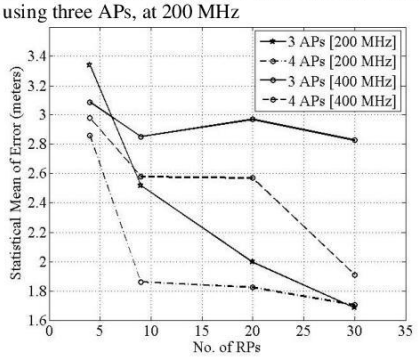

Fig. 7. Statistical mean error for the vector algorithm.

The statistical mean of error was also reduced as shown in fig. 7. Moreover, the performance shows more stability as the number of RPs increases; error deviation was reduced and the high error estimates were less common. For thirty, twenty, nine and four RPs the error for 85% of locations was less than (2.7, 3.2, 4.8, 6.15) m respectively. Thus, increasing the number of RPs improves localization and enhances stability.

Table 6: Success Rates for different sets of RPs, APs and frequencies.

No. of APs	No. Of RPs	200 MHz	400 MHz
	4 RPs	65%	67%
3 APs	9 RPs	58%	47%
	20 RPs	49%	32%
	30 RPs	49%	32.7%
4 APs	4 RPs	78%	72%
	9 RPs	72%	58%
	20 RPs	58%	54%
	30 RPs	52%	61%

Fig. 7 shows the statistical mean error for the vector algorithm using three and four APs at different frequencies. The figure shows that the overall performance of the algorithm is poor for low-resolution radio maps. It improves gradually as the number of APs and RPs in the system increases. The system performance at 200 MHz improves steadily until it reaches a maximum level of accuracy. As shown in the metrics in table 6, the algorithm performance does not give satisfactory accuracy at 400 MHz except for the system that used thirty RPs and four APs. In general, the performance at 200 MHz is significantly better than at 400 MHz, however high-resolution radio maps and adequate numbers of APs will improve the algorithm's performance to acceptable levels.

It can be noted that the success rate decreases as the number of RPs increases, as shown in table 6, although the localization error improved. This can be justified thus: the algorithm is considered successful when the estimated location is the closest RP to the test point. When the number of RPs in the radio map is limited, the RPs will be large distances away, and it is expected that they will be exposed to different fading parameters, so it will be easier for the algorithm to estimate the closest RP. However, as the number of RPs increases, they become closer to each other, and they will have more similar propagation environments, and thus comparable RSS readings. It will be more difficult for the algorithm to estimate the closest RP, and therefore the error will be enhanced.

Fig. 8 shows the localization performance using four APs for different numbers of RPs, showing the outstanding performance of the algorithm especially with a high-resolution radio map, and they underline the importance of the number of APs in determining the overall system performance. They also suggest that even low-resolution systems could provide a system with good accuracy as long as there were an adequate number of APs in the

system. If we exclude the 4 RPs system, the algorithm shows stability and robustness, with deviations constant for the other systems. The most interesting result obtained is the performance of the localization using nine RPs, which is almost the same as for those using twenty and thirty RPs in the 0-2 m window, and outperforms them slightly in the 2-4 m window. For thirty, twenty, nine and four RPs the error for 85% of locations was less than (3.37, 3.2, 2.28, 5.385) m respectively. This may be considered as the optimum system, which has good performance metrics with only a few RPs used.

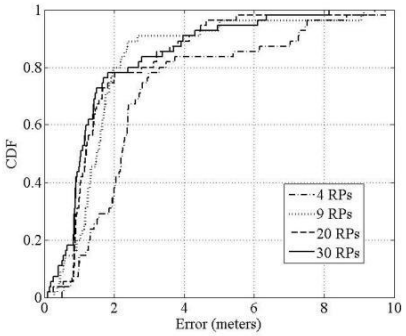

Fig. 8. Localization error for the vector algorithm using four APs, at 200 MHz.

Fig. 9 shows a localization error comparison between the three AP and four AP systems. The four AP system shows better performance, with a success rate enhanced from 58% to 74%. The statistical mean of error was improved from 2.52 m to 1.86 m. Standard deviation was reduced from 2.12 m to 1.7 m. The error performances of the two systems are almost the same in the 0-1 m window, but they do vary in the 1-2 m window.

P(Error $\leq$ 2m) for three RPs was about 0.6 whereas it was around 0.8 for the four RP system. This accuracy is satisfactory for many applications. The effect of adding an extra AP to the system is obvious as all the metrics reflect enhancement in performance.

Fig. 10 shows the localization performance for the vector algorithm using three and four APs with a radio map resolution of thirty RPs. The success rate was enhanced from 49% to 52%, and the mean error has changed slightly from 1.68 m to 1.7 m. Standard deviation remained the same at 1.68 m. The performance of the two systems is effectively identical. It is clear that increasing the number of RP points will make the need for more APs less. In addition, increasing the number of RPs will enhance the performance of localization but the enhancement obtained may become insignificant, as the accuracy will saturate at a certain level.

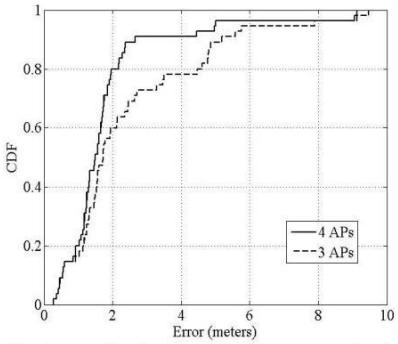

Fig. 9. Localization error for the vector algorithm using nine RPs.

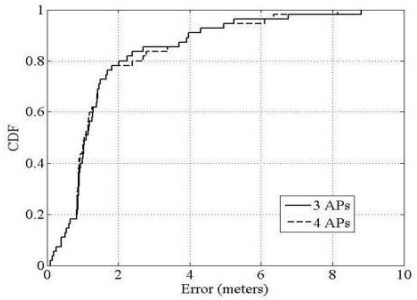

Fig. 10. Localization error for the vector algorithm using twenty RPs, at 200 MHz.

As mentioned above, two operating frequencies, 200 MHz and 400 MHz, were used to conduct the experiments. In general, the localization performance with 200 MHz is better. A justification for such results can be found in propagation theory. When a signal travels in space over a surface, as well as the direct wave there is also a ground wave traveling with it. Due to the different paths that the

signals take, a phase shift of 180 degrees occurs every λ/2, leading to destructive interference and thus reduced power at those points. For example, at 400 MHz, this happens every 0.375 m, so test points at such locations will be completely irrelevant to the RP measurements. As the power readings in the area around the RP will change significantly, mapping the received power vector with the location will result in weaknesses in RSS-based algorithms. At 200 MHz, cancellation occurs every 0.75 m and so the fluctuation in power readings is slower than with 400 MHz. Fig. 11 shows the performance of the vector algorithm for two different operating frequencies and a radio map resolution of twenty RPs. The algorithm performance with 200 MHz is clearly better than with 400 MHz. The error for 85% of locations was less than 3.2 m (three and four APs at 200 MHz), 6.3m (three APs at 400 MHz) and 6.6m (four APs at 400 MHz). Moreover, table 7 shows that the algorithm performance at 200 MHz with the use of three APs only is better than its performance with the use of four APs at 400 MHz provided that the statistical mean of error increased to about 60 cm for most studied cases. These results emphasize the importance of the operating frequency in determining the algorithm performance.

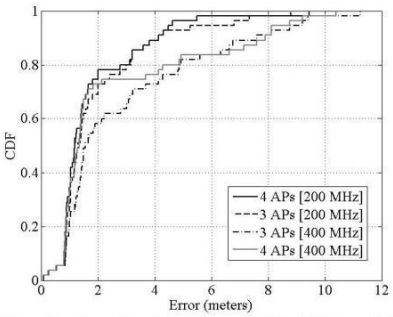

Fig. 11. Localization error at 200 MHz and 400 MHz, for twenty RPs.

Table 7: Performance metrics of the vector algorithm for 200 MHz and 400 MHz.

No. of APs	Metric	200 MHz	400 MHz
	Success rate	49%	32.7%
3 APs	Mean	2 m	2.97 m
	Standard deviation	1.75 m	2.27 m
4 APs	Success rate	58%	54%
	Mean	1.82 m	2.57 m
	Standard deviation	1.61 m	2.75 m

IV. CONCLUSIONS

The paper compares two indoor localization algorithms using received signal strength, the vector algorithm, and the CRSS algorithm. The experiment was carried out at 200 MHz and 400 MHz, and the localization performance was tested for different numbers of access points (AP), and for different numbers of reference points (RP). In the vector algorithm, increasing the number of RPs enhances the localization process up to a certain limit, while increasing the number of APs will also result in better performance. Experiments show that increasing the number of RPs will compensate for a reduction in the number of APs, which seems to be attractive commercially. The CRSS algorithm suffers from ambiguity since more than one RP may have the same matrix, and increasing the number of RPs will only make the ambiguity worse. Reducing the number of the APs will increase the algorithm's ambiguity.

It is noted that a lower frequency is better for localization than a higher one. Based on the experimental results the vector algorithm is better in terms of accuracy, cost, and effort.

Acknowledgment

The authors would like to acknowledge support from the TSB-KTP project grant No. 008734 with the Seven Technologies Group, Leeds, United Kingdom.

REFERENCES

[1] Z. Yang Y. Liu, *Location, Localization, and Localizability Location-awareness Technology for Wireless Networks*, 1st ed. New York, United States: Springer, 2011.

[2] K. Pour, and D. Kasper, "A Robust Model-based Approach to Indoor Positioning Using Signal Strength," in *Personal, Indoor and Mobile Radio Communications, 2008. PIMRC 2008. IEEE 19th*

International Symposium on, Cannes, 2008, pp. 1-5, 2008.

[3] H.Ahn, and W. Yu, "Environmental-Adaptive RSSI-Based Indoor Localization," Automation Science and Engineering, IEEE Transactions on, vol. 6, no. 4, pp. 626- 633, Oct. 2009.

[4] Kharidia, S.A.; Qiang Ye; Sampalli, S.; Jie Cheng; Hongwei Du; Lei Wang, "HILL: A Hybrid Indoor Localization Scheme," in *Mobile Ad-hoc and Sensor Networks (MSN), 2014 10th International Conference on* , vol., no., pp.201-206, 19-21 Dec. 2014

[5] D. Munoz, F. Bouchereasus, and C. Caldera, Position Location Techniques and Applications, 1st ed. Burlington, United States: Academic Press, 2009.

[6] A. Ladd, "On the feasibility of using wireless ethernet for indoor localization," Robotics and Automation, *IEEE Transactions on*, vol. 20, no. 3, pp. 555-559, June 2004.

[7] D. Moeinfar, H. Shamsi, F. Nafar,"Design and Implementation of a Low-Power Active RFID for Container Tracking at 2.4 GHz Frequency," Advances *in Internet of Things*, Vol.2 No.2,pp. 13-22, 2012 [Online]. Available: DOI:10.4236/ait.2012.22003

[8] Y. Cui, Q. Wang, H. Yuan, X. Song, X. Hu, and L. Zhao, "Relative Localization in Wireless Sensor Networks for Measurement of Electric Fields under HVDC Transmission Lines," *Sensors*, vol. 15, no. 2, pp. 3540–3564, Feb. 2015 [Online]. Available: http://dx.doi.org/10.3390/s150203540

[9] Chapre, Y.; Mohapatra, P.; Jha, S.; Seneviratne, A., "Received signal strength indicator and its analysis in a typical WLAN system (short paper)," in *Local Computer Networks (LCN), 2013 IEEE 38th Conference on* , vol., no., pp.304-307, 21-24 Oct. 2013

[10] Lisheng Xu; Feifei Yang; Yuqi Jiang; Lei Zhang; Cong Feng; Nan Bao, "Variation of Received Signal Strength in Wireless Sensor Network," in *Advanced Computer Control (ICACC), 2011 3rd International Conference on* , vol., no., pp.151-154, 18-20 Jan. 2011

[11] Ullah, K.; Custodio, I.V.; Shah, N.; dos Santos Moreira, E., "An Experimental Study on the Behavior of Received Signal Strength in Indoor Environment," in *Frontiers of Information Technology (FIT), 2013 11th International Conference on* , vol., no., pp.259-264, 16-18 Dec. 2013

[12] Shchekotov, M., "Indoor localization methods based on Wi-Fi lateration and signal strength data collection," in *Open Innovations Association (FRUCT), 2015 17TH Conference of* , vol., no., pp.186-191, 20-24 April 2015

[13] Chuenurajit, T.; Phimmasean, S.; Cherntanomwong, P., "Robustness of 3D indoor localization based on fingerprint technique in wireless sensor networks," in *Electrical Engineering/Electronics, Computer, Telecommunications and Information Technology (ECTI-CON), 2013 10th International Conference on* , vol., no., pp.1-6, 15-17 May 2013

[14] Bshara, M.; Orguner, U.; Gustafsson, F.; Van Biesen, L., "Fingerprinting Localization in Wireless Networks Based on Received-Signal-Strength Measurements: A Case Study on WiMAX Networks," in *Vehicular Technology, IEEE Transactions on* , vol.59, no.1, pp.283-294, Jan. 2010

[15] L. Xie, Y. Wang, and X. Xue, "A New Indoor Localization Method Based on Inversion Propagation Model," *6th International Conference on in Wireless Communications Networking and Mobile Computing (WiCOM), 2010*, Chengdu, China, 2010, pp. 1-4, 2010

[16] Y A S Dama, H Hammad, R Zaid, R Zaid, R A Abd-Alhameed, P S Excell, A comparision between vector algorithm and CRSS algorithm for indoor localization, IET conference on Ninth CEM International Conference on Computation in Electromagnetics, Imperial College, London, UK, session 3, P3-4, pp. 1-2, 31 March - 01 April 2014

[17] Obeidat, H.A.; Abd-Alhameed, R.A.; Noras, J.M.; Zhu, S.; Ghazaany, T.; Ali, N.T.; Elkhazmi, E., "Indoor localization using received signal strength," in *Design and Test Symposium (IDT), 2013 8th International* , vol., no., pp.1-6, 16-18 Dec. 2013

[18] K. Pour, and J. Perez, "Robust Indoor Positioning Based on Received Signal Strength," *2nd International Conference on, Birmingham in Pervasive Computing and Applications, 2007. ICPCA 2007*, UK, 2007, pp. 693- 698, 2007.

[19] Obeidat, H.A.; Shuaieb, W.; Alhassan, H.; Samarah, K.; Abousitta, M.; Abd-Alhameed, R.A.; Jones, S.M.R.; Noras, J.M., "Location based services using received Signal Strength algorithms," *Internet Technologies and Applications (ITA), 2015*, pp. 411-413, 8-11 Sept. 2015.

Huthaifa Obeidat was born in Jordan, he received his BSc degree in Electrical Engineering from Jordan University of Science and Technology 2011, he was awarded MSc degree in Personal Mobile and Satellite Communication from the University of Bradford 2013. Since then, he worked as lecturer in Communication and Electronics department at Jerash University in Jordan. Currently he is a PhD student at the University of Bradford. His research interests include Radiowave Propagation, Antenna and Location Based Services.

Yousef Dama is an Assistant professor in Telecommunications Engineering at An-Najah National University, Palestine. He received his BSc in electrical engineering from An-Najah national University, Palestine, in 2005, MSc degree in Personal Mobile and Satellite Communications from University of Bradford, UK, in 2006, and his PhD in Broadband Wireless Systems Engineering from University of Bradford, UK, in 2013. He has published about 40 academic journals and referred conference papers. His current research interests includes diversity techniques, space time coded orthogonal frequency division multiplexing, Propagation channel modelling, and spatial envelope correlation of MIMO system for broadband wireless systems, and also he is enthusiasm for antenna array implementation, optimization, radio frequency designs, and novel localization applications.

Raed A. Abd-Alhameed is Professor of Electromagnetic and Radio Frequency Engineering at the University of Bradford. Currently, he is the leader of the RF, antenna design and electromagnetic research in the School of Engineering and Informatics, Bradford University. He is Principal Investigator for several funded projects from EPSRC, EU, TSB, RDP and has led several successful knowledge transfer programmes for Pace PLC, YW PLC, Datong of Seven Technologies Group, WiMAC and ITEG Ltd. He has published over 400 academic journal and conference papers and is co-author of three books and several book chapters. Prof. Abd-Alhameed is a Fellow of the Institution of Engineering and Technology, Fellow of Higher Education Academy, and a Chartered Engineer in the U.K.

Fun Hu is Professor of Wireless Communications Engineering at University of Bradford, UK. Prof. Hu has received considerable funding support through participations and contributions to many flagship projects funded by the UK funding councils, EU, ESA and TSB. Her major research is in integrated mobile, wireless and satellite communication networks with particular applications to vehicular communications networks including aircrafts and trains. She is the Head of the Future Ubiquitous Research Group and has published over 100 papers in scientific journals and international conferences, and co-authored 1 book, edited two books and contributed to 5 book chapters.

Rami Qahwaji is Professor of Visual Computing at Bradford University. He is originally trained as an Electrical Engineer and had MSc in Control and Computer Engineering. His research interests include: 2D/3D image processing, machine learning, signal processing and the design of machine vision systems with proven track record in the fields of satellite imaging, medical imaging, data visualisation and applied data mining working with various medical and industrial collaborators. He led the development of software systems that are being used by NHS, NASA, European Space Agency and other companies. His research has been funded by EPSRC, EU FP7, NHS, ERDF, European Space Agency (ESA), TSB, Yorkshire Forward, and more. He has over 120 refereed publications and has supervised 20 completed PhD projects. Rami is also Fellow of the Institution of Engineering and Technology (FIET), Charted Engineer (CEng) and Fellow of the Higher Education Academy (FHEA).

James Noras is a Senior Lecturer in the School of Engineering and Informatics at the University of Bradford, UK, and has published 59 journal papers and 93 conference papers, in fundamental semiconductor physics, analogue and digital circuit design, digital signal processing and RF system design and evaluation. He is the director of three internationally franchised B.Eng. courses in Electrical and Electronic Engineering, has successfully supervised 18 Ph.D. students, and is currently supervising the research of three Ph.D. students. His main research interests are now in digital system design and implementation, DSP and coding for communication systems, and localization algorithms for

Location Based Services using Received Signal Strength Algorithms

H.A. Obeidat[1], W. Shuaieb[1], H Alhassan[1], K. Samarah[1,2], M. Abousitta[1], R.A. Abd-Alhameed[1], J.M. Noras[1]
[1]School of Engineering and Informatics, University of Bradford, Bradford, UK
h.a.obeidat@student.bradford.ac.uk; r.a.a.abd@bradford.ac.uk
University of Mutah, Al-Karak, Jordon

***Abstract*—A comparison is carried out among indoor localization algorithms using received signal strength, namely the vector algorithm, and the Modified Comparative Received Signal Strength (MCRSS) algorithm. The study considered comparisons on the performance of the proposed algorithms. The experiments were carried out in a simulated environment for 3rd floor of Chesham Building, University of Bradford using ray tracing software and MATLAB. Results justify a preference for use of the MCRSS algorithm.**

Keywords— MCRSS; Indoor localization; Ray tracing; RSS.

I. INTRODUCTION

Indoor localization has become one of the most attractive areas in the research nowadays. Localization is defined as the process by which a target can be located in a space. If the process is to locate the target in an outdoor environment it is referred as outdoor localization, however if the target to be located within a building, this type of localization is called indoor localization.

Localization was employed by sailors, who knew the directions in the sea based on celestial objects location. In 1920, sea-based navigation was improved by the use of shore-transmitter [1]. In 1960s the US army evolved satellite based localization which is promoted later to global positioning system (GPS) [2]. In 1983 GPS was utilized for public usage, the accuracy enhanced from 100 m as achieved in 1990 to 10m as achieved in 2000 [2]. GPS is highly desired for outdoor localization, where LoS mode is the dominant mode propagation; however it is not practical to be used in indoor localization due to its weakness to penetrate buildings as well as the high cost required [3].

Indoor environment causes particular propagation problems. Because of the building constructions, furniture, and people inside, the multipath phenomenon and shadowing arise, this in turn would affect the position location resolution [4]. The main problems that face the indoor localization systems can be summarized as; First: reflection from obstacles, which occurs due to the multipath. Second: the attenuation due to losses caused by obstacles that exists between the transmitters and receivers, in addition to the lossy nature of the transmission medium. Finally: the noise level which industriously degrade the performance of the system, and hence affect the accuracy of localization [5].

Indoor localization can be carried out by personal area network, Wireless LANs, or wireless ad-hoc networks, where outdoor localization is carried out by GPS, GSM, and UMTS [4].

Indoor localization can take place in many environments such as hospitals, evacuations, and even households [6]. In hospitals, patients' movements within the hospital facilities could be tracked to provide quick assist when needed. Firefighter locations can be identified during evacuations, and firefighting activities, if anyone suffered suffocation and fell down or was trapped, he could be located and rescued [7]. Indoor localization can be used for household usage; the mother can know the location for her kid inside the house.

There are so many techniques to perform localization; the most powerful technique is the one that gives high accuracy with less computation [4]. Localization can be carried out through so many methods. Based on time duration for the signal travelling between the transmitter and the target; the location can be estimated by Time of Arrival (TOA) location method [8]. Based on the strength of the received signal, the location is evaluated using Received Signal Strength (RSS) method [9]. The third technique uses the direction of the transmitted signal from the target to find the location; this technique is Angle of Arrival (AOA) [10]. Both of the RSS localization method and the TOA localization method are based on distance measurements [4]; where the AOA localization method based on angle measurements. Other techniques are based on area, hop count, and neighborhood [11]. For any type of localization, a procedure of two steps should be followed during the localization process; the first step is to have information about the geographic area to be tested, the second is to estimate the location for targets according to the collected data [12]. The design for the localization algorithm depends on so many factors, these include the availability of the resources, the required accuracy, and the nature of the area to be covered (i.e. the building details); however no algorithm is absolute favorable [13,14].

II. PROPOSED ALGORITHMS

The Proposed algorithms are based on Radio Frequency Fingerprinting, this paper considered the benefits and drawbacks of the algorithms. In the first algorithm, the collected RSS readings from the access point (AP) at the reference point (RP) forms a vector. The readings are organized with respect to the AP order in the facility. The radiomap is constructed from the generated vectors. For the test point (TP); the same procedure is applied, the test node's vector will be compared to the database to estimate the closest location, and this is done by estimating the Euclidean distance, the one with smallest distance is considered to be the closest to the TP.

The second algorithm is MCRSS algorithm, we extend the work done by authors in [15-17], the algorithm is based on RF-Fingerprinting too. In the offline phase the radiomap is constructed from matrices rather than vectors as in the previous algorithm, the vectors in the last approach are converted to a matrix as illustrated in the equations below

This algorithm highlights the presence of receiver sensitivity R_{sens}.

$$M_{\alpha}(x,y)=\left[c_{ij}(x,y)\right] \qquad i,j=1,2,\cdots,\alpha \tag{1}$$

$$c_{ij}(x,y)=\begin{cases} +1 & R_i(x,y)>R_j(x,y) \\ -1 & R_i(x,y)<R_j(x,y) \\ 0 & R_i(x,y)=R_j(x,y) \\ +2 & R_i(x,y)>R_{sens}>R_j(x,y) \\ +2 & R_j(x,y)>R_{sens}>R_i(x,y) \\ 3 & R_{sens}>[R_j(x,y),R_i(x,y)] \end{cases} \tag{2}$$

$$c_{ij}(x,y)=0 \text{ for all } i=j. \tag{3}$$

Where $M_{\alpha}(\mathcal{X},\mathcal{Y})$ is the constructed matrix, $c_{ij}(\mathcal{X},\mathcal{Y})$ is the entry for the matrix at row i and column j. $(\mathcal{X},\mathcal{Y})$ is the location for the mobile which is considered to be known. $R_i(\mathcal{X},\mathcal{Y})$ is the RSS from the transmitter or access point (i) at the tag's location $(\mathcal{X},\mathcal{Y})$.

In the on-line phase the location of the test devices is to be estimated, the TP RSS readings is converted to a matrix as in the off-line phase. A tag's location is estimated by comparing its constraint matrix with those in the radio map. The closest matrix is the one with the smallest Euclidean distance, thus the corresponding location for the closest matrix is assumed to be the closest location to the tag.

The inherent redundancy that exists in each constraint matrix gives rise to an acceptable performance for the positioning algorithm and makes the system more strong.

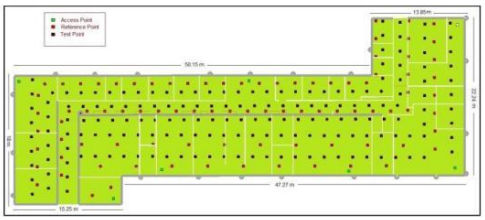

Fig.1 The distribution of APs, RPs, and test points within the floor.

III. SIMULATION AND RESULTS

The adopted floor for the experiment was the third floor in Chesham building in Bradford University. The model for the building was constructed also by the *Wireless Insite*® software. The floor has concrete walls, a polystyrene wall, and wooden doors. A layout of the adopted floor is demonstrated in fig.1.

The floor structure is considered appropriate to test the performance of our algorithm in indoor environment. The access points were planted in an organized way to provide a proper coverage. Although the reference points (RP) were also placed in an organized way, their distribution can't be fully uniform as the floor structure is more complicated; more RPs were added in the corridor and close to the walls to improve the localization accuracy in these areas. The system operates at 200 MHz.

1) Vector Algorithm:

This algorithm is deemed successful as long as the estimated location is the closest to the actual location of the mobile terminal. When the estimated RP is not the closest to the actual location of the mobile terminal, then the algorithm is said to have failed. The percentage of correctly estimated locations gives the *success rate*.

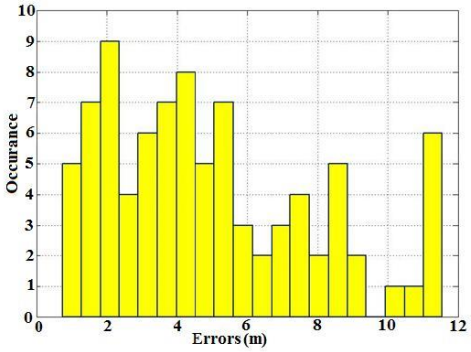

Fig.2 Histogram of LE for the vector algorithm in the floor.

Fig. 2 show the localization performance for the vector algorithm in a floor environment. The achieved success rate is 20%. The statistical mean of error is 5 meters. The standard deviation is 2.97 meters. As the figure shows, $P\,(Error \leq 4\,meters) = 0.44$ and $P\,(Error \leq 6\,meters) = 0.7$.

Considering the floor dimensions and sophistication, the algorithm performance is sufficient to meet the accuracy requirements for many applications (mean error is less than 10% of the floor dimensions).

2) MCRSS Algorithm:

A severe drawback of the MCRSS algorithm was exposed during the analysis of the results obtained in the project, termed "the ambiguity problem". During the process of generating the MCRSS radio map, it was noted that some RPs construct the same constraint matrix. Although each RP is likely to have unique power readings, RP's received power is found frequently to have the same relative power readings as other RPs. Since 7 APs were used, the resultant constraint matrix is (7×7). It was expected that the localization performance will be improved as the size of matrix was larger and hence the effect of ambiguity

reduced. However, the ambiguity problem still exists almost for the half of the measurements as the table below shows.

Table1. The occurrence of the ambiguity problem using MCRSS algorithm in the floor

No. of Estimated Locations	Occurrence
1	46
2	22
3	11
4	4
5	2
6	2

Table.1 shows the number of estimated locations resulted when deploying the CRSS algorithm. Among 87 test points, more than half of the test points (46 out of 87) were linked to a single RP for each test point (no ambiguity). One fourth (22 out of 87) of the test points where linked to 2 RPs for each test point. One eighth (11 out of 87) of the test points were linked to 3 RPs for each test point.

Fig. 3 shows the performance comparison between the vector and MCRSS algorithms. Although the algorithm considered failing all the time, however, it was represented for the purpose of comparison with the vector algorithm. As expected, the vector algorithm outperforms the MCRSS algorithm. Although the plots look comparable, the vector algorithm does not suffer from the ambiguity problem. Moreover, the upper bound for the vector error is restricted to 11 meters as shown above which reflects more stability. Although that the MCRSS algorithm was enhanced, and more APs were used, the ambiguity still exists; the localization performance could not match the vector algorithm.

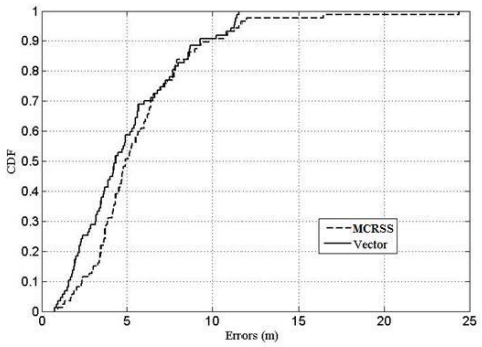

Fig.3 LE comparison between MCRSS and Vector algorithms in the floor.

Conclusion

The paper compares set of indoor localization algorithms using received signal strength, the vector algorithm, the MCRSS algorithm. The experiment was carried out at 200 MHz in a simulated environment for 3rd floor Chesham Building, University of Bradford, UK. The vector algorithm shows acceptable performance as majority of errors are less than 10% of the floor dimensions. The MCRSS algorithm suffers from ambiguity since more than one RP may have the same matrix. Based on the experimental results the vector algorithm is better in terms of accuracy, cost, and effort.

REFERENCES

[1] Goswami, S.: Indoor Location Technologies. Springer, New York (2013)

[2] G. Frost, I. Lachow, *et al*, *The Global Positioning System Assessing National Policies*, 1st ed., Santa Monica, United States: RAND Corporation, 1995.

[3] A. Ladd, "On the feasibility of using wireless ethernet for indoor localization," Robotics and Automation, *IEEE Transactions on*, vol. 20, no. 3, pp. 555-559, June 2004.

[4] Z. Yang Y. Liu, *Location, Localization, and Localizability Location-awareness Technology for Wireless Networks*, 1st ed. New York, United States: Springer, 2011.

[5] J. Andersen, T. Rappaport, and S. Yoshida, "Propagation measurements and models for wireless communications channels," *IEEE Communications Magazine*, vol. 33, no. 1, pp. 42-49, Jan 1995.

[6] M. Zhang, S. Zhang, J. Cao, "Fusing Received Signal Strength from Multiple Access Points for WLAN User Location Estimation," in *Internet Computing in Science and Engineering, 2008. ICICSE '08. International Conference on*, pp.173-180.

[7] Y. Ji, S. Biaz, S. Wu, and B. Qi, "Impact of Building Environment on the Performance of Dynamic Indoor Localization," in *Wireless and Microwave Technology Conference, 2006. WAMICON '06. IEEE Annual*, pp.1-5.

[8] X. Li, and K. Pahlavan, N. Alsindi, "Performance of TOA estimation algorithms in different indoor multipath conditions," in *Wireless Communications and Networking Conference*, 2004 IEEE, pp. 495-500.

[9] M. Robinson, "Received signal strength based location estimation of a wireless LAN client," in *Wireless Communications and Networking Conference*, 2005 IEEE, Los Angeles, 2005, pp. 2350 - 2354.

[10] C. Lam, and A. Singer, "Bayesian Beamforming for DOA Uncertainty: Theory and Implementation," *Signal Processing, IEEE Transactions on*, vol. 54, no. 11, pp. 4435- 4445, Nov. 2006.

[11] Pastina, D.; Colone, F.; Martelli, T.; Falcone, P., "Parasitic exploitation of WiFi signals for indoor radar surveillance," *Vehicular Technology, IEEE Transactions on* , vol.PP, no.99, pp.1,1

[12] Xiao, W., Ni, W., Toh, Y.: Integrated wi-fi fingerprinting and inertial sensing for indoor positioning. In: International Conference on Indoor Positioning and Indoor Navigation. IEEE, New York (2011)

[13] Y. López, M. Gómez, J.o Álvarez, F. Andrés, "Evaluation of an RSS based indoor localization system," *Sensors and Actuators A: Physical*, vol. 167, no. 1, pp. 110-116, Feb. 2011.

[14] "Wireless Medium Access Control (MAC) and Physical Layer (PHY) Specifications for Low-Rate Wireless Personal Area Networks (LR-WPANs)," IEEE, 802.15.4, 2008.

[15] K. Pour, and J. Perez, "Robust Indoor Positioning Based on Received Signal Strength," *2nd International Conference on, Birmingham in Pervasive Computing and Applications, 2007. ICPCA 2007*, UK, 2007, pp. 693- 698, 2007.

[16] Obeidat, H.A.; Abd-Alhameed, R.A.; Noras, J.M.; Zhu, S.; Ghazaany, T.; Ali, N.T.; Elkhazmi, E., "Indoor localization using received signal strength," *Design and Test Symposium (IDT), 2013 8th International* , pp.1-6, 16-18 Dec. 2013.

[17] H. Obeidat, "Indoor localization using received signal strength," MSc. dissertation, School of Engineering, Design and Technology, University of Bradford, Bradford, UK, 2013.

Performance Comparative Study Between Vector And ECOLOCATION Algorithms For Indoor Positioning

H. Obeidat[1], O. Obeidat[2], W. Shuaieb[1], A. Alabdullah[1],Y. Dama[3], M.S. Binmelha[1], S. Jones[1], R. Abd-Alhameed[1]
[1]School of Electrical Engineering and Computer Science, University of Bradford, Bradford, UK
[2]College of Engineering, Wayne State University, Detroit, USA
[3] Department of Telecommunication Engineering, An Najah National University, Nablus, Palestine
{h.a.obeidat, r.a.a.abd}@bradford.ac.uk

***Abstract*— a comparative study of performance is conducted between two indoor positioning algorithms described in the Literature, the Vector and Ecolocation algorithms. Both use received signal strength (RSS) to implement a radio frequency fingerprinting technique. The experiment is conducted using commercial ray tracing software called Wireless Insite and Matlab. The Vector algorithm performs better than the Ecolocation algorithm, which suffers heavily from an ambiguity issue. For the Vector algorithm, the median position error was 2.79 m and 90% of errors were less than 5.72 m**

Keywords— Ecolocation; Indoor localization; Ray tracing; RF-fingerprinting, RSS; Vector Algorithm.

I. INTRODUCTION

In free space, received signal strength (RSS) reduces monotonically with distance according to an inverse square law. However, in a cluttered, multipath environment the relationship of RSS and distance is multi-valued. Fingerprinting is a technique that seeks to unambiguously recognize a mobile terminal's location from the pattern of RSS seen from a number of spatially distributed transmitting sources [1]. In many indoor environments radiolocation is possible by making opportunistic use of existing wireless local area network signals [2].

One advantage of using RSS in positioning is that it does not require additional hardware other than the power detectors which are already built-in in to Bluetooth, infrared, Wi-Fi, UWB, Zigbee devices. This makes the use of RSS for positioning attractive [3]. In comparisons between UWB and Zigbee positioning technologies, it was found that the former gives better results but is more expensive to be deployed [4]. Another advantage in positioning using RSS is that it does not depend on timing information therefore no further synchronization between the operating devices is required [5]. RSS positioning works fine over short distances which is the case for the indoor scenarios; however the performance degrades for outdoor scenarios where other techniques like Time of arrival (TOA) are preferable [6]. RSS positioning algorithms require training and matching algorithms [7]. Recently, localization systems take advantage of the existing infrastructure of WLAN systems which characterized by its low cost and ability to work for many years [8]; however many of these systems operate in the 2.4 GHz band, where many other applications including Bluetooth devices and microwave ovens are operating in the same band, which introduces some interference and degrades the localization performance [2]. RSS positioning is prone to shadowing, non-line of sight (NLOS) and works less accurately in low signal to noise ratio (SNR) conditions [6].

RSS Fluctuations with time reduce positioning accuracy [9], which occurred due to temporal, human and interference factors. Temporal factors include the change of RSS measurements due to change in environmental temperature, human factor include the effect of human body as it has over 50% of water which can alter the RSS especially with movements, while interference factors which are due to existence of other systems operating in the same frequency band [10] [11].

In the literature many algorithms have been proposed for positioning using RSS, the main categories including radio-frequency (RF) fingerprinting, probabilistic estimation, range based techniques, Kernel based algorithms and proximity based techniques [12].

The present research compares two RF-fingerprinting indoor positioning algorithms, the Vector algorithm and the Ecolocation algorithm. It is an extension of previous work [13] [14] [15]. Section II offers a brief explanation of the proposed algorithms and the environmental setup. Section III introduces a discussion of the results. Conclusions are presented in Section IV.

II. PROPOSED ALGORITHMS

The indoor environment is both complex and dynamic due to the severe effect of multipath, movement of people and objects and dynamics of potentially interfering radio sources, which makes the use of range based algorithms insufficient; however RF-fingerprinting methods use multi-parameter data about the indoor channel and hence provide better estimation [4] [16].

Two stages are followed in RF – fingerprinting algorithms [17]; the offline phase (the training stage) and the online phase (real time stage). In the offline stage, a large number of *reference points* (RP) locations are selected. This may be accomplished by dividing the area into grids. At the center of each grid RSS data are collected from the surrounding access

points (APs). The system stores the location of the fingerprints along with its corresponding RSS measurements and this information is termed a *Radio Map* [18]. In order to reduce the effect of noise, measurements are performed over a period of time and then averaged.

In the next stage, RSS at the mobile from the surrounding APs are recorded at positions called *test point*s (TP), the collected readings are compared with the radio map data. Algorithms differ in the method used to make that comparison.

One possible method is to estimate the smallest Euclidean distance between the TP and the radio map subspace [19]. The RP with the lowest corresponding value is considered as the closest RF to the TP [18] as shown in equation (1).

$$(\hat{x},\hat{y}) = \arg\min_{x_i,y_i} \sqrt{\sum_{i=1}^{N} \left(RSS_{TP} - RSS_{(x_i,y_i)}\right)^2} \qquad (1)$$

where N is the total number of RPs, RSS_{TP} is the TP received signal strength and $(\hat{x},\hat{y})$ is the estimated location of the mobile. Other methods return the k-nearest locations which have the lowest values of equation (1) [20]. Increasing the number of RPs will enhance the positioning however it will cost more time and effort to build the radio map, additionally the data base should be regularly updated in case of changes in the environment layout or employing new APs [12] [21].

In our experiments the advantages and drawbacks of using two proposed localization algorithms were investigated. Both algorithms are RF-Fingerprinting based algorithms. The first algorithm is the vector algorithm [19], where the collected received signal strength measurements from the RPs are stored and arranged in vectors according to AP order. These vectors are used to build the radio map, in the next stage the location of the mobile is inferred by estimating the Euclidean distance between the TP's RSS and the data base in the radio map as mentioned above.

The second algorithm is **E**rror **CO**ntrolling **LOCA**liza**TION** (ECOLOCATION) [22] [23], the algorithm links the higher signal strength to the closest AP as shown in equation (2) [23] where i and j are APs:

$$R_i > R_j \rightarrow d_i < d_j, \text{ for all } i < j \qquad (2)$$

Similar to vector algorithm, ECOLOCATION has two phases, in the training phase a matrix is assembled based on comparative distances between the mobile and α surrounding APs, as shown in equations (3-5). (x_k, y_k) are the reference points, $d_i(x_k, y_k)$ is the distance between the k^{th} RP and the i^{th} AP, $M_k(x_k, y_k)$ is the matrix generated for the k^{th} RP and $\mathrm{c_{ij}}(x_k, y_k)$ is the entry for that matrix at row i and column j. The set of matrices generated at this stage is the idealized Radio Map indicating which APs are nearest.

$$M_k(x_k, y_k) = \left[\mathrm{c_{ij}}(x_k, y_k)\right].\ i,j = 1,2,\ldots,\alpha \qquad (3)$$

$$\mathrm{c_{ij}}(x_k, y_k) = \begin{cases} +1 & d_i(x_k, y_k) < d_j(x_k, y_k) \\ -1 & d_i(x_k, y_k) > d_j(x_k, y_k) \\ 0 & d_i(x_k, y_k) = d_j(x_k, y_k) \end{cases} \qquad (4)$$

$$\mathrm{c_{ij}}(x_k, y_k) = 0 \text{ for all } i = j. \qquad (5)$$

In the online phase, at any given position (x, y), RSS from the surrounding APs are measured and converted into a further matrix M_ρ as shown in equations (6-8). To test the algorithm, matrices are constructed for a number of sample positions.

$$M_\rho(x,y) = \left[\mathrm{e_{ij}}(x,y)\right].\ i,j = 1,2,\ldots,\rho \qquad (6)$$

$$\mathrm{e_{ij}}(x,y) = \begin{cases} +1 & \mathrm{R_i}(x,y) > \mathrm{R_j}(x,y) \\ -1 & \mathrm{R_i}(x,y) < \mathrm{R_j}(x,y) \\ 0 & \mathrm{R_i}(x,y) = \mathrm{R_j}(x,y) \end{cases} \qquad (7)$$

$$\mathrm{e_{ij}}(x,y) = 0 \text{ for all } i = j. \qquad (8)$$

where (x, y) is the TP location, $M_\rho(x, y)$ is the matrix generated for the TP, $\mathrm{e_{ij}}(x, y)$ is the entry for the matrix at row i and column j and $\mathrm{R_i}(x, y)$ is the RSS from the i^{th} AP at the tag's location (x, y).

The matrix M_ρ is compared with all the matrices M_k in the Radio Map. The Euclidean distance (e) between elements of M_ρ and M_k with the same matrix indices is estimated as shown in equation (9). The RP whose matrix has least Euclidean distance is considered as the closest RP.

$$e = \sqrt{\sum_{i=1}^{N}\sum_{j=1}^{N} (c_{ij} - e_{ij})^2} \qquad (9)$$

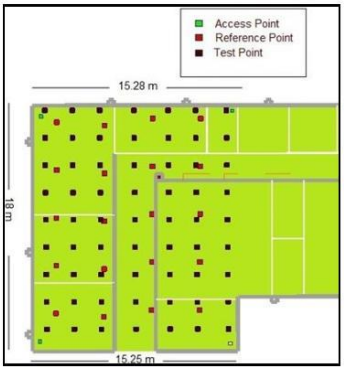

Figure 1: The distribution of APs, RPs, and Test Points in the floor.

III. SIMULATION AND RESULTS

The adopted scenario for the experiment is a simulated model using Wireless Insite for the 3rd floor in Chesham building at the University of Bradford. With the development in the software technologies, combining the uniform theory of diffraction (UTD) with shoot and bouncing rays (SBR) ray tracing become an efficient tool for signal parameters estimation [24]. Ray tracing estimation accuracy depends on many factors including the fine detailed design of the implemented scenario which in case was not carefully designed it may affect the phases of the electromagnetic rays and lead to errors in signal parameters predictions [25]. The model considered material type and electrical properties; the

floor has different types of walls, concrete block and stud partition, wooden doors and glass windows. A top view of the simulated floor is presented in Figure 1, the APs used are linear dipole and mounted in a way to provide proper coverage; the system operates at 200 MHz.

1) Vector Algorithm:

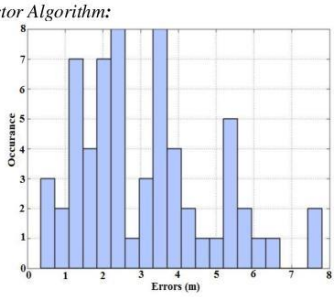

Figure 2: Histogram of positioning error for the vector algorithm.

As seen in Figure 2, there are some large errors, however, the median error of approximately 2.79 m makes the technique useable in some applications. 90% of results are within 5.7 m. The standard deviation is 1.76 m.

2) Ecolocation Algorithm:

During generation the matrices for both offline and online phases, it was observed that some matrices are identical due to the way that matrices are made. Matrix elements are assigned values depending firstly on the ascending order of distances to transmitters in the offline case and secondly on the ascending order of received power in the online case. For example, if the room has four transmitters and the distances to these transmitters from two different places are respectively: $d_1 = [2.5\ \ 5\ \ 7\ \ 9]$ and $d_2 = [3\ \ 5.5\ \ 6\ \ 8.5]$, when applying equations (3-5) both locations will create the same matrix. The same thing is observed in the online phase, such a problem is termed as ambiguity issue as shown in Figure 4. For a four-AP system, the maximum number of unique generated matrices is 8 as shown in Table 1 and Figure 3, this exclude the possibility of having RP with exactly equal distances to two or more AP as it unlikely to happen.

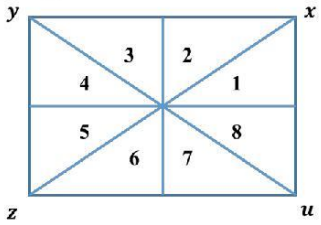

Figure 3: Boundaries of distance based comparative regions.

Figure 3 illustrates the boundaries of the distance-based comparative regions for a rectangular shaped coverage area with four APs, the ascending order of distances to the four APs in each region is identical, as shown in Table 1.

Table 1: Possible arrangements for distance based matrices for four APs.

Region	Distance based comparative order
1	$d_x < d_u < d_y < d_z$
2	$d_x < d_y < d_u < d_z$
3	$d_y < d_x < d_z < d_u$
4	$d_y < d_z < d_x < d_u$
5	$d_z < d_y < d_u < d_x$
6	$d_z < d_u < d_y < d_x$
7	$d_u < d_z < d_x < d_y$
8	$d_u < d_x < d_z < d_y$

The shape of regions in Figure 3 depends on the area under study, number of APs and their deployment. If more than one RP is located in each region, ambiguity will arise. In fact the optimum location for RPs would be at the centre of area in each region. Therefore if the number of APs increases there will be more regions which reduces the ambiguity, on the other hand, increasing the number of RPs will make the ambiguity issue worse. In our experiment the shape of the area under study is rectangular, with four APs, so the regions are triangular. If RPs were optimally located, the r.m.s. error of distances to the centre of the triangle found to be 2.622 m which represents the best possible performance for the Ecolocation algorithm in the absence of ambiguity and multipath (this can insure the credibility of equation 2). Furthermore, it was found that different pairs of matrices can have the same Euclidean distance, which compounds the ambiguity issue.

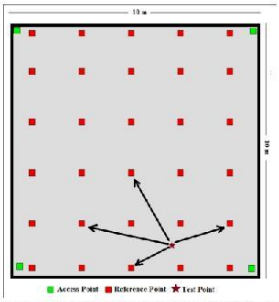

Figure 4 Example of ambiguity arising with RSS measurements.

Figure 5 shows the occurrence of estimated locations resulted due to ambiguity problem. Less than one quarter of the TPs (15 out of 63) have no ambiguity. The case where each TP is linked to 2 RPs was recorded for 5 TPs, while in the case where each TP is linked to 3 RPs it was recorded for 21 TPs which nearly third of the total number of TPs, the severity of ambiguity problem is shown as (4 out of 63) of the TPs were linked to 8 RPs for each TP.

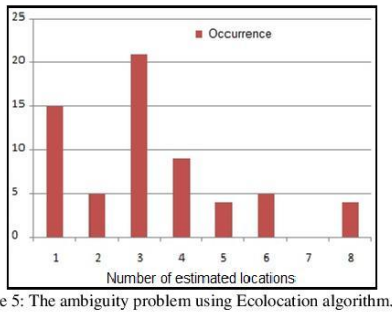

Figure 5: The ambiguity problem using Ecolocation algorithm.

Figure 6 presents a comparative performance between the introduced algorithms, as shown in the figure comparing to Ecolocation algorithm the vector algorithm has much better performance. For example, the probability of having error less or equal to 4 m using the vector algorithm is around 75% while using the Ecolocation algorithm it is even less than 5%. Because it suffers from the ambiguity problem, positioning using the Ecolocation algorithm is not as accurate as the vector algorithm which does not suffer from this effect.

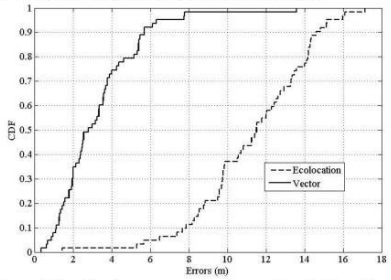

Figure 6: Positioning error comparison using the introduced algorithms.

CONCLUSION

A comparative performance study was undertaken between two indoor positioning methods proposed in the literature, namely the vector and Ecolocation algorithms. The experiment was conducted at 200 MHz in a simulated environment for the 3rd floor of Chesham building of university of Bradford. The Vector algorithm shows superior performance compared to the Ecolocation algorithm which suffer heavily from an ambiguity issue; only one quarter of the results are free from ambiguity. The median distance error was quite large for the Vector algorithm, at 2.79 m with 90% of errors less than 5.7 m. However, for the Ecolocation algorithm the median was 11.5 m.

References

1. Sayrafian-Pour, K. and D. Kaspar. *A robust model-based approach to indoor positioning using signal strength*. in *Personal, Indoor and Mobile Radio Communications, 2008. PIMRC 2008. IEEE 19th International Symposium on*. 2008. IEEE.
2. Ladd, A.M., et al., *On the feasibility of using wireless ethernet for indoor localization*. IEEE Transactions on Robotics and Automation, 2004. **20**(3): p. 555-559.
3. Obeidat, H., et al. *Indoor localization using received signal strength*. in *Design and Test Symposium (IDT), 2013 8th International*. 2013. IEEE.
4. Ahn, H.-S. and W. Yu, *Environmental-adaptive RSSI-based indoor localization*. Automation Science and Engineering, IEEE Transactions on, 2009. **6**(4): p. 626-633.
5. Bouchereau, F. and D. Brady. *Bounds on range-resolution degradation using RSSI measurements*. in *Communications, 2004 IEEE International Conference on*. 2004. IEEE.
6. Munoz, D., et al., *Position location techniques and applications*. 2009: Academic Press.
7. Hatami, A., et al. *On RSS and TOA based indoor geolocation-a comparative performance evaluation*. in *Wireless Communications and Networking Conference, 2006. WCNC 2006. IEEE*. 2006. IEEE.
8. Shchekotov, M. *Indoor localization methods based on Wi-Fi lateration and signal strength data collection*. in *Open Innovations Association (FRUCT), 2015 17TH Conference of*. 2015. IEEE.
9. Chapre, Y., et al. *Received signal strength indicator and its analysis in a typical WLAN system (short paper)*. in *Local Computer Networks (LCN), 2013 IEEE 38th Conference on*. 2013. IEEE.
10. Xu, L., et al. *Variation of received signal strength in wireless sensor network*. in *Advanced Computer Control (ICACC), 2011 3rd International Conference on*. 2011. IEEE.
11. Ullah, K., et al. *An Experimental Study on the Behavior of Received Signal Strength in Indoor Environment*. in *Frontiers of Information Technology (FIT), 2013 11th International Conference on*. 2013. IEEE.
12. Zekavat, R. and R.M. Buehrer, *Handbook of position location: Theory, practice and advances*. Vol. 27. 2011: John Wiley & Sons.
13. Obeidat, H.A., et al., *A Comparison between Vector Algorithm and CRSS Algorithms for Indoor Localization using Received Signal Strength*. 2016.
14. H. A. Obeidat et al., "Location based services using received Signal Strength algorithms," *2015 Internet Technologies and Applications (ITA)*, Wrexham, 2015, pp. 411-413.
15. Dama, Y., et al. *A comparison between vector algorithm and CRSS algorithm for indoor localization*. in *Computation in Electromagnetics (CEM 2014), 9th IET International Conference on*. 2014. IET.
16. Khanbashi, N.A., et al. *Real time evaluation of RF fingerprints in wireless LAN localization systems*. in *Positioning Navigation and Communication (WPNC), 2013 10th Workshop on*. 2013.
17. Alkasi, U., M.A. Shayokh, and H.P. Partal. *An experimental comparison study on indoor localization: RF fingerprinting and Multilateration methods*. in *Electronics, Computer and Computation (ICECCO), 2013 International Conference on*. 2013.
18. Xie, L., Y. Wang, and X. Xue. *A new indoor localization method based on inversion propagation model*. in *Wireless Communications Networking and Mobile Computing (WiCOM), 2010 6th International Conference on*. 2010. IEEE.
19. Bahl, P. and V.N. Padmanabhan. *RADAR: An in-building RF-based user location and tracking system*. in *INFOCOM 2000. Nineteenth Annual Joint Conference of the IEEE Computer and Communications Societies. Proceedings. IEEE*. 2000. Ieee.
20. Li, D., et al. *A feature scaling based k-nearest neighbor algorithm for indoor positioning system*. in *2014 IEEE Global Communications Conference*. 2014.
21. Feng, C., et al., *Received-signal-strength-based indoor positioning using compressive sensing*. Mobile Computing, IEEE Transactions on, 2012. **11**(12): p. 1983-1993.
22. Sayrafian-Pour, K. and J. Perez. *Robust indoor positioning based on received signal strength*. in *Pervasive Computing and Applications, 2007. ICPCA 2007. 2nd International Conference on*. 2007. IEEE.
23. Yedavalli, K., et al. *Ecolocation: a sequence based technique for RF localization in wireless sensor networks*. in *Proceedings of the 4th international symposium on Information processing in sensor networks*. 2005. IEEE Press.
24. Dama, Y., et al. *RSSI evaluation for multi-story building*. in *Internet Technologies and Applications (ITA), 2015*. 2015. IEEE.
25. Fuschini, F., et al., *Analysis of In-Room mm-Wave Propagation: Directional Channel Measurements and Ray Tracing Simulations*. Journal of Infrared, Millimeter, and Terahertz Waves, 2017: p. 1-18.